N84-27956

JPL PUBLICATION 84-12

Land Mobile Satellite Service (LMSS) Channel Simulator: An End-to-End Hardware Simulation and Study of the LMSS Communications Links

Ali B. Salmasi
James C. Springett
Joe T. Sumida
Paul H. Richter
Contributors

Ali B. Salmasi
Editor

May 1, 1984

NASA
National Aeronautics and
Space Administration

Jet Propulsion Laboratory
California Institute of Technology
Pasadena, California

JPL PUBLICATION 84-12

Land Mobile Satellite Service (LMSS) Channel Simulator: An End-to-End Hardware Simulation and Study of the LMSS Communications Links

Ali B. Salmasi
James C. Springett
Joe T. Sumida
Paul H. Richter
Contributors

Ali B. Salmasi
Editor

May 1, 1984

NASA
National Aeronautics and
Space Administration

Jet Propulsion Laboratory
California Institute of Technology
Pasadena, California

The research described in this publication was carried out by the Jet Propulsion Laboratory, California Institute of Technology, under a contract with the National Aeronautics and Space Administration.

ACKNOWLEDGMENT

The authors wish to express their deep gratitude to J. C. Packard, and acknowledge his fervent efforts, for the implementation and testing of all the hardware in the LMSS channel simulator laboratory. We also acknowledge F. J. Kollar for his immeasurable contributions to the design and implementation of the audio evaluation facility and testing procedures.

ABSTRACT

This report describes the design and implementation of the Land Mobile Satellite Service (LMSS) channel simulator as a facility for an end-to-end hardware simulation of the LMSS communications links, primarily with the mobile terminal. A number of studies are reported which show the applications of the channel simulator as a facility for validation and assessment of the LMSS design requirements and capabilities by performing quantitative measurements and qualitative audio evaluations for various link design parameters and channel impairments under simulated LMSS operating conditions.

As a first application, the LMSS channel simulator has been used in the evaluation of a system based on the voice processing and modulation (e.g., NBFM with 30 kHz of channel spacing and a 2-kHz rms frequency deviation for average talkers) selected for the Bell System's Advanced Mobile Phone Service (AMPS). The various details of the hardware design, qualitative audio evaluation techniques, signal-to-channel impairment measurement techniques, the justifications for criteria of different parameter selection in regards to the voice processing and modulation methods, and the results of a number of parametric studies are further described in this report.

CONTENTS

Tables

SECTION 1

SUMMARY

1.1 BACKGROUND

The Land Mobile Satellite Service (LMSS) channel simulator has been designed and implemented as a facility for an end-to-end hardware simulation of the LMSS communications links, primarily with the mobile terminal. The general objective of the simulator development is to provide a facility for validation and assessment of the LMSS design requirements and capabilities by performing quantitative measurements and qualitative subjective audio evaluations for various link-design parameters and channel impairments under simulated LMSS operating conditions. As an immediate application, this channel simulator will be used for evaluation of MSAT-X communications links (Ref. 1).

In designing satellite communications systems for multiple carrier operation such as MSAT-X, there is an enoromous need to be able to identify sets of communication-link parameters which provide an "acceptable" quality audio or data signal at the output of the receiver for the specific type of voice processing, modulation, coding, and/or satellite processing envisioned for the satellite system. Examples of these link parameters are rms frequency deviation ("modulation index"), IF bandwidth, Carrier-to-Noise ratio (C/N), Carrier-to-cochannel/adjacent channel Interference ratio (C/I), Carrier-to-Multipath Fading ratio (C/MF), Carrier-to-Intermodulation noise ratio (C/IM) and Bit Error Rate (BER).

The purpose of a facility such as the LMSS channel simulator is to provide accurate hardware simulation of mobile-satellite-mobile communication links as close to the actual environmental and operating conditions as possible. It also provides a tool to test the mobile equipments under evaluation. Quantitative baseband signal-to-channel impairment ratio measurements, bit-error-rate measurement, and qualitative subjective evaluations can be performed to determine sets of link parameters which provide the desired quality baseband audio signal. Once these sets of link parameters are determined, the communication systems designer can make trade-off studies between different link parameters and identify the optimum set which will result in the optimum system design in terms of the system capacity and system cost.

As a first application, the LMSS channel simulator has been used in the evaluation of a system based on the voice processing (e.g., 2:1 companding) and modulation (e.g., NBFM with a 2-kHz rms frequency deviation for the average talker) selected for the Bell System's Advanced Mobile Phone Service (AMPS) (Ref. 2). Therefore, so far, all of the quantitative and qualitative measurements and subjective tests have been geared towards determination of sets of link parameters that would provide the desired quality audio signal at the mobile receiver output for an AMPS-compatible type of system (i.e., 2:1 companding and 30 kHz of channel spacing). This defines the first phase of the LMSS channel simulator activities, which are described in this report.

1.2 IMPORTANT RESULTS

The quantitative and qualitative measurements, and subjective tests, performed with the LMSS channel simulator have provided a large number of possible trade-offs between different link parameters and have identified some optimum system designs. In Section 4, it will be shown that acceptable intelligibility can be achieved with surprisingly high amounts of noise, interference, and multipath fading---even for the relatively low modulation index chosen (11.5 kHz bandwidth of NBFM) for the measurements. For example, in the absence of noise and multipath fading, 97-percent sentence intelligibility is possible with a C/I ratio as low as 2 dB, and for 92-percent sentence intelligibility this ratio can be less than 1 dB. Similarly, for a carrier-to-multipath fading ratio of 5 dB (i.e., typical partial shadowing conditions for direct line-of-sight signal) and a carrier-to-noise ratio of 8 dB, which corresponds to the system FM threshold, a carrier-to-interference ratio about 13 dB will result in 97-percent sentence intelligibility, while a value of 92-percent sentence intelligibility can be achieved with a carrier-to-interference ratio of only 6 dB.

Furthermore, the results of subjective quality evaluation tests in Section 4 have shown the existence of a three-way trade-off between C/N (dependent on carrier power and receiver sensitivity), C/I (dependent on the antenna beam patterns, the number of beams, and the frequency reuse pattern), and modulation index (dependent on IF bandwidth and the required receiver output signal-to-noise ratio) for each value of C/MF (dependent on mobile environments and the percentage of time and locations that undisrupted communications are required). As an example, for a fixed amount of rms frequency deviation (i.e., the same value used in AMPS modulation) and a C/MF of 20 dB (i.e., no shadowing conditions and a mobile antenna with good low elevation angle signal discrimination), a combination of 17 dB for C/I and about 9 dB for C/N provides a standard city-telephone-link-quality signal, while a combination of 9 dB for C/I and about 14 dB for C/N provides the exact same quality signal. These results are extremely important since they provide a basis for further system evaluation by means of a cost sensitivity analysis for these design parameters.

In Appendix C, some important derivations of a number of useful new formulas for the predictions of the noise performance of mobile FM receivers are presented. In Appendix D, a novel technique is shown for measurement of the mobile FM output signal-to-noise ratio in the presence of narrowband Gaussian noise and rapid Rayleigh fading, with or without the satellite direct line-of-sight signal. In Section 5 of this report, the various theoretical formulas provided in Appendix C are compared with the results of the experimental measurements obtained using the measurement technique described in Appendix D. For example, it is shown that for small values of C/MF, $(C/MF) \leq 0$ dB, the receiver output signal-to-noise ratio is well predicted by the values obtained by theoretical formulas for the case of no direct line-of-sight signal, $(C/MF) = -\infty$, or the AMPS case. Similarly, for large values of C/MF, $(C/MF) \geq 20$ dB, the output signal-to-noise ratio is well predicted by the values obtained by theoretical formulas for the case of no multipath fading signal being present or $(C/MF) = \infty$.

SECTION 2

INTRODUCTION*

2.1 BACKGROUND

During the next decade, mobile radios will take a quantum leap in technology and service with the introduction of cellular mobile radiotelephone systems. Their sophisticated control system and efficient use of the spectrum will provide a grade of service superior to that presently available. Furthermore, the system is expandable with growing markets and, indeed, should be less costly to the user as the system grows. Many believe that the elastic nature of the market will create a spiral effect of decreasing prices and increasing market demand. While recent mobile radio market forecasts differ in their assessments, even the most pessimistic foresees a remarkably strong growth curve in the next 20 years and beyond. This huge potential for a good quality mobile telephone service has been recognized by American Telephone and Telegraph (AT&T), which is now testing a "cellular" Advanced Mobile Phone Service (AMPS) in Chicago that overcomes the capacity and service-quality limitations of present operational systems and has the potential to reduce subscriber costs. Motorola, together with American Radio Telephone Service, is testing a similar concept in the Washington-Baltimore area.

As sophisticated as the cellular mobile radiotelephone concept is, the fact remains that the majority of the geographical area of the country, and a significant portion of the population of the country represented by that area, will not be served by these advanced systems, at least for many years to come. This is due primarily to the fact that these systems are not particularly cost effective in less densely populated areas. However, market assessments conducted by the National Aeronautics and Space Administration (NASA) have consistently shown that in the less-populated areas of the country, a strong market exists for dispatch, radio-telephone, and emergency services.

A number of studies conducted under NASA sponsorship by Jet Propulsion Laboratory (JPL) conclude that the solution to a truly domestic and ubiquitous mobile radio service will be composed of cellular systems serving the metropolitan areas, integrated with and complemented by a satellite system serving the rural and remote areas. A broad spectra of Land Mobile Satellite Service (LMSS) systems have been studied (Ref. 1) from simple single-beam satellites with very limited capacity, but with readily available technology, to the large-antenna, high-capacity satellite requiring future technology. Within a few years, one of the more simple systems could be launched to serve a limited user community. More complicated, higher-capacity systems would follow and lead to a relatively large satellite in the 1990s.

---

*This section is a summary of the baseline design of the LMSS ground segment provided in Chapter 4 of Ref. 1.

2.2 MOBILE RADIO EQUIPMENT FOR LMSS

Communication satellites, in one sense, can be grouped into two categories. The first category, which includes most of the present-day satellites, communicate with fairly powerful ground stations having large antennas and complex receivers. This permits the satellite antenna to be relatively unsophisticated. The geographically dispersed users of this class of satellite are connected, via terrestrial means, to ground stations where the channels are trunked and relayed to the satellite. A classical example of this class of satellite is the INTELSAT series.

The second category of communication satellites, which will flourish in the next two decades, and of which Mobile Satellite (MSAT) is an example, provide service directly to the user's premises. Here, hundreds of thousands of users directly access the satellite through inexpensive transceivers and small antennas mounted on their rooftops or car tops. The economics of providing direct-to-the-user service dictate the user's equipment, which is produced in quantities of hundreds of thousands, to be inexpensive.

Because MSAT provides direct-to-the-user service, it must communicate with small mobile antennas and a fairly simple transceiver. This establishes the first constraint in designing the mobile equipment for MSAT. The second constraint is imposed by the likelihood of integrating the satellite and the terrestrial mobile systems. In the future, the integration of the LMSS with the terrestrial cellular system will allow for a truly ubiquitous mobile radio service. Anticipating such an integration, the technical parameters for LMSS mobile terminals should be selected to allow a subscriber to use the same set of equipment for both the terrestrial and the satellite systems. For this reason, it is strongly desired that the LMSS mobile equipment be compatible with the planned cellular mobile telephone system as typified by Bell System's AMPS. Since the modulation scheme has a strong impact on the makeup of the mobile transceiver, Section 2.2.1 discusses the rationale for selecting the modulation scheme for MSAT.

2.2.1 Selection of Voice Link Modulation

Any system that involves the transmission of voice signals must contend with a wide range of differing inputs (i.e., the highly variable nature of the speaking population). The voice dynamic range of a given speaker when engaged in telephonic communication is typically 20 dB, while the dynamic range over the total population of speakers, from the softest to the loudest is some 30 dB. Thus, the voice link must be able to efficiently accommodate an overall input dynamic range of 50 dB.

A second very important consideration is the quality of the speech reproduced at the output of the transmission system. Significant measures in this regard are articulation or intelligibility, signal-to-noise ratio (SNR), crosstalk, and speaker identification. Generally, the voice quality from the LMSS should be roughly on a par with that considered acceptable for the present-day toll service.

From the communication engineer's perspective, nothing could be less desirable than the aforementioned characteristics. Beset by pragmatic matters, such as available transmitter power constraints, channel bandwidth limitations, and system design dictums such as "maximize the number of channels," "be compatible with interfacing and tandem systems," and "let's use the most advanced techniques available," the task of specifying a modulation system for the LMSS becomes arduous.

However, the most binding constraint on the selection of a modulation scheme for the LMSS is the assurance that the mobile transceiver used in the Land Mobile Satellite System does not significantly differ from the equipment used in a terrestrial cellular mobile system such as the AMPS. This compatibility requirement is desirable so that the equipment already under development for the cellular system can be used, with some modifications, for the LMSS, thus reducing the cost for a user who subscribes to both services.

It is within this framework that the selection of a baseline modulation technique for the LMSS is summarized. Trade-offs and alternatives are outlined, and possible future options are discussed.

2.2.1.1 Digital Modulation. The heart of the modulation trade-offs involves the issue of whether digital or analog methods should be used. For a digital system, the voice signal, which is inherently analog at its source, must be digitized in some fashion. Because of a total UHF RF band limitation of 10 MHz, it is decided that the bandwidth of each individual voice channel, irrespective of modulation form, should not, at the very most, exceed 30 kHz. Thus, the maximum bit rate which can be accommodated using Quadrature Phase-Shift Keying (QPSK) of the carrier is on the order of 32 kbps. A speech-encoding technique capable of this bit rate is adaptive delta modulation (ADM). However, system output speech quality is considerably below toll-grade transmission*, and the resulting overall capacity of the LMSS is considered marginal due to the required 30-kHz channel bandwidth.

In addition to ADM, other digital speech-encoding algorithms, such as adaptive predictive coding (APC) and linear predictive coefficient (LPC) vocoding, are potential candidates. These methods have the potential for reducing the bit rate to as little as 2.4 kbps (thus permitting channel bandwidths as small as perhaps 4 kHz); however, their relatively large encoder hardware complexity, plus their synthetic quality voice reproduction, presently make them undesirable.

Apart from the speech-encoding problem, a digital modulation system also involves the need for synchronization, which fosters a moderately complex mobile receiver design. Taking the speech-encoding and digital-synchronization issues together, it was decided that digital modulation

---

*Throughout the trade-off activity leading to the baseline LMSS design and performance specifications, the issue as to whether the LMSS should provide toll-grade quality was addressed. After much study, it was concluded that a system capable of somewhat less than toll-grade service will be necessary if an acceptable system capacity is to be obtained considering all constraints imposed.

results in mobile equipment which does not comply with the self-imposed system requirement of remaining compatible with the cellular mobile system. However, because of the rapidly falling cost of LSI circuitry, digital modulation will continue to be an attractive option for systems proposed for the 1990s. Its use for the LMSS baseline design, however, was precluded mainly because of the compatibility issue.

2.2.1.2 Analog Modulation. Turning now to analog modulation forms, only two generic types of modulation have been seriously considered for the LMSS; narrowband frequency modulation (NBFM) and single-sideband (SSB) modulation. SSB modulation has the distinct property that the required RF bandwidth need not be much larger than the highest effective frequency of the speech signal. Typically, 4- to 5-kHz channels will suffice. On the other hand, conventional NBFM requires 25- to 30-kHz channels.

SSB modulation, as applied to the LMSS, would operate with a suppressed carrier in order to achieve high transmitter power utilization efficiency and preclude carrier intermodulation terms. As a result, very accurate and highly stable carrier frequencies are needed so that the frequency difference between the received signal and receiver's estimate of the proper carrier frequency is less than 35 Hz. This is essential if good reproduced speech intelligibility and naturalness are to be obtained. For the UHF 800-MHz band, this requirement can be met only through the use of an AFC pilot and an oven-stabilized crystal oscillator within the mobile transceiver. Contrastingly, the use of NBFM can operate with frequency errors as large as several kHz, thereby significantly reducing the frequency tolerance requirements of an NBFM system relative to the use of SSB modulation. NBFM mobile transceivers need only relatively simple temperature-compensated crystal oscillators.

From a link-design point of view, the performance of NBFM and SSB can effectively be made equivalent when a form of speech signal companding known as envelope normalization is employed. This will be discussed subsequently.

Bell System's Advanced Mobile Phone Service (AMPS), an experimental urban cellular mobile telephone system, operating in the 800-MHz band, makes use of NBFM. It is fair to state that a strong compelling reason for NBFM being selected as the modulation technique for the baseline LMSS is the desire to be "compatible" with AMPS. The basic reasoning is that because both AMPS and LMSS operate in the same RF band, AMPS serving urban environments and LMSS covering suburban/rural/remote areas, a subscriber could obtain complete CONUS coverage with a universal set of mobile equipment. Thus, the LMSS baseline system will use NBFM, but not identically to the AMPS, as will now be outlined.

In the introductory paragraph, it was stated that the dynamic range of the speaking population is on the order of 50 dB. Reduction of this range by means of electrical signal processing is necessary if an efficient communication system is to result. The method used is known by the term compandor (contraction of the words compressor and expander). The principle involves compression (or reduction) of the speech signal dynamic range at the transmitter prior to modulation, and a corresponding expansion of the received signal prior to listening reproduction. Ideally, the companding operation is transparent, so that a listener will not perceive that modification of the speaker's signal has occurred.

Apart from reducing the speech dynamic range, companding produces other tangible benefits. First, the weak speech segments or syllables are critical to good articulation. Compression acts to amplify these segments, with the result that the weak syllable SNR, and therefore intelligibility, is increased relative to a system that does not make use of companding. Secondly, the expansion process acts as a noise and crosstalk suppressor between utterances and during speech pauses. Consequently, there is a large subjective SNR improvement apparent to the listener, and less distraction and annoyance from cochannel signals (arising from frequency reuse).

The AMPS system uses a form of compression which halves (in dB) the speech dynamic range (2:1 compression). Using this compression technique, channels with a bandwidth of 30 kHz are required. However, it seems unlikely that by the mid-1990s any band-limited system would be so wasteful as to use 30-kHz voice channels. Therefore, an LMSS operating in the 90s should be designed, not to be compatible with today's cellular system, but rather with the cellular system expected to be operating in that time period. Accordingly, the LMSS conceptual design assumes a 15-kHz channel bandwidth.

To limit the channel bandwidth to 15 kHz, a different compression algorithm must be used. The proposed compression algorithm for the LMSS reduces the speech dynamic range to 0 dB. Known as envelope normalization (EN), the operation involves dividing the speech waveform by its own exact envelope, then frequency modulating the transmitted signal in the most optimum manner possible. The result from a total system perspective is a uniform received voice SNR for all speakers, and a reduction of the required 30-kHz channel spacing for AMPS to a 15-kHz channel spacing for LMSS. With the EN approach, it is necessary to transmit the speech envelope modulated onto a pilot or subcarrier placed above the speech band in order to effect the expansion process within the receiver.

Table 1 presents speech and modulation performance parameters for the baseline LMSS NBFM system. Also shown for comparison are the parameters that would have resulted for the LMSS system if either the AMPS companding and modulation characteristics or SSB had been used.

As can be seen, the LMSS EN systems, based on EN NBFM or 2:1 compression NBFM, differ only in the companding algorithm and the resulting peak deviation, channel bandwidth, and transmitter power. The cellular mobile equipment therefore must be somewhat modified for use in the LMSS. However, the modification is not as extensive as that required for a drastically different scheme, such as digital modulation.

2.2.2 Voice-Operated Switch (VOX)

A final consideration is given to the use of VOX (voice-operated transmission) to minimize the prime power and transmitter size for the spacecraft-to-mobile link. A well-known characteristic of conversational speech is that the interword, short-pause, and listening intervals amount to about 60 percent of the running speech pattern. Since it is considered wasteful to transmit a carrier wave during silence periods, the speech-bearing component of the signal (and its associated power) should correspondingly be suppressed. The average transmitter power is thereby reduced by a factor of 0.4 (-4 dB).

Table 1. Modulation and Performance Parameters for Three Modulation Techniques

Parameter	LMSS (Using EN NBFM)	Option 1 (Using SSB)	Option 2 (Using NBFM Similar to AMPS)
Companded Speech			
Compandor	EN	EN	2:1
Speaking population compressed dynamic range, dB	0	0	25
Modulation			
Transmitter peak deviation, kHz	2.1	---	12
Channel bandwidth, kHz	15	4	30
Preemphasis, dB/octave	6	6	6
Relative transmitter power	p	0.84 p	2.2 p
Received Speech			
Minimum link voice rms SNR, dB	22	22	23.3
Minimum link weak-syllable SNR, dB	22	22	18.3
Subjective voice SNR improvement, dB	10-15	10-15	6-12
Intelligibility, %	95 to 98	90	90

With a VOXed signal, provision must be made within the receiver to squelch the increased noise level presented to the listener due to the sudden loss of the input speech carrier. Conventional squelch methods are ineffective, and the necessary control can be effected only through the use of an envelope modulated pilot, mentioned earlier. With SSB modulation, the entire VOX process is naturally and easily implemented (especially with EN) since the transmitted power is directly proportional to the speech and pilot signal components. With NBFM, the realization of VOX is not so simple since normally the transmitter power is independent of the modulation. Thus, it is necessary to detect the speech silence intervals (an inherent feature of the EN process) and synonymously switch off the carrier. The pilot in this case will consequently have to be a separate low-power carrier, since the control signal must be present at all times.

SECTION 3

LMSS CHANNEL SIMULATOR DESIGN DESCRIPTION AND CONSIDERATIONS

A descriptive block diagram of the LMSS channel simulator used for the study of an AMPS compatible type of system (e.g., NBFM with 30 kHz of channel spacing and 2-kHz rms frequency deviation for average talkers) is shown in Figure 1. The simulator consists of three subsystems: (1) signal-path simulator, (2) audio evaluation area, and (3) computer controller. The signal-path simulator provides the end-to-end simulation of the process which the voice signal is subjected to under the actual LMSS operating conditions. The audio evaluation area provides a facility for subjective testing of the effects of various link design parameters and constraints. The computer controller basically performs the task of data acquisition and analysis, and, in the future, will also provide signal conditioning not implemented in hardware. It should be pointed out that, in the past, a requirement of the LMSS system design was that it be compatible with the Advanced Mobile Phone Service (AMPS). As such, in this study, the type of voice processing, modulation, and overall performance criteria of the AMPS has strongly influenced the LMSS channel simulator design. A brief description of each subsystem follows.

3.1 SIGNAL-PATH SIMULATOR

A more detailed block diagram of the LMSS signal-path simulator is shown in Figure 2. It can be seen that it is comprised of four main subsystems:

(1) Mobile FM transmitter - conditioner.

(2) Interference transmitter - conditioner.

(3) Space-path simulator.

(4) Mobile FM receiver - deconditioner.

The satellite-segment simulator shown with the dashed lines has not been included in this study and it is shown in Figure 2 for the sake of future studies. The two transmitter-conditioner combinations are exactly identical, and they can both operate at the same carrier frequency or at different frequencies. One transmitter is used to produce the desired mobile carrier, while the second transmitter generates the independent interfering carrier(s) from one or more interference sources. The generation of multiple interference is basically achieved through the use of the method discussed in Section F.4 of Appendix F, with the second transmitter providing only one interfering carrier. This point will be explained in more detail in the space-path simulator subsection. However, it should be pointed out that due to the flexibility available in setting the operating carrier frequencies of each transmitter (with some limitations as discussed later), both cases of multiple (or single) cochannel and adjacent channel interference can be simulated.

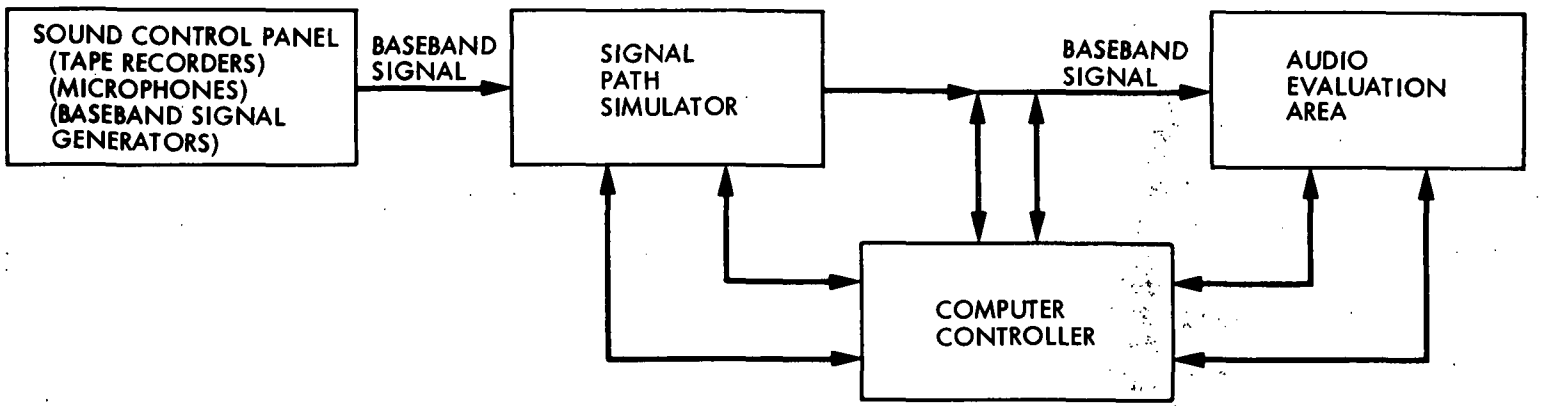

Figure 1. A Simplified Block Diagram of the LMSS Channel Simulator

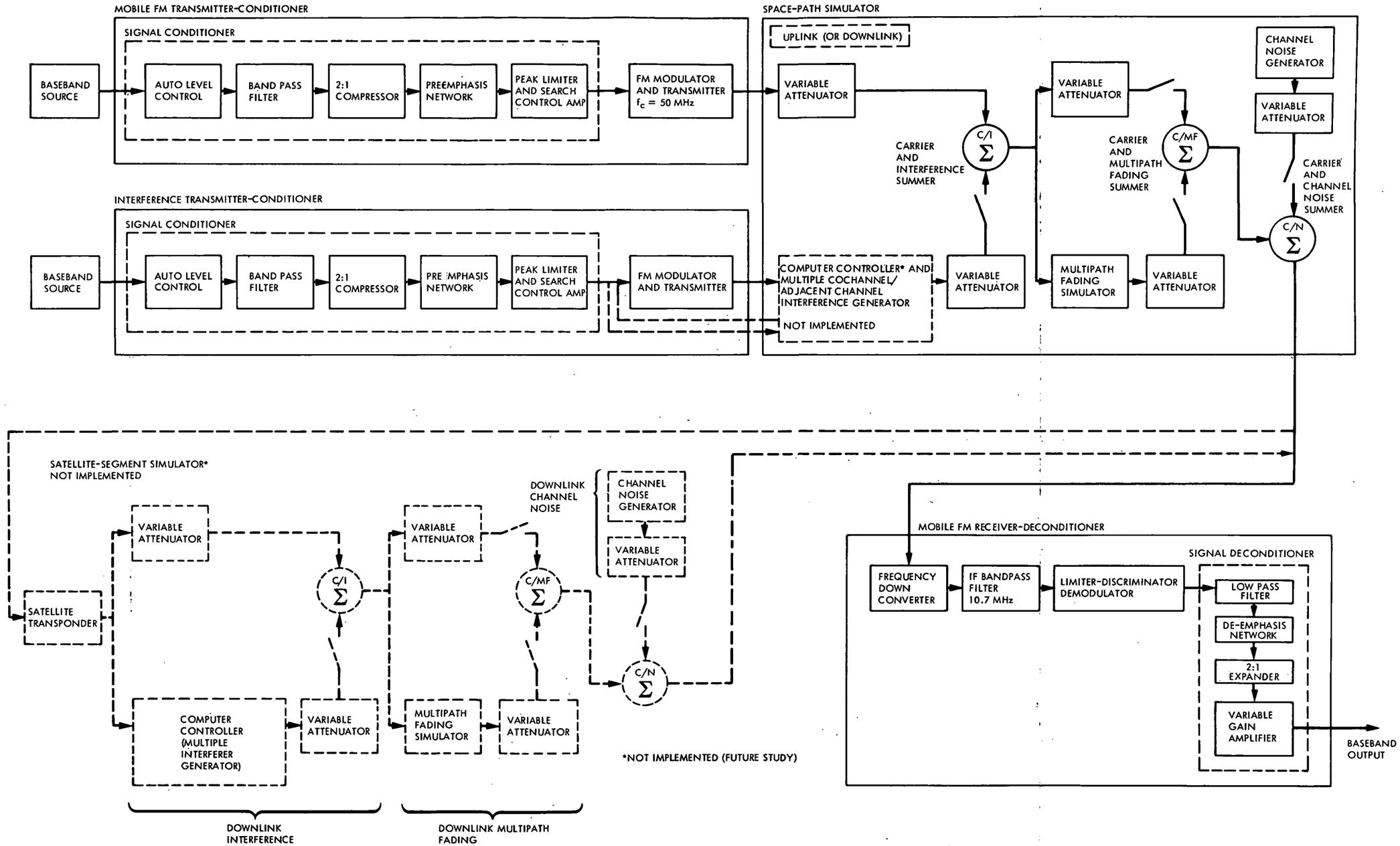

Figure 2. Block Diagram of the Signal-Path Simulator of the LMSS Channel Simulator

3.2 FM TRANSMITTER-CONDITIONER

A block diagram of the FM transmitter-conditioner circuitry is provided in Figure 3. It can be seen that each transmitter-conditioner consists of the following internal functions:

(1) An automatic level control (ALC) amplifier, which acts as a feedback amplifier, maintains a predetermined constant rms level at the input of the band-pass filter. ALC responds only to the rms signal level variations rather than signal amplitude variations and, in this case, it can accommodate up to 30 dB (dynamic range) of input signal rms level variations.

(2) A band-pass filter (BPF) made up of a combination of a 5th-order Butterworth low-pass filter (LPF) and a 3rd-order Butterworth high-pass filter (HPF), which removes the undesired out-of-band frequency components contained in the baseband audio signal. Being active filter designs, the LPF has a -3 dB frequency bandwidth of 3 kHz and a roll-off rate of 30 dB per octave, while the HPF has a -3 dB frequency bandwidth of 300 Hz and a roll-off rate of 18 dB per octave.

(3) A 2:1 compandor compressor makes up the next audio processing block. A compressor is defined as a device which operates on the voice waveform to attenuate strong syllables and amplify weak syllables with respect to some chosen reference level. The 2:1 compandor (i.e., the word compandor is coined from a contraction of compressor and expander) has been found to provide important improvements in AMPS voice transmission quality (Ref. 2). The syllabic compandor is made up of a matched compressor-expander pair with carefully controlled time constants. Both are variable gain devices, with the signal-dependent "gain" of the compressor matched by a complementary signal-dependent "loss" of the expander so that speech may be transmitted without perceptible distortion and level changes. Appendix E describes the rationale for companding for the LMSS voice links and explains the various qualitative and quantitative noise control advantages provided by the 2:1 compandor. However, besides the noise control advantages, the 2:1 compressor produces an output audio signal dynamic range (in dB) which is about half of the input signal dynamic range (in dB). This provides an effective means of reducing the amount of clipping distortion and also provides a more desirable range of rms frequency deviation. The compressor's response time, or time constant, is 22 ms, which is slow enough to operate primarily on the slower syllabic variations; also, it does not significantly affect the speech-crest factor and spectral content. The compandor in this application is designed for attack and recovery times of 3 and 13.5 ms, respectively, which are the CCITT recommended nominal values that are compatible with the AMPS design. This 2:1 compandor compressor can accommodate up to 70 dB (dynamic range) of input-signal rms-level variations, which are not faster than the 22-ms R-C time constant of its LPF.

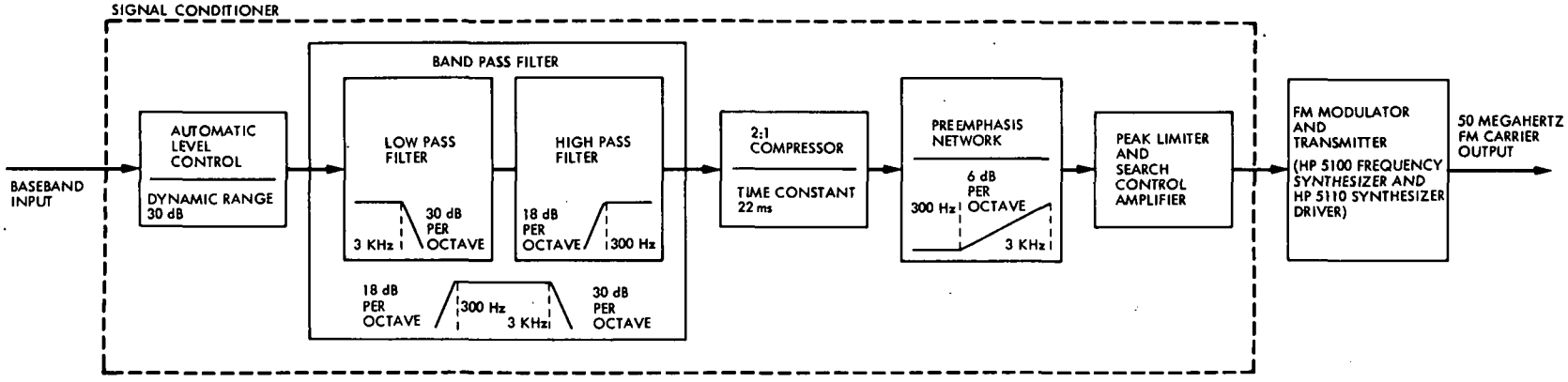

Figure 3. Block Diagram of the FM Transmitter - Conditioner

(4) A preemphasis network provides a 6-dB-per-octave accentuation of the audio frequency band beginning at a frequency of 300 Hz. The use of emphasis filtering to improve performance in the presence of channel impairments is consistent with standard design approaches. However, it has been shown (Ref. 2) that besides the noise suppression effect as in most FM systems, where the noise characteristics are different from those of the mobile FM communications, the emphasis filtering (i.e., the de-emphasis network portion) here primarily shapes the spectrum of the major noise component (i.e., the "clicks" noise) and, therefore, improves the subjective quality of the audio signal at the receiver output.

(5) A peak limiter and a search control amplifier make up the last block in the signal conditioner of the FM transmitter-conditioner. The peak limiter is basically a clipper which clips the peaks of input signals larger than a predetermined level and effectively establishes the peak-to-rms-voltage level of the signal at the modulator input. This type of peak limiting prevents overdeviation of the FM transmitter and controls the amount of spectrum spill into adjacent channels.

The search control amplifier is a biased interface amplifier which sets the dc-voltage level of the baseband signal at a predetermined required level suitable for direct FM modulation. This amplifier also controls the signal dc-voltage drift from the bias level and, hence, it provides one level of stabilization of the carrier frequency.

(6) The FM modulator and transmitter block consists of an HP frequency synthesizer (model 5100 A), driven by an HP synthesizer driver (model 5110 A), which provides a very stable direct FM modulation at carrier frequencies of up to about 50 MHz. A voltage-vs-frequency characteristics curve of the direct FM VCO of an HP frequency synthesizer is given in Figure 4. In this figure it is shown that if the carrier frequency f_c is set at, for example, 49.95 MHz and the modulator input signal is limited to zero-to-peak values of 1 volt, then a peak frequency deviation of 9.4 kHz is achieved. It should be noted that since the maximum output frequency of the HP model 5100 A frequency synthesizer is 50 MHz, for direct FM modulation the carrier frequency should be set slightly lower than the nominal 50-MHz value by at least as much as the value of peak frequency deviation in order to allow frequency swings on both sides of the value chosen for f_c. This was practiced in all of the quantitative and qualitative testing performed using the FM transmitter-conditioner; however, for the sake of convenience, throughout this report we refer to a 50-MHz carrier frequency rather than a 49.95-MHz carrier frequency. The reason for choosing a carrier frequency close to 50 MHz

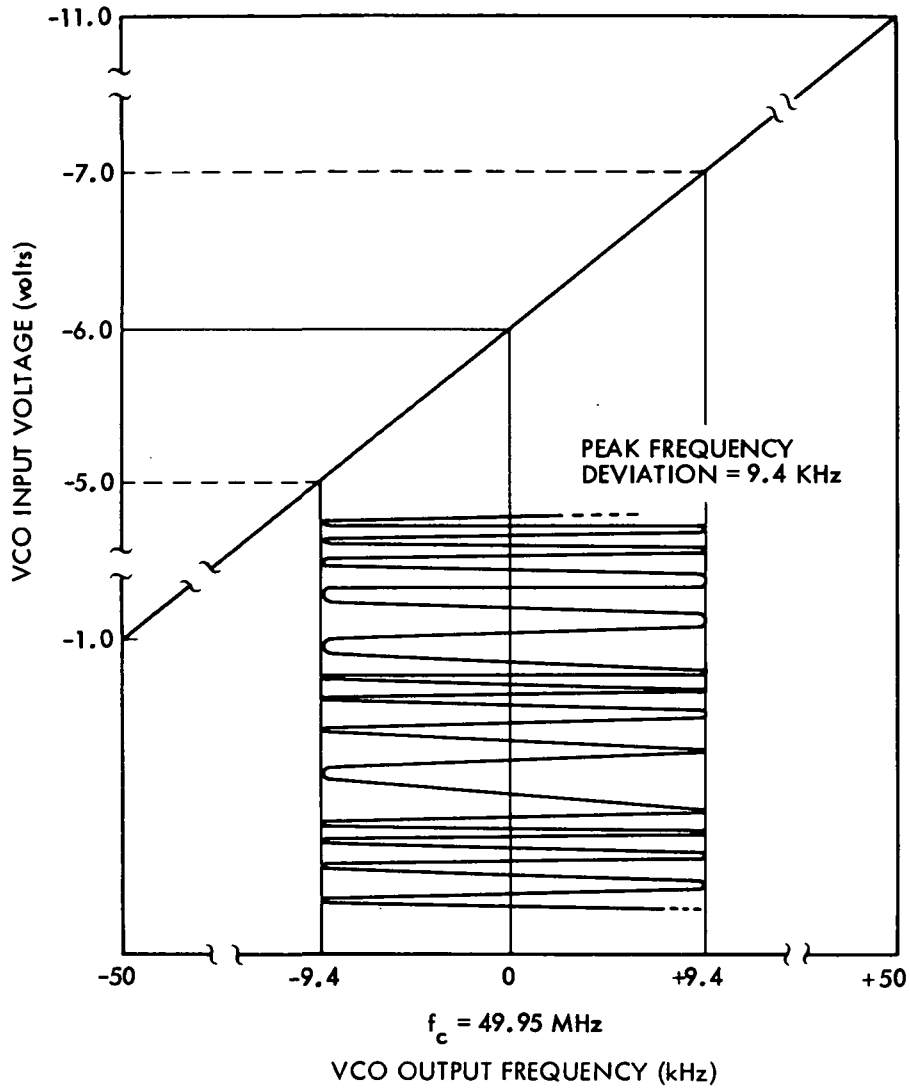

Figure 4. Voltage vs. Frequency Characteristics of Direct FM VCO

is for the sake of compatibility with the equipment which was already available before the design of the signal-path simulator.

3.3 SPACE-PATH SIMULATOR

Radio signals transmitted from a mobile to the satellite, or from the satellite to a mobile, are subject not only to the same significant propagation-path losses that are encountered in other types of terrestrial mobile communications, but are also subject to many other types of impairments. The transmitted signal in both uplink and downlink is affected by various types of scattering and multipath phenomenon, which can cause severe signal fading attributable to the mobile-radio communications medium. Furthermore, the faded signal will be received in the presence of various types of impairments including the channel background noise, random FM, system-generated cochannel and adjacent channel interference, intermodulation interference, and man-made environmental noise. The purpose of the space-path simulator is to simulate the actual LMSS environmental conditioning that the transmitted signal experiences and, moreover, to create and add the various mentioned types of impairments to the transmitted signal as much as possible.

It should be noted that even though the satellite-segment simulator has not been used in this study, it can be reasonably assumed that the aggregate effects of the uplink and downlink channel background noise, multipath fading, and cochannel/adjacent channel interference can be mostly simulated through the space-path simulator by selecting appropriate values for different parameters of impairments. However, the effects of the satellite transponder on the uplink Rayleigh-faded, or Rician-faded, multipath signal and cochannel/adjacent channel interference, and the fact that the downlink signal is again subject to multipath phenomenon with more of different cochannel/adjacent channel interference added to it, will not be observed as additional impairments at the mobile receiver output of the channel simulator. Also, the other important type of impairment not present at the mobile receiver input is the intermodulation interference generated at the satellite because of TWTA nonlinearities. Therefore, in general, the satellite-segment simulator should be an integral part of the signal-path simulator in order to observe the full effects of all types of impairments mentioned on the subjective quality of the receiver output signal. A brief description of the simulation process by which each one of the impairments is introduced follows.

(1) Cochannel and Adjacent Channel Interference. A primary object of high-capacity land mobile satellite communications is to conserve the frequency spectrum by reusing frequency channels in geographic areas located as close to each other as possible. The factor which limits the reuse of frequency channels is cochannel interference. In the case of adjacent channel interference, only the tails of the adjacent channel signals enter the FM demodulator through the IF filter. Both cochannel and adjacent channel interference will be present as an impairment to the signal quality in a high-capacity system. Furthermore, in a satellite system such as LMSS, because of various mobile transmitters sharing the same

channel, cochannel interference exists on the uplink at the satellite receiver as well as the downlink at the mobile receiver; this is the result of interbeam cochannel interference originating from the satellite multiple-beam antenna. The normal and worst-case levels of cochannel interference depend upon a number of system design parameters (Ref. 3) such as the number of beams (or number of mobile transmitters in the uplink case), frequency reuse pattern, and transmitting antenna (mobile or satellite) beam patterns. These parameters are determined by the system designers according to the established criteria of the system cost and performance objectives.

In reference to Figure 1, the interference transmitter-conditioner provides the space-path simulator with a single interfering carrier at either the desired carrier frequency (i.e., 50 MHz) or at a different frequency, depending on the case of the cochannel/adjacent channel interference being simulated. The multiple interference generator uses this single interfering carrier for generation of a composite multiple cochannel/adjacent channel interfering carrier by using the technique described in Appendix F. Here the ratio of desired carrier to interfering carrier power, C/I, was set by variable step attenuators.

(2) Multipath Fading Simulator. One may identify the propagation channels involved in land mobile satellite communications as: (1) direct line-of-sight (LOS)/ground reflections and scattering; (2) ionospheric scintillation; (3) tropospheric refraction; (4) LOS tropospheric scattering; and (5) ionospheric refraction (HF). Other propagation channels may be defined, but these five are the primary channels for the system design studies. The channel of major importance in land mobile satellite communications is the direct LOS/ground reflections and scattering. This channel consists of a "distortion-free" direct LOS path between transmitter and receiver, plus a collection of many ground-reflected radio paths between transmitter and receiver which exist solely because of intervention of the earth's surface as a reflector. The propagation effects on the direct LOS path normally do not need to be simulated, since they effect the strength of the signal on the long-term basis only and can be accommodated by increasing the carrier power or tolerating the loss of carrier for a certain percentage of the time. Hence, the only propagation channel simulated by the spacepath simulator is one that assumes that the received signal at the mobile, or at the satellite, is the net result of many EM waves that arrive via multiple paths (multipath ground reflections) formed by diffraction and scattering plus a nondistorted direct LOS signal which could be totally eliminated at option (i.e., due to total shadowing). Furthermore, the direct LOS signal and the multipath fading signal could be modeled either as the desired or wanted

signal, or as the desired signal plus the cochannel/ adjacent channel interfering signal depending upon the carrier-to-interference ratio set before propagation channel simulation. It should be noted that in the downlink where the desired signal and the interfering signals are all subject to the same local terrain, the effect of multipath fading is the same for both signals. However, this is not the case in the uplink where the desired signal and the interfering signals all originate from different locations, different local terrains, and thus are subject to different levels of multipath fading. In general, it is possible for the desired signal to experience a more severe fade than its cochannel interferers in the uplink and thus result in the receiver loss of desired signal capture in the downlink; this introduces impairments into the baseband response.

Based on analyses of the statistical nature of a mobile fading signal and its effects on envelope and phase, a fading simulator can be configured either from hardware or a combination of hardware and software. The multipath fading simulator, shown in the space-path simulator section of Figure 2, provides an RF signal with a Rayleigh distributed envelope and a uniformly distributed phase component. Figure 5 shows the building blocks of this Rayleigh multipath fading simulator which consists of two Gaussian noise sources, two variable shaping filters, and two balanced mixers, which add their modulated inputs in quadrature (Ref. 4). The simulation of the fading spectrum appropriate to mobile radio is obtained by properly shaping the spectrum of the noise sources. The theoretical fading spectrum (Ref. 4) is simulated by passing the output of each noise source through a shaping filter whose response is shown in Figure 6. The shaping filter has a theoretical frequency response that peaks at a Doppler frequency, $f_D = V/\lambda$, corresponding to a vehicle speed V and a carrier wavelength λ, and then drops off sharply at the rate of 18 dB per octave. A set of shaping filters was designed to be switched in, thereby simulating different vehicle speeds of 15 mph, 55 mph, and 80 mph. Moreover, it is also capable of simulating different types of mobile environments (e.g., road surfaces and local terrain) by varying the statistics of the diffusely scattered multipath signal. However, since the direct LOS signal is present for a majority of the time and the local terrain is drastically different at different locations within CONUS, it was deemed unnecessary to simulate selective fading along with multipath fading. Furthermore, different values of the carrier-to-multipath fading ratio, C/MF, where the carrier is the direct LOS signal present at the receiving antenna, can be obtained by way of variable step attenuators. A detailed block diagram of the multipath fading simulator is provided in Appendix G.

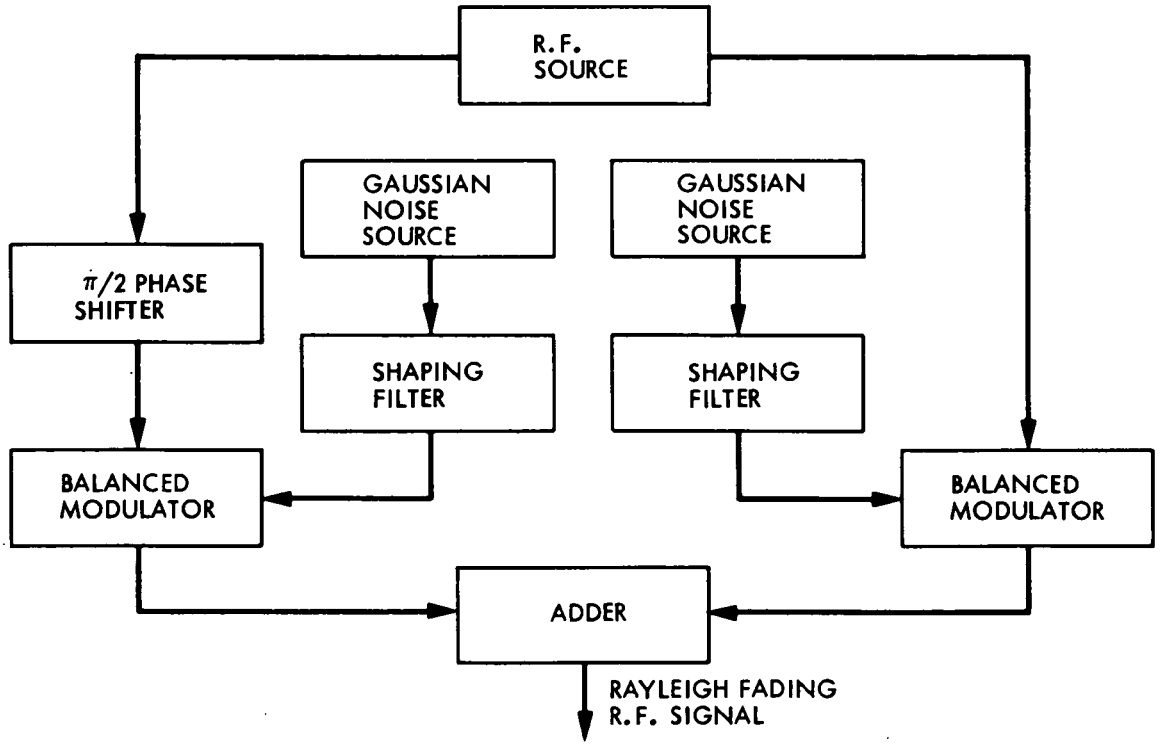

Figure 5. Multipath Fading Simulator Block Diagram

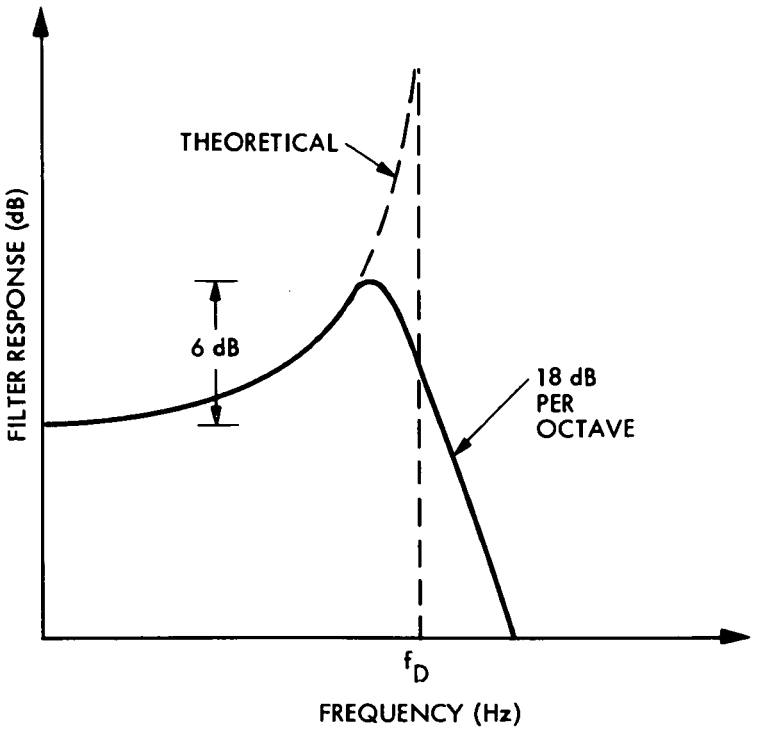

Figure 6. Shaping Filter Frequency Response

(3) Channel Background Noise. The channel noise generator is a Rohde & Swartz model SKTU. The excess noise from this unit can be manually controlled, whereby the maximum limit is 15 dB above KTB. The absolute noise power level from the noise source is not adequate; therefore its output is used as an input to a high-gain, broadband, noise amplifier whose center frequency is about 50 MHz. This is the primary reason for choosing a carrier frequency close to 50 MHz. The noise amplifier is comprised of two sections: the preamplifier, whose gain is variable as a function of a control current, and a power amplifier. The power amplifier is followed by a noise filter whose bandwidth is considerably narrower than the amplifier's bandwidth. As a result, the simulator system noise bandwidth is somewhat established by the bandwidth of the noise filter which is 14.148 MHz. This bandwidth is reasonably large enough, compared to the noise bandwidth of the IF filter, which does not limit the system performance or testing capabilities in any way. Different values of carrier-to-channel noise ratio, C/N, are obtained by using a variable step attenuator.

3.4 FM RECEIVER-DECONDITIONER

A functional block diagram of the FM receiver-deconditioner is provided in Figure 7. The deconditioner not only removes the predistortions of the baseband (audio) signal induced by the conditioner of the transmitter, but also suppresses receiver noise and interference relative to the speech signal (which was one of the reasons for predistortions), and thereby improves the subjective quality of the receiver output signal. The mobile FM receiver-deconditioner consists of the following internal functions:

(1) A down converter performs the task of translating the 50-MHz carrier to the intermediate frequency (IF) of 10.7 MHz of the receiver. The IF frequency of 10.7 MHz used in commercial FM broadcast receivers was selected as the receiver IF frequency for the sake of compatibility and convenience. It can be seen that the frequency down conversion is accomplished by frequency mixing which is generated by the multiplication of the 50-MHz carrier by a 60.7-MHz carrier producing the sum and difference frequencies of 110.7 MHz and 10.7 MHz, respectively. Furthermore, three stages of tuned amplification provide the IF amplification and selectivity in the receiver before the IF filter.

(2) An 8th-order integrated crystal BPF with an IF center frequency of 10.7 MHz filters the difference beat frequency produced as a result of the down conversion mixing. This filter constitutes the IF filter for all of the narrowband FM testing performed using the channel simulator and it has an essentially flat band-pass frequency characteristic, with a

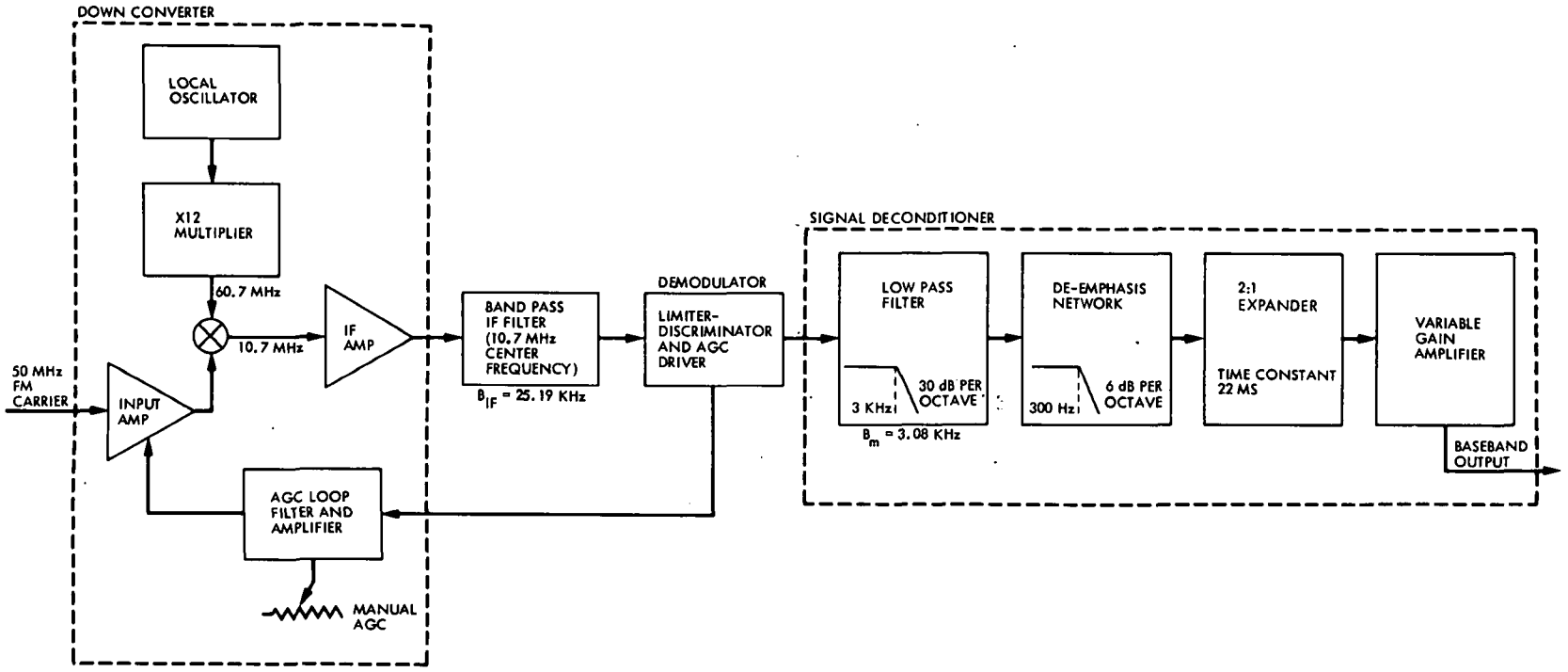

Figure 7. Block Diagram of the FM Receiver - Deconditioner

noise bandwidth, B_{IF}, which has been carefully measured to be 25.192 kHz. However, a ceramic BPF with an IF center frequency of 10.7 MHz and a noise bandwidth of 224.925 kHz is also implemented in the FM receiver, which can be switched for wideband FM applications. The frequency response of this filter is essentially flat over its 3-dB bandwidth which is 200 kHz.

(3) The limiter and narrowband FM discriminator is a commercial integrated circuit (National Semiconductor Corporation, IC #LM3089) which has three stages of limiting, with IF amplification, followed by a quadrature demodulator. Along with the IF limiting amplifier and detector, the following functions are provided by the IC: (1) a mute logic circuit that can mute or squelch the audio output circuit when tuning between stations; however; this feature was not used in any of the channel simulator tests performed; (2) an IF level or signal-strength meter circuit which provides a dc logarithmic output as a function of IF input levels from 10 μV to 100 mV (four decades); (3) a separate AFC output which can also be used to drive a center-tune meter for precise visual tuning at each carrier frequency; (4) a delayed AGC output to control front-end gain.

Furthermore, the IF amplifier consists of three direct-coupled amplifier-limiter stages and the FM demodulation is performed accurately with a fully balanced multiplier circuit. The FM discriminator of this IC has a linear frequency range of 24 kHz at the IF frequency of 10.7-MHz. On a typical detector S curve, this means a 12-kHz linear range on each side of the 10.7 MHz IF frequency as shown in Figure 8. Moreover, four IF peak or level detectors provide the delayed AGC, IF level, and mute-control functions. A more detailed circuit description of this IC can be found in Appendix G.

Also, for wideband FM applications, an exactly similar commercial IC is implemented in the FM receiver which can be switched for cases with a much larger peak frequency deviation of the corresponding modulated carrier. The linear frequency range of this wideband FM discriminator is 240 kHz (i.e., 120-kHz linear range on each side of the 10.7-MHz IF frequency) as can be seen from Figure 9.

(4) The postdetection filter is a 5th-order Butterworth multiple feedback (active) LPF with a -3-dB frequency bandwidth of 3 kHz and a roll-off rate of 30 dB per octave. The noise bandwidth, B_m, of this LPF is carefully measured to be 3.08 kHz.

(5) The de-emphasis network restores the baseband signal spectral preemphasizing, which occurred at the conditioner portion of the transmitter, to that which existed prior to the

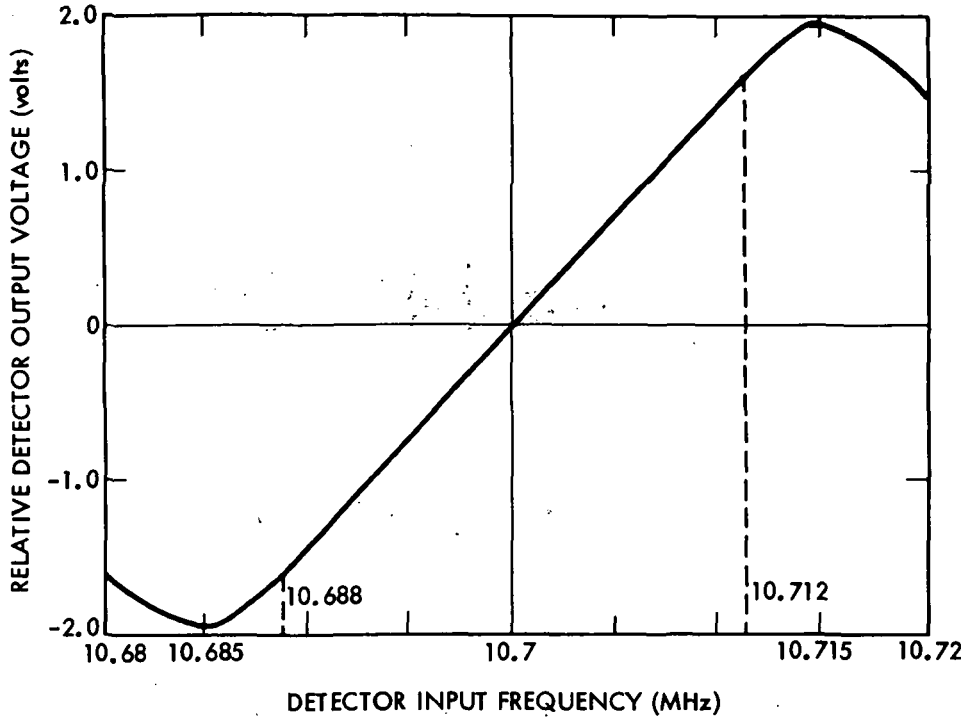

Figure 8. Narrowband FM Detector S Curve

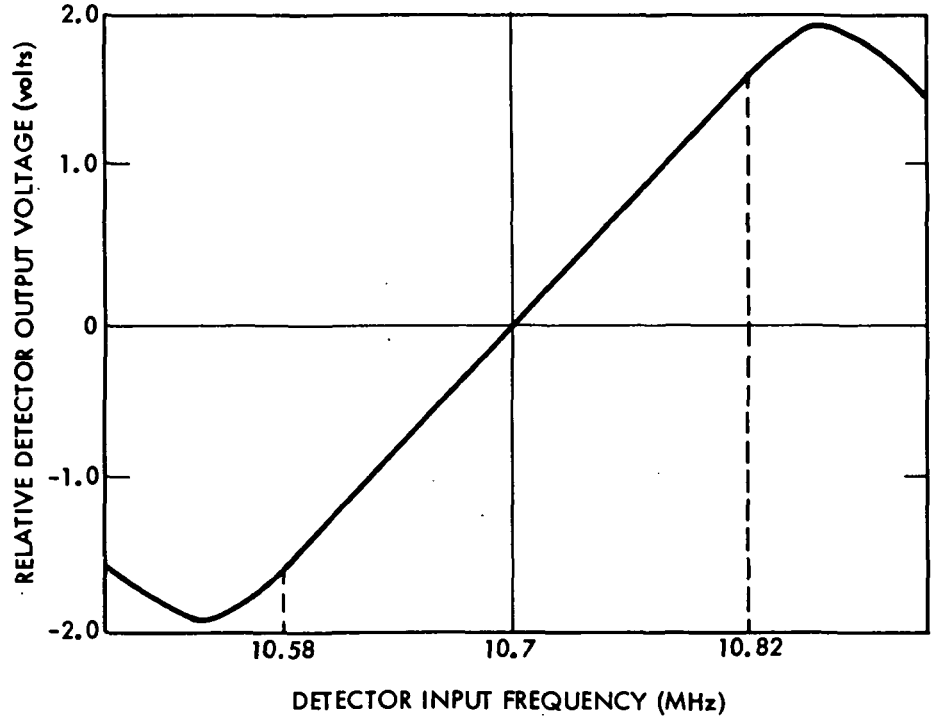

Figure 9. Wideband FM Detector S Curve

preemphasis operation. Naturally, the de-emphasis network provides a 6-dB-per-octave attenuation of the audio frequency band beginning at a frequency of 300 Hz, which is the exact inverse of the preemphasis filter frequency response. In such a process, the high-frequency components of the noise at the LPF output are also attenuated, thereby effectively increasing the output signal-to-noise ratio of the system. Furthermore, as mentioned before, the de-emphasis network primarily shapes the spectrum of the "clicks" noise in the case of mobile FM communications and, therefore, improves the subjective quality of the audio signal at the receiver output. This effect is especially noticeable in situations of severe direct LOS shadowing which results in low values of the carrier-to-multipath fading ratio. Some quantitative discussions of the noise reduction effects of emphasis filtering are provided in later chapters and Appendices.

(6) The receiver 2:1 expander removes the transmitter-conditioner predistortion created by the compandor compressor by reestablishing the audio-signal dynamic range present before compression. This is accomplished by exactly reversing the time domain operation performed by the compressor (see Appendix E for more details). Moreover, when the baseband input level is small, as during the audio speech signal pauses, the expander is instrumental in producing the "quieting" of noise and interference by virtue of its gain reduction properties. Also, it has been shown (Ref. 2) that for low-level impairments whose average level varies slowly with respect to the expander response time (e.g., such a random FM, Gaussian noise, and the cochannel carrier offset "wobbling tone"), the expander output signal-to-impairment ratio (in dB) is improved by a factor that approaches the companding law, which is 2:1 in this case. This is the typical quieting mechanism for wire-line systems. Furthermore, the finite response time of the expander has a large effect on suppression of the audio impairments of mobile radio. This is due to the fact that the expander is normally in a high-loss state in the absence of an applied audio signal (Ref. 2). Thermal noise clicks present in the receiver-audio-LPF response may be larger in amplitude than levels corresponding to nominal talkers. However, individual clicks at the input to the audio receiver last only about 0.3 ms and lack sufficient energy in the loss-control bandwidth to cause the expander to change from its high-loss state fast enough to respond to them. Since expander-loss control is achieved through integration of the received baseband signal by means of a LPF with a time constant of 22 ms (same as compressor), the expander will not be fully driven from its high-loss state by a burst of clicks or cochannel interference lasting less than 22 ms. This inertia in the expander response results from the CCITT attack-time standard, which is made large enough to prevent excessive voice distortion at low frequencies due to compandor action.

For mobile telephone operation, this specification serves a dual purpose by inhibiting the expander response to bursts of clicks and interference. This, in conjunction with receiver quieting during the absence of speech, enables the 2:1 compandor/de-emphasis combination to provide a very effective subjective improvement in transmission quality in the presence of mobile radio impairments.

(7) Finally, the variable-gain audio power amplifier, which is a variable operational amplifier, provides the necessary drive level to operate speakers and other output transducers.

In Appendix G, detailed circuit diagrams along with complete functional characteristics are provided for each one of the functional elements in the signal-path simulator. For the sake of convenience, the description of the audio evaluation area and facilities is presented in Section 4.

SECTION 4

AUDIO EVALUATION

4.1 APPROACH

The audio evaluation program was designed with two goals in mind: first, to determine the simulator operating conditions that would result in satisfactory overall performance, and second, to determine the limits of simulator operating parameters that would permit intelligible communication. In the first instance, subjective responses were used to determine how people judged the system performance when compared with a standard telephone circuit, while in the latter, standard intelligibility tests were administered and scored to determine those conditions which, while far from ideal, would nevertheless permit intelligible communication in the presence of noise, interference, and fading.

The results of these evaluations, when combined with cumulative probability distributions for the various degradations expected in an actual operating system, will provide the data necessary to produce a design in accordance with specified performance criteria, and hence permit the selection of the most economical configuration that will satisfy such criteria.

In addition to the above goals, there was a third which, while subsidiary to the main purposes of this investigation, nonetheless has significance for future work as well as affecting economies in the present. This was to automate the testing and evaluation procedures as much as was deemed desirable to achieve greater reproducibility and reduce the labor required. Although time did not permit full automation of all of the tests performed, significant progress toward this goal was achieved.

The following sections describe the testing facility, intelligibility and subjective test procedures, and the results obtained. Details are left for the appendices.

4.2 AUDIO EVALUATION FACILITY

To conduct the simulator audio evaluation, two sound-proofed booths were built into the laboratory area to accommodate the personnel and equipment used for conducting the tests. Figure 10 shows the physical arrangement of these, and Figure 11 gives the plan of the general layout, including the equipment incorporated into each booth.

Consideration of available space, funds, and convenience led to the location of these booths close to the simulator hardware and the computer, with the result that their acoustical performance, while adequate for the purpose at hand, is not good enough for audiometric work. The main reasons for this are the location of heavy equipment adjacent to the laboratory in which the booths were built, and the relatively long reverberation time of the laboratory necessitated by the presence of the equipment itself.

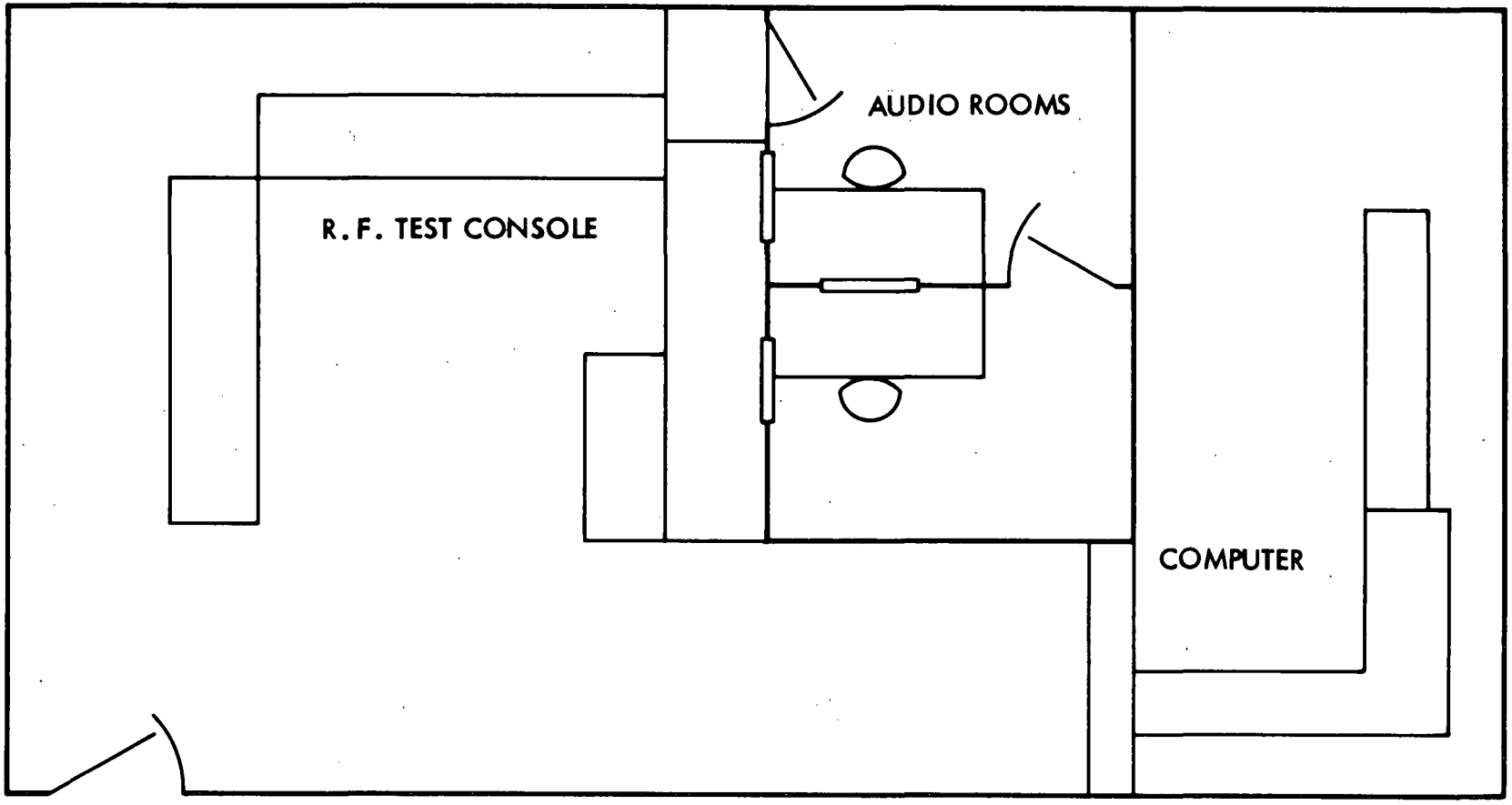

Figure 10. Plan View of Sound-Proofed Booths Used in Audio Evaluation Work

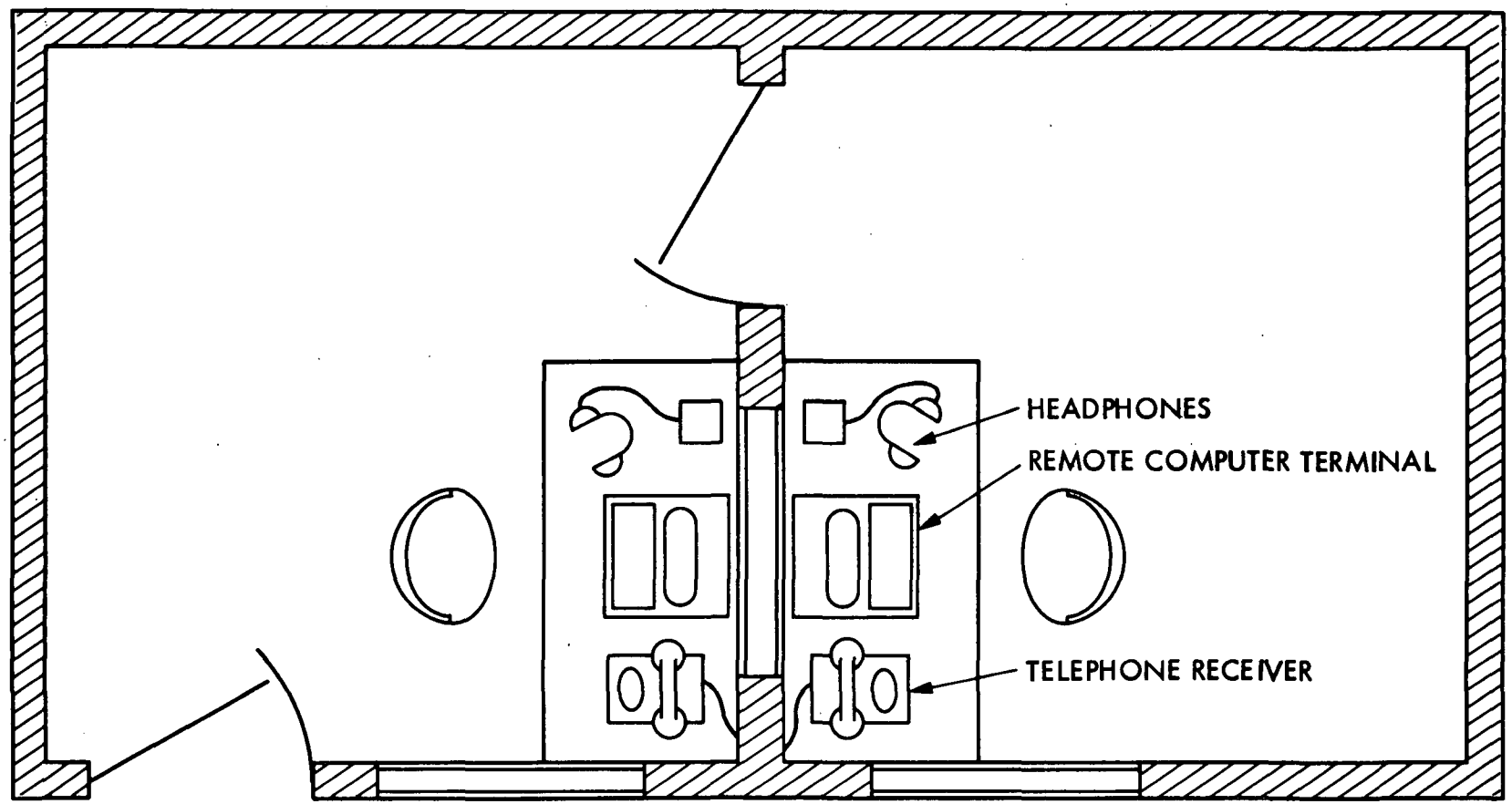

Figure 11. Detail of Sound-Proofed Booths, Showing Arrangement of Equipment

Measurements of the ambient noise levels in the two booths resulted in the spectrum level values shown in the graphs of Figure 12 (see Appendix A for measurement details). Included in the figure for comparison purposes is a typical long-term averaged speech spectrum measured 1 meter from the lips of the talker. From this it can be seen that while the ambient noise levels in the booths are relatively high, especially at low frequencies, it is possible to provide a speech spectrum at least 30 dB above noise between the low and high frequency cutoffs of the simulator (300 Hz to 3 kHz) without the overall level being too high for listener comfort. The significance of the 30-dB figure quoted here is that speech-to-noise levels greater than this do not result in measurable loss of intelligibility (Ref. 5), so that intelligibility testing could readily be carried out in such an environment.*

To provide an audio response at the listener's ear that is a faithful reproduction of the audio output of the simulator receiver, high-fidelity earphones (KOSS ESP-9) were used in the testing booths. These provided, in addition, a further attenuation of the ambient noise as shown by the lower curves of Figure 12, although this is less than might be expected at low frequencies. The reason for this is that while the manufacturer's specification for earphone attenuation is nominally 40 dB, ambient sound is also conducted around the earphone cups through the listener's cranium, thus contributing to an enhanced sound level at the listener's ear (see Appendix A for a discussion of the measurement technique used to determine the perceived noise level when the listener is wearing earphones).

In contrast to the arrangement described above, a conventional telephone handset was used to conduct subjective evaluations of the simulator performance. The decision to use this listening device instead of the high-fidelity earphones was based upon two considerations. First, the standard telephone circuit used for comparison purposes transmits objectionable high-frequency distortion which can be heard in high-fidelity earphones but is eliminated by the handset characteristics. Second, the use of an environment that is not absolutely quiet for subjective comparisons between the simulator and a telephone was considered desirable in that it provided a more normal listening environment without the danger of contributing to detectable degradation of performance. Such an environment was considered desirable because it tends to relax the listener more than one that is perfectly quiet, a situation that is also enhanced by the use of a telephone rather than earphones.

4.3 INTELLIGIBILITY TESTS

4.3.1 Design and Execution of the Tests

As mentioned above, the purpose of conducting intelligibility tests on the channel simulator was to determine the limits of noise, interference, and fading that could be tolerated singly and in combination, and still produce

*The long-term averaged speech spectrum shown in Figure 12 has been augumented by 12 dB since it is the speech peaks that must be compared with the noise level to determine channel intelligibility (Ref. 5).

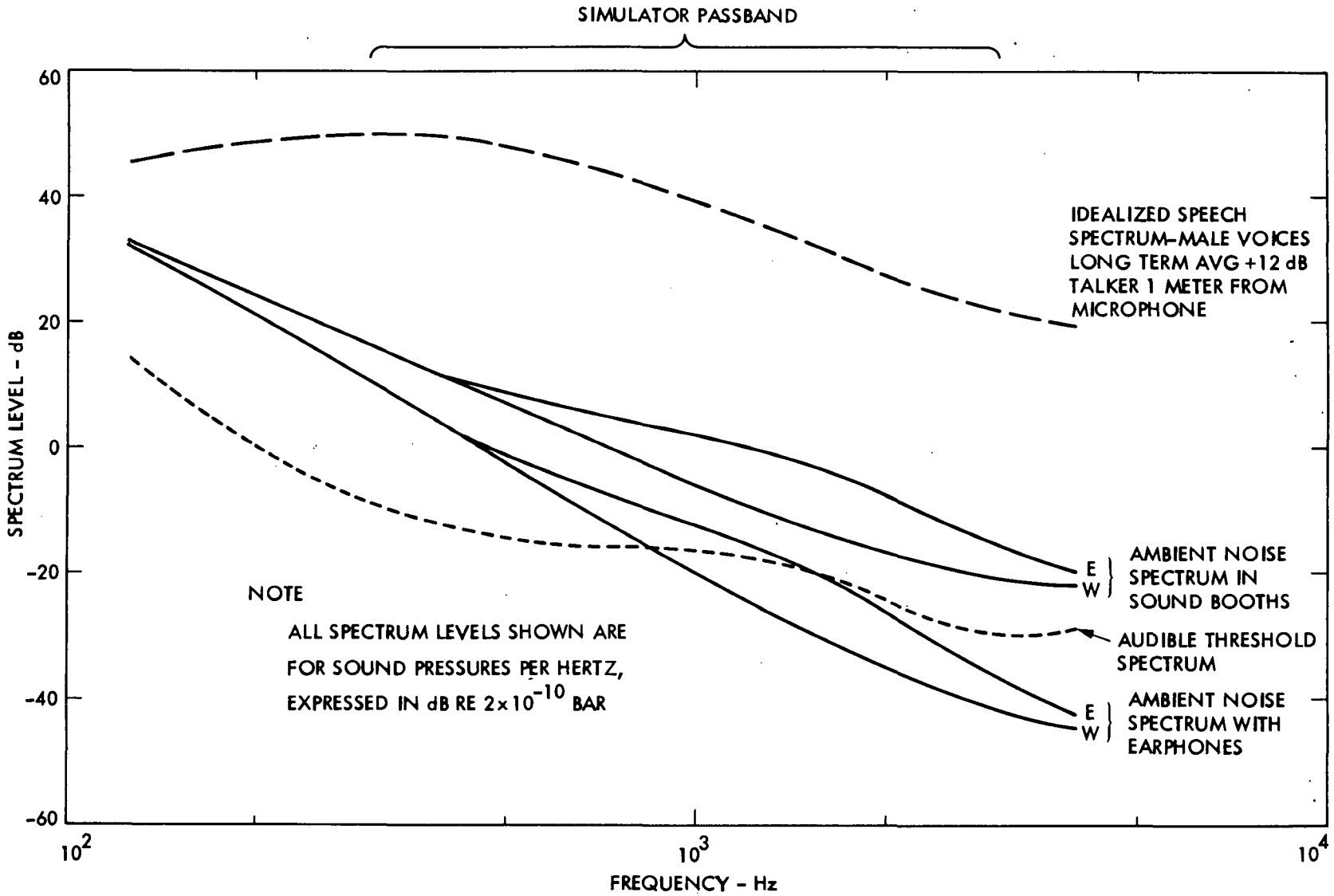

Figure 12. Ambient Noise Spectra for Sound-Proofed Booths. A typical speech spectrum at a distance of 1 meter from the talker, and the average audible threshold spectrum are shown for comparison

a usable communication channel. In view of the fact that such testing involves a great deal of time and labor if conducted manually, using standard jury evaluation methods, it was decided at the outset to automate this portion of the evaluation as much as practicable. To this end, computer terminals were installed in each of the booths so that the testing could be administered and scored by computer.

The test material used for these evaluations was a 1000-word source of phonetically balanced monosyllabic words (PB word lists) taken from Ref. 6 and recorded onto low-noise audio magnetic recording tape (Scotch Brand #208, 1.5 mil) by means of a high-fidelity recording system. This consisted of a B&K Model 2203/1613 Sound Level Meter used as a microphone, feeding directly into an AKAI GX-625 Reel-to-Reel Tape Recorder (1/2 track).

The PB words were read onto one track of the tape in 50-word groups with 4-second spacing between words and 10-second spacing between 50-word groups. A total of 20 groups was recorded onto two separate reels, making 1000 words in all. Simultaneously, a digital-code sequence representing each word was generated by the computer and read onto the second track of the tape so that the start of the code sequence began 2 seconds after the beginning of the utterance of each word. The digital encoding was accomplished by amplitude modulating an ultrasonic carrier (f = 20 kHz) at a 1200-baud rate. The resulting timing sequence is shown in Figure 13, where it can be seen that the two tracks of the audio tape contain audible speech and digitally coded versions of the words, spaced 4 seconds apart, with the digital track delayed by 2 seconds relative to the speech track.

During playback for testing, the listeners in each booth simultaneously received in their earphones a word which had been transmitted through the simulator. They then had 2 seconds to decide what word they had heard before the digital track activated the display terminal with the written version of the actual word that had been spoken into the simulator. The listeners were instructed to press a response button only if the word displayed sounded like the word they thought they had heard, i.e., words sounding the same but having different spelling, for example ONE and WON, were considered identical for this evaluation. If no response was recorded by the end of the fourth second, i.e., 2 seconds after the correct word was displayed on the terminal, the computer scored this as a "miss". Thus, at the end of each 50-word group, the computer scored the responses from each booth and produced a hard copy display showing the percent correct as well as the entire 50-word list, with those words missed being marked by an asterisk. In addition, the name of the listener, date, and the specific channel conditions being simulated were also listed on the computer printout. The system block diagram for playback is shown in Figure 14, and an example of the computer printout in Figure 15.

Each 50-word list was used to test for a specific simulator configuration, and individual lists were randomly selected in the course of testing so as to avoid any systematic bias due to differences in the intrinsic intelligibility of the lists themselves. The latter should be small in any case, owing to the careful manner by which these lists were originally created.

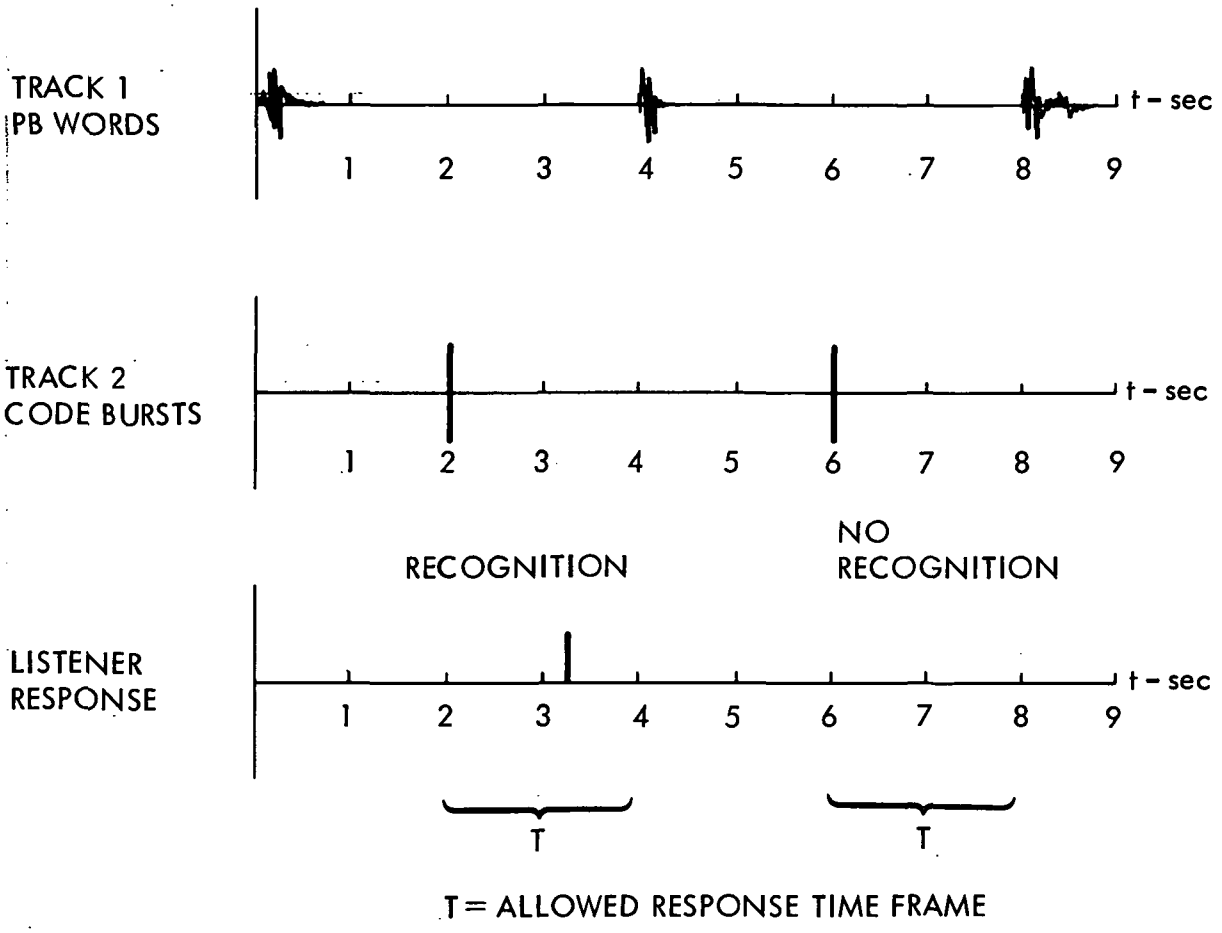

Figure 13. Timing Sequence for Intelligibility Testing

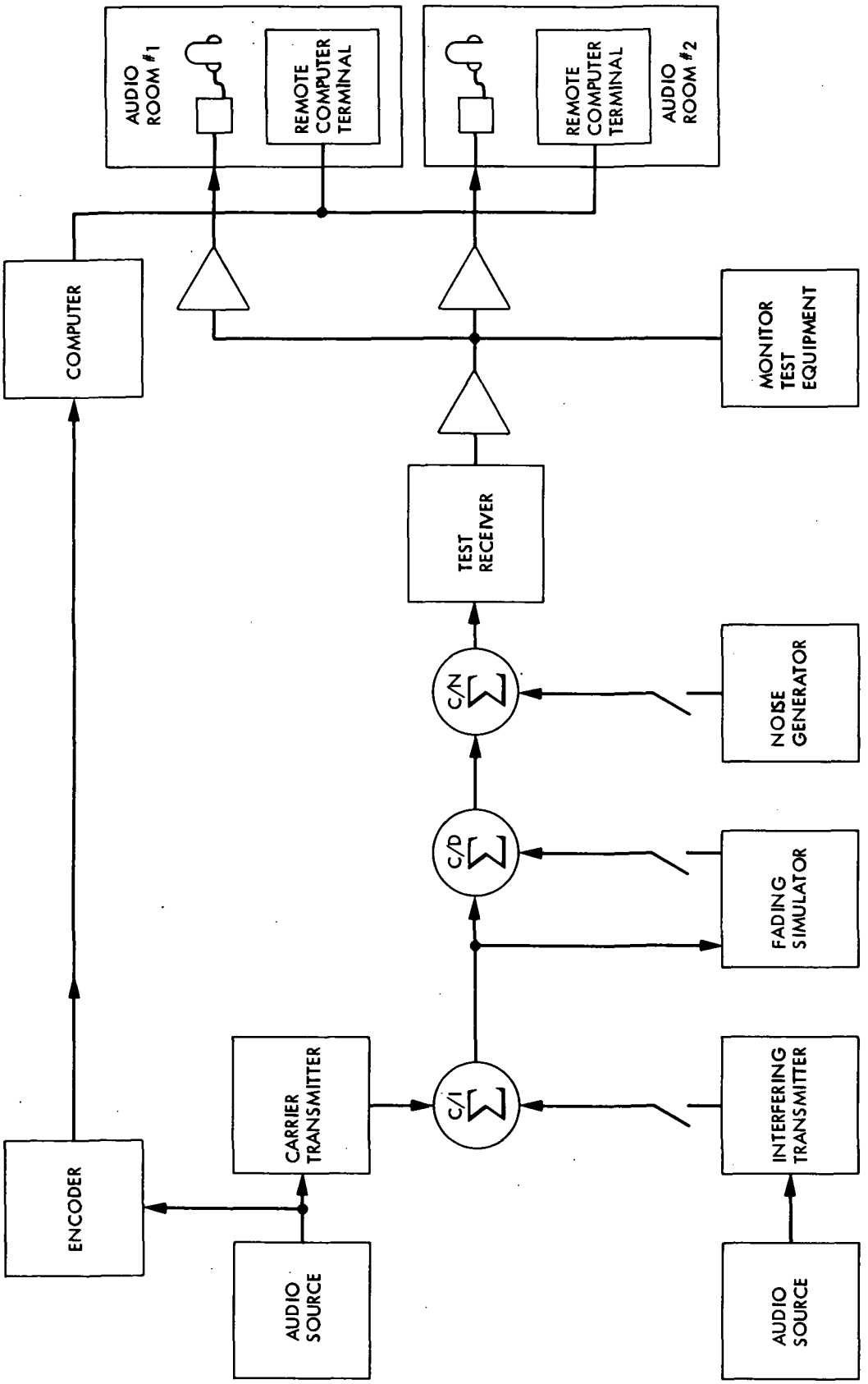

Figure 14. Block Diagram for Intelligibility Test Setup

PETER KINMAN 10-01-82 54.00 PERCENT CORRECT WORD LIST 12

TEST CONDITIONS -

VEHICLE SPEED = 55 mPh INTERFERENCE RATIO = 5.00 dB CLOCK RATE = 900.0 Hz
C/N = 16.00 dB C/I = 2.00 dB

*LOOSE	HUG	*ROVE	CLING
*CLUTCH	*CHAFE	PRIEST	*DONE
BLUFF	*FOUGHT	*PARK	FLOOD
JAW	TILE	THROB	*FOOT
KNIFE	*SHUT	*SOD	*ROMP
CHAIR	SET	CHINK	*WOVE
HEAR	JAZZ	*JOLT	GNASH
SKY	BALL	WAGE	GREET
DEPTH	FED	*VINE	CAVE
*REEK	LASH	DIME	*LAUGH
*RIPE	LEDGE	*CAD	*AND
OUT	*FRILL	*CHAP	
*ASS	FLOG	*HUNCH	

Figure 15. Typical Computer Printout of Intelligibility Test Results

4.3.2 Test Results

A summary of the test results obtained under the testing conditions is shown in Figure 16. Here, percent intelligibility is plotted as a function of the carrier-to-noise ratio, C/N, in dB, with the carrier-to-interference ratio, C/I, in dB, serving as a parameter. The four sets of graphs shown in these figures display the results for each of four different fading conditions represented by values of the carrier-to-multipath fading ratio, C/MF, where the carrier is the direct LOS signal, of 20 dB, 5 dB, and -20 dB.

In all cases tested, the fading simulator was set for Rayleigh fading conditions corresponding to a vehicle speed of 91 km/h (55 mph) and a smooth reflecting background. However, a nondistorted direct LOS signal was added to the Rayleigh-faded multipath signal to create the Rician-faded signal, which is typical of a LMSS communications channel. The transmitter modulation was set to a value of $\delta_{rms} = .15$,* and the earphone level was set 14 dB higher than the speech curve shown in Figure 12. This resulted in a comfortable listening level (Sound Pressure Level = 79 dB) and a speech-to-ambient noise ratio under clear channel conditions of greater than 53 dB at all frequencies within the simulator passband.

The results shown in Figure 16 have been used to determine "Intelligibility Thresholds" for the system as shown in Figure 17. Here, curves have been drawn which give values of C/N and C/I for which the PB word scores have the constant percentage values shown. The percentages shown in parentheses give the corresponding intelligibility scores one would expect for tests run with sentences rather than PB words. These have been determined from established correlations between the two kinds of tests as provided, for example, in Figure 15 of Ref. 7.

4.3.3 Discussion of Intelligibility Test Results

The curves of Figure 17 indicate that acceptable intelligibility can be achieved with surprisingly high amounts of noise, interference, and fading-even for the relatively low modulation index chosen for the measurements. For example, in the absence of noise and multipath fading, 97-percent sentence intelligibility is possible with a C/I ratio as low as 2 dB, and for 92-percent sentence intelligibility this ratio can be less than 1 dB. Similarly for a carrier-to-multipath fading ratio of 5 dB (i.e., typical partial shadowing conditions) and a carrier-to-noise ratio of 8 dB, corresponding to the system threshold, a C/I ratio of about 13 dB will result in 97-percent sentence intelligibility, while a value of 92-percent can be achieved with C/I = 6 dB.

Since the carrier and interfering transmitters operate independently of one another (see Figure 14) and are relatively stable, a frequency difference exists between the two (i.e., due to differences in vehicle speed), resulting in a fluctuation of the audio output at the difference frequency. In our measurements, this frequency difference was approximately 200 Hz so that the fluctuation was too rapid for the ear to detect directly. However,

*See Appendix C for definition of this term.

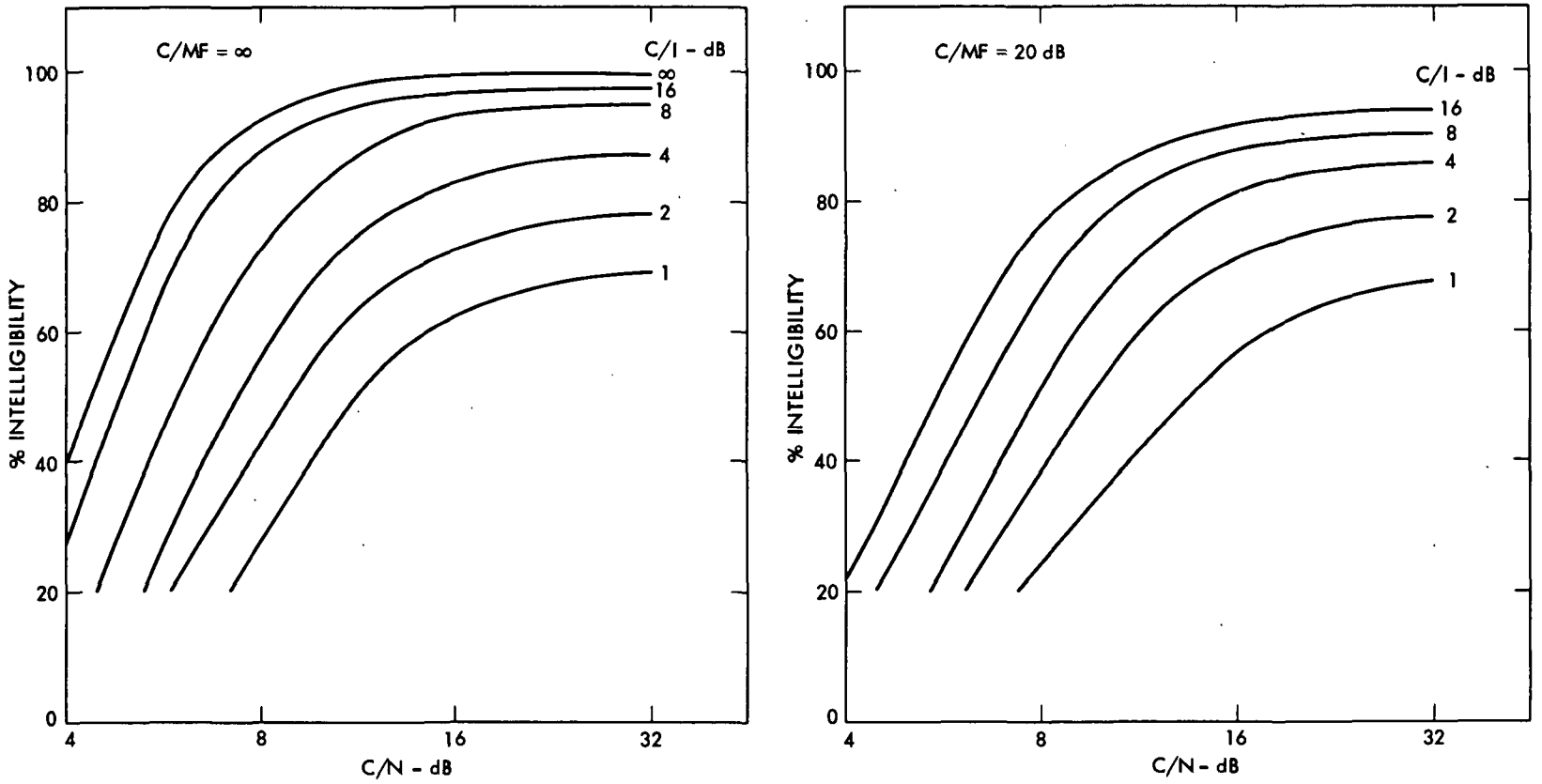

Figure 16. Summary of Intelligibility Test Results as a Function of Carrier-to-Noise Ratio C/N, Carrier-to-Interference Ratio C/I, and Carrier-to-Multipath Fading Ratio C/MF. In all cases the multipath fading corresponded to reflection from a smooth surface and a vehicle speed of 91 km/h (55 mph). The modulation index $\delta = \Delta f/Bm$, where Δf = rms frequency deviation and B_m = audio bandwidth, was set to $\delta = 0.15$ in all cases

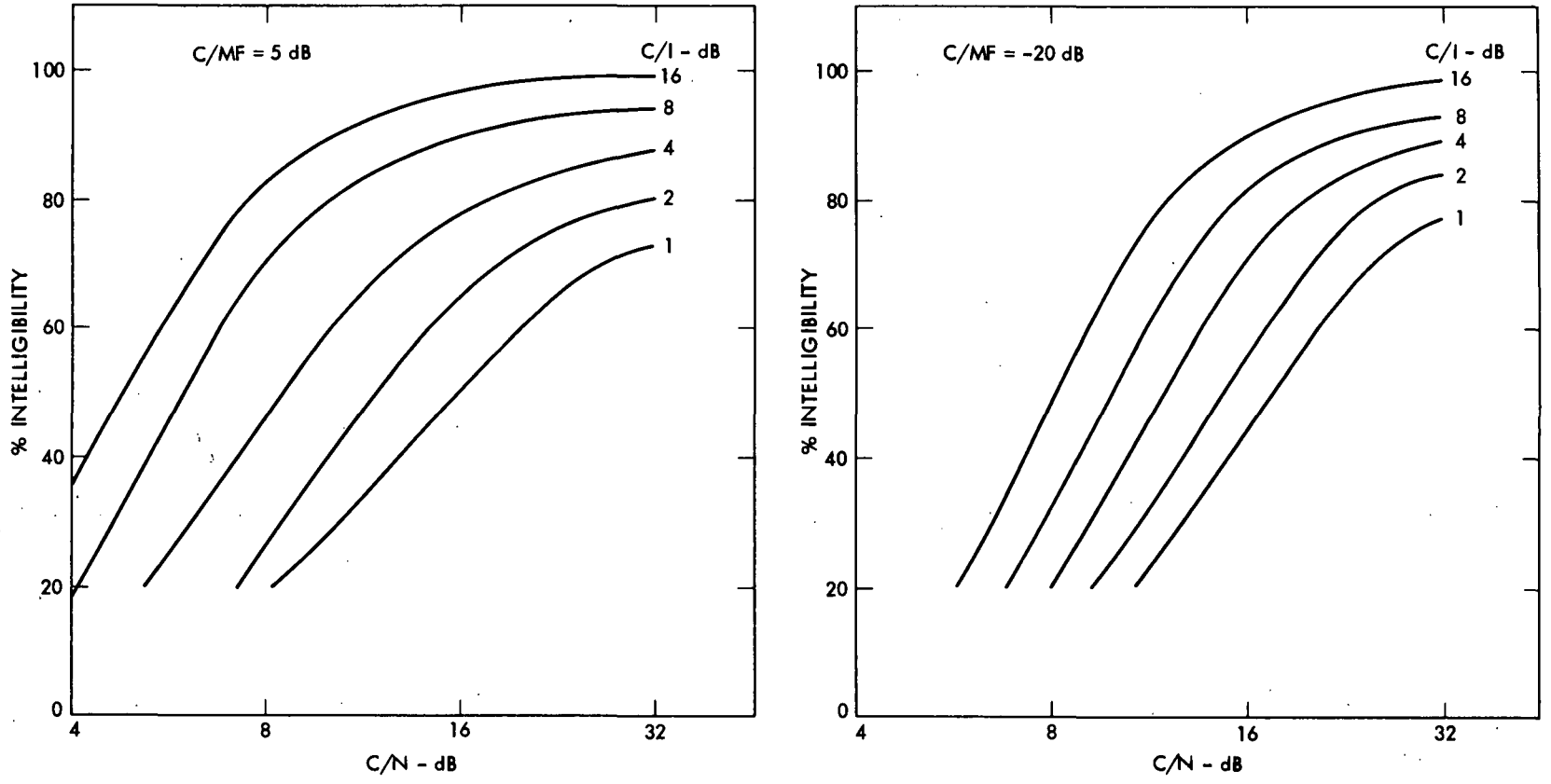

Figure 16. Summary of Intelligibility Test Results as a Function of Carrier-to-Noise Ratio C/N, Carrier-to-Interference Ratio C/I, and Carrier-to-Multipath Fading Ratio C/MF. In all cases the multipath fading corresponded to reflection from a smooth surface and a vehicle speed of 91 km/h (55 mph). The modulation index $\delta = \Delta f/Bm$, where Δf = rms frequency deviation and B_m = audio bandwidth, was set to $\delta = 0.15$ in all cases. (Continued)

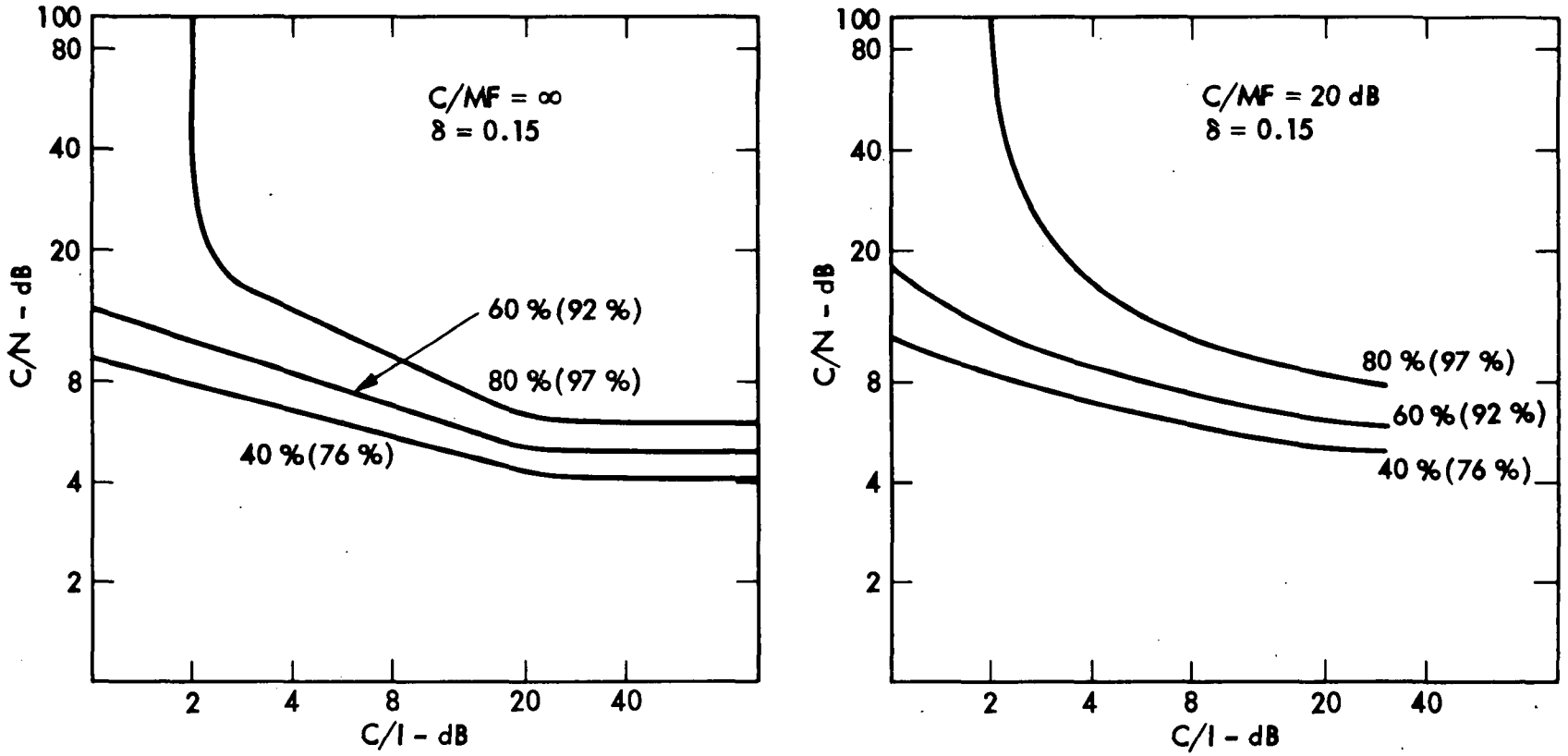

Figure 17. Intelligibility Thresholds as a Function of C/N and C/I for Four Conditions of Multipath Fading. The percentages outside the brackets represent the measured PB word scores while those inside the brackets represent the corresponding sentence scores (first presentation to listeners). The latter were obtained from the correlation presented in Figure 15 of Ref. 7

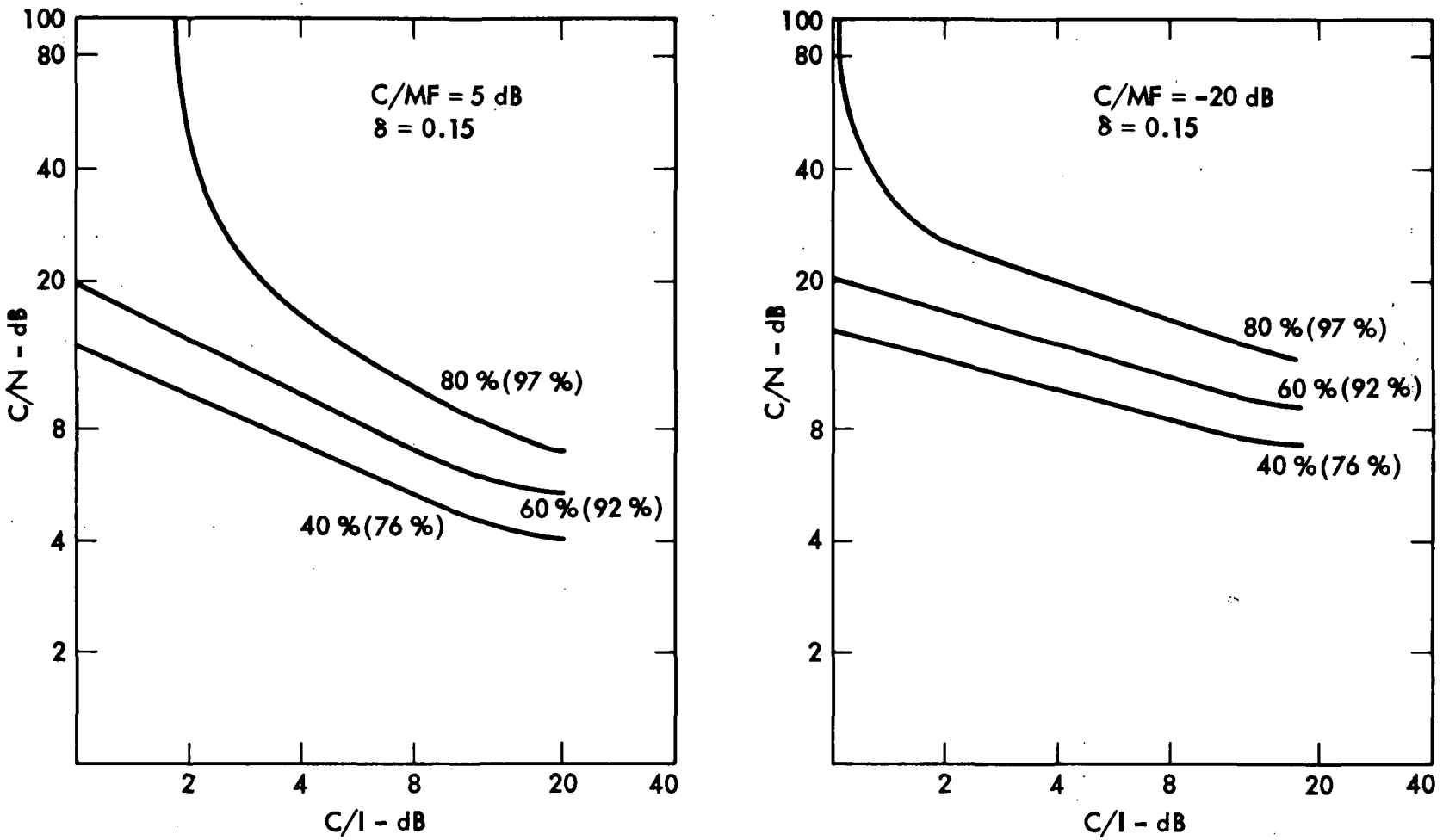

Figure 17. Intelligibility Thresholds as a Function of C/N and C/I for Four Conditions of Multipath Fading. The percentages outside the brackets represent the measured PB word scores while those inside the brackets represent the corresponding sentence scores (first presentation to listeners). The latter were obtained from the correlation presented in Figure 15 of Ref. 7. (Continued)

it is well known that the human ear-brain combination responds to such a waveform resulting from the summation of two frequencies to produce the sensation of "aural harmonics." These have frequencies given by $f = nf_1 - mf_2$, where f_1 and f_2 are the two frequencies responsible for the beat pattern, and n and m are integers. The most prominent frequency heard will be for $n = m = 1$, the beat frequency, with those next in prominence corresponding to small values of n and m.

The result then, is to produce a garbling of the speech due to the interference of the fundamental glottal pulse frequency and its harmonics with aural harmonics, resulting in a loss of intelligibility even when no interfering modulation is present on the interfering carrier. Such a circumstance is a contributing factor to the results shown in Figure 17, and since the actual value of the beat frequency in an operating LMSS will be a random variable, the effects on intelligibility cannot be determined with precision. In particular, if the beat frequency is below approximately 30 Hz, then the fluctuations will be perceived directly and the effects on speech intelligibility, especially for low values of C/I, can be expected to be greater than those represented by the data shown in Figure 17.

4.4 SUBJECTIVE QUALITY EVALUATION

4.4.1 Design and Execution of the Tests

The subjective quality evaluation was carried out on the basis of comparison with a standard telephone link between two southern California cities located approximately 20 miles apart. Listeners were asked to judge the performance of the LMSS simulator for the channel conditions under test by first listening to a tape recording of test sentences transmitted over the telephone link, and then listening to the same sentences spoken by the same talkers transmitted through the simulator.

The test material chosen for these evaluations (Ref. 8) consists of a tape recording of three male and three female talkers uttering short sentences.* Each talker speaks 15 sentences in 1 to 1.5 minutes, and the evaluation of a given channel condition was based on one 15-sentence test per listener, each condition being evaluated by four to ten listeners. Talkers were randomly selected so that each condition was evaluated with several different talkers.**

The comparison tape was produced by connecting the output of a tape recorder directly to a telephone transmitter located in the first city,

*This material was designed by Dynastat Inc. to be used in determining what they term a Diagnostic Acceptability Measure (DAM) for a speech system (Ref. 8).

**After preliminary testing it was found that two of the female talkers were consistently judged lower than the remaining four talkers, and as a result it was decided that the tests would be conducted using only the 3-male and 1-female talkers.

dialing the second city, and recording the transmitted signal directly from a telephone receiver onto tape. After each sentence a new connection was established by redialing and this procedure was carried out a total of twenty times, thus producing a comparison tape with a variety of noise and interference conditions deemed to be representative of the existing telephone network for intercity calls.

Figure 18 shows the block diagram for the test arrangement used in the subjective evaluation phase of the LMSS simulator testing program. It was decided that for the listening device for this phase, a standard telephone receiver would replace the high-fidelity earphones used in the intelligibility testing phase. The reasons for this choice were twofold. First, it was discovered that the comparison tape contained a high-frequency noise component that could be heard over the earphones but not through the standard telephone receiver because of its high-frequency filtering characteristics. Second, it was felt that realistic subjective evaluation could best be carried out in an environment more closely resembling that of, say, a quiet office than a carefully controlled laboratory space. (For further details of the comparison tape preparation and testing procedures, see Appendix A.)

The evaluations were carried out by means of a questionnaire asking the listeners to evaluate the system quality on a Subjective Quality Factor scale ranging from 1 to 5, with 3 corresponding to the average, i.e., the standard telephone link, 1 corresponding to poor quality and 5 corresponding to excellent quality.

4.4.2 Test Results

The results of the subjective evaluations are summarized in Figure 19 where the Subjective Quality Factor is plotted as a function of C/I for various values of C/N, and two values each of C/MF and δ_{rms}. These graphs were obtained by drawing smooth curves through points obtained by averaging the numerical Subjective Quality Factors assigned by all listeners for a given channel condition. (For a more detailed discussion of the data analysis, see Appendix A.)

Figure 20 shows Acceptability Thresholds plotted as a function of C/N and C/I for the two values each of C/MF and δ_{rms} used in Figure 19. These were obtained in a manner analogous to that used to determine the Intelligibility Thresholds discussed in Subsection 4.3.2 and shown in Figure 17. In the present instance, the Acceptability Threshold corresponds to those conditions for which the Subjective Quality Factor is equal to 3, i.e., equivalent to an average telephone link, so that values of C/N and C/I greater than those determined by the curves of Figure 20 define simulator link conditions that provide a better-than-average qualitative evaluation.

Finally, in Figure 21 we show a comparison of Intelligibility and Acceptability Thresholds for the case of C/MF = 20 dB and $\delta_{rms} = 0.15$. Extrapolation of the PB word-and-sentence intelligibilities corresponding to the Acceptability Threshold curve show results of 93 percent and 99 percent, respectively.

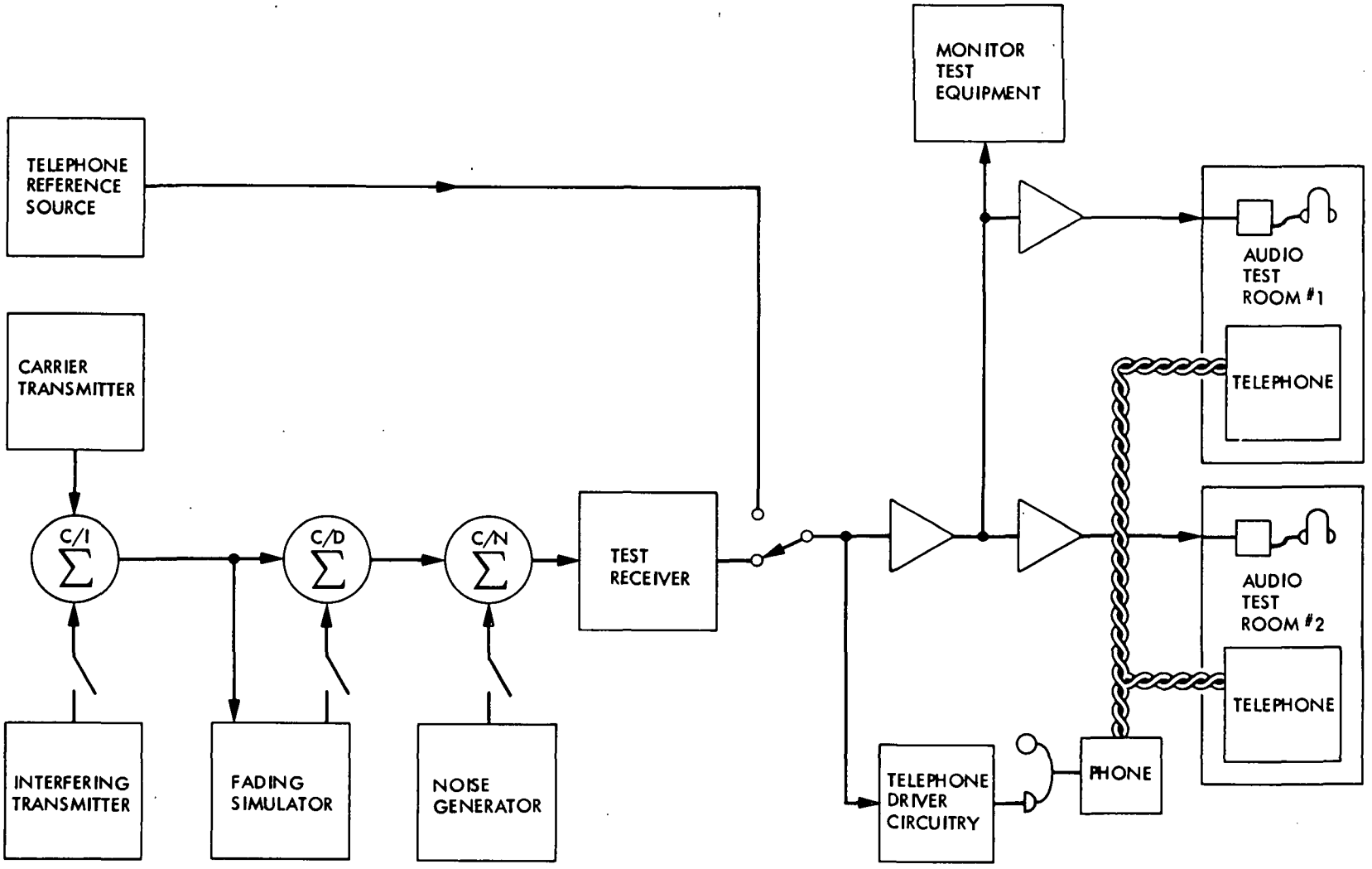

Figure 18. Block Diagram for Subjective Evaluation Test Setup

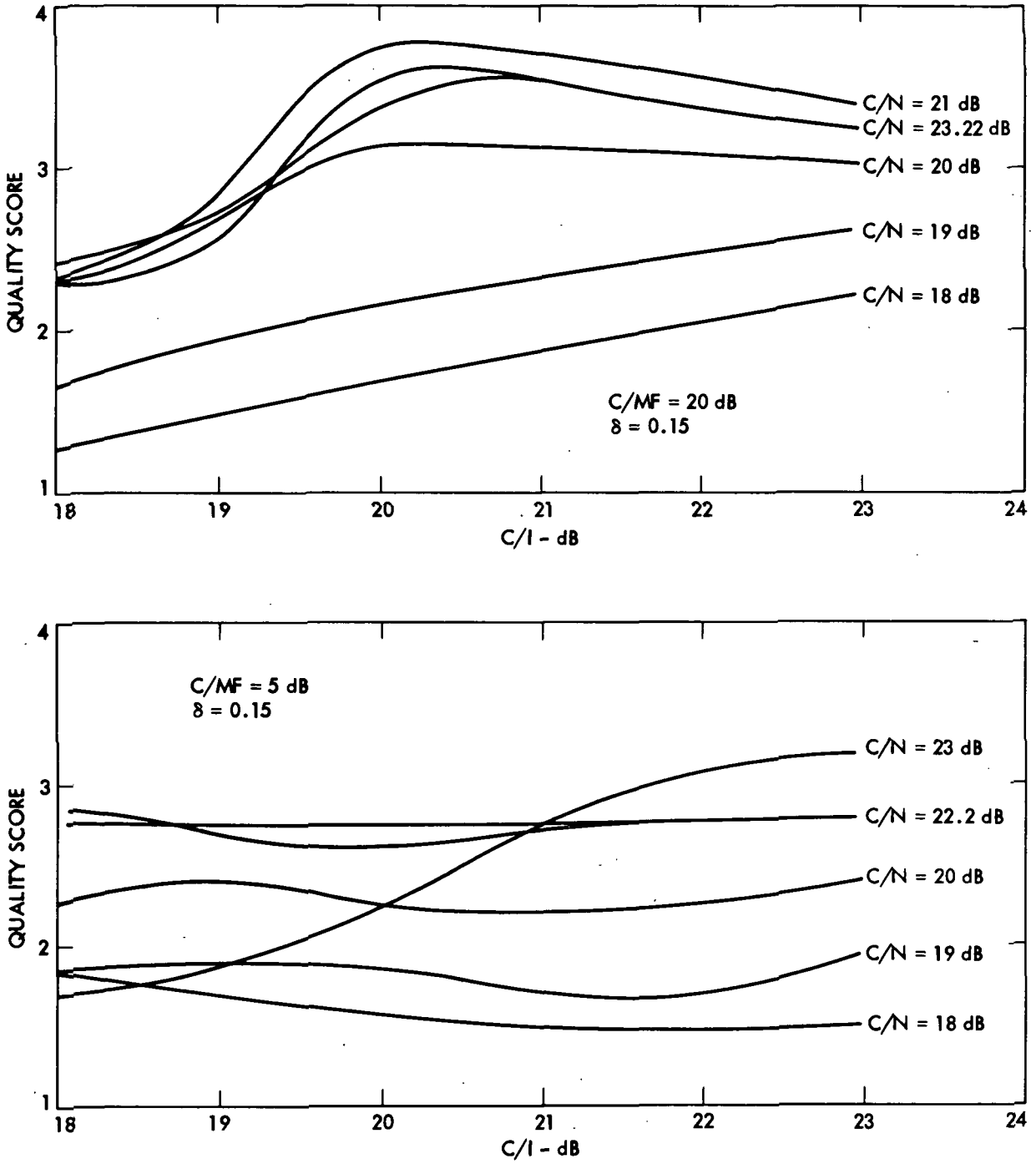

Figure 19. Summary of Subjective Quality Test Results as a Function of C/N, C/I, C/MF, and δ. Fading conditions were identical to those used in the intelligibilty tests (see Figure 7)

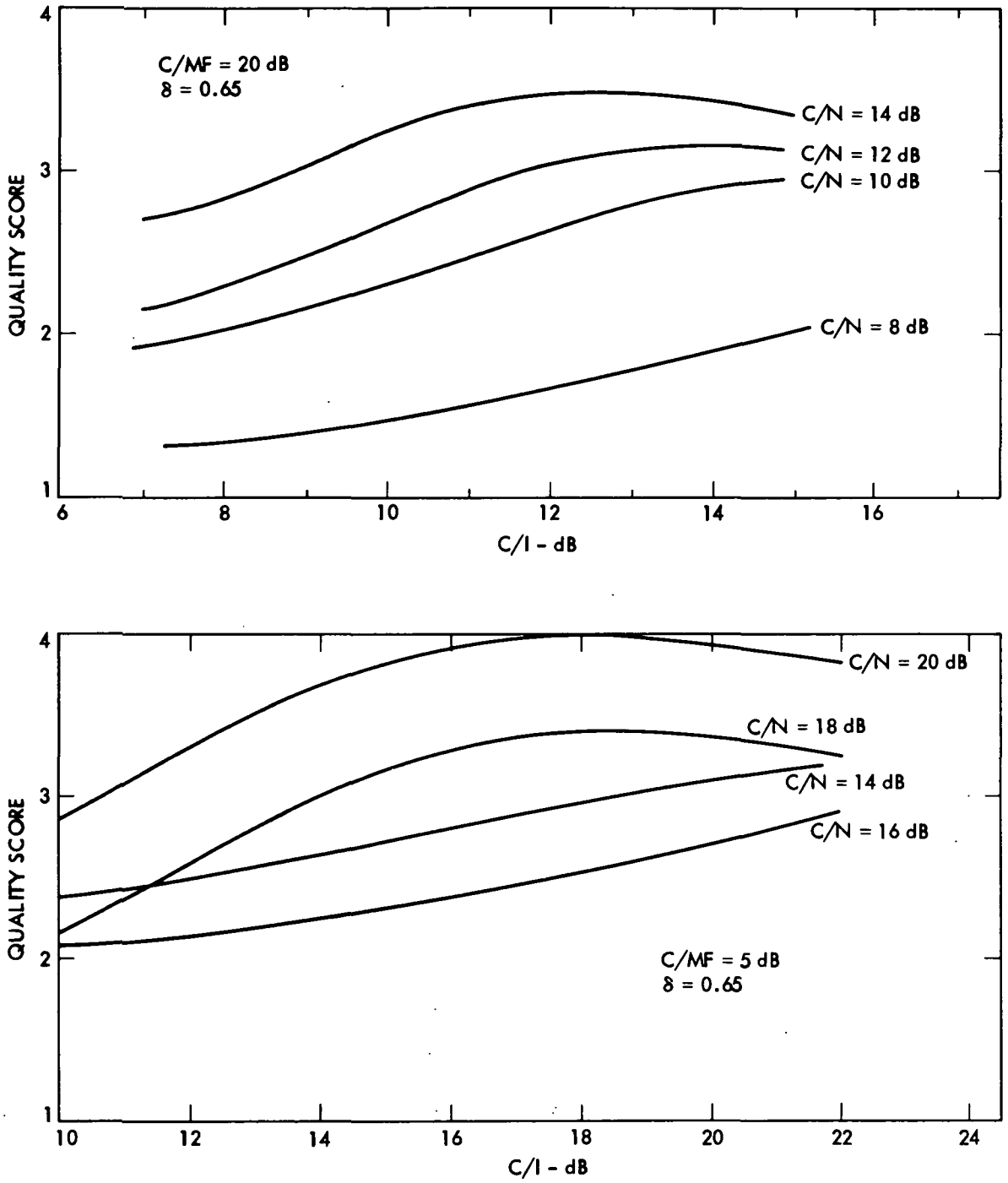

Figure 19. Summary of Subjective Quality Test Results as a Function of C/N, C/I, C/MF, and δ. Fading conditions were identical to those used in the intelligibilty tests (see Figure 7). (Continued)

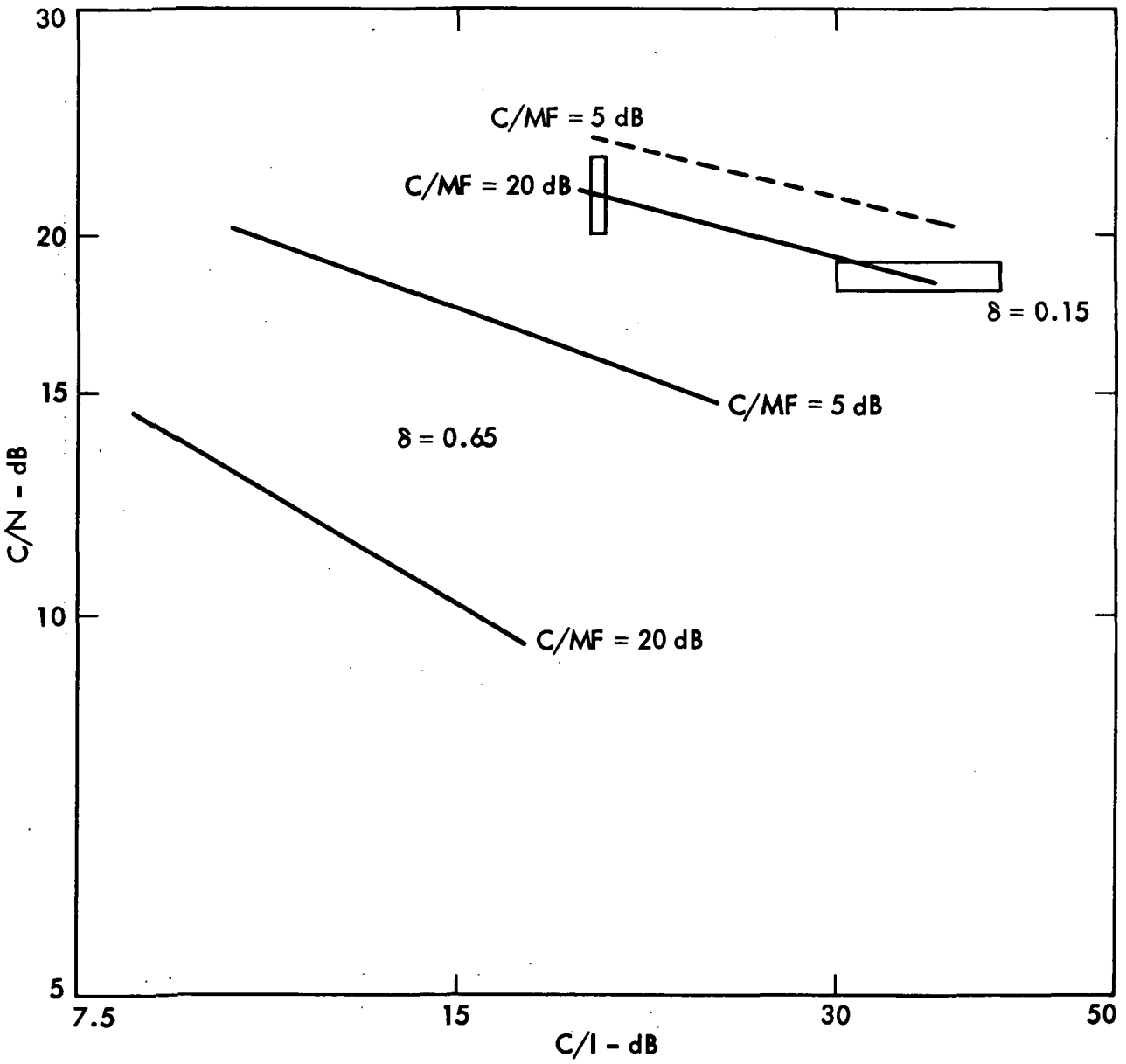

Figure 20. Acceptbility Thresholds as a Function of C/N and C/I for Two Values of C/MF and Two Values of δ

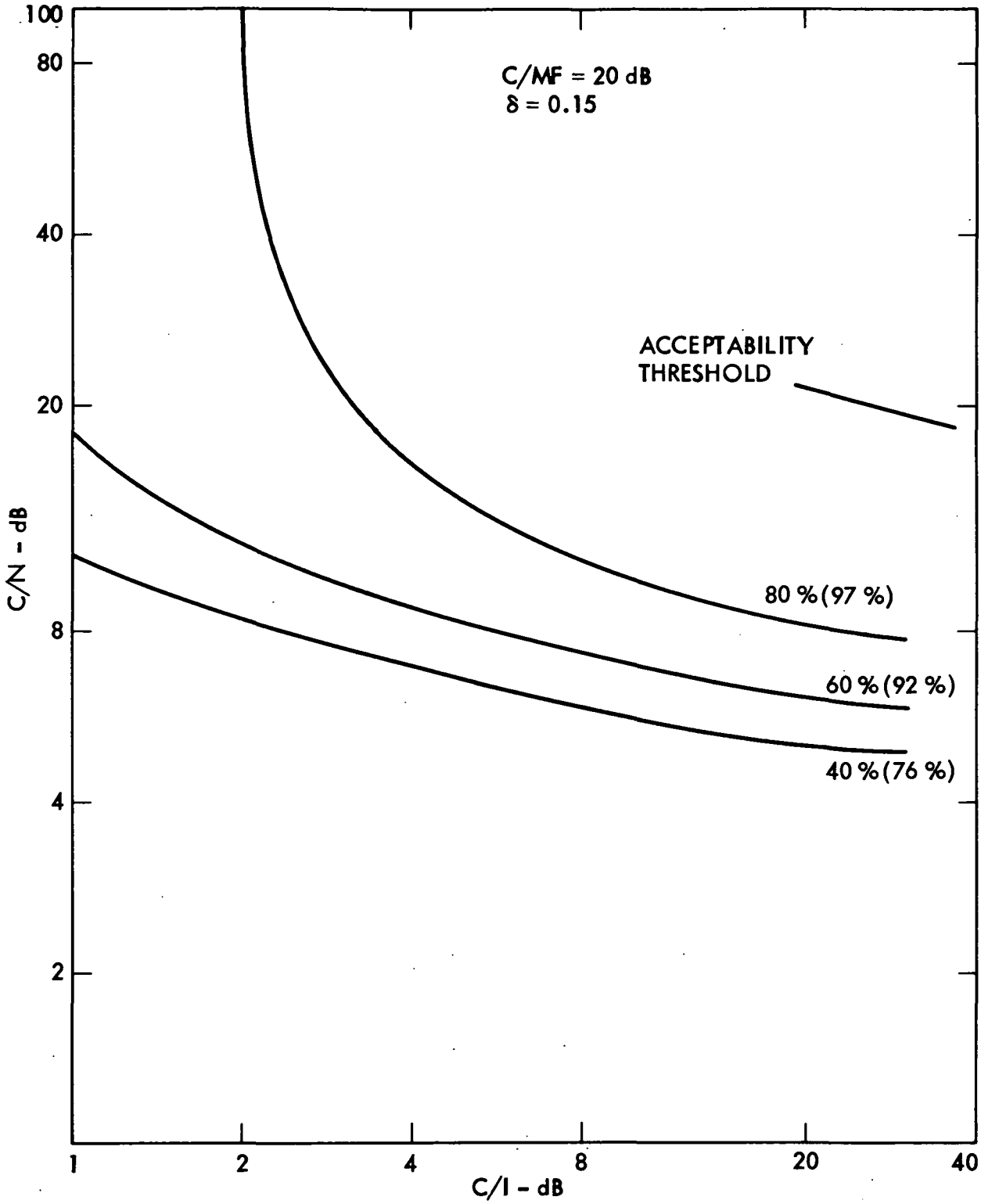

Figure 21. Comparison of Intelligibility and Acceptability Thresholds for C/MF = 20 dB and δ = 0.15. The extrapolated PB word intelligibility for the acceptability threshold is 93% corresponding to a sentence intelligibility of 99%

4.4.3 Discussion of Subjective Quality Evaluation Test Results

Examination of Figure 20 reveals that the Acceptability Threshold curves shown are separated by constant C/N, independent of C/I. For example, for $\delta_{rms} = 0.65$, the C/MF = 20 dB and C/MF = 5 dB curves are everywhere 7.2 dB apart in C/N, while for the C/MF = 20 dB the $\delta_{rms} = 0.15$ and $\delta_{rms} = 0.65$ curves (extrapolated) are 12.7 dB apart in C/N. The value of $\delta_{rms} = 0.65$ corresponds to $\Delta f_{rms} = 2$ kHz, which is the value chosen for AMPS rms frequency deviation.

These observations can be understood in terms of the results shown in Figures 21 and 22 as follows. (For a more detailed analysis, see Appendix C). Figure 21 indicates that constant acceptability corresponds approximately to constant intelligibility. Thus, we can assume that for all conditions represented by points on the curves of Figure 21, the PB word intelligibility is approximately 93 percent. If the nature of the baseband noise spectrum did not change as the system conditions changed from C/MF = 20 dB to C/MF = 5 dB holding both δ_{rms} and C/I constant, then the baseband signal-to-noise ratio S_0/N_0 would also remain constant, because constant intelligibility implies constant S_0/N_0 for a given noise spectrum (see Appendix A).

From the measured S_0/N_0 data presented in Figure 22, we see that for above FM threshold conditions, the C/MF = 20 dB and C/MF = 5 dB curves are separated by the nearly constant C/N value of 5.3 dB for a constant S_0/N_0. In fact, the analysis in Appendix C shows that since the noise spectrum in the absence of fading is parabolic, whereas the click noise introduced by fading tends to be white, a constant intelligibility under conditions of increased fading could occur only as a result of a slight <u>increase</u> in S_0/N_0, thus resulting in a somewhat greater change of C/N. The results of Appendix C are in good agreement with the observed differences of 7.2 dB in C/N quoted above.

Before leaving this point it should be mentioned that while the conditions represented in the data of Figure 22 (Gaussian modulation, $\delta_{rms} = 0.49$, $C/I = \infty$) do not correspond exactly to those represented by the data of Figure 20 (voice modulation, $\delta_{rms} = 0.65$, C/I = 10 to 20 dB), they are sufficiently close to render the above conclusion valid.

The constant difference of 12.7 dB in C/N observed as δ_{rms} changes from 0.15 to 0.65, holding C/MF constant (= 20 dB), can be understood on the basis of the "above threshold" theoretical relationship (see Appendix C) between the baseband signal-to-noise ratio, SNR, carrier-to-noise ratio, CNR, and modulation index δ_{rms},

$$SNR = 3\,\delta_{rms}^2 \left(\frac{B_{IF}}{B_m}\right) (CNR)$$

where

B_{IF} = IF bandwidth

B_m = baseband bandwidth

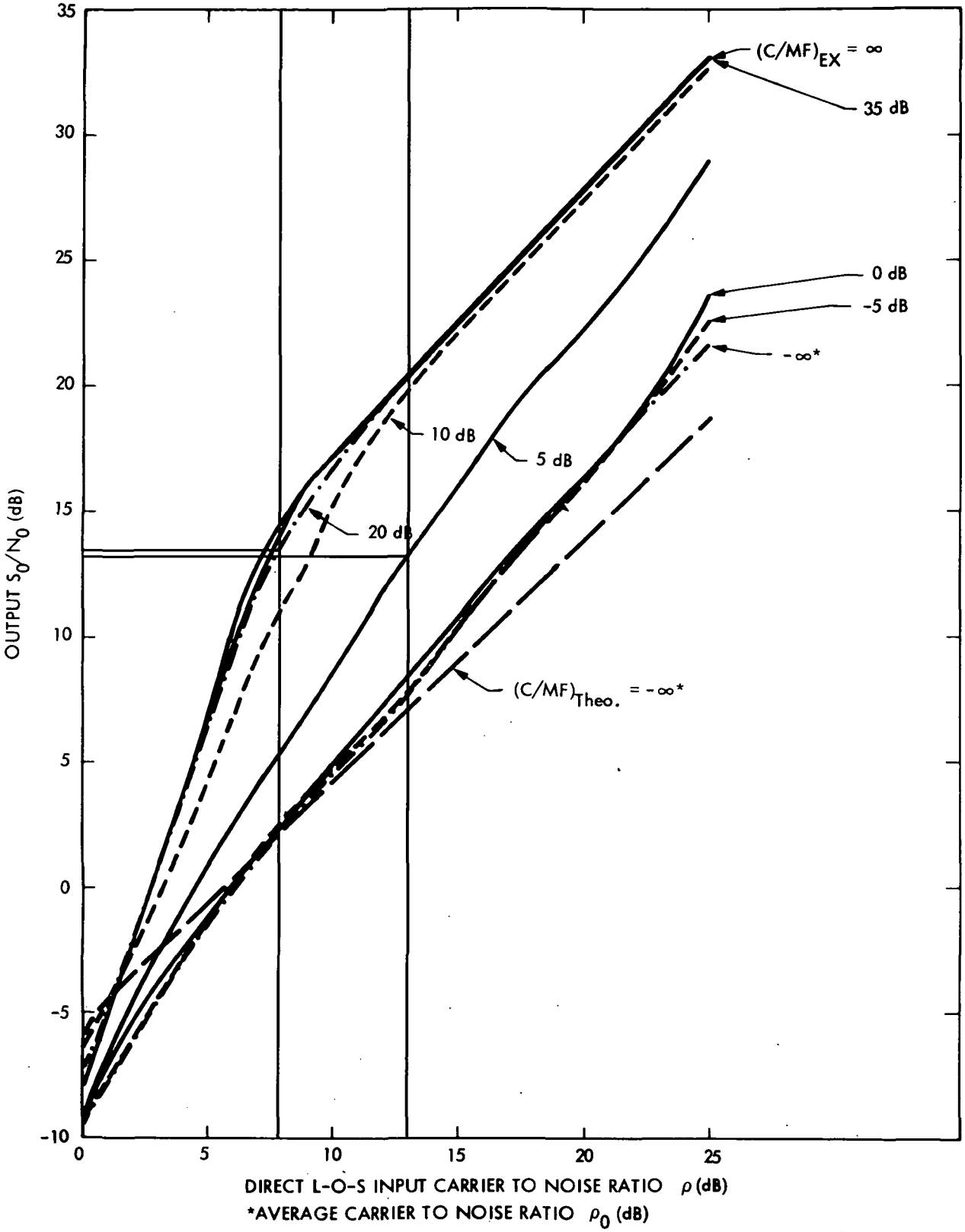

Figure 22. Measured S_0/N_0 Data Showing a Constant Difference of 5.3 dB in C/N Value for the C/MF = 20 dB and C/MF = 5 dB Curves (Gaussian modulation with $\delta_{rms} = 0.49$)

In terms of decibels, the above may be written

$$S_0/N_0 = K + 20 \log \delta_{rms} + C/N$$

where

$$K = 10 \log 3\left(\frac{B_{IF}}{B_m}\right), \quad \frac{S_0}{N_0} = 10 \log (SNR), \quad \frac{C}{N} = 10 \log (CNR)$$

Now, as δ_{rms} changes (and C/N also changes) and C/MF remains constant, the nature of the noise spectrum does not change, so that S_0/N_0 = constant. The above relation then yields a change in C/N of 12.74 dB for a change in δ_{rms} from 0.15 to 0.65, in excellent agreement with the observations of Figure 20.

We are now in a position to use the above observations and analysis to extend our acceptability threshold data to values of C/MF and δ_{rms} not covered in the measurements summarized in Figure 20. In particular, we see that we may extend the data to include C/MF = $-\infty$ (no direct LOS signal) from the results of Figure 22, and we may consider higher modulation indices by means of the above equation, taking S_0/N_0 = constant. The results of this process are depicted in Figure 23, where we have displayed acceptability threshold curves for C/MF = $-\infty$, and δ_{rms} = 0.15, 0.65, and 1.30.

The results shown in Figure 23 warrant some discussion. First, while constraints of time and money did not permit the carrying out of jury testing to confirm the acceptability thresholds predicted by the above analysis, a number of tests were run under several of the conditions indicated in the figure, and the results were recorded for individual listening by laboratory personnel. These tests indicate that the channel quality obtained in all cases is comparable to that represented by the results shown in Figure 20, i.e., the resulting speech quality is comparable to a standard telephone circuit.

A second comment has to do with the δ_{rms} = 1.30 curve. The value of δ_{rms} = 0.65 corresponds to Δf_{rms} = 2 kHz, which is the value chosen for AMPS. While doubling this figure to 4 kHz does result in some clipping of the speech waveform, this does not appear to result in noticeable distortion in the system speech output, which remains of high quality.

In summary then, the results shown in Figure 23 imply the existence of a three-way tradeoff in C/N (transmitter power), C/I (antenna and feed design), and δ_{rms} (modulation), which can provide the basis for further system evaluation by means of a cost sensitivity analysis of these three design parameters.

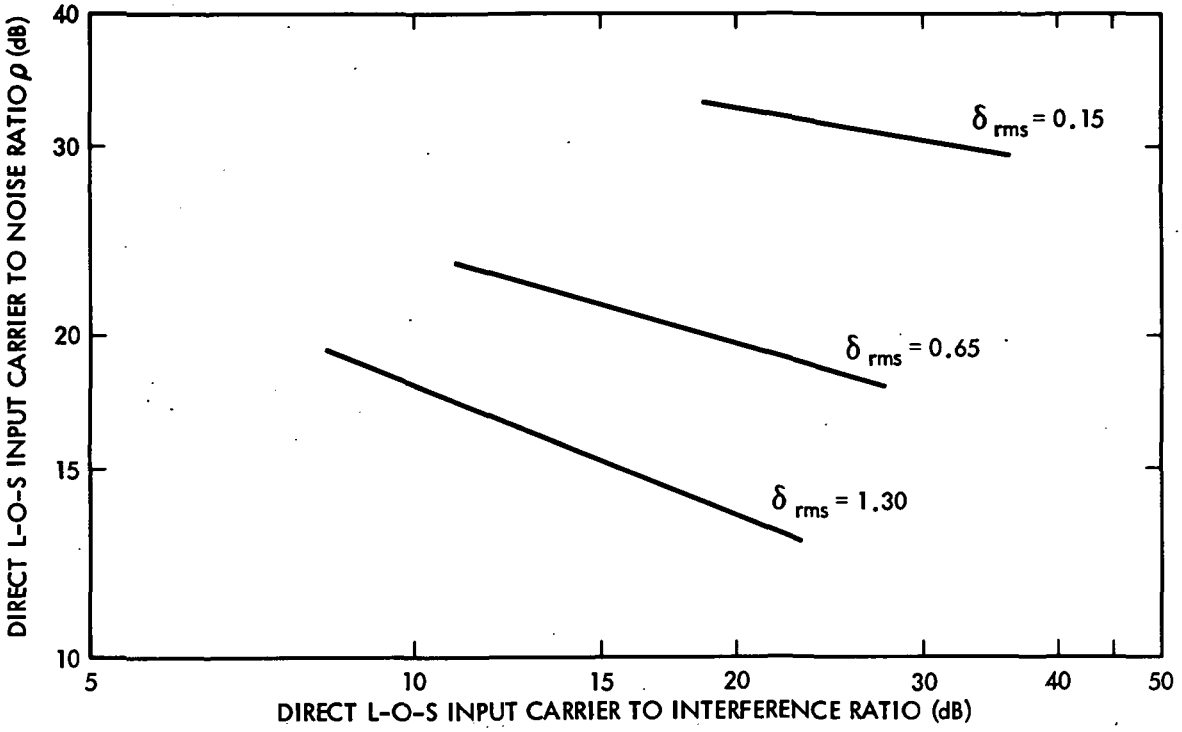

Figure 23. Acceptability Thresholds, C/MF = - ∞

SECTION 5

EXPERIMENTAL SNR MEASUREMENT RESULTS

With the LMSS channel simulator, a large number of experiments have been carried out, including the FM receiver output SNR as a function of input CNR measurements under various conditions of narrowband Gaussian noise, rapid Rayleigh fading or Rician fading, and cochannel/adjacent channel interference. In this section, the various theoretical formulas provided in Appendix C are compared with the results of the experimental measurements obtained using the measurement technique described in Appendix D. For a complete definition of the parameters, refer to Section C.3 of Appendix C.

5.1 VALUES OF THE KEY SYSTEM PARAMETERS

The LMSS channel simulator is designed to provide a facility for subjective audio evaluation of the effects of various link design parameters and constraints under simulated LMSS operating conditions. The following parameters were calculated (see Appendix B) and verified by measurements in the laboratory and from the characteristics of the channel simulator system components:

noise bandwidth of IF carrier filter $\triangleq B_{IF} = 25.19$ kHz

noise bandwidth of baseband filter $\triangleq B_m = 3.08$ kHz

$$\left(\frac{B_{IF}}{B_m}\right) \triangleq K = 8.18, \quad \delta \triangleq \left(\frac{\Delta f}{B_m}\right)$$

$$\delta_{rms} \triangleq \left(\frac{\Delta f_{rms}}{B_m}\right)$$

$$\beta \triangleq \left(\frac{\Delta f}{f_m}\right)$$

where Δf = peak frequency deviation, Δf_{rms} = rms frequency deviation, and f_m = frequency of pure sinusoid.

5.2 SNR VERSUS CNR IN THE NONFADING CASE

Figure 24 shows the experimentally determined curve for the receiver output SNR as a function of input CNR for a sinusoidal modulation with a $\delta = 1.79$ and $\beta = 5.52$, where the experimental curve is denoted by EX. In this case, it can be seen that Equation (C-37) derived in Appendix C by extending the output autocorrelation model totally agrees with the experimental results and is more accurate than the other models in the subthreshold region. Figure 25 shows somewhat similar results for a sinusoidal modulation with a $\delta = 0.2$ and $\beta = 2.4$. Furthermore, Figure 26 shows the experimental and theoretical results obtained for a Gaussian process modulation with a $\delta_{rms} = 0.49$. Again, Equation (C-43) derived for Gaussian process modulation by extending the output autocorrelation model is more accurate than the other models in the subthreshold region. In Appendix D, Section D.2, it is shown that the measured SNR may be very slightly higher than theoretical predictions (i.e., 0.2 to 0.3 dB) because of the distortion components included in the signal output.

A simple expression (Ref. 9) has been obtained for a value of $\rho \triangleq$ CNR at threshold by approximating the results provided in Ref. C-5, , Equations (C-44) and (C-45); this expression is:

$$\rho_{dB,threshold} = 6.64 + 12.9 \log_{10} B_{IF} - 2.9 \log_{10} B_m$$

where, for values of $B_{IF} = 25.19$ kHz and $B_m = 3.08$ kHz, we obtain

$$\rho_{dB,threshold} = 53.3 \text{ (dB)}$$

where, from Figures 24, 25, and 26, it is clearly seen that the value of ρ at FM threshold is about 9 dB.

It should be noted that in presentation of the results reported in Refs. C-2 and C-5, the signal-suppression factor, $(1 - \exp(-\rho))^2$, was added to their results as can be seen from Equations (C-26), (C-44), and (C-45). Figures 24, 25 and 26 show that if the signal-suppression factor was not added to Equations (C-26), (C-44), and (C-45), then the theoretical results provided by the zero-crossing model and the simple formula would have been more inaccurate as compared with the experimental results in the FM subthreshold region. Therefore, it is again verified that the Rice's clicks theory is inaccurate in the FM subthreshold region; the formulas (C-37) and (C-43) derived in Appendix C of this report by extending the output autocorrelation function model are most accurate for determination of the FM threshold.

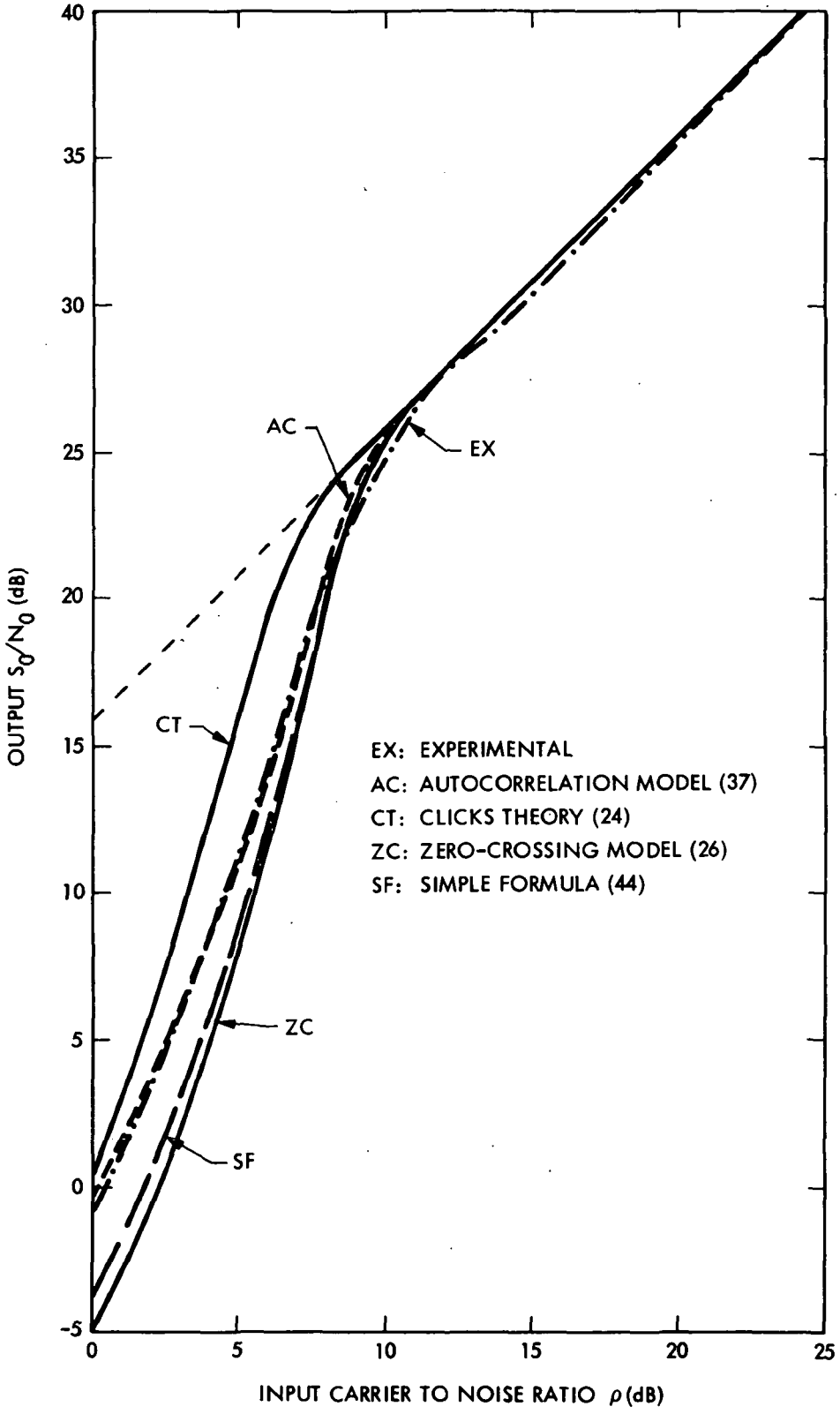

Figure 24. Output SNR for a Sinusoidal Modulation with $\delta = 1.79$ and $\beta = 5.52$. (The numbers inside the parenthesis denote the corresponding equation numbers in Appendix C)

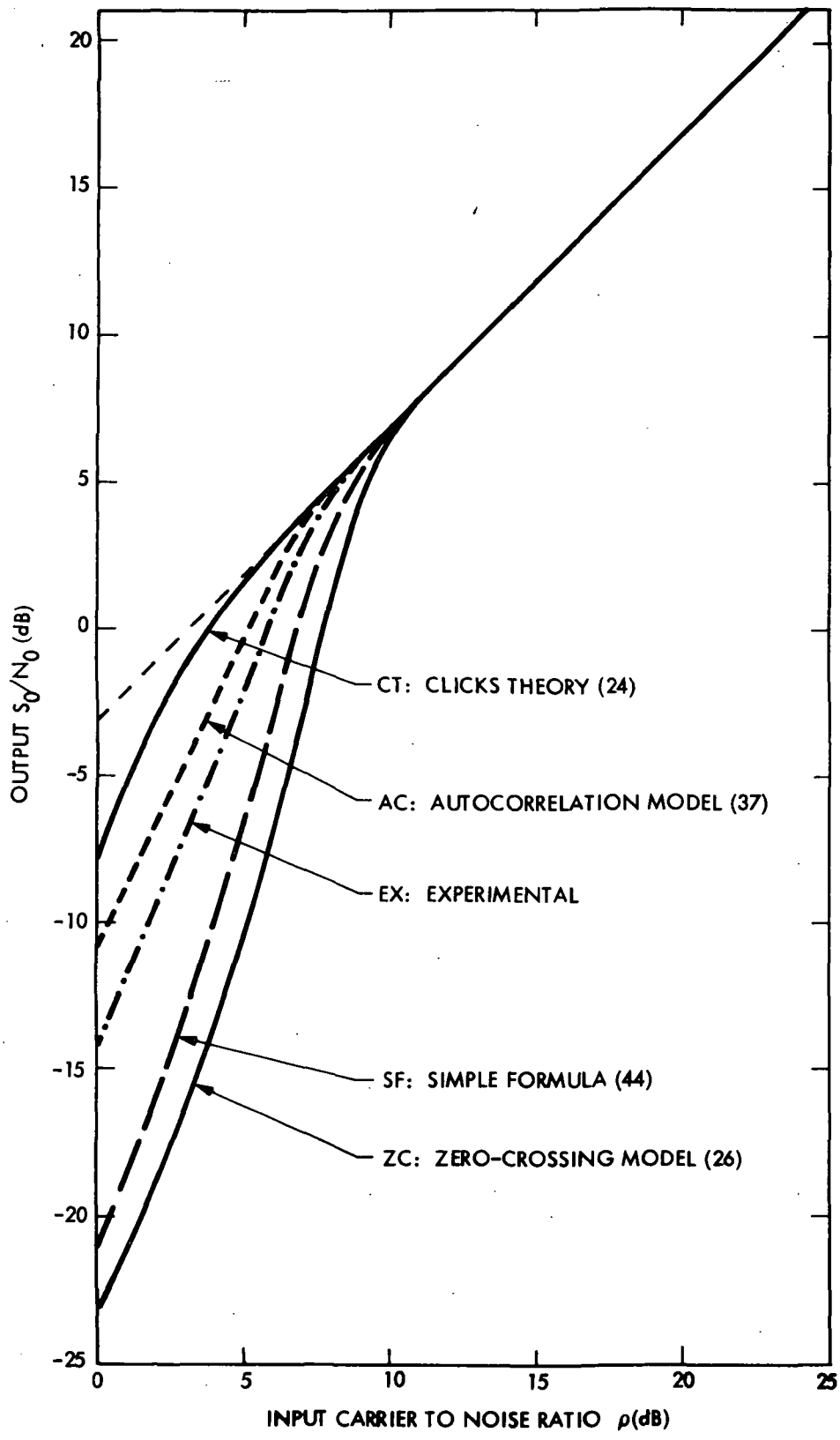

Figure 25. Output SNR for a Sinusoidal Modulation with $\delta = 0.2$ and $\beta = 2.4$. (The numbers inside the parenthesis denote the corresponding equation numbers in Appendix C)

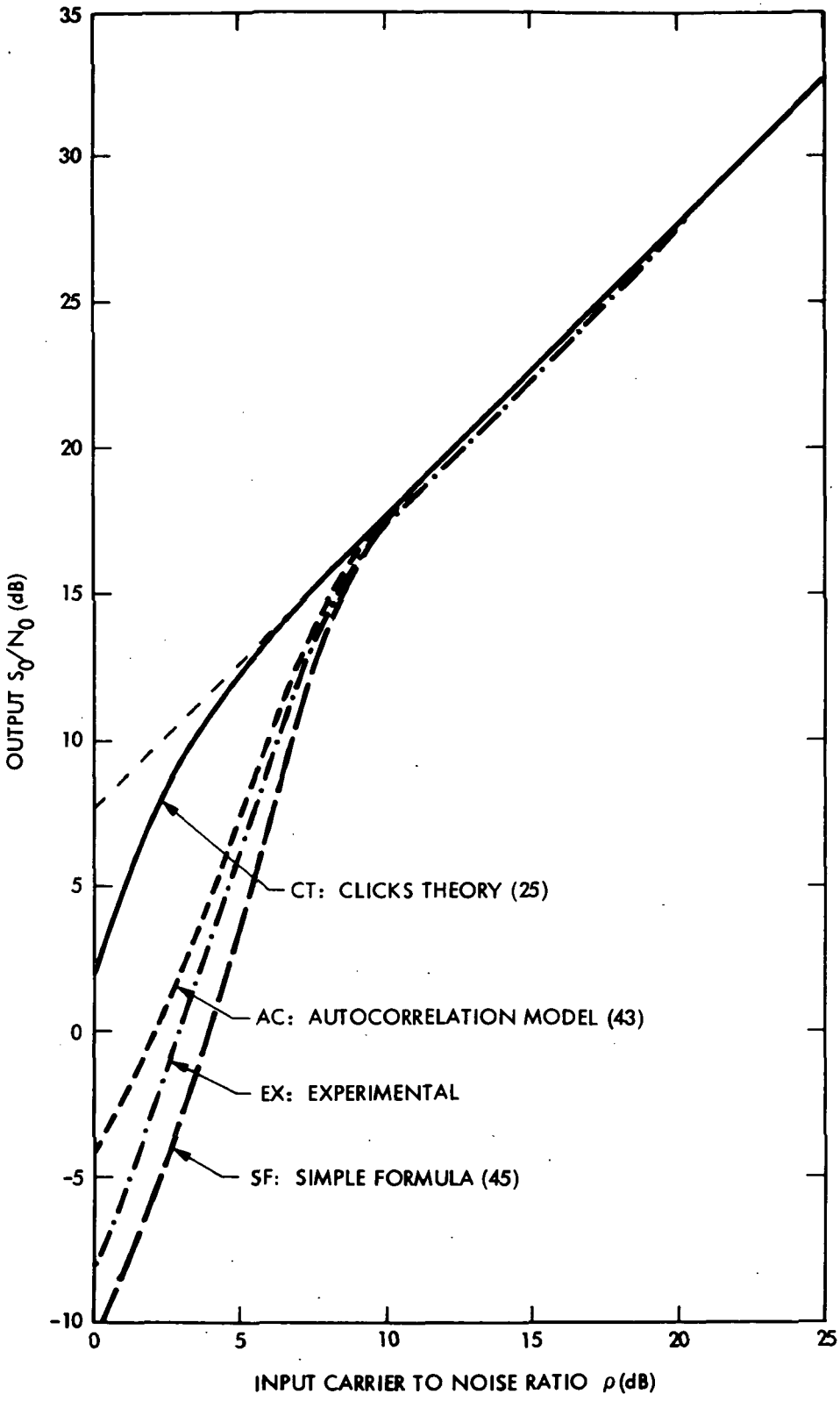

Figure 26. Output SNR for a Gaussian Modulation with $\delta_{rms} = 0.49$. (The numbers inside the parenthesis denote the corresponding equation numbers in Appendix C)

5.3 SNR VERSUS CNR IN THE RAPID RAYLEIGH FADING CASE

Figure 27 shows the experimental results obtained for the receiver output SNR, as a function of input CNR, for a Gaussian process modulation with a $\delta_{rms} = 0.49$, a vehicle speed of 55 mph and different values of carrier-to-multipath fading ratio, C/MF, where the carrier is the satellite direct LOS signal present at the mobile antenna. It should be noted that the curve shown for the case of $(C/MF)_{EX} = \infty$, where infinity denotes the fact of no multipath fading signal being present, is the same as the experimental results shown in Figure 26. Furthermore, the curves for the cases of $(C/MF)_{EX} = -\infty$ and $(C/MF)_{Theo.} = -\infty$, where minus infinity denotes the fact of no satellite direct LOS signal being present, are shown as a function of input ρ_0 meaning that the carrier is the multipath fading signal present at the mobile antenna. To the author's knowledge, there are no theoretical results available for the case of a satellite direct LOS signal plus a rapid Rayleigh fading signal; in Figure 27, the theoretical results shown (curve of $(C/MF)_{Theo.} = -\infty$) are for the case of rapid Rayleigh multipath fading signal present which was obtained by using Equations (C-51) and (C-52).

From Figure 27, it can be seen that the theoretical results, $\overline{S}/\overline{N}$, provided by (C-51) and (C-52) is mostly inaccurate as compared with the experimental results. However, it is further observed that the accuracy of the theoretically calculated $\overline{S}/\overline{N}$ is somewhat acceptable for values of ρ_0 about the FM threshold, which is observed only for large values of C/MF. Nevertheless, experimental results verify the theoretically predicted fact that rapid Rayleigh fading alters the output SNR performance, which is seen to wash out the sharp FM threshold and destroy the capture properties of FM.

5.4 DISCUSSION OF SNR MEASUREMENT RESULTS FOR THE RICIAN FADING CASE

In this section, the SNR measurements for the case of direct LOS signal plus rapid Rayleigh faded signal, which provides a Rician faded signal, are presented.

In Figure 27, it is of interest to note that for small values of C/MF, $(C/MF) \leq 0$ dB, the output SNR is well predicted by the output SNR values obtained for the case of no direct LOS signal or $(C/MF) = -\infty$. Similarly, for large values of C/MF, $(C/MF) \geq 20$ dB, the output SNR is well predicted by the output SNR values obtained for the case of no multipath fading signal or $(C/MF) = \infty$. Therefore, for C/MF greater than 20 dB, formulas (C-37) and (C-43) can be used to predict the FM receiver output SNR. Figures 28 through 37 show similar types of results.

Figure 28 shows that in the absence of emphasis filtering and companding, the FM receiver output SNR is exactly the same for voice and Gaussian modulations. Figure 29 shows the noise reduction properties of emphasis filtering and companding for voice modulation as opposed to Gaussian modulation, which, in this case, is as high as 10 dB. This effect is expected, as explained earlier in Section 3 and Appendix E, since the emphasis filtering and companding takes advantage of the special shape of the voice spectrum to suppress channel white noise at the receiver. Figure 30 shows that cochannel interference creates a smoother curve around the FM threshold region and has a washout effect on the sharp FM threshold similar to the effects of rapid Rayleigh fading. Furthermore, it shows a 5-dB increase in receiver output SNR for a 10-dB increase in C/I around the FM threshold region

which is of interest. Figure 31 shows the same type of results presented in Figure 27 with the effects of emphasis filtering and companding included. In both Figures 31 and 27, trends are similar; however, comparing the figures, increases of up to 12 dB in output SNR are noticeable due to the effects of emphasis filtering and companding for voice modulation even in the presence of multipath fading. Figure 32 shows that the combined effects of emphasis filtering and companding on output SNR for voice modulation in the presence of multipath fading would be on the order of a 10-dB increase. Figure 33 depicts probably the most important results in terms of the validity of Gaussian modulation when the effects of full signal conditioning, emphasis filtering, and companding are observed in the presence of multipath fading. Figure 33 shows that full signal conditioning has a negative effect on output SNR for a Gaussian modulation when there is no direct LOS. However, this is not true for voice modulation as will be seen in other examples. Figure 34 shows results similar to Figure 31 for a Gaussian modulation. Figure 35 shows the effects of emphasis filtering and companding, singly and in combination, on output SNR for a Gaussian modulation. It can be seen that in this case most of the 2-dB increase in the output SNR due to the combined effect comes from emphasis filtering. Figure 36 depicts the effects of emphasis filtering and companding, singly and in combination, on output SNR for a voice modulation. It can be seen that the 10-dB increase in output SNR due to the combined effect is equally attributable to emphasis filtering and companding. Figure 37 shows also that half of the 10-dB difference in output SNR between Gaussian modulation and voice modulation shown in Figure 29 is attributable to emphasis filtering (also see Figure 28).

In this section, the important contributions of full signal conditioning, emphasis filtering, and companding for voice modulation in the presence of multipath fading has been shown. Further, it is shown that in laboratory experiments, Gaussian modulation should not be a direct substitute for voice modulation, especially when signal conditioning is used and other types of impairments besides channel noise are present.

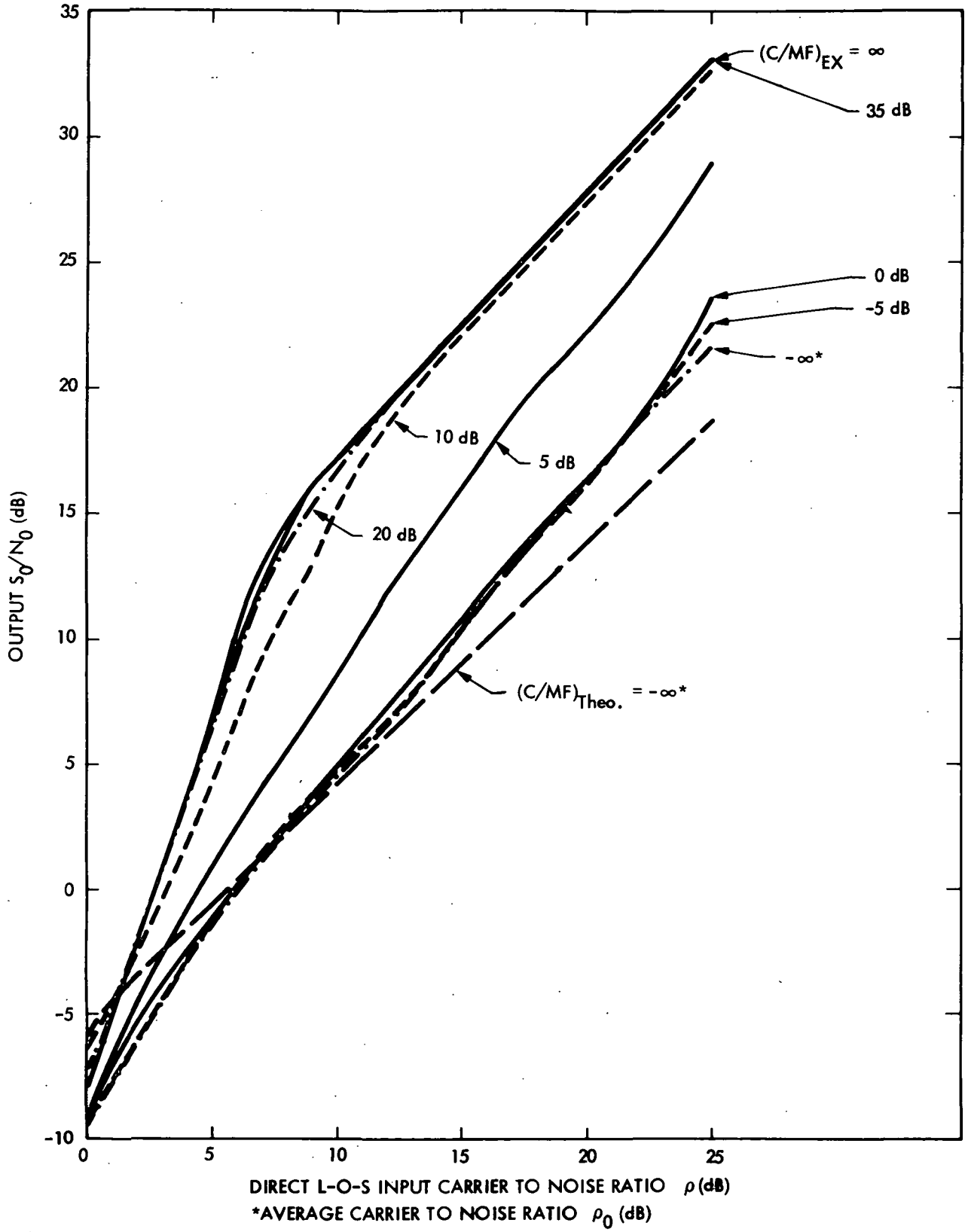

Figure 27. Experimental Output SNR for a Gaussian Modulation with $\delta_{rms} = 0.49$ and Various Values of $(C/MF)_{EX}$ (Rician Fading)

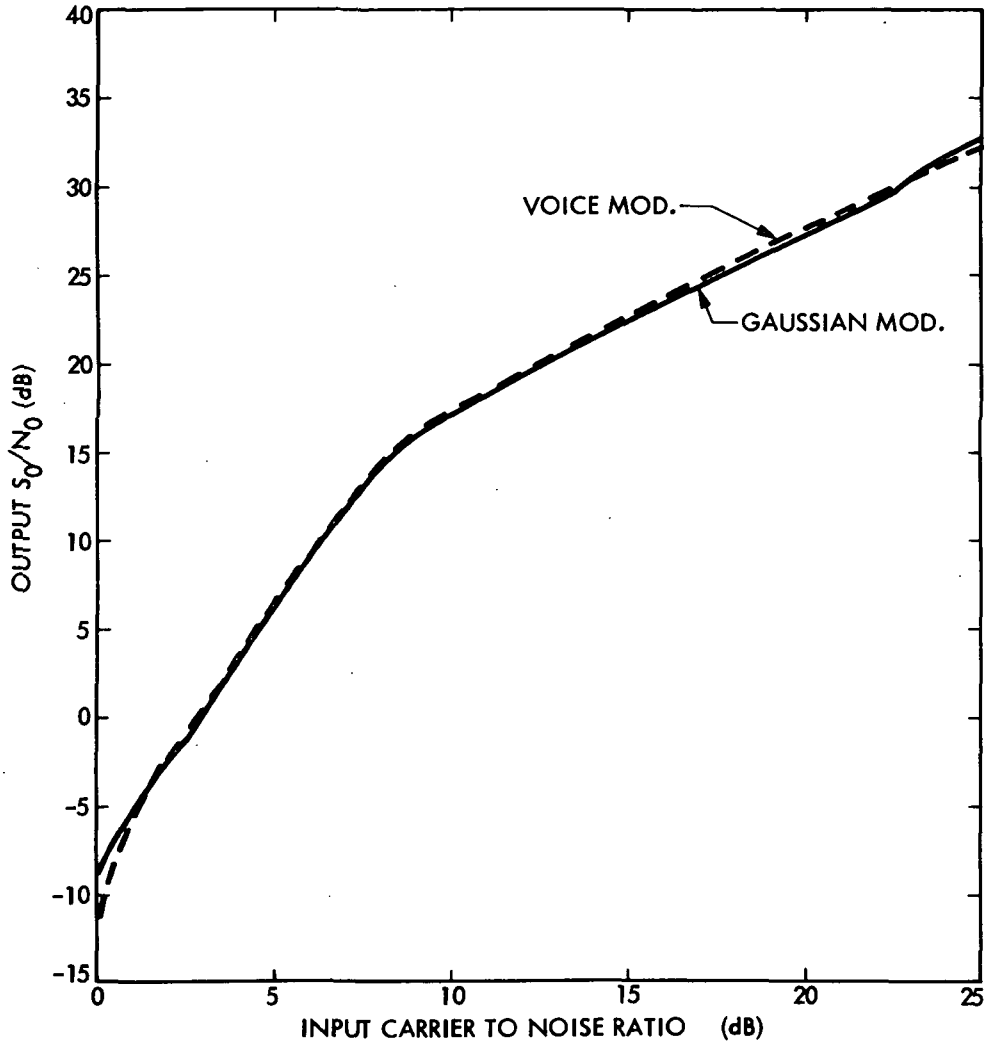

Figure 28. Output SNR for a Gaussian Modulation and a Voice Modulation with $\delta_{rms} = 0.49$ and no Emphasis Filtering or Companding (no multipath fading or interference)

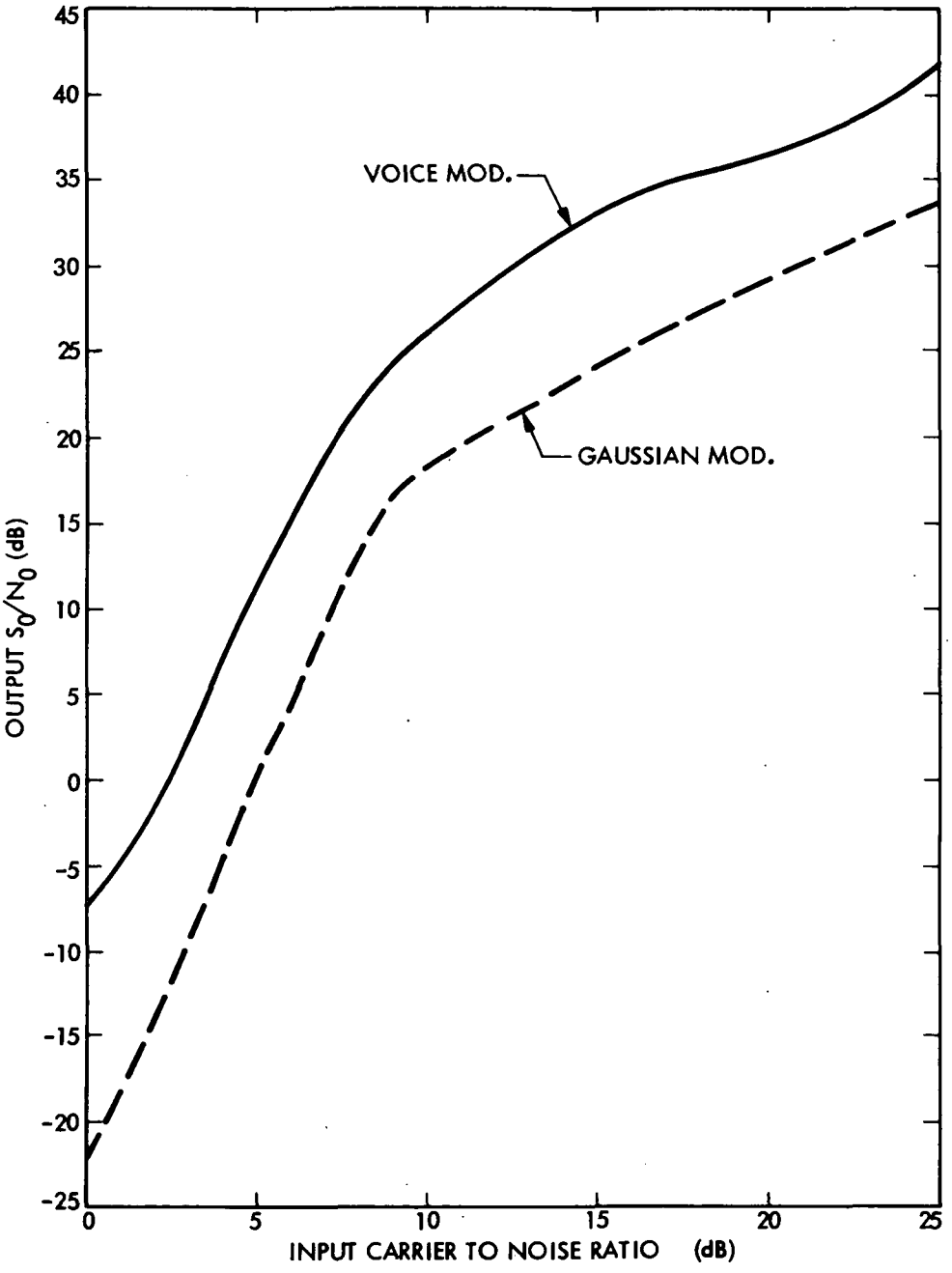

Figure 29. Output SNR for a Gaussian Modulation and a Voice Modulation with $\delta_{rms} = 0.49$ and the Effects of Emphasis Filtering and Companding Included (no multipath fading or interference)

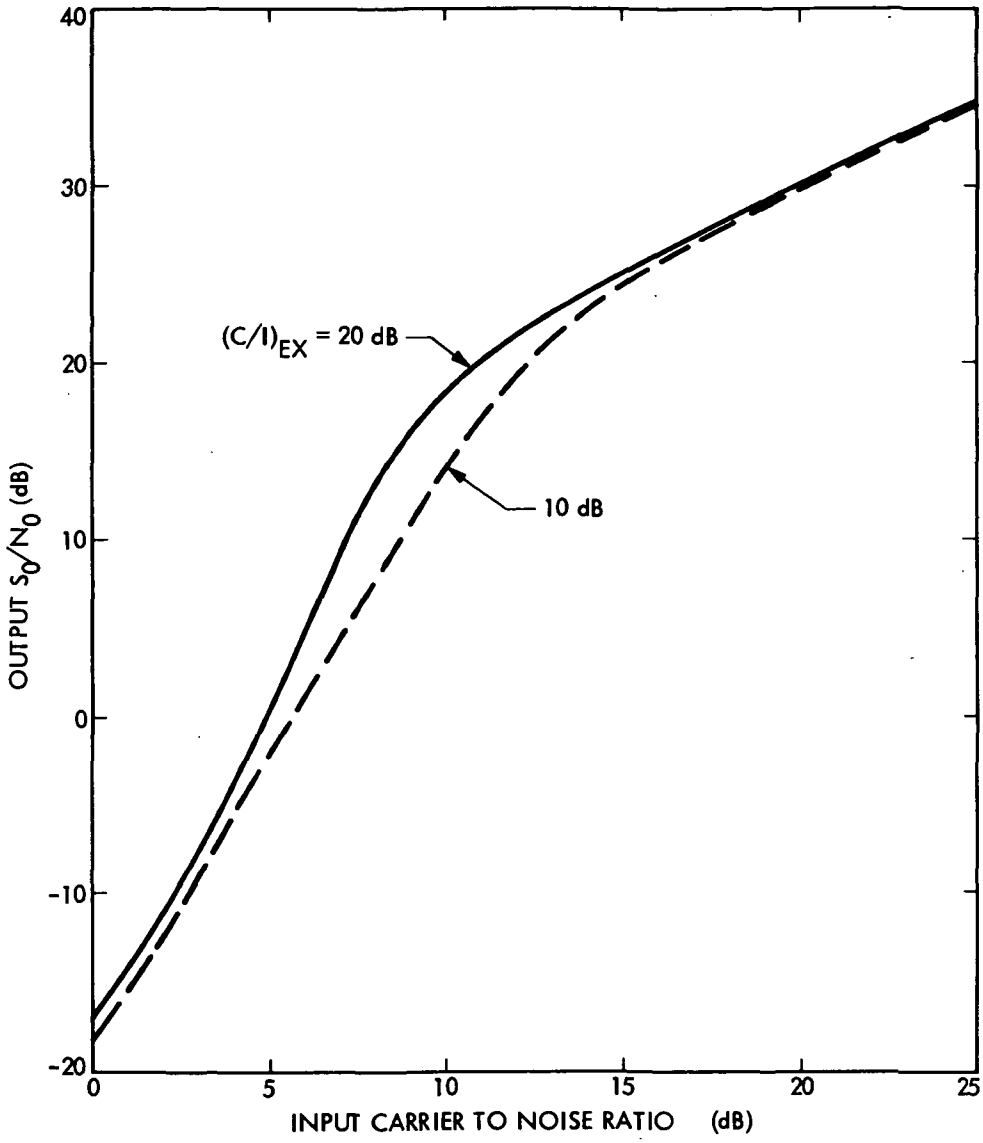

Figure 30. Output SNR for a Gaussian Modulation with $\delta_{rms} = 0.49$ and Different Values of (C/I) (no multipath fading)

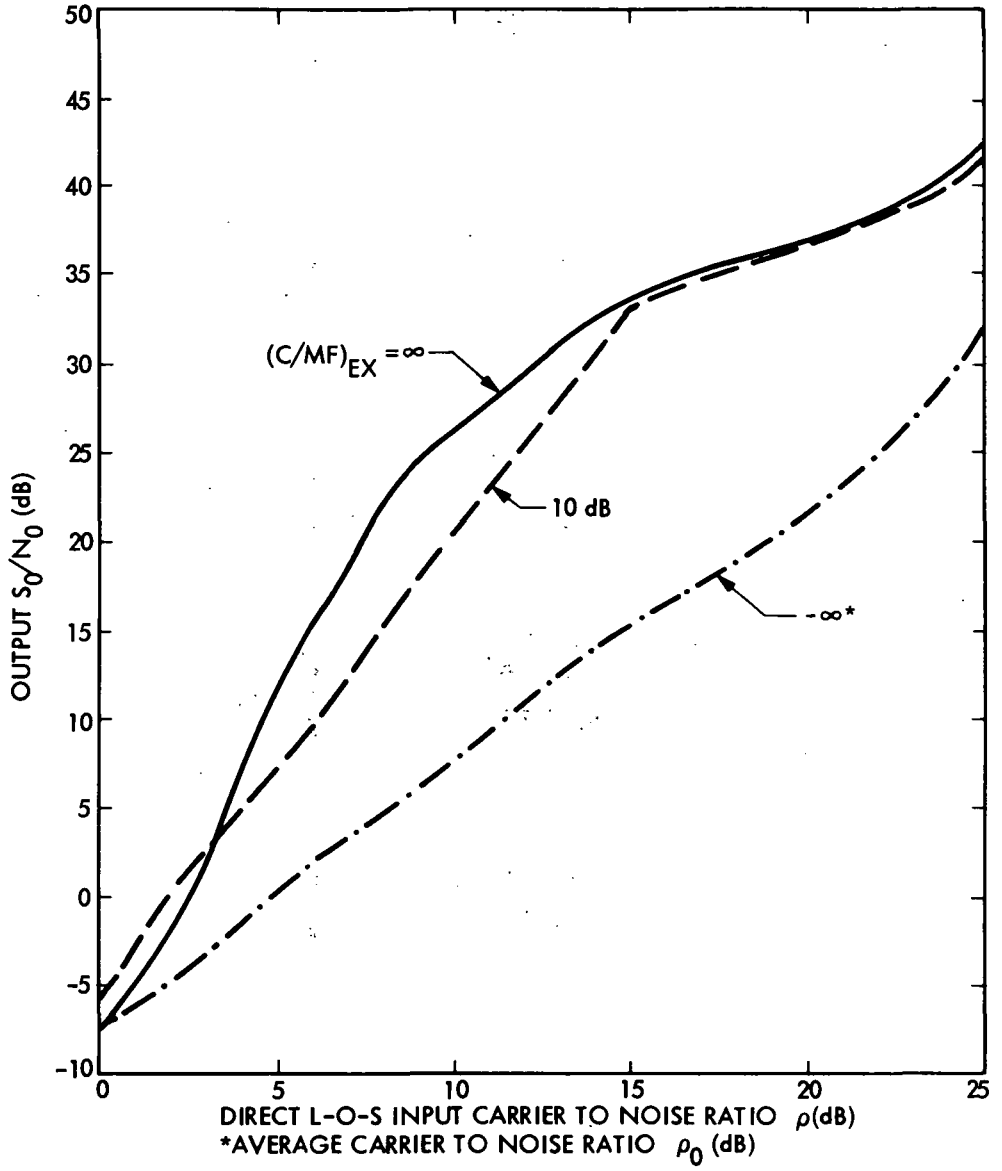

Figure 31. Output SNR for a Voice Modulation with $\delta_{rms} = 0.49$ and Effects of Emphasis Filtering and Companding Included (no interference)

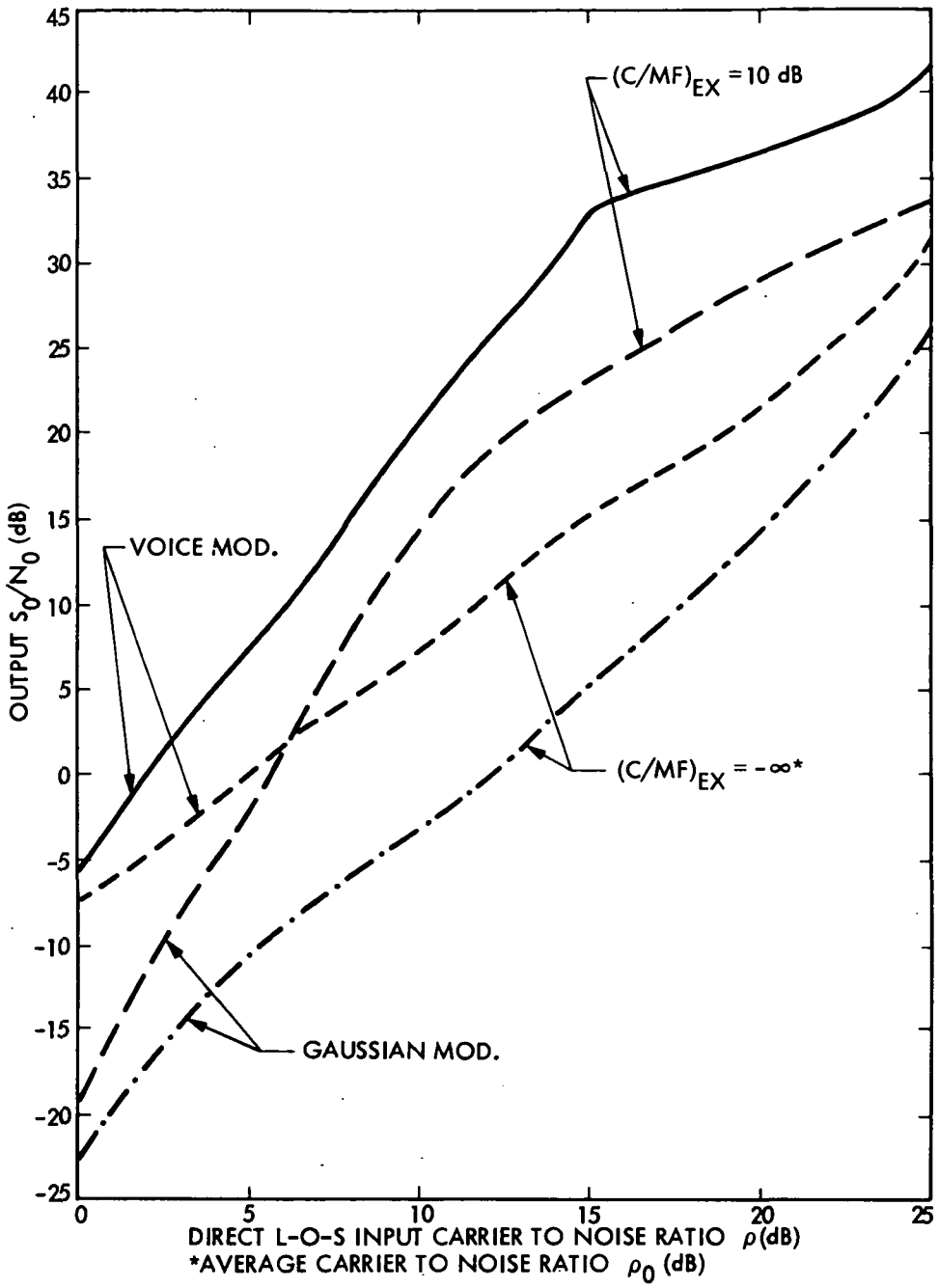

Figure 32. Comparison of Output SNR for a Gaussian Modulation and a Voice Modulation With δ_{rms} = 0.49 and the Effects of Emphasis Filtering and Companding Included (no interference)

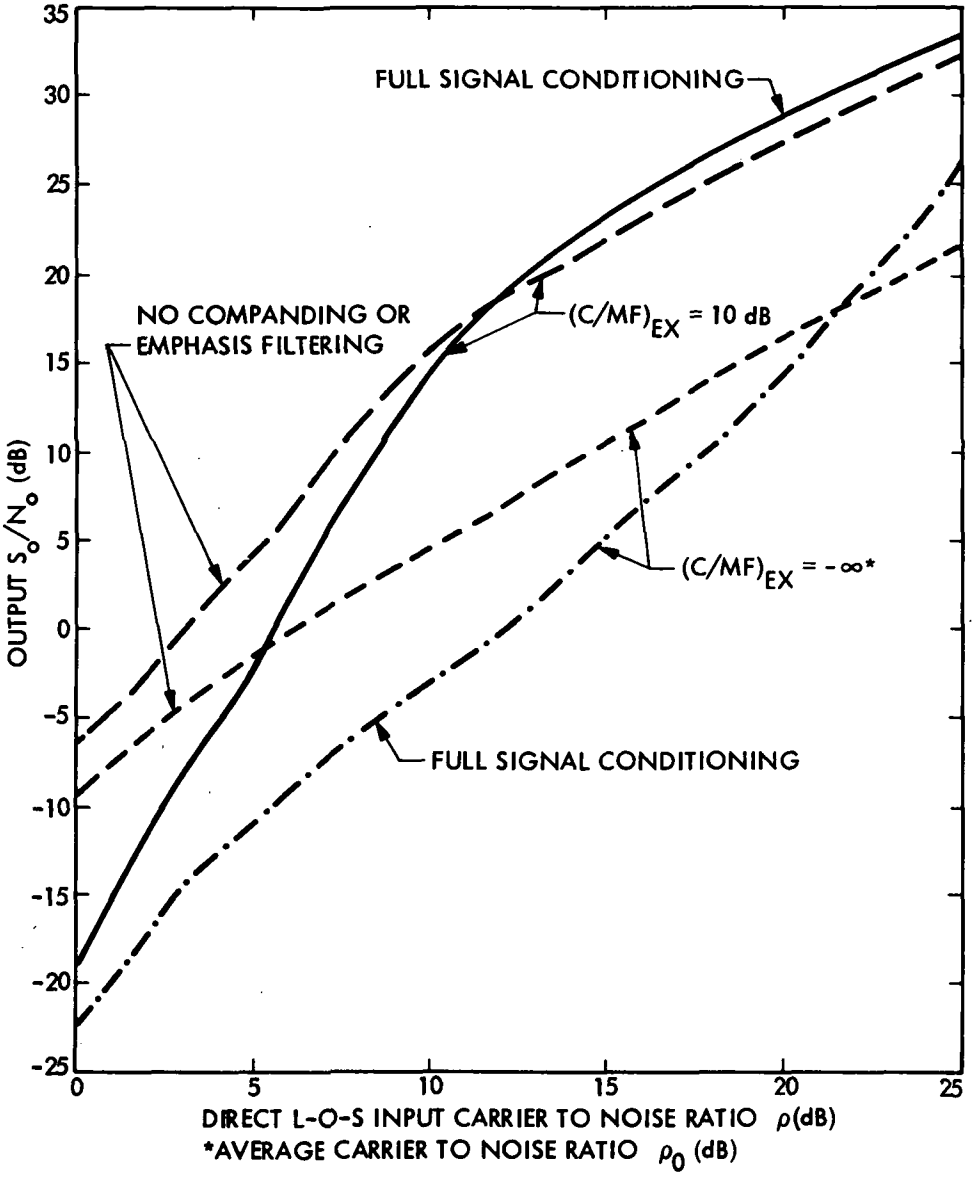

Figure 33. Output SNR for a Gaussian Modulation with $\delta_{rms} = 0.49$ (no interference)

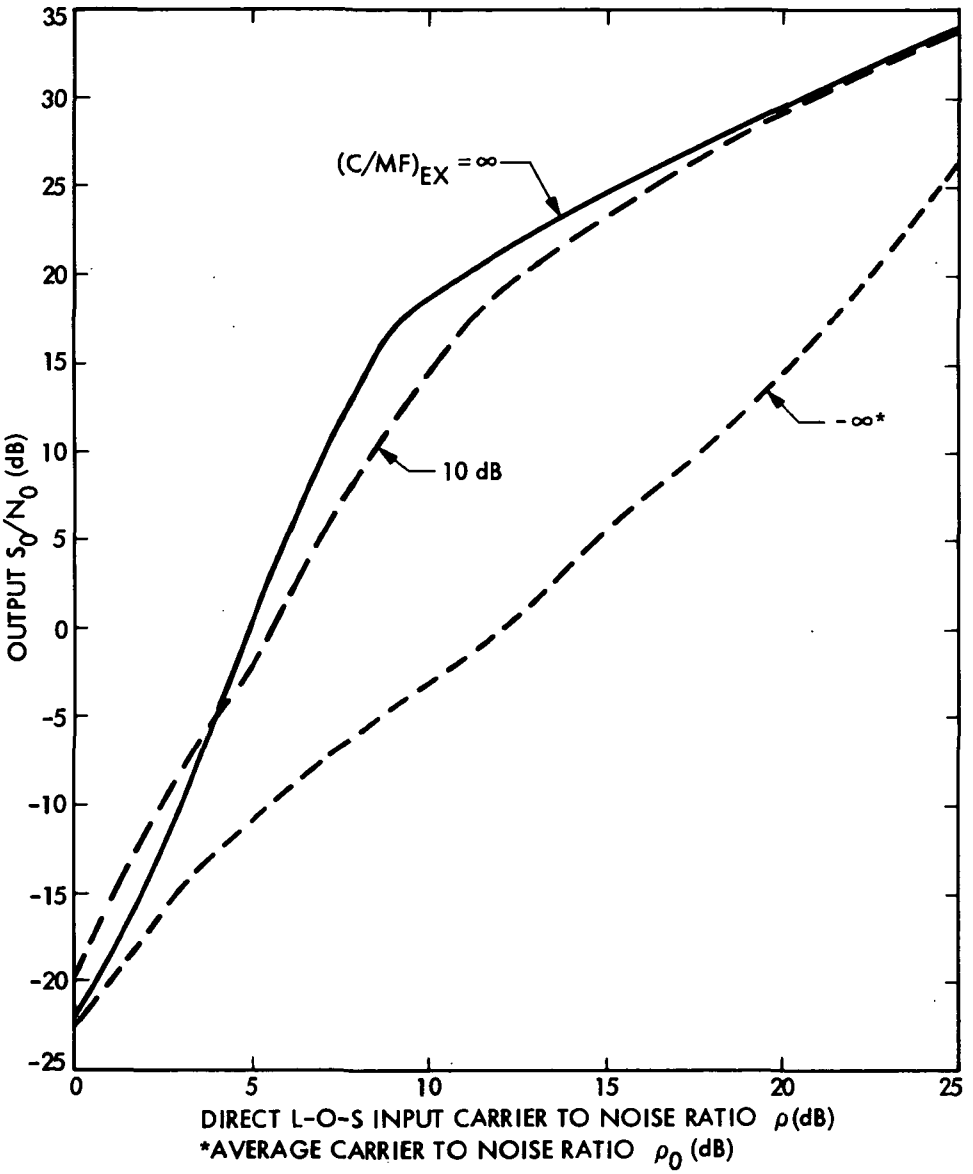

Figure 34. Output SNR for a Gaussian Modulation With $\delta_{rms} = 0.49$ and the Effects of Emphasis Filtering and Companding Included (no interference)

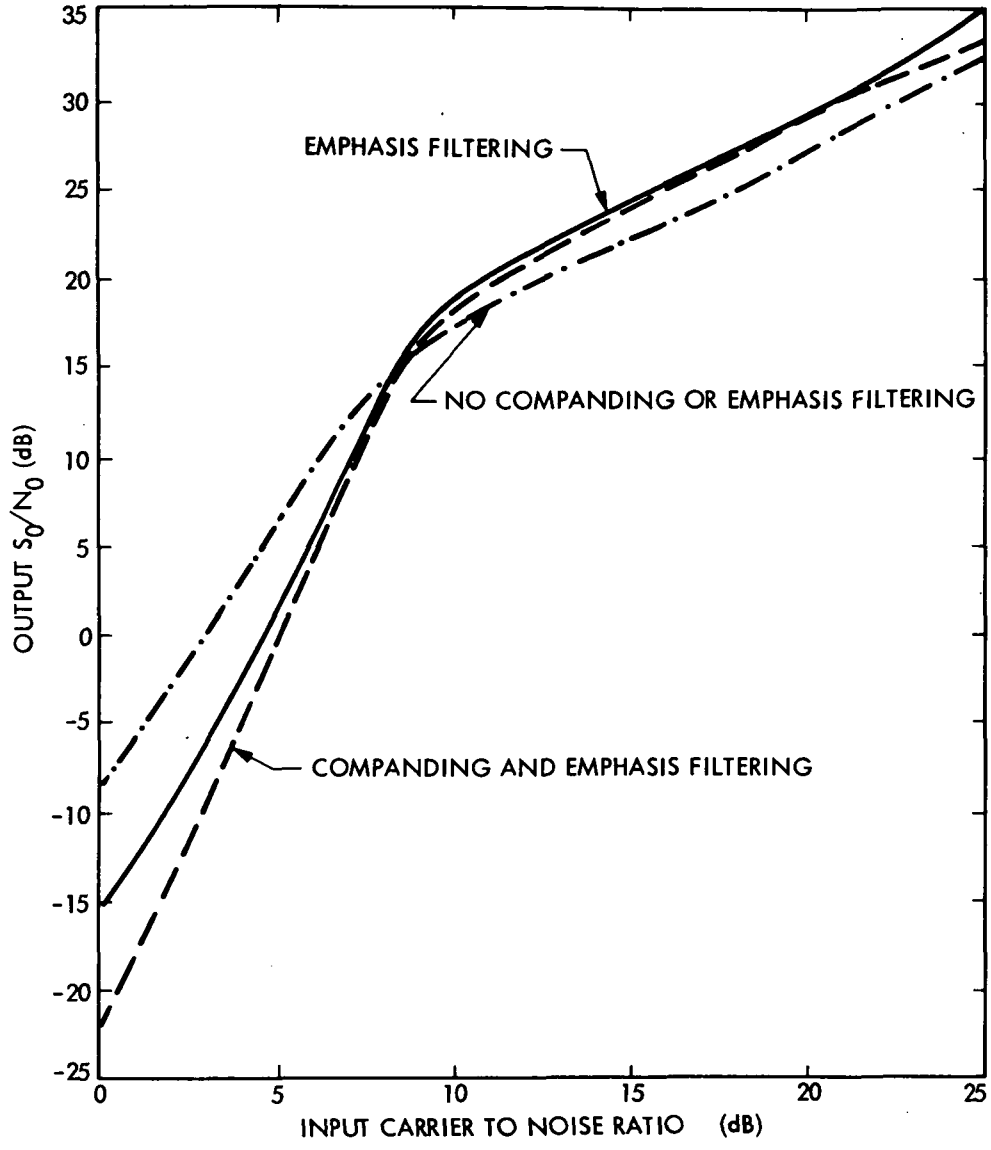

Figure 35. Output SNR for a Gaussian Modulation With δ_{rms} = 0.49 (no multipath fading or interference)

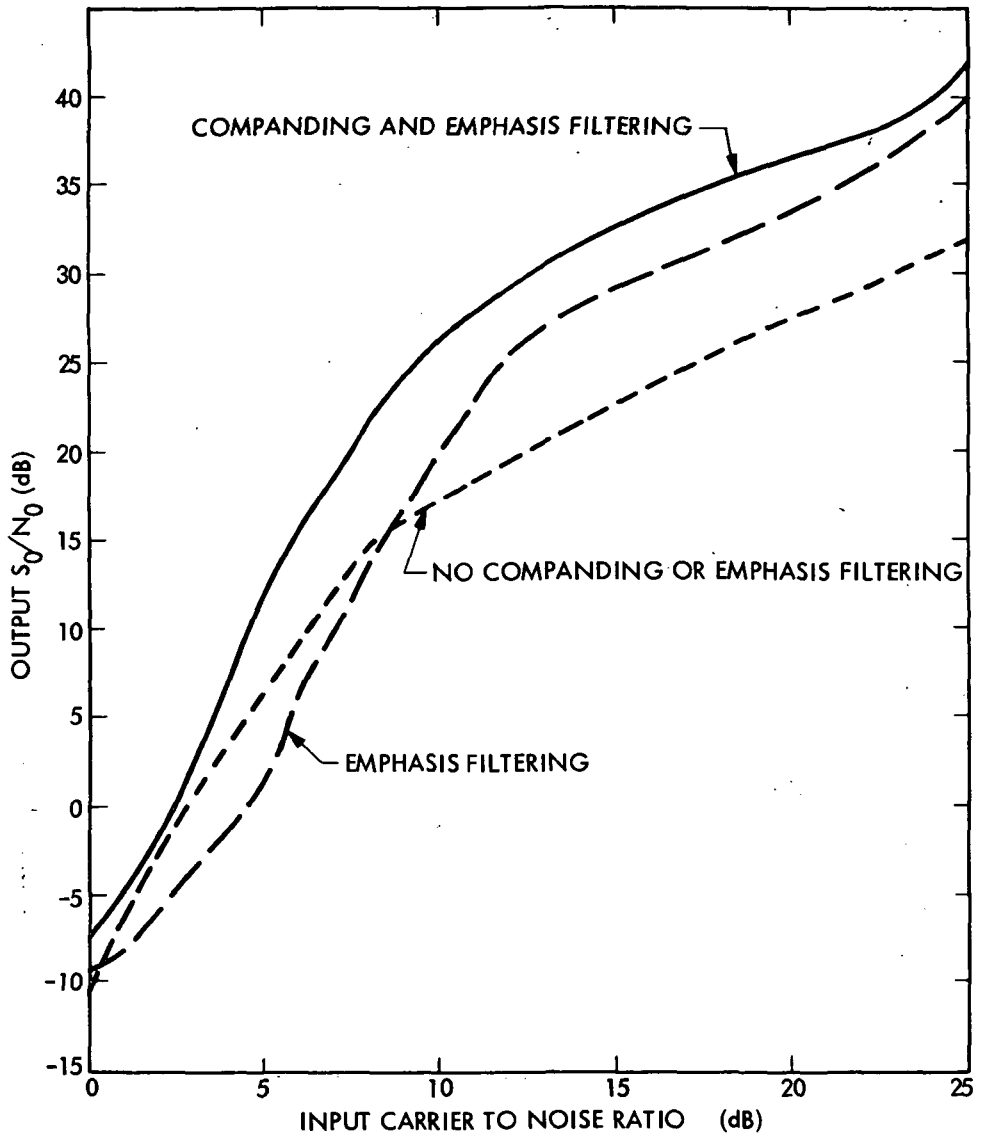

Figure 36. Output SNR for a Voice Modulation With $\delta_{rms} = 0.49$ (no multipath fading or interference)

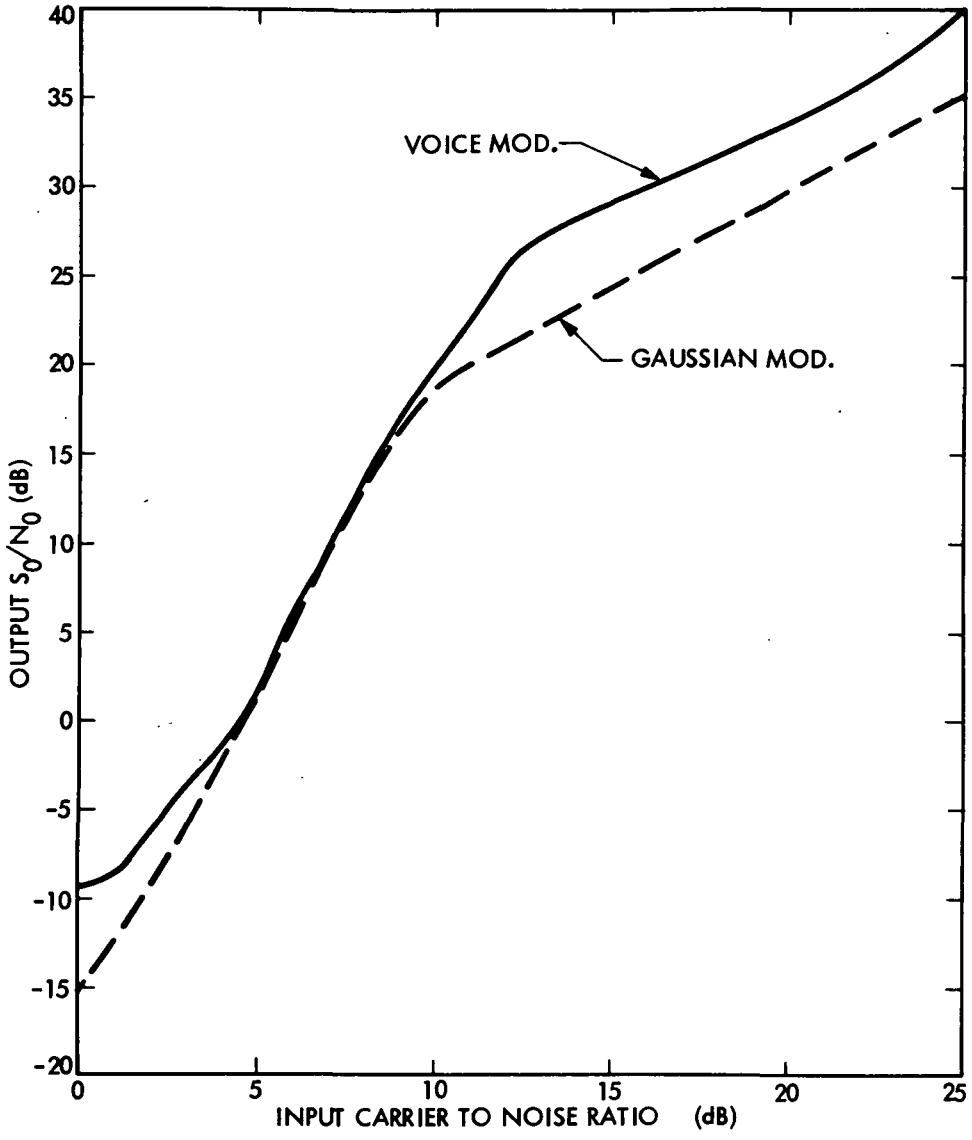

Figure 37. Output SNR for a Gaussian Modulation and a Voice Modulation with $\delta_{rms} = 0.49$ and the Effects of Emphasis Filtering Included (no multipath fading or interference)

SECTION 6

REFERENCES

1. Land Mobile Satellite Service (LMSS): A Conceptual System Design and Identification of the Critical Technologies, F. Naderi, editor. Pulication No. 82-19, Jet Propulsion Laboratory, Pasadena, California, Feburuary 15, 1982.

2. Arrendondo, G. A., Feggeler, J.C., Smith, J. I., "Advanced Mobile Phone Service: Voice and Data Transmission", B.S.T.J., Vol. 58, No. 1, January 1979, pp. 97-122.

3. Salmasi, A. B., A Parametric Analysis of Performance Characteristics of Satellite-Borne Multiple-Beam Antennas, Publication No. 80-52, Jet Propulsion Laboratory, Pasadena, California, March 15, 1982.

4. Arrendondo, G. A., Chriss, W. H., and Walker, E. H., "A Multipath Fading Simulator for Mobile Radio," IEEE Trans. Veh. Tech., Vol. VT-22, No. 4, November 1973.

5. Criteria for Permissible Ambient Noise During Audiometric Testing, ANSI S3.1, Table C1, p-7, 1977. American National Standards Institute, Inc., New York, New York.

6. Method for The Measurement of Monosyllabic Word Intelligibility, ANSI S3.2, 1960 (R1971). American National Standards Institute, Inc., New York, New York.

7. Methods for the Calculation of the Articulation Index, ANSI S3.5, 1969. American National Standards Institute, Inc., New York, New York.

8. A collection of tapes entitled A Diagnostic Acceptability Measure (DAM) for a Speech System. Dynastat, Inc., Austin, Texas.

9. Boudreau, P. M., and Davies, N. G., "Modulation and Speech Processing for Single Channel Per Carrier Satellite Communications," Record of the 1971 IEEE International Conference on Communications, 71C28-COM, pp. 19-9 to 19-15.

APPENDICES

APPENDIX A

CONSIDERATIONS FOR AUDIO EVALUATION STUDIES

A.1 ARTICULATION - BASEBAND SIGNAL-TO-NOISE RATIO RELATION

The relationship between such system parameters as C/N, C/I, and C/MF on the one hand and intelligibility scores on the other can be arrived at by a three-step procedure. First, the baseband signal-to-noise ratio S_0/N_0 is obtained as a function of the above parameters, singly and in combination, either on the basis of theoretical considerations or direct measurements on the system. In the second step the relationship between S_0/N_0 and the system Articulation Index (AI) is established by calculating each of these parameters for the particular noise spectrum associated with each type of interference, i.e., RF noise, cochannel interference, and multipath fading. Finally, the correlation between AI and intelligibility scores for the particular type of articulation tests and test conditions used is combined with the above to obtain relationships between C/N, C/I, and C/MF, and intelligibility scores.

The above procedure finds application in making direct comparisons with intelligibility scores measured as a function of C/N, C/I, and C/MF, and provides insight into the functioning of the overall system so that the results of subjective audio evaluation can be understood in terms of system performance.

An example of the procedure is shown in the following, and use is made of the results to illustrate some general features of the subjective evaluations described in Section 4.3.

We begin with the S_0/N_0 vs C/N results shown in Figure A-1. These are analogous to those shown in Figure 22 of Section 4, the difference being that here $\delta = 0.2$ ($\delta_{rms} = 0.14$) so that comparison can be made with the intelligibility test results, for which $\delta_{rms} = 0.15$ (see Figure 16, Section 4).

Figure A-2 shows the four audio output spectral density curves required for calculating both S_0/N_0 and AI for the three types of interference considered, and hence for determining the requisite relationship between S_0/N_0 and AI. The top curve represents the average speech spectrum, and the remaining three curves the three types of baseband noise spectra associated with C/N, C/I, and C/MF. Note that the cochannel interference spectrum matches the speech spectrum. The RF noise spectrum (C/N) has the typical quadratic frequency dependence at the discriminator output, increasing 6 dB/octave. However, this is subsequently modified by the de-emphasis network which superimposes a 6 dB/octave decrease, resulting in the essentially flat spectrum shown. Similarly, for large amounts of fading the baseband noise spectrum at the discriminator is essentially flat (frequent "click" noise), so that after passing through the de-emphasis network it decreases at 6 dB/octave as shown. Also shown in Figure A-2 is the threshold of hearing curve.

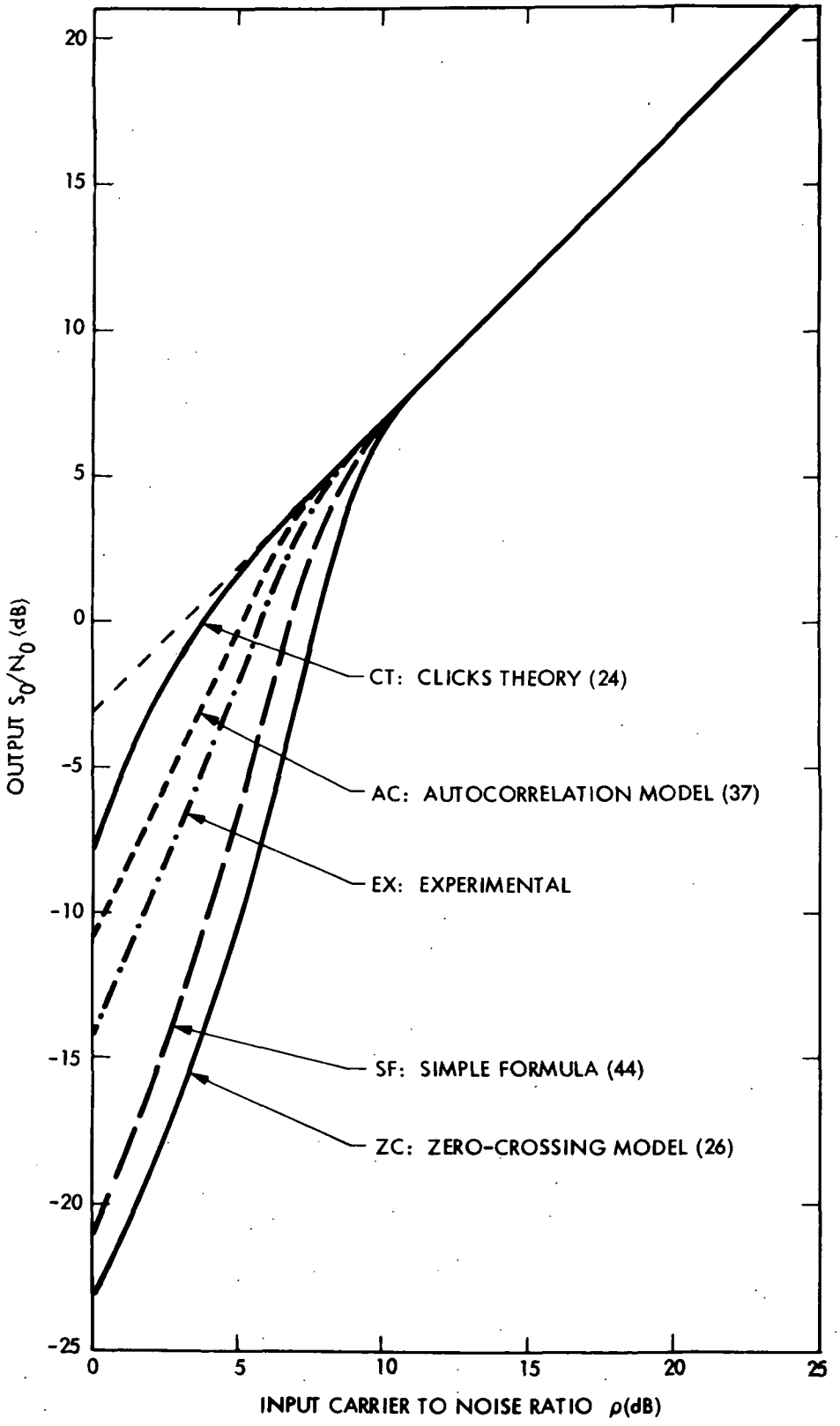

Figure A-1. S_0/N_0 vs C/N Results for a $\delta_{rms} = 0.2$ and $\beta = 2.4$, which is used for comparison purposes with the intelligibility test results

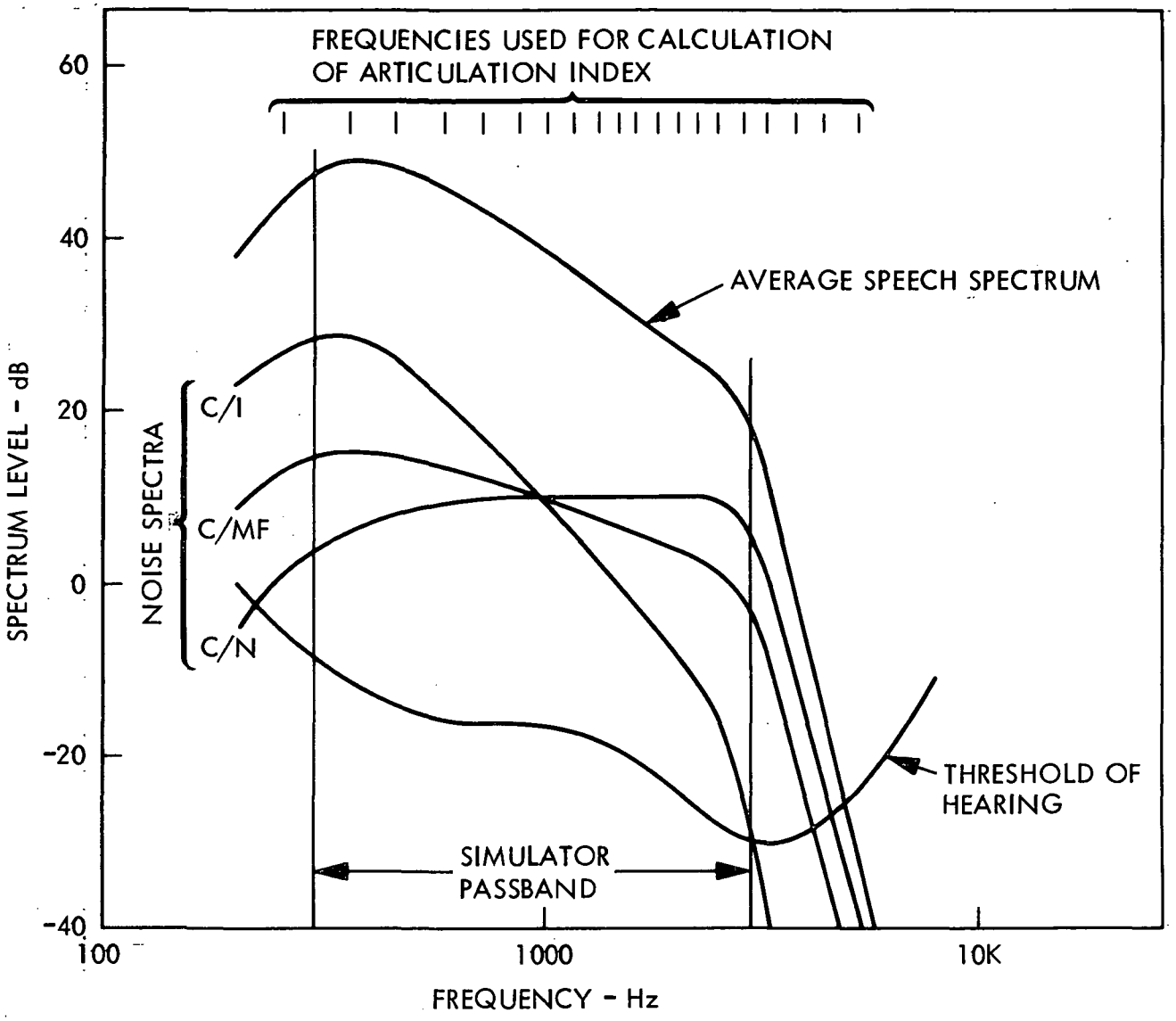

Figure A-2. Calculation of S_0/N_0 and AI

The three noise spectra illustrate the spectral shapes involved in the S_0/N_0 and AI calculations. The relationship between S_0/N_0 and AI for a given type of interference is determined by raising and lowering the corresponding noise spectrum shown and computing S_0/N_0 and AI for each position of the curve. The calculation of S_0/N_0 involves straightforward integration of the speech and noise spectra separately, while the calculation of AI requires the calculation of S(f)/N(f) at each of the 20 frequencies shown in the figure, summing of the results and division by 600 (see Ref. 7 for details).

The results of the above calculations are shown in Figure A-3. Note the difference between the curves for the three different types of interfering noise spectra.

The final step in the procedure is contained in the results shown in Figure A-4, taken from Ref. 7, which illustrate the various correlations obtained between articulation scores and AI. As mentioned earlier, such correlation depends on the nature of the test material as well as the methods of conducting the tests and the personnel involved, so that the results shown in Figure A-3 should be taken as typical but not necessarily representative of a given set of evaluations.

Comparison of Figures A-3 and A-4, with the measured articulation scores shown in Figure 16a of Section 4, for C/MF = ∞ and C/I = ∞, using the C/N curve of Figure A-3, shows that the curve of Figure A-4 labeled "Test Vocabulary Limited to 256 PB Words" provides the best fit to the measurements of Figure 16a. While the actual tests involved 1000 PB words, the fit using the 256 PB word correlation is not unreasonable given the variability expected due to the nature of the talker and method of testing. More extensive testing, providing better statistics, would have permitted a more accurate determination of the proper correlation peculiar to our own testing methods and personnel.

As a final example of the use of the relationship shown in Figure A-3, we consider the constant difference in C/N that appears between curves of different C/MF shown in Figure 20 of Section 4. For $\delta_{rms} = 0.65$, this difference amounts to 7.2 dB as one moves from the C/MF = 20 dB to the C/MF = 5 dB curve at constant C/I. As explained in the discussion of Section 4.4.3, such a change in C/N implies an increase in S_0/N_0 of approximately 2 dB, as seen from Figure 22 of Section 4.

From Figure 20, Section 4, we may infer that for large C/I, the limiting value of C/N resulting in acceptable performance with C/MF = 20 dB and $\delta_{rms} = 0.65$ is approximately 8 dB. From Figure 22 of Section 4 we see that this corresponds to S_0/N_0 = 13 dB. However, the curves of Figure 22 were obtained with $\delta_{rms} = 0.49$, and since 20 log (0.65/0.49) = 2.5 dB, the corresponding value of S_0/N_0 for $\delta_{rms} = 0.65$ is 13 + 2.5 = 15.5 dB. Referring back to Figure A-3, we see that for C/N type noise, S_0/N_0 = 15.5 dB corresponds to AI = 0.6.

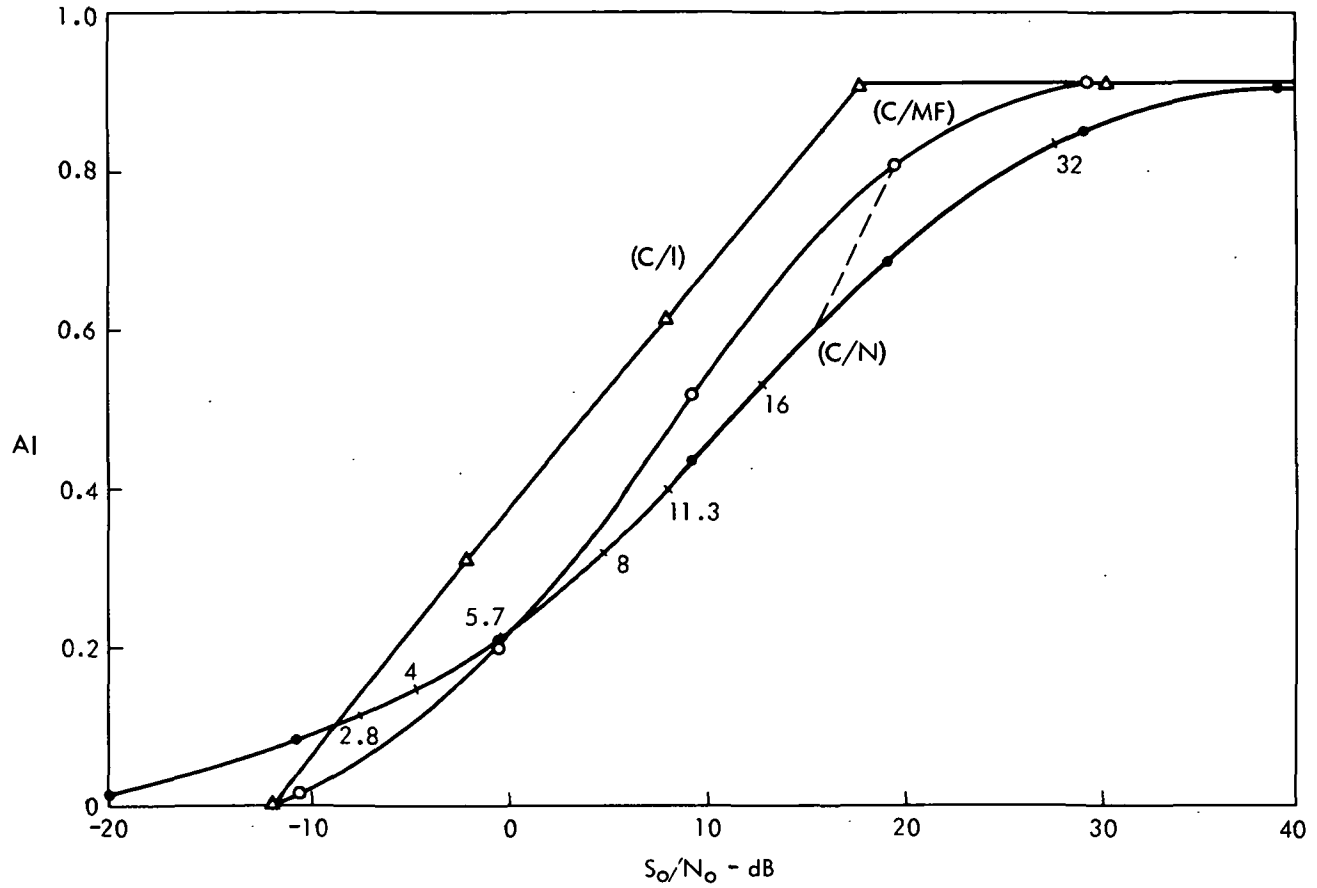

Figure A-3. Articulation Index vs Baseband Signal-to-Noise Ratio for Various Types of Interfering Noise Spectra

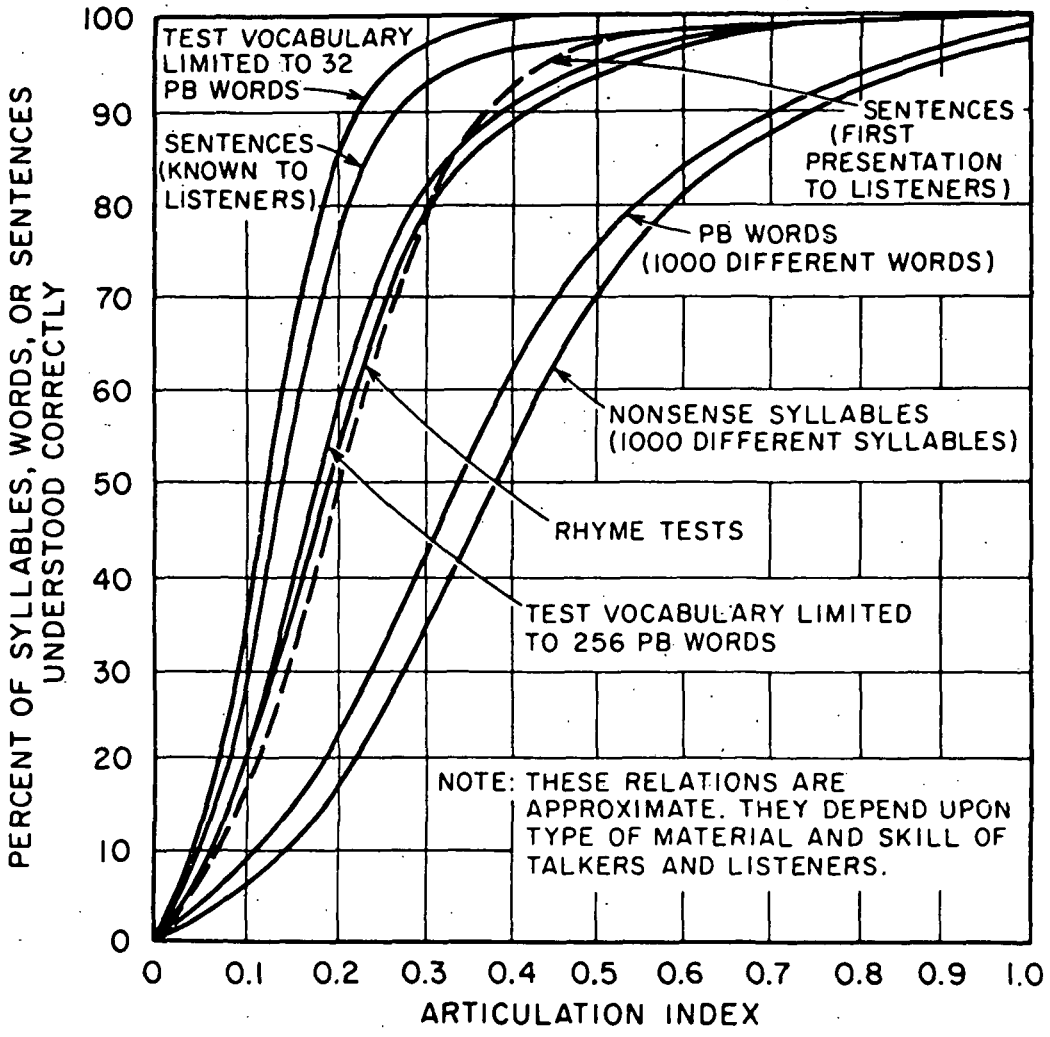

Figure A-4. Relation Between AI and Various Measures of Speech Intelligibility

If we now make the assumption that for C/N = 8 + 7.2 = 15 dB, and C/MF = 5 dB, the character of the noise is essentially white, corresponding to pure fading, then, following the line in Figure A-3 from the C/N curve at S_0/N_0 = 15.5 dB to the C/MF curve at S_0/N_0 = 15.5 + 2 = 17.5 dB, we find AI = 0.8. Referring to Figure A-4 we see that as AI varies from 0.6 to 0.8, the sentence intelligibility varies from 98% to 99%, thus verifying the observation made in Section 4.4.3 that curves of equal acceptability correspond approximately to curves of equal intelligibility.

As a final observation, we note that according to Figure 20, Section 4, the asymptotic acceptability threshold value of C/N for C/MF = 20 dB and δ_{rms} = 0.15 (C/I → ∞) is approximately 18 dB, and from Figure A-1 we see that this corresponds to S_0/N_0 = 15 dB, in good agreement with the value of 15.5 dB found above for δ_{rms} = 0.65. Thus, for the case δ_{rms} = 0.15 we find the same value of AI = 0.6 for acceptable system performance, as is expected. Also, the asymptotic acceptability threshold value of C/N for C/MF = 5 dB and δ_{rms} = 0.65 dB (C/I → ∞) is approximately 18 dB which, according to Figure 22 of Section 4, corresponds once again to S_0/N_0 = 13 dB (δ_{rms} = 0.49), giving the same corrected value of 15.5 dB for δ_{rms} = 0.65.

A.2 MEASUREMENT OF AMBIENT NOISE LEVELS IN SOUND BOOTHS

Ambient noise level measurements were made in each sound booth by means of a B&K Model 2203/1613 Precision Sound Level Meter - Octave Filter Set combination. This instrument utilizes a 2.54-cm (1-in.) precision condenser microphone, which, in conjunction with the octave band filter set, permits accurate sound level measurements (±1 dB) over the frequency range of 22 - 15,000 Hz and sound pressure levels (SPL) of 22 - 134 dB. The instrument was calibrated by Bruel and Kjaer immediately prior to use by instruments whose accuracy is traceable to the National Bureau of Standards.

Within each sound booth, measurements were made at several positions and heights, and the results averaged to yield the spectrum levels shown in Figure 12 of Section 4. In addition to the monotonic decrease in level with frequency, the data indicate a difference in levels between the two booths at higher frequencies. This is caused by the higher transmittance of the entrance door as discussed below.

Since the measured spectrum levels were higher than had been expected when the sound booths were planned, an attempt was made to determine the cause of the excess noise to see if corrective measures could be taken to reduce it. To this end transmittance measurements of various parts of the structure were made by measuring the spectrum levels at each inside and outside surface while a high-level white-noise source (∿100 dB) was emitting inside the booths. The transmittance measurements were then combined with absorption coefficient data for the various materials used in the construction of the booths to calculate the expected room attenuation spectrum on the basis of a simple model, described below. The absorption coefficients were obtained from published data from various sources, and represent the best estimate of the properties of the materials used.

The model used in the calculations is depicted in Figure A-5, where we show a sound booth partially isolated from its surroundings by the enclosing structure that forms the booth. The sound intensity inside the booth is given by the relation

$$I_2 = \frac{P_2}{A_2}$$

where

P_2 = sound power inside the booth,

$A_2 = \sum_i \alpha_i S_i$,

α_i = absorption coefficient of the ith surface inside the booth,

S_i = surface area of the ith surface inside the booth,

and the sum is over all internal surfaces in the booth.

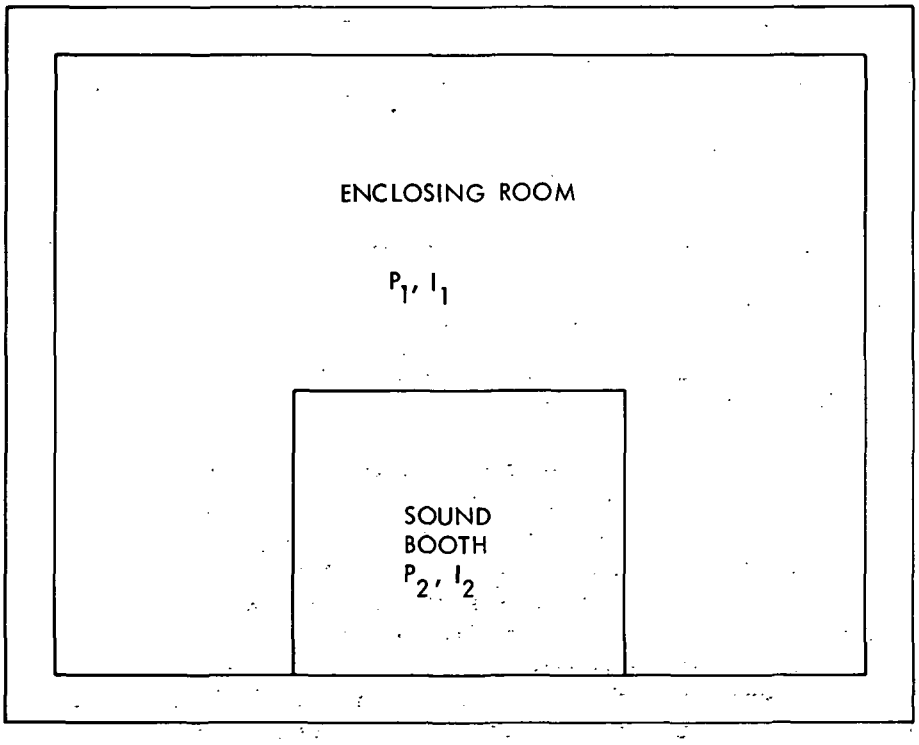

Figure A-5. Model for Calculation of Sound Booth Attenuation

The power inside the booth is due to transmission of sound through the structure from the surroundings, and is given by

$$P_2 = I_1 \sum_j t_j S_j$$

where

I_1 = sound intensity outside the booth,

t_j = transmittance of the jth surface forming the enclosure,

S_j = surface area of the jth surface forming the enclosure,

and the sum is over all surfaces forming the enclosure.

The intensity I_1 is due to sources inside the room surrounding the booth as well as sounds transmitted into that room from outside. Combining the above two equations we obtain

$$\frac{I_2}{I_1} = \frac{\sum_j t_j S_j}{\sum_i \alpha_i S_i}$$

from which we find the booth attenuation to be given by

$$\Delta L = L_1 - L_2 = 10 \log \frac{I_1}{I_2} = 10 \log \left(\sum_i \alpha_i S_i \right) - 10 \log \left(\sum_j t_j S_j \right) .$$

The above model is based on the simplifying assumption that sound energy lost to the booth by transmission from the surroundings and subsequent absorption in the booth is small, and that a negligible amount of sound transmitted into the booth subsequently escapes by retransmission to the surroundings. Both of the assumptions are supported by the results discussed below.

The application of the above model to each sound booth separately permits comparisons to be made between calculations and room attenuation measurements and so provides insight into the contributions made to the background noise level in the booths by various parts of the structure.

The data for the two booths are listed in tabular form as a function of frequency in Tables A-1 and A-2, and the results of the calculations are plotted in Figure A-6, where comparison is made with the measured room attenuation $\Delta L = L_1 - L_2$, where L_1 and L_2 are the average measured noise levels inside and outside the booth, respectively.

Table A-1. Acoustical Data for West Sound Booth

f - Hz		Walls	Windows	Doors	Floor	Ceiling	Σ	10 Log Σ	ΔL
	S_1	263	16.7	24.5	64	64			
	S_2	220	8.3	0	64	64			
125	α	0.11	0.18	0.20	0.08	0.11			
	t	2.71	3.16	17.9	10.0	12.7			
	αS_1	28.9	3.0	4.9	5.1	7.0	48.9	16.9	
	tS_2	0.596	0.026	0	0.640	0.813	2.075	3.2	13.7
250	α	0.22	0.06	0.15	0.27	0.22			
	t	1.36	2.24	25.0	3.55	15.9			
	αS_1	57.9	1.0	3.7	17.3	14.1	94.0	19.7	
	tS_2	0.299	0.019	0	0.227	1.018	1.563	1.9	17.8
500	α	0.44	0.04	0.10	0.39	0.44			
	t	0.41	1.78	1.41	0.89	7.94			
	αS_1	115.7	0.7	2.5	25.0	28.2	172.1	22.4	
	tS_2	0.090	0.015	0	0.057	0.508	0.670	-1.7	24.1
1000	α	0.73	0.03	0.09	0.34	0.73			
	t	0.86	0.89	4.90	1.00	4.46			
	αS_1	192	0.5	2.2	21.8	46.7	263.2	24.2	
	tS_2	0.189	0.007	0	0.064	0.285	0.545	-2.6	26.8
2000	α	0.90	0.02	0.09	0.48	0.90			
	t	0.38	0.63	21.7	0.40	0.25			
	αS_1	236.7	0.3	2.2	30.7	57.6	327.5	25.2	
	tS_2	0.084	0.005	0	0.026	0.016	0.131	-8.8	34.0
4000	α	0.90	0.02	0.09	0.63	0.90			
	t	0.07	0.14	18.2	0.56	0.20			
	αS_1	236.7	0.3	2.2	40.3	57.6	337.1	25.3	
	tS_2	0.015	0.001	0	0.036	0.013	0.065	-11.9	37.2

NOTES: S_1 refers to inside absorbing areas in 0.093 m^2

S_2 refers to enclosure transmitting areas in 0.093 m^2

t values quoted must be multiplied by 10^{-3}

Table A-2. Acoustical Data for East Sound Booth

f - Hz		Walls	Windows	Doors	Floor	Ceiling	Σ	10 Log Σ	ΔL
	S_1	238	16.7	49	64	64			
	S_2	119	8.3	24.5	64	64			
125	α	0.11	0.18	0.20	0.08	0.11			
	t	2.71	3.16	12.6	10.0	12.7			
	αS_1	26.2	3.0	9.8	5.1	7.0	51.1	17.1	
	tS_2	0.332	0.026	0.309	0.640	0.813	2.120	3.3	13.8
250	α	0.22	0.06	0.15	0.27	0.22			
	t	1.36	2.24	25.1	3.55	15.9			
	αS_1	52.4	1.0	7.4	17.3	14.1	92.2	19.6	
	tS_2	0.162	0.019	0.615	0.227	1.018	2.041	3.1	16.5
500	α	0.44	0.04	0.10	0.39	0.44			
	t	0.41	1.78	6.31	0.89	7.94			
	αS_1	104.7	0.7	4.9	25.0	28.2	163.5	22.1	
	tS_2	0.049	0.015	0.155	0.057	0.508	0.784	-1.1	23.2
1000	α	0.73	0.03	0.09	0.34	0.73			
	t	0.86	0.89	7.94	1.00	4.46			
	αS_1	173.7	0.5	4.4	21.8	46.7	247.1	23.9	
	tS_2	0.102	0.007	0.195	0.064	0.285	0.653	-1.9	25.8
2000	α	0.90	0.02	0.09	0.48	0.90			
	t	0.38	0.63	10.00	0.40	0.25			
	αS_1	214.2	0.3	4.4	30.7	57.6	307.2	24.9	
	tS_2	0.045	0.005	0.245	0.026	0.016	0.337	-4.7	29.6
4000	α	0.90	0.02	0.09	0.63	0.90			
	t	0.07	0.14	3.16	0.56	0.20			
	αS_1	214.2	0.3	4.4	40.3	57.6	316.8	25.0	
	tS_2	0.008	0.001	0.077	0.036	0.013	0.135	-8.7	33.7

NOTES: S_1 refers to inside absorbing areas in 0.093 m^2

S_2 refers to enclosure transmitting areas in 0.093 m^2

t values quoted must be multiplied by 10^{-3}

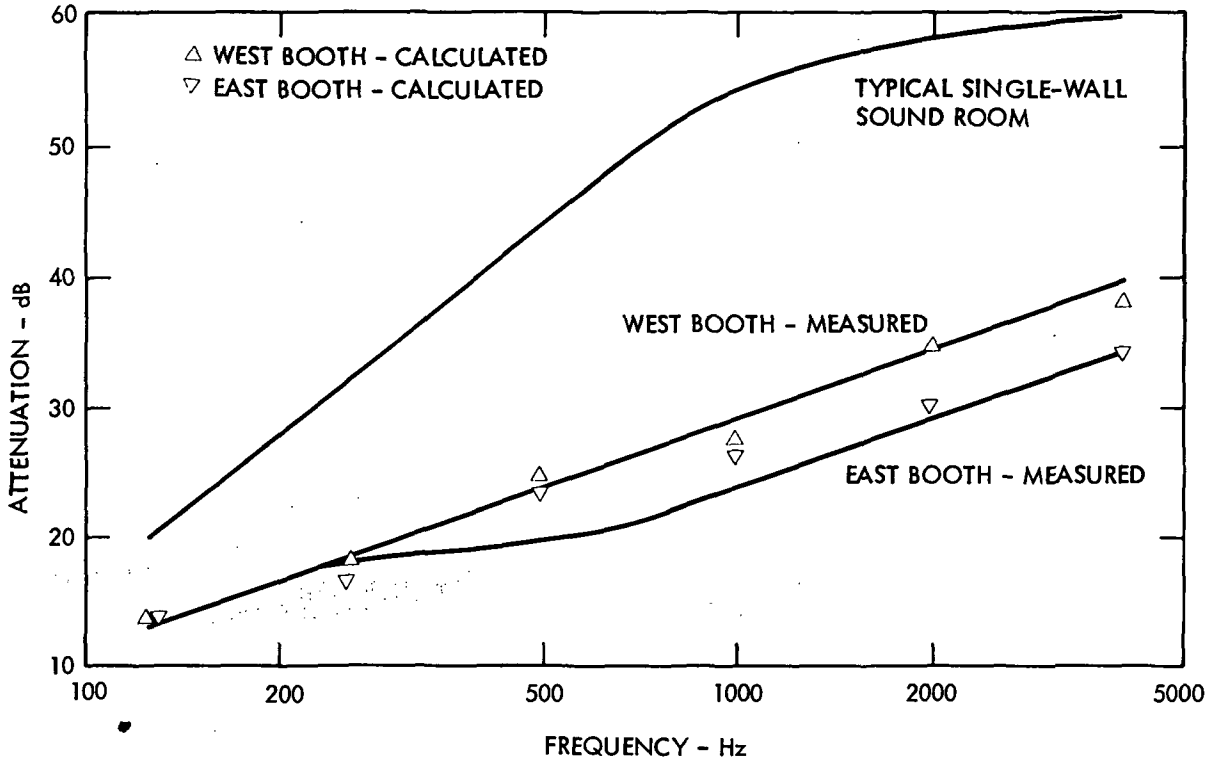

Figure A-6. Comparison of the Measured and Calculated Attenuation Values for the Sound Booths

It is seen from Figure A-6 that the agreement is remarkably good, given the difficulties of making transmittance measurements and estimating absorption coefficients. Also shown in the figure is an attenuation curve for a typical, single-wall sound room (Ref. 5), from which it is seen that the sound booths' performance is up to 20-dB poorer than expected for a well-constructed room.

Analysis of Tables A-1 and A-2 indicates that the principal cause for this behavior is the relatively low attenuation afforded by the major parts of the structure, namely, the walls, floor, and ceiling. Also, these parts of the structure account for most of the room absorption, with relatively little contribution from the doors and windows. Since the absorption coefficients for the walls, floor, and ceiling are relatively high to begin with, no significant improvement could be achieved by trying to further increase these values.

For example, if the booths were completely lined with material whose absorption coefficient is unity, this would result in less than 3 dB of improvements at 1000 hz. On the other hand, the data of Tables A-1 and A-2 show that the attenuation of the major structure is only of the order of 30 dB or so, whereas a 48.83 kg/m^2 wall should have an attenuation of 50 to 60 dB at 1000 Hz (Ref. A-1). We conclude from this that, short of major reconstruction, no significant improvement in performance of the sound booths is possible.

It is also to be noted from the data in the tables that the major contribution to higher observed noise levels in the East Booth at frequencies above about 1000 Hz is conduction through the entrance door.

A.3 Measurement of Earphone Attenuation

The attenuation of ambient noise afforded a listener wearing earphones was determined by a substitution method using the arrangement shown in Figure A-7. White noise from the generator is amplified and then passed through an octave band filter to the earphone power supply. A switch on the supply permits the amplified octave band noise signal to be applied either to the earphones or an audio power amplifier - loudspeaker combination.

With the switch in the earphone position the amplifier gain was adjusted until a comfortable listening level was achieved. The value of this level was determined from the rms voltmeter reading by comparison with the calibration curve supplied by the earphone manufacturer, and was chosen to be 75-dB SPL. This was deemed loud enough to mask the normal ambient noise level in the room, and yet not too loud for comfortable listening.

With the earphone level thus set, the switch was thrown to the loudspeaker position and the power amplifier adjusted until the perceived loudness equalled that previously heard. Switching back and forth between the

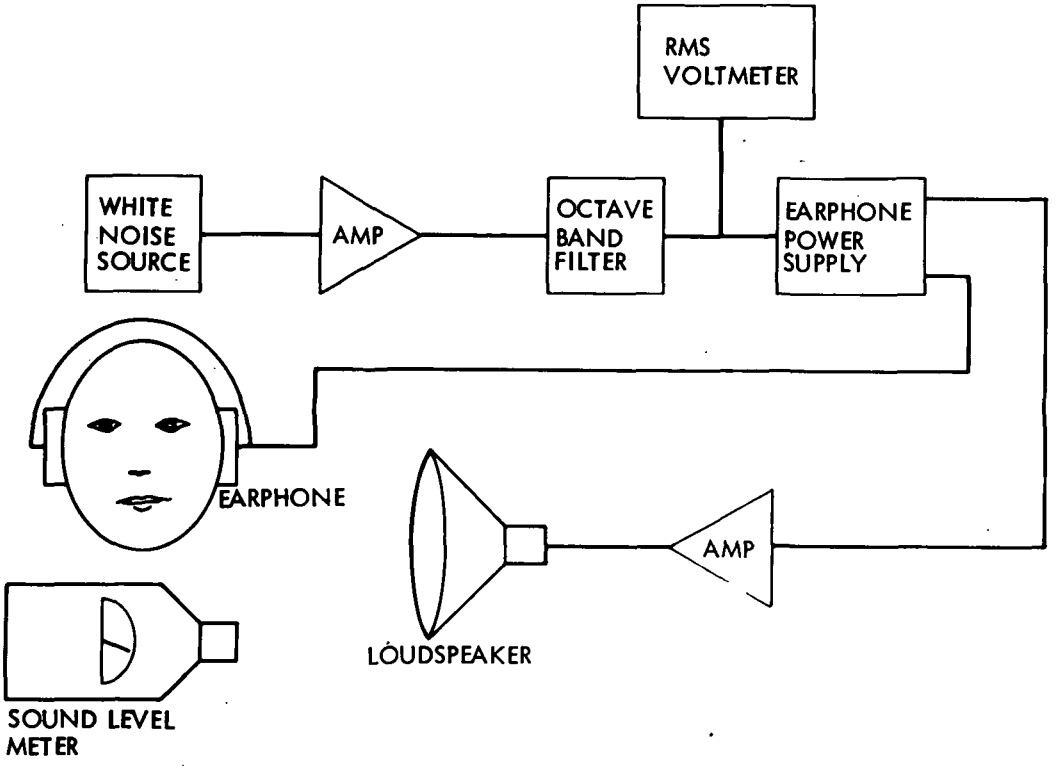

Figure A-7. Test Setup for Measurement of Earphone Attenuation

two positions permitted this comparison to be made with a repeatability of ±1.5 dB. With the switch in the loudspeaker position, the ambient SPL in the vicinity of the listener's head was then measured with the sound level meter. The attenuation provided by the earphones for the octave band selected is then given by the difference between the latter level and 75 dB.

The results are shown in Figure A-8. As noted earlier (see Section 4.2), the measured attenuation is significantly lower than the value quoted by the earphone manufacturer. However, the latter was measured by means of a small microphone placed inside a dummy head on which the earphones were placed, and it is expected that such an arrangement, which does not take into account bone conduction by the listener's cranium and other leakage paths in the head, will yield attenuation values considerably higher than the direct method used above.

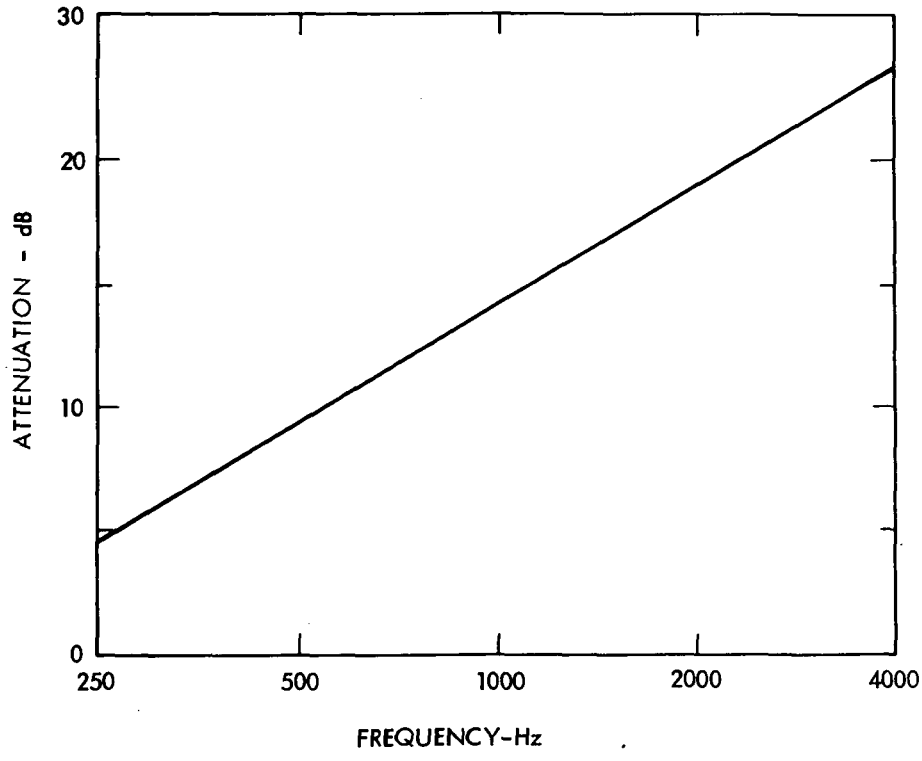

Figure A-8. Measured Attenuation Characteristics of KOSS-ESP9 Earphones

REFERENCE

A-1. King, A.J., "Noise Reduction", Chapter 8, p. 185, in Technical Aspects of Sound, E.G. Richardson, Editor. Elsevier Publishing Co., London, England, 1953.

APPENDIX B

IF BANDWIDTH CONSIDERATIONS FOR LMSS NBFM

B.1 GENERAL REVIEW

The demodulation portion of the carrier subsystem at the receiver is shown in Figure B-1. The antenna signal is processed in the RF and IF stages, and the output of the IF filter stage serves as the input to the receiver carrier demodulator. This input is the sum of the IF carrier and the IF noise waveform which can be written as

$$x_{IF}(t) = c(t) + n(t) \tag{B-1}$$

where the carrier and noise are referred to the demodulator input. The carrier $c(t)$ is at the IF frequency ω_c and the narrowband IF noise $n(t)$ is white Gaussian noise shaped by the IF filter. The power spectral density of $n(t)$, $S_n(\omega)$, is narrowband and is assumed to be symmetric about ω_c (i.e., bandwidth about ω_c is much smaller than ω_c).

This narrowband, zero mean, Gaussian noise has the quadrature expansion

$$n(t) = n_c(t) \cos(\omega_c t + \psi) - n_s(t) \sin(\omega_c t + \psi) \tag{B-2}$$

relative to the frequency ω_c and for any arbitrary phase angle ψ (in the literature, Ψ is conveniently taken to be zero without affecting the final results). $n_c(t)$ is the in-phase component and $n_s(t)$ is the quadrature component of $n(t)$, which are sometimes simply called the quadrature components. The quadrature components $n_c(t)$ and $n_s(t)$ are independent stationary Gaussian processes with zero mean, each having a power spectral density of

$$S_{n_c}(\omega) = S_{n_s}(\omega) = 2S_n(\omega + \omega_c) = N_0 \left| \tilde{H}_{IF}(\omega) \right|^2 \tag{B-3}$$

where

$$N_0 = KT^{o}_{eq} G_1$$

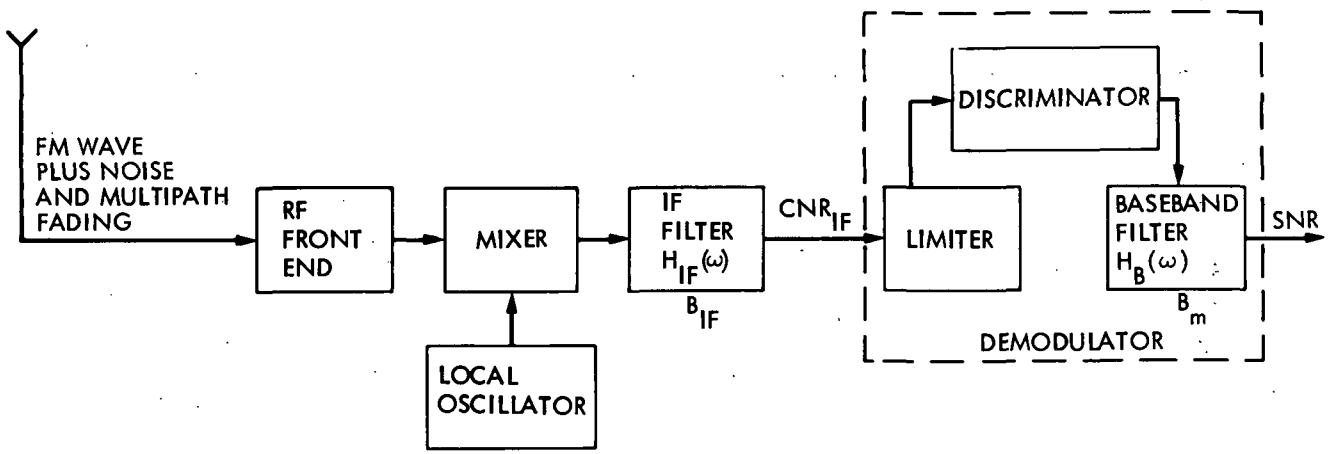

Figure B-1. A Conventional FM Receiver

and $\tilde{H}_{IF}(\omega)$ is the low-frequency equivalent of the IF bandpass filter function $H_{IF}(\omega)$. The gain G_1 accounts for the total receiver gain from antenna to demodulator input and KT^o_{eq} is the equivalent one-sided noise spectral level at the antenna output terminals (i.e., K is the Boltzmann constant and T^o_{eq} is the equivalent overall noise temperature at the RF front-end filter input). From Equation (B-3), it can be seen that the power of $n_c(t)$, $n_s(t)$, and n(t) is equal and, furthermore,

$$R_n(\tau) = R(\tau) \cos(\omega_c \tau) \tag{B-4}$$

where $R_n(\tau)$ is the autocorrelation function of n(t) and $R(\tau)$ is the autocorrelation function of both $n_c(t)$ and $n_s(t)$. The quadrature components are usually regarded as low frequency or "slowly varying" functions, and n(t) can be interpreted as a "modulation" of the quadrature components onto the carrier at ω_c.

It is often convenient to write the zero-mean, stationary, narrowband Gaussian noise process in Equation (B-2) in terms of its complex expansion

$$\begin{aligned} n(t) &= n_c(t) \cos(\omega_c t + \psi) - n_s(t) \sin(\omega_c t + \psi) \\ &= \mathrm{Re}\left\{ r(t)\, e^{j\theta(t)}\, e^{j(\omega_c t + \psi)} \right\} \\ &= r(t) \cos[\omega_c t + \psi + \theta(t)] \end{aligned} \tag{B-5}$$

where

$$\left.\begin{aligned} r(t) &= \left[n_c^2(t) + n_s^2(t) \right]^{1/2} \\ \theta(t) &= \tan^{-1}\left[\frac{n_s(t)}{n_c(t)} \right] \end{aligned}\right\} \tag{B-6}$$

The random process r(t) is the envelope of the bandpass noise, whereas $\theta(t)$ is the phase process. The envelope process has been shown to have the Rayleigh probability density at any t, given by

$$f_r(v) = \frac{v}{\alpha^2} e^{-v^2/2\alpha^2}, \quad v \geq 0 \tag{B-7}$$

where the mean-square value is $\overline{r^2(t)} = 2\alpha^2 = P_n$, the mean value is $\overline{r(t)} = \sqrt{\pi/2}\,\alpha$, and the variance is $\sigma_r^2 = (2 - \frac{\pi}{2})\,\alpha^2$. The phase process, $\theta(t)$, has a uniform probability density at any t, given by

$$f_\theta(\theta) = \frac{1}{2\pi}, \quad -\pi \leq \theta \leq \pi \tag{B-8}$$

and is independent of the envelope process.

We are now interested in determining the performance of a conventional FM demodulator system that operates on the IF waveform given in Equation (B-1). This will be discussed in this appendix and Appendix C.

In frequency modulation the baseband waveform m(t) is used to modulate the frequency of the RF carrier. The general FM carrier has the form

$$c(t) = A \cos\left[\omega_c t + \Delta\omega \int m(t)\,dt + \psi\right] \tag{B-9}$$

where A is the carrier amplitude, $\Delta\omega$ is the frequency deviation coefficient in rps/V, and ψ is again the carrier phase. The power in an FM carrier with any deterministic modulating waveform m(t) is easily determined and given by

$$P_c = \frac{A^2}{2} \tag{B-10}$$

The preceding carrier given by Equation (B-9) has an instantaneous radian frequency defined as

$$\omega(t) = \frac{d}{dt}\left[\omega_c t + \Delta\omega \int m(t)\,dt + \psi\right] \tag{B-11}$$

$$= \omega_c + \Delta\omega\, m(t)$$

which therefore varies in proportion to the modulating signal m(t) as desired. The frequency deviation coefficient, $\Delta\omega$ ($\triangleq 2\pi\Delta f$), determines the amount of frequency variation given to the carrier. If m(t) is normalized to a unit peak value, then $\Delta\omega$ is the maximum frequency deviation, or "peak frequency deviation," in rps that the carrier will undergo. From the above definition, Equation (B-11), we define the instantaneous frequency as

$$f(t) = f_c + \Delta f\, m(t) \tag{B-12}$$

where $\Delta f = \Delta\omega/2\pi$. Furthermore, the deviaton of the instantaneous frequency from the carrier frequency is

$$v(t) \triangleq f(t) - f_c = \Delta f\, m(t) \tag{B-13}$$

which is referred to as "instantaneous frequency deviation."

B.2 FM SPECTRAL ANALYSIS

Before starting the analysis of the threshold characteristic of an ideal FM discriminator, since FM is a nonlinear, or exponential, type of modulation, it is necessary to review the important concepts regarding the spectrum of an FM signal as it relates to the later discussions.

An exact description of FM spectra is difficult, if not impossible, save for certain simple modulating signals. This of course, merely reflects the fact that FM is a nonlinear process. Therefore, instead of attempting the analysis with an arbitrary modulating signal m(t), an alternate tactic is to examine the case of a sinusoidal modulating signal and then formulate general conclusions based on this case. This approach is admittedly indirect but it simplifies the analysis and yields "acceptable" results.

Sine Wave Modulation

Consider the case where the baseband modulating signal is a pure sinusoid at frequency ω_m and phase θ_m. That is, let

$$m(t) = A_m \cos(\omega_m t + \theta_m) \tag{B-14}$$

Substituting Equation (B-14) into Equation (B-9), we then have

$$c(t) = A \cos \left[\omega_c t + \beta \sin (\omega_m t + \theta_m) + \psi \right] \tag{B-15}$$

where

$$\beta = \frac{A_m \Delta\omega}{\omega_m} \tag{B-16}$$

or if m(t) is normalized to a unit peak value, so $A_m = 1$ and $\Delta\omega$ is the peak frequency deviation, then Equation (B-16) is simplified to the more common form of

$$\beta = \frac{\Delta\omega}{\omega_m} = \frac{\Delta f}{f_m} \tag{B-17}$$

which is referred to as the "FM modulation index." The FM modulation index, β, has two rather unusual properties: it is strictly defined only for tone modulation, and it depends on both the amplitude and frequency of the modulating tone.

We wish to determine the frequency transform of c(t) given by Equation (B-15). However, rather than formally transforming, we can instead write

$$\begin{aligned} c(t) &= A \, \mathrm{Re} \left\{ \exp (j\omega_c t + j\psi) \exp \left[j\beta \sin (\omega_m t + \theta_m) \right] \right\} \\ &= A \left\{ \cos (\omega_c t + \psi) \cos \left[\beta \sin (\omega_m t + \theta_m) \right] \right. \\ &\quad \left. - \sin (\omega_c t + \psi) \sin \left[\beta \sin (\omega_m t + \theta_m) \right] \right\} \\ &= A \sum_{n=\infty}^{\infty} J_n(\beta) \cos \left[(\omega_c + n\omega_m)t + n\theta_m + \psi \right] \end{aligned} \tag{B-18}$$

where the coefficients $J_n(\beta)$ are Bessel functions of the first kind, of order n and argument β. These Bessel coefficients possess rather unique properties. A formal definition for $J_n(\beta)$ is given by

$$J_n(\beta) \triangleq \frac{1}{2\pi}\int_{-\pi}^{\pi} e^{j(\beta \sin \lambda - n\lambda)}\, d\lambda \qquad \text{(B-19)}$$

where $J_{-n}(\beta) = (-1)^n J_n(\beta)$. Examining Equation (B-18), we see that the FM spectrum consists of a carrier frequency line plus an infinite number of sideband lines at frequencies $f_c \pm nf_m$. Figure B-2 illustrates a typical spectrum for an FM signal where all lines are equally spaced by the modulating frequency and the odd-order lower sideband lines are reversed in phase (i.e., have negative amplitudes) compared to the unmodulated carrier. Several of the Bessel functions which determine the amplitudes of the spectral components in the Fourier expansion are plotted in Figure B-3. We note that, for $\beta = 0$, $J_0(0) = 1$, while all other J_n's are zero. Thus, as expected when there is no modulation, only the carrier, of normalized amplitude unity, is present, while all sidebands have zero amplitude. When β departs slightly from zero, $J_1(\beta)$ acquires a magnitude which is significant in comparison with unity, while all higher-order J's are negligible in comparison. That such is the case may be seen either from Figure B-3 or from the approximations, which apply when $\beta \ll 1$,

$$J_0(\beta) \doteq 1 - \left(\frac{\beta}{2}\right)^2, \quad \beta \ll 1$$

$$J_n(\beta) \doteq \frac{1}{n!}\left(\frac{\beta}{2}\right)^n, \quad n \neq 0 \text{ and } \beta \ll 1 \qquad \text{(B-20)}$$

Accordingly, for β very small, the FM signal is composed of a carrier and a single pair of sidebands with frequencies $f_c \pm f_m$. An FM signal which is so constituted, that is, a signal where $\beta \ll 1$ so that only a single sideband pair is of significant magnitude, is called a "narrowband" FM signal. Hence, narrowband FM is much like AM save for the phase reversal of the lower sideband line. On the other hand, if $\beta \gg 1$, there will be many sideband lines, as seen from Figure B-3, and the FM signal is called "wideband" FM. Hence, large β implies a large bandwidth to accommodate the extensive sideband structure which is in agreement with our physical interpretation of large frequency deviation. Another respect in which FM is unlike the linear-modulation schemes is that the relative amplitude of the carrier line $J_0(\beta)$ varies with the modulation index and hence depends on the modulating signal. Thus, the carrier frequency component of an FM signal "contains" part of the message information. Nonetheless, there will be spectra in which the carrier line has zero amplitude since $J_0(\beta) = 0$ when $\beta = 2.4, 5.5$, etc.

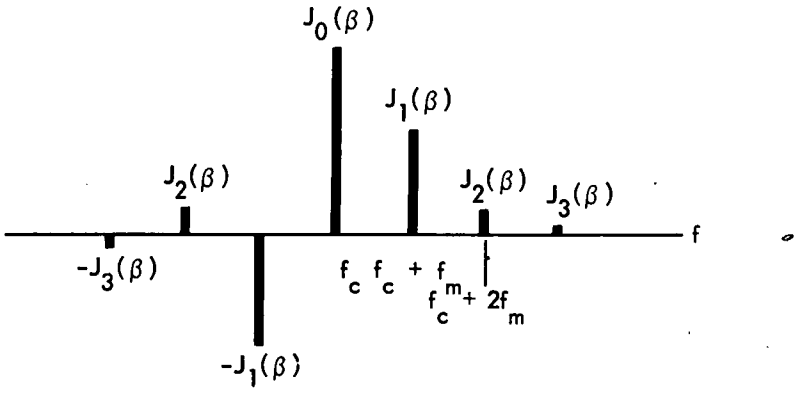

Figure B-2. FM Line Spectrum for Tone Modulation

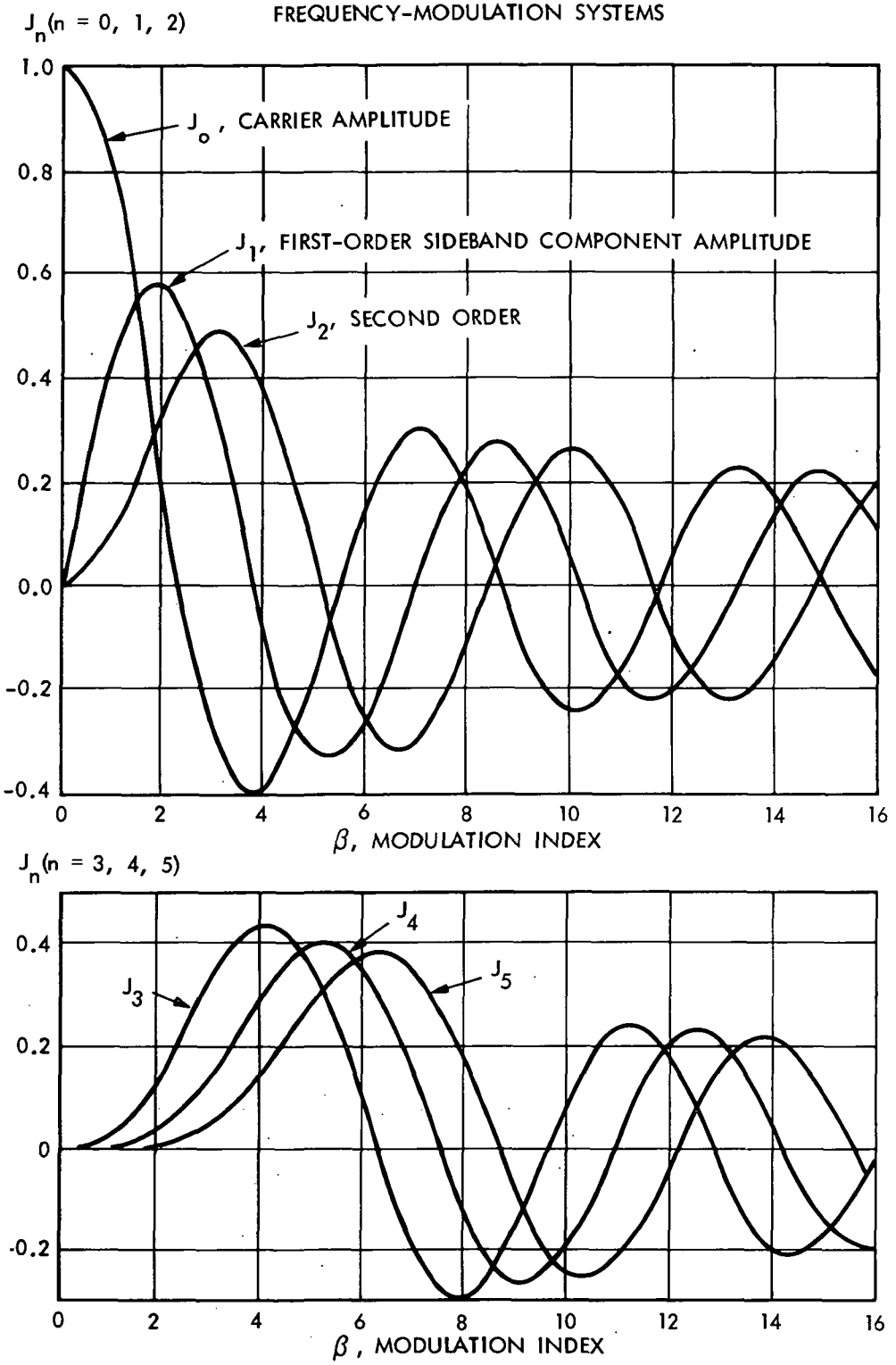

Figure B-3. The Bessel Functions J_n (β) Plotted as a Function of β for n = 0, 1, 2, •••, 5

It is to be expected that such should be the case on the basis of the following considerations. The envelope of an FM signal has a constant amplitude. Therefore, the power of such a signal is a constant independent of the modulation, since the power of a periodic waveform depends only on the square of its amplitude and not on its frequency as given by Equation (B-10). When the carrier is modulated to generate an FM signal, the power in the sidebands may appear only at the expense of the power originally in the carrier. Another way of arriving at the same conclusion is to make use of the identity

$$J_0^2 + 2J_1^2 + 2J_2^2 + 2J_3^2 + \ldots = 1 \qquad \text{(B-21)}$$

and from Equation (B-18), after some algebraic manipulations,

$$P_c = \overline{c^2(t)} = \frac{A^2}{2}\left(J_0^2 + 2\sum_{n=1}^{\infty} J_n^2\right) = \frac{A^2}{2} \qquad \text{(B-22)}$$

B.2.1 IF Bandwidth of an FM Signal

In principle, when an FM signal is modulated, we see from Equation (B-18) that the number of sidebands is infinite and the bandwidth required to encompass such a signal is similarly infinite in extent. (It should be pointed out that each of the bandwidths defined here are along the positive frequency axis only, and are always the positive frequency or one-sided bandwidths). As a matter of practice, it turns out that for any β, so large a fraction of the total power is confined to the sidebands that lie within some finite bandwidth that no serious distortion of the signal results if the sidebands outside this bandwidth are lost. In particular we see that $J_n(\beta) \ll 1$ for $\beta \ll n$. Hence, only significant terms exist up to values of n slightly greater than the value of β. How many such sideband components need to be considered may be seen from an examination of Table B-1 where $J_n(\beta)$ is tabulated for various values of n and of β.

It has been found experimentally in the past that the distortion resulting from bandlimiting an FM signal is tolerable as long as 98 percent or more of the power is passed by the bandlimiting filter. The merits of this definition are examined later, especially since the term "tolerable" means different things in different applications. In each column of Table B-1 a line has been drawn after the entries that account for at least 98 percent of the power. We note that the horizontal lines in this table always occur just after $n = \beta + 1$. Thus, for sinusoidal modulation, an "adequate" bandwidth, B, to transmit or receive the FM signal is

Table B-1. Values of the Bessel Functions $J_n(\beta)$ for Various Orders n and Integral values of β

n \ β	1	2	3	4	5	6	7	8	9	10
0	0.7652	0.2239	-0.2601	-0.3971	-0.1776	0.1506	0.3001	0.1717	-0.09033	-0.2459
1	0.4401	0.5767	0.3391	-0.06604	-0.3276	-0.2767	-0.004683	0.2346	0.2453	0.04347
2	0.1149	0.3528	0.4861	0.3641	0.04657	-0.2429	-0.3014	-0.1130	0.1448	0.2546
3	0.01956	0.1289	0.3091	0.4302	0.3648	0.1148	-0.1676	-0.2911	-0.1809	0.05838
4	0.002477	0.03400	0.1320	0.2811	0.3912	0.3576	0.1578	-0.1054	-0.2655	-0.2196
5		0.007040	0.04303	0.1321	0.2611	0.3621	0.3479	0.1858	-0.05504	-0.2341
6		0.001202	0.01139	0.04909	0.1310	0.2458	0.3392	0.3376	0.2043	-0.01446
7			0.002547	0.01518	0.05338	0.1296	0.2336	0.3206	0.3275	0.2167
8				0.004029	0.01841	0.05653	0.1280	0.2235	0.3051	0.3179
9					0.005520	0.02117	0.05892	0.1263	0.2149	0.2919
10					0.001468	0.006964	0.02354	0.06077	0.1247	0.2075
11						0.002048	0.008335	0.02560	0.06222	0.1231
12							0.002656	0.009624	0.02739	0.06337
13								0.003275	0.01083	0.02897
14								0.001019	0.003895	0.01196
15									0.001286	0.004508
16										0.001567

$$B = 2(\beta + 1) f_m$$

$$\doteq 2(\Delta f + f_m) \qquad \text{(B-23)}$$

where $\beta = \Delta f / f_m$ from Equation (B-17) was used in Equation (B-23). Expressed in words, the bandwidth is twice the sum of the peak frequency deviation and the modulating frequency of the sinusoidal signal. This rule for bandwidth is called Carson's rule. As a matter of interest, from Table B-1, the table of Bessel functions published in Ref. B-1, it may be verified that the rule given in Equation (B-23) holds up without exception up to $\beta = 29$, which is the largest value of β for which J_n is tabulated there. The bandwidth of an FM signal for the two cases of narrowband FM and wideband FM, Equation (B-23), is seen to have the simple approximations of $B \doteq 2fm$ for $\beta << 1$ (narrowband FM) and $B \doteq 2\Delta f$ for $\beta >> 1$ (wideband FM).

In some cases, the 98-percent power rule, or the Carson's rule, does not satisfy the requirements of an initial tentative design of a system. Hence, other criteria have been proposed by various authors (Refs. B-2 through B-4). One of the commonly used criterion is to define all sideband components having relative amplitude $|J_n(\beta)| > \epsilon$ as being significant, where ϵ ranges from 0.01 to 0.1 according to the application. Then, if $|J_M(\beta)| > \epsilon$ and $|J_{M+1}(\beta)| < \epsilon$ there are M significant sideband pairs and $(2M + 1)$ significant lines all told. The bandwidth is thus defined as

$$B \doteq 2 M(\beta) f_m, \quad M \geq 1 \qquad \text{(B-24)}$$

since the lines are spaced by f_m and M depends on the modulation index β. The condition $M \geq 1$ has been included in Equation (B-24) to account for the fact that B cannot be less than $2f_m$ as seen from Equation (B-23). Figure B-4 shows M as a continuous function of β for $\epsilon = 0.01$ and 0.1. Experimental studies (Ref. B-2) indicate that $\epsilon = 0.01$ is often overly conservative, while $\epsilon = 0.1$ may result in small but noticeable distortion. Values of M between these two bounds, as indicated by the dashed line, are acceptable for most purposes and yield more conservative results than the Carson's rule (i.e., compare values of $\beta + 1$ to the values of $M(\beta)$ given by the dashed line).

We now focus attention on the transmission or reception bandwidth B required when m(t) is an aribtrary modulating signal having the baseband message bandwidth W and satisfies the normalization convention $|m(t)| \leq 1$. However, we have to use the previous conclusions drawn about tone modulation to determine the bandwidth of the FM signal in this general case. This is done by extrapolating the case of tone modulation to the case of an arbitrary modulating signal. Admittedly, this procedure ignores the fact that superposition is not applicable to FM. However, it has been shown by experimental methods (Ref. B-2) that the results obtained in this manner are, in general, good approximations.

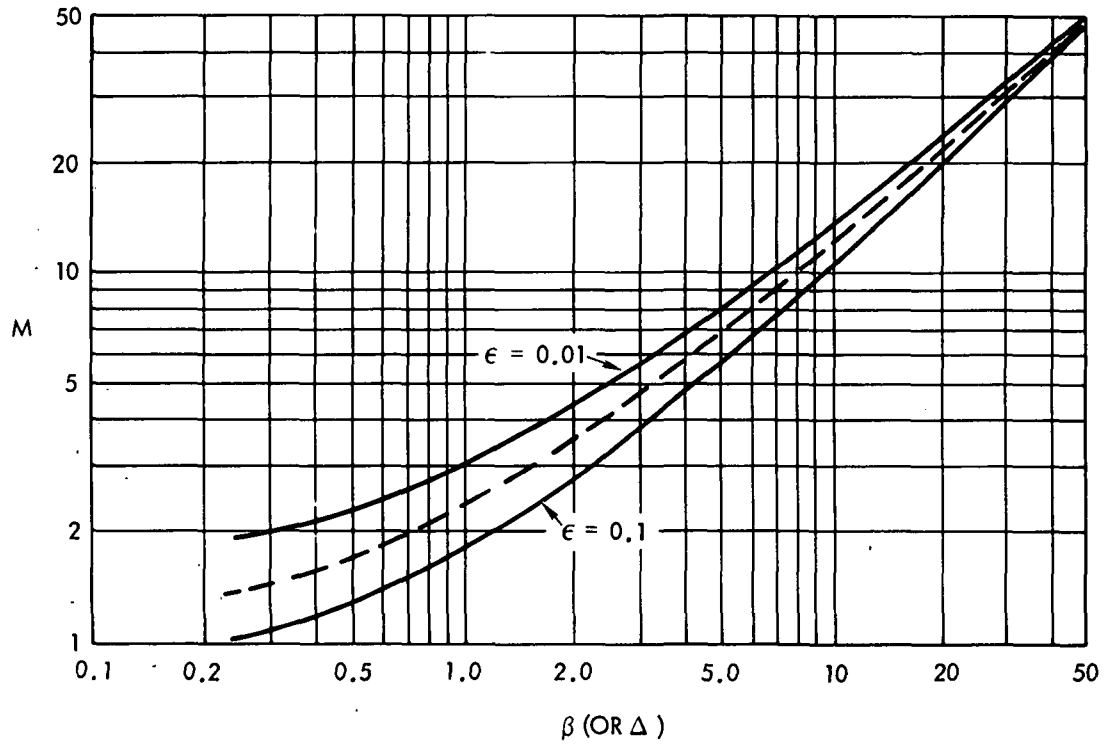

Figure B-4. The Number of Significant Sideband Pairs as a Function of β (or Δ)

For this case of an arbitrary modulating signal, a new parameter called the "deviation ratio" is defined as

$$\Delta \triangleq \frac{\Delta f}{W} \tag{B-25}$$

which is the peak frequency deviation divided by the maximum baseband frequency of the modulating signal - somewhat analogous to the modulation index in the case of sinusoidal modulation. The transmission (reception) bandwidth required for the FM signal with the arbitrary m(t) as the modulating signal is approximated by

$$B \doteq 2\, M(\Delta) W, \quad M \geq 1 \tag{B-26}$$

where Δ is treated just like β in determining $M(\Delta)$, say from Figure B-4.

Lacking appropriate curves or tables for $M(\Delta)$, there are several approximations to B that can be invoked. A convenient relation is again provided by the Carson's rule, for arbitrary modulations, as

$$B \doteq 2\,(\Delta + 1)W = 2\,(\Delta f + W) \tag{B-27}$$

With extreme values of the deviation ratio from Equation (B-27), it is seen that

$$B \doteq \begin{cases} 2\,\Delta f, & \Delta \gg 1 \text{ (wideband FM)} \\ 2\,W, & \Delta \ll 1 \text{ (narrowband FM)} \end{cases} \tag{B-28}$$

paralleling our results for tone modulation with β very large or very small. Perversely, the majority of actual FM systems have $2 < \Delta < 10$, for which Carson's rule somewhat underestimates the transmission bandwidth. A better approximation for equipment design is then

$$B \doteq 2\,(\Delta f + 2W) = 2\,(\Delta + 2)\,W, \quad \Delta \geq 2 \tag{B-29}$$

which would be used, for example, to determine the 3-dB bandwidths of RF and IF amplifiers.

Narrowband and Wideband FM

Our bandwidth investigations point to the conclusion that there are two special FM cases, which correspond to $\beta << 1$ for narrowband FM and $\beta >> 1$ for wideband FM. These cases have such distinctly different properties that for the sake of later analysis, we have to acquire a good understanding of their spectrum and bandwidth at this time.

Narrowband FM (NBFM) is in many ways similar to double-sideband linear modulation. We found that, just as in AM, sinusoidal modulation of the carrier gives rise to two sidebands at frequencies $(f_c + f_m)$ and $(f_c - f_m)$. We can extend the result now to the case of an arbitrary modulating waveform. Using Equation (B-9) for the general FM carrier, let

$$\phi(t) \triangleq 2\pi \Delta f \int m(t)\, dt \tag{B-30}$$

and assume that

$$\left|\phi(t)\right|_{max} = \Delta << 1 \tag{B-31}$$

which we take as the defining condition for NBFM as in Equation (B-28). Then the modulated wave is, from Equation (B-9) with $\Psi = 0$ for convenience,

$$\begin{aligned} c(t) &= A \cos\left[\omega_c t + \phi(t)\right] \\ &\doteq A\left[\cos \omega_c t \cos \phi(t) - \sin \omega_c t \sin \phi(t)\right] \\ &\doteq A \cos \omega_c t - A\, \phi(t) \sin \omega_c t \end{aligned} \tag{B-32}$$

where the approximations $\cos \phi \doteq 1$ and $\sin \phi \doteq \phi$ have been used due to the condition set by Equation (B-31). It can be seen that Equation (B-32) is in quadrature-carrier form and its spectrum can be easily determined. However, initially, we should note that $\phi(t)$ is proportional to the integral of m(t), as in Equation (B-30), and its Fourier transform is given by

$$\Phi(f) = \mathcal{F}\{\phi(t)\} = 2\pi\Delta f\left[\frac{M(f)}{j2\pi f}\right] \qquad \text{(B-33)}$$

$$= -j\, M(f)\, (\Delta f/f)$$

where M(f) is the Fourier transform of the arbitrary modulating waveform m(t). Then, the frequency spectrum of the carrier signal is easily determined by taking the Fourier transform of Equation (B-32) and using Equation (B-33)

$$C(f) \doteq \frac{A}{2}\left[\delta(f - f_c) + \delta(f + f_c)\right] + \frac{A\Delta f}{2}\left[\frac{M(f - f_c)}{f - f_c} - \frac{M(f + f_c)}{f + f_c}\right] \qquad \text{(B-34)}$$

which has the same general form as an AM spectrum. Therefore, if m(t) is band-limited in W, then $B \doteq 2W$ as expected from Equation (B-28).

The distinguishing feature of wideband FM (WBFM) is that $\Delta >> 1$ and hence its bandwidth is large compared to the message bandwidth. In fact, it was shown earlier that B is independent of the message bandwidth, $B \doteq 2\Delta f$ as in Equation (B-28). However, there is no simple approximation for the WBFM waveform c(t), for the case of an arbitrary modulating waveform, but there is an approximation for the power spectral density of the carrier $S_c(f)$ in terms of the probability density function $f_m(m)$ of the modulating signal. The two-sided power spectral density of the carrier is given by Ref. B-2:

$$S_c(f) = \frac{A^2}{4\Delta f}\left[f_m\left(\frac{f - f_c}{\Delta f}\right) + f_m\left(\frac{f + f_c}{\Delta f}\right)\right] \qquad \text{(B-35)}$$

where A is the carrier amplitude as before. Subject to the condition $\Delta >> 1$, Equation (B-35) may be used whenever the PDF of m(t) exists, at least in the sense of relative frequency of occurance. As an example, let m(t) be a Gaussian random signal process with the probability density function (assuming $\overline{m(t)} = 0$)

$$f(m) = \frac{1}{\sigma_m\sqrt{2\pi}}\, e^{-m^2/2\sigma_m^2} \qquad \text{(B-36)}$$

where, in this case, the variance of this stationary random process has the property

$$\sigma_m^2 = \overline{m^2(t)} = R_m(0) = P_m \tag{B-37}$$

where, again, $R_m(\tau)$ is the autocorrelation function of the process m(t) and P_m is the average rms power of the same process. Because of the random nature of m(t), the usual convention $|m(t)| \leq 1$ cannot be applied. However, recalling Tchebycheff's inequality, we can require that $\sigma_m = 1/K$ and so Prob $[|m(t)| > 1] \leq 1/K^2$ can be made arbitrarily small by making σ_m small. Now, using Equations (B-34) and (B-36), the two-sided power spectral density of the carrier is determined to be

$$S_c(f) = \frac{A^2}{4\sqrt{2\pi}\,\Delta f_{rms}} \left[e^{-(f-f_c)^2/2\Delta f_{rms}^2} + e^{-(f+f_c)^2/2\Delta f_{rms}^2} \right] \tag{B-38}$$

where

$$\Delta f_{rms} \triangleq \sigma_m \Delta f = \sqrt{\overline{m^2(t)}\,\Delta f} \tag{B-39}$$

which is the "rms frequency deviation" that the carrier will undergo for a random arbitrary signal such as m(t) with $\overline{m(t)} = 0$. The two-sided power spectral density of the carrier represented by Equation (B-38) is shown in Figure B-5 and, moreover, it shows that $(\Delta f_{rms})^2$ is also the variance of the Gaussian power spectrum density. As a check, it is easily verified that using Equation (B-38) for $S_c(f)$,

$$\int_{-\infty}^{+\infty} S_c(f)\, df = \frac{A^2}{2} = P_c \tag{B-40}$$

which was given earlier in Equation (B-10).

We now seek to determine the bandwidth B of a rectangular bandpass filter centered at f_c which will pass 98 percent of the power of the FM waveform with the power spectral density given by Equation (B-38). (Ref. B-5).

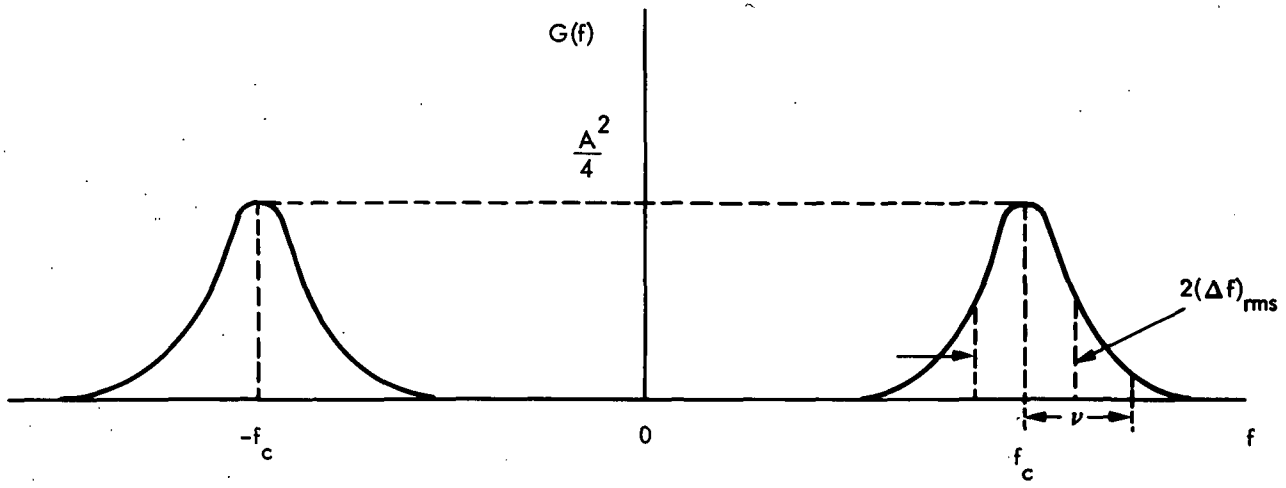

Figure B-5. The Power Spectral Density of a Carrier f_c Frequency Modulated by a Baseband Signal With a Gaussian Amplitude Distribution. The Variable ν is a Measure of the Departure of Frequency from the Carrier Frequency

Recognizing that each of the terms in Equation (B-38) makes equal contributions to the power and using the variable $\nu \triangleq f \pm f_c$ (see Equation (B-13)), we find that B is determined by the equation

$$\frac{1}{\sqrt{2\pi}\ \Delta f_{rms}} \int_{-B/2}^{B/2} e^{-\nu^2/2(\Delta f_{rms})^2}\, d\nu = 0.98 \qquad \text{(B-41)}$$

which yields

$$\text{erf}\left(\frac{B}{2\sqrt{2}\ \Delta f_{rms}}\right) = 0.98 \qquad \text{(B-42)}$$

and using a table of values of the error functions gives

$$B = 2\sqrt{2}\ (1.645)\ \Delta f_{rms} = 4.6\ \Delta f_{rms} \qquad \text{(B-43)}$$

The above example was for a Gaussian modulated WBFM signal. When the modulating signal has a continuous spectral density and gives rise to an FM signal with sidebands that have a continuous spectral density, a bandwidth definition often used is defined by

$$B \triangleq 2 \left[\frac{\int_{-\infty}^{+\infty} \nu^2 S_c(\nu)\, d\nu}{\int_{-\infty}^{+\infty} S_c(\nu)\, d\nu} \right]^{1/2} \qquad \text{(B-44)}$$

This definition yields an "rms bandwidth" that is twice the radius of gyration of the area under the power spectral density plot.

In LMSS channel simulator laboratory measurements, it has been discovered that for the Gaussian modulation, or other types of modulations that resemble Gaussian modulation (i.e., voice modulation), a better general approximation to the FM IF bandwidth is

$$B \doteq 2.5\ (3.5\ \Delta f_{rms} + W) \qquad \text{(B-45)}$$

where 3.5 Δf_{rms} is somewhat equivalent to the values of peak frequency deviation, Δf, observed 90 percent of the time. As an example, in the case of AMPS NBFM, Δf_{rms} is equal to 2 kHz, with which Equation (B-45) provides an IF bandwidth equal to 25 kHz for a voice bandwidth of W = 3 kHz.

REFERENCES

B-1. Jahnke, E., and Ende, F., Tables of Functions, Dover Publications Inc., New York, 1945.

B-2. Carlson, A.B., Communication Systems, McGraw-Hill, New York, 1975.

B-3. Schwartz, M., Bennet, R., and Stein, S., Communication Systems and Techniques, McGraw-Hill, New York, 1966.

B-4. Abramson, N., "Bandwidth and Spectra of Phase-and-Frequency-Modulated Waves," IEEE Trans. Comm. Systems, Vol. CS-11, pp. 407-414, Dec. 1963.

B-5. Taub, H., and Schilling, D.L., Principles of Communication Systems, McGraw-Hill, New York, 1971.

APPENDIX C

THEORETICAL CONSIDERATIONS OF NOISE AND MULTIPATH FADING PERFORMANCE OF MOBILE FM RECEIVER

C.1 INTRODUCTION

In this appendix the noise performance of a mobile FM receiver under the three conditions of a line-of-sight signal, a rapid Rayleigh fading signal, and a line-of-sight signal plus a rapid Rayleigh fading signal is examined. The nonfading case of a line-of-sight signal plus the narrowband Gaussian noise has been analyzed by use of various theoretical models (Refs. C-1 through C-9). It has been shown (Refs. C-2 and C-5) that the results obtained using the Rice's "clicks" theory is inaccurate in the FM subthreshold region as compared with experimental data. In the next section, the results obtained for the receiver output signal-to-noise ratio as a function of the IF carrier-to-noise ratio by Rice's "clicks" model (Ref. C-1), Kibe's "zero-crossing" analysis (Ref. C-2) Shimbo's "output autocorrelation function" method (Refs. C-3 through C-5), and Davis's "empirical formulation" model (Ref. C-6) are presented. Furthermore, the results of the "zero-crossing" analysis and the "output autocorrelation function" are extended and a number of useful formulas are derived. In Section C.4, the available results for the case of rapid Rayleigh fading are examined. It was shown, in Section 5 of this report, that the formulas obtained in this appendix by extending the "output autocorrelation function" model have the best agreement with the experimental measurements and are most accurate for determination of the FM threshold. Finally, since there are no theoretical results available for the case of a line-of-sight signal plus a rapid Rayleigh fading signal, to the author's best knowledge for this case, some general guidelines for determination of the FM receiver output signal-to-noise ratio are discussed in Section 5, based on the experimental results.

C.2 PRELIMINARY CONSIDERATIONS

The demodulation portion of the carrier subsystem at the receiver is shown in Figure C-1. The antenna signal is processed in the RF and IF stages, and the output of the IF filter stage serves as the input to the receiver carrier demodulator. This input is the sum of the IF carrier and the IF noise waveform which can be written as

$$x_{IF}(t) = c(t) + n(t) \tag{C-1}$$

where the carrier $c(t)$ is at the IF frequency ω_c and the narrowband IF noise $n(t)$ is white Gaussian noise shaped by the IF filter.

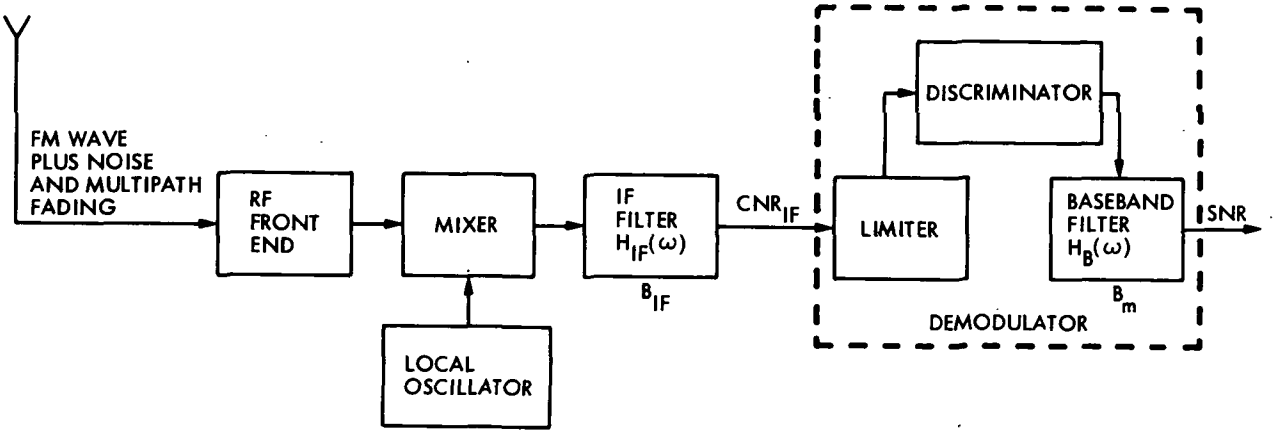

Figure C-1. A Conventional FM Receiver

The general FM carrier has the form

$$c(t) = A[\cos \omega_c t + \Delta\omega \int m(t)\, dt + \psi] \qquad \text{(C-2)}$$

where A is the carrier amplitude, m(t) is the baseband modulating waveform, $\Delta\omega = 2\pi\Delta f$ is the maximum or "peak" frequency deviation in rps/V (i.e., for an m(t) which is normalized to a unit peak value), and ψ is the arbitrary carrier phase angle. It is well known that the power in an FM carrier with any modulating waveform m(t) is given by $P_c = A^2/2$.

The narrowband IF noise n(t) has a power spectral density, $S_n(\omega)$, which is assumed to be symmetric about ω_c with a two-sided value of

$$s_n(\omega) = \begin{cases} \frac{\eta}{2} & |f - f_c| \leq B_{IF} \\ 0 & \text{elsewhere} \end{cases} \qquad \text{(C-3)}$$

where $\eta/2$ is the spectral density of white noise and B_{IF} is the noise bandwidth of the IF carrier filter. This narrowband, zero mean, Gaussian noise has the quadrature expansion

$$n(t) = n_c(t) \cos(\omega_c t + \psi) - n_s(t) \sin(\omega_c t + \psi) \qquad \text{(C-4)}$$

relative to the frequency ω_c and for any arbitrary phase angle ψ.

$n_c(t)$ and $n_s(t)$ are the in-phase and quadrature components of $n(t)$, respectively, which are independent stationary Gaussian processes with zero mean; each has a power spectral density of

$$S_{n_c}(\omega) = S_{n_s}(\omega) = 2S_n(\omega + \omega_c) = \eta, \quad |f| \leq \frac{B_{IF}}{2} \tag{C-5}$$

and, therefore, $P_n = P_{n_c} = P_{n_s} = \eta B_{IF}$.

It is often mathematically convenient to express $n(t)$ in terms of an envelope function and a phase function represented as

$$n(t) = r(t) \cos [\omega_c t + \theta(t) + \psi] \tag{C-6}$$

where

$$\begin{aligned} r(t) &= \left[n_c^2(t) + n_s^2(t) \right]^{1/2} \\ \theta(t) &= \arctan \left(\frac{n_s(t)}{n_c(t)} \right) \end{aligned} \tag{C-7}$$

The random process $r(t)$ is the envelope of the bandpass noise, and $\theta(t)$ is the phase process. The envelope process is well known to have the Rayleigh probability density at any t, given by

$$p_r(\tau) = \frac{\tau}{\alpha^2} e^{-\tau^2/2\alpha^2}, \quad \tau \geq 0 \tag{C-8}$$

where the mean-square value is $\overline{r^2(t)} = 2\alpha^2 = P_n$, the mean value is $\overline{r(t)} = \sqrt{\pi/2}\alpha$, and the variance of r about the mean is $\sigma_r^2 = [2 - (\pi/2)]\alpha^2$. The phase process, $\theta(t)$, has a uniform probability density at any t, given by

$$p_\theta(\theta) = \frac{1}{2\pi}, \quad -\pi \leq \theta \leq \pi \tag{C-9}$$

and is independent of the envelope process.

C.3 NOISE PERFORMANCE OF AN FM RECEIVER

In this section, the properties of the signal-to-noise ratio (SNR) at the output of an idealized FM receiver with a limiter-balanced discriminator, as shown in Figure C-1, are examined. It is well known that for high carrier-to-noise ratios (CNRs) the expressions relating the demodulator output SNR and input CNR for the sinusoidal and Gaussian random process baseband modulations above FM thresholds are as follows:

$$\frac{S_0}{N_0} = \frac{3}{2}\left(\frac{\Delta f}{B_m}\right)^2 \left(\frac{B_{IF}}{B_m}\right) \text{CNR (sinusoidal modulation)} \qquad \text{(C-10)}$$

$$\frac{S_0}{N_0} = 3\left(\frac{\Delta f_{rms}}{B_m}\right)^2 \left(\frac{B_{IF}}{B_m}\right) \text{CNR (Gaussian modulation)} \qquad \text{(C-11)}$$

where B_m is the noise bandwidth of the baseband filter in the demodulator and Δf_{rms} is the rms frequency deviation produced by the Gaussian process modulating signal given by

$$\Delta f_{rms} = \Delta f \sqrt{\overline{m^2(t)}} \qquad \text{(C-12)}$$

Using Equations (C-2) and (C-3), the value of CNR in Equations (C-10) and (C-11) is

$$\rho \triangleq \text{CNR} = \frac{P_c}{N_c} = \frac{A^2}{2\eta B_{IF}} \qquad \text{(C-13)}$$

since the carrier power was given to be $A^2/2$. Furthermore, some authors have named the ratios $(\Delta f/B_m)$ and $(\Delta f_{rms}/B_m)$ as the "modulation index", and the "rms modulation index", and denoted them by β and β_{rms}, respectively. However, it should be noted that the FM modulation index, β, is strictly defined only for tone modulation and is given by

$$\beta \triangleq \frac{\Delta\omega}{\omega_m} = \frac{\Delta f}{f_m} \qquad \text{(C-14)}$$

where f_m is the frequency of a pure sinusoid and Δf is the peak frequency deviation as in Equation (C-10). To avoid confusion, the following notation will be used

$$\left.\begin{aligned} \delta &\triangleq \left(\frac{\Delta f}{B_m}\right) \\ \delta_{rms} &\triangleq \left(\frac{\Delta f_{rms}}{B_m}\right) \\ \kappa &\triangleq \left(\frac{B_{IF}}{B_m}\right) \end{aligned}\right\} \qquad \text{(C-15)}$$

Hence Equations (C-10) and (C-11) can be expressed as

$$\frac{S_0}{N_0} = \frac{3}{2}\kappa\rho\delta^2 \quad \text{(sinusoidal modulation)} \qquad \text{(C-16)}$$

$$\frac{S_0}{N_0} = 3\kappa\rho\delta_{rms}^2 \quad \text{(Gaussian modulation)} \qquad \text{(C-17)}$$

Again, it should be noted that δ is the same as β, only if the receiver is designed such that $B_m = f_m$.

C.3.1 Rice's "Clicks" Model

In derivations of Equations (C-16) and (C-17), it was assumed that the noise output of the demodulator is just the background thermal-type noise ("smooth noise") due to the large value of CNR. However, it has been observed (Ref. C-1) that at lower values of CNR, at the onset of FM threshold, a pulse-type noise ("spike-noise") waveform appears which is superimposed on top of the smooth noise. If we were to listen to the FM receiver output, we would hear individual snaps or clicks; as CNR is reduced still further, these clicks merge into a crackling or sputtering noise. It has been shown that although the frequency of occurrence of a spike noise is small, the noise energy associated with a spike is very large compared with the energy of the smooth noise occurring during a comparable time interval. Hence the spike noise greatly increases the total noise output and thereby causes a threshold.

Rice's "clicks" model is based on the fact that the total output noise power is the sum of the Gaussian smooth noise, N_G, and the spike noise, N_S,

$$N_0 = N_G + N_S \tag{C-18}$$

Furthermore, Rice has shown (Ref. C-1) that the total number of spikes occurring per second in the presence of a carrier alone (no modulation) is much smaller than that in a modulated carrier. For the case of an unmodulated carrier, the spike noise N_S is easily determined (Ref. C-7). If the amount of baseband modulation is small, $m(t) << 1$, then using the value of spike noise N_S obtained for the unmodulated carrier case yields a good approximation for the receiver output SNR, valid for $\rho \geq 2$, which is (Ref. C-7)

$$\frac{S_0}{N_0} \doteq \frac{3\kappa\delta^2\,\overline{m^2(t)}\,\rho(1 - e^{-\rho})^2}{1 + \sqrt{3}\,\kappa^2\rho\ \mathrm{erfc}\ (\sqrt{\rho})}, \quad \rho \geq 2 \tag{C-19}$$

where erfc (x) is the complementary error function. The condition $\rho \geq 2$ is given in Ref. C-1, since the approximations made for the N_0 in the derivation of Equation (C-19) do not hold for smaller values. Futhermore, it is shown (Ref. C-1) that the presence of the noise reduces the signal at the discriminator output by the factor $(1 - e^{-\rho})$. This signal-suppression effect, or the noise "capture" effect, is included in Equation (C-19).

The threshold effect is evident in Equation (C-19). At very-high CNR, the complementary error function approaches zero. The right-hand member of the denominator of Equation (C-19) becomes zero, and S_0/N_0 varies linearly with CNR. Furthermore, in this case, for sinusoidal modulation, $\overline{m^2(t)} = 1/2$, since Δf is taken as peak frequency deviation, which means m(t) is normalized to a unit peak value, then Equation (C-19) is simply reduced to Equation (C-16). Similarly, for Gaussian modulation, Equation (C-19) will be reduced to Equation (C-17), since from Equation (C-12)

$$\delta_{rms} = \delta\sqrt{\overline{m^2(t)}} \tag{C-20}$$

It was mentioned that the total number of spikes occurring per second in the presence of a carrier alone (no modulation) is much smaller than that in a modulated carrier. For the case of a modulated carrier, the spike noise N_S is not easily determined and only approximate formulas are available for special types of modulations. Specifically in this case, only the sinusoidal and Gaussian modulations have been treated in the literature (Equations (C-1) and (C-7)).

For the case of sinusoidal modulation, the receiver output SNR, valid for $\rho \geq 2$, has an approximation given by Ref. C-1:

$$\frac{S_0}{N_0} \approx \frac{(3/2)\kappa\rho\beta^2(1 - e^{-\rho})^2}{C + 24\kappa\rho\Phi\beta}, \quad \rho \geq 2 \tag{C-21}$$

where β is the FM modulation index as defined by Equation (C-14) and C is a constant computed from

$$C = J_0^2(\beta) + J_\ell^2(\beta) + 2\sum_{n=1}^{\ell-1} J_n^2(\beta)$$

where $J_n(\beta)$ is the Bessel function of the first kind, of order n and argument β, and $\ell = [\beta]$ is the integer whose magnitude does not exceed the magnitude of β and whose sign is the same as the sign of β which is always positive. It can easily be verified from

$$J_0^2(\beta) + 2\sum_{n=1}^{\infty} J_n^2(\beta) = 1$$

for any β, that the constant C is always ≤ 1. Furthermore, Φ in the denominator of Equation (C-21) is approximately obtained from

$$\Phi \approx \frac{e^{-\rho}}{2\pi}\left[1 + \left(\frac{\pi}{12\rho}\right)^{1/2} e^{-3\rho/2} I_0\left(\frac{3\rho}{2}\right)\right] \tag{C-22}$$

where $I_0(\ )$ is the modified Bessel function of the first-kind of zero order.

An approximation of Equation (C-21) can be found by assuming that the value of spike noise N_S determined in the case of a modulated carrier is the same for all values of CNR above and below FM threshold. Then, using

$$e^{-z} I_0(z) \approx 1/\sqrt{2\pi z} \quad \text{for } z >> 1$$

the parameter Φ given by Equation (C-22) is reduced to

$$\Phi \approx \frac{e^{-\rho}}{2\pi}\left[1 + \frac{1}{6\rho}\right] \approx \frac{e^{-\rho}}{2\pi}, \quad \frac{3\rho}{2} >> 1$$

Hence, making the further assumptions c = 1 and $B_m = f_m$, Equation (C-21) can be rewritten as

$$\frac{S_0}{N_0} \approx \frac{(3/2)\kappa\rho\delta^2(1 - e^{-\rho})^2}{1 + (12\delta/\pi)\kappa\rho e^{-\rho}}, \quad \rho \geq 2 \tag{C-23}$$

where for large values of ρ, Equation (C-23) is reduced to Equation (C-16).

Since B_m is not always equal to f_m for this same case of sinusoidal modulation, a better approximation than Equation (C-23), which is more convenient than Equation (C-21), is shown to be (Ref. C-7):

$$\frac{S_0}{N_0} \approx \frac{(3/2)\delta^2\kappa\rho(1 - e^{-\rho})^2}{1 + (12\delta/\pi)\kappa\rho \exp\left[-\kappa\rho/2(\delta + 1)\right]}, \quad \rho \geq 2 \tag{C-24}$$

A somewhat similar expression is found for receiver output SNR by using the Rice's clicks model, when the baseband modulation is a Gaussian random process, which is given by (Ref. C-7)

$$\frac{S_0}{N_0} \approx \frac{3\delta_{rms}^2 \kappa\rho(1 - e^{-\rho})^2}{1 + 6\sqrt{2/\pi}\,\delta_{rms}^2 \kappa\rho e^{-\rho}}, \quad \rho \geq 2 \tag{C-25}$$

Again, it is easily seen that for large values of ρ, Equations (C-24) and (C-25) will be reduced to Equations (C-16) and (C-17).

It has been shown (Refs. C-8 and C-9) that the expected number of clicks per second at the output of a conventional FM discriminator is smaller than the number given by Rice (Ref. C-1). The difference between the two numbers is due to a number of clicks that do not exist in practice. These nonexistent clicks are called false clicks. These false clicks further complicate Rice's model in the subthreshold region. However, in any analysis of the discriminator, the difference is small, and it does not affect the output SNR appreciably. However, in the analysis of threshold extending demodulators, which remove a large number of clicks, the difference can become very important. The probability of false clicks as a function of the demodulator input CNR is plotted (Ref. C-8) in Figure C-2. To account for the effect of false clicks on the output SNR, the second term of the denominators in Equations (C-19), (C-21), (C-23), (C-24), and (C-25) should be multiplied by the factor $(1 - P_{FC})$ for values of P_{FC} read from Figure C-2 at each value of CNR.

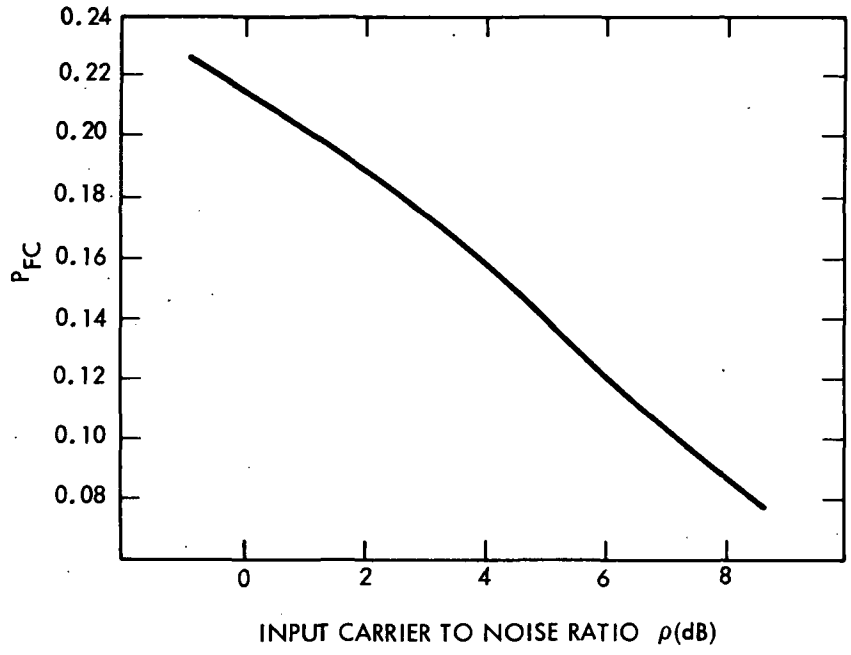

Figure C-2. Probability of False Clicks

C.3.2 "Zero-Crossing" Analysis

Stumper's basic idea of "zero-crossing FM detection" has been extended (Ref. C-1) for calculation of noise power due to clicks in the FM subthreshold region. According to this model, the demodulator output noise is looked upon as the changes in position and number of the zero crossings of the FM signal when narrowband Gaussian noise or any interfering signal are present. It is shown (Ref. C-2) that in the subthreshold region, the output SNR measured by experimental methods are better approximated by the zero-crossing model than by the Rice's clicks model (Ref. C-1) discussed in the preceding subsection.

The general receiver output SNR as a function of input CNR for sinusoidal type of modulation, predicted by the zero-crossing model, can be expressed as (Ref. C-2)

$$\frac{S_0}{N_0} \approx \frac{(3/2)\delta^2 k\rho (1 - e^{-\rho})^2}{1 + 6(\kappa/B_m)\,\Omega\rho e^{-\rho}} \qquad \text{(C-26)}$$

where the signal-suppression factor, $(1 - e^{-\rho})^2$, has been added to Equation (C-26) and the factor Ω is computed by

$$\Omega = \frac{1}{2\pi}\left[\frac{B_{IF}}{2\sqrt{3}}\int_0^{2\pi}\sqrt{1 + a^2\cos^2(\omega_m t)}\,d(\omega_m t)\right]$$

where ω_m is the baseband sinusoidal modulation radian frequency, $a = 2\sqrt{3}\,(\Delta f/B_{IF})$, and the above integral is an elliptic integral that can be computed only by numerical methods. For large values of ρ, Equation (C-26) is reduced to Equation (C-16).

For the sake of convenience, the above elliptic integral will be expressed in terms of a complete elliptic integral of the second kind for which extensive tables are available.

The elliptic integral in Equation (C-27) can be written as

$$\int_0^{2\pi}\sqrt{1 + a^2\cos^2 x}\,dx = \sqrt{(1 + a^2)}\int_0^{2\pi}\sqrt{1 - \left(\frac{a^2}{1 + a^2}\right)\sin^2 x}\,dx$$

where, using a table of integrals (Ref. C-10),

$$\int_0^{\phi}\sqrt{1 - m^2\sin^2 x}\,dx \triangleq E(m, \phi), \quad m^2 < 1$$

$$\triangleq mE\left(\frac{1}{m}, \alpha\right) - \left(\frac{m^2 - 1}{m}\right)F\left(\frac{1}{m}, \alpha\right), \quad m^2 > 1$$

where $E(m, \phi)$ is the elliptic integral of the second kind, $F(m, \phi)$ is the elliptic integral of the first kind, and

$$\alpha = \arcsin(m \sin \phi)$$

Furthermore (Ref. C-10),

$$E(m, \phi + n\pi) = nE(m, \pi) + E(m, \phi)$$

$$= 2n\,E\left(m, \frac{\pi}{2}\right) + E(m, \phi), \quad m = 0, 1, 2, \ldots$$

where $E\left(m, \frac{\pi}{2}\right)$ is the complete elliptic integral of the second kind.

Therefore,

$$\int_0^{2\pi} \sqrt{1 + a^2 \cos^2 x}\, dx = 4\sqrt{1 + a^2}\, E\left(\frac{a}{\sqrt{1 + a^2}}, \frac{\pi}{2}\right)$$

since

$$\left(\frac{a^2}{1 + a^2}\right) < 1$$

is always true. Hence

$$\Omega = B_{IF}\left(\sqrt{1 + a^2}/\pi\sqrt{3}\right) E\left(\frac{a}{\sqrt{1 + a^2}}, \frac{\pi}{2}\right) \qquad \text{(C-27)}$$

C.3.3 "Output Autocorrelation Function" Method

The previous results shown for the demodulator output SNR had been obtained mostly by heuristic methods. However, the exact solution of the output SNR is available for both sinusoidal and Gaussian process types of modulation; it is obtained from the exact autocorrelation function of the FM discriminator output when the input noise is a narrowband, zero-mean, Gaussian process (Refs. C-3 and C-4). Nevertheless, it is difficult to evaluate the exact solutions provided by the above method since it involves many integrals of Bessel functions of different kinds and many Bessel function expansions are usually required to obtain a solution for each of the six output noise components.

It has been shown (Refs. C-3 and C-4) that the exact results for the demodulator output spike noise can be approximated by rather simple formulas if it is assumed that the contributing components have an almost flat power spectra in the baseband frequency region and the Fourier integrals of their autocorrelation functions at zero frequency can be determined by the region of small τ. Under these assumptions, for sinusoidal modulation, the spike noise is determined by (Ref. C-3)

$$N_S \approx B_m \left\{ -\sqrt{2\pi}\,\gamma''(0) e^{-\rho} \left[-\frac{\rho\gamma''(0)}{2} \right]^{-1/2} \left[1 - \frac{4\pi^2(\Delta f)^2\rho}{\gamma''(0)} \right]^{-1/2} \left[1 - \frac{4\pi^2(\Delta f)^2\rho}{\gamma''(0)} D \right] \right\} \tag{C-28}$$

where

$$D \approx \ln 4 \left[1 - \frac{4\pi^2(\Delta f)^2\rho}{\gamma''(0)} \right] \tag{C-29}$$

and $\gamma''(\tau)$ is the second derivative, with respect to τ (" denotes the second derivative), of the normalized autocorrelation function of the input noise quadrature components $R_{n_s}(\tau)$ and $R_{n_c}(\tau)$, which are given by

$$\gamma''(\tau) \triangleq \frac{R''_{n_{sc}}(\tau)}{\eta B_{IF}} = \frac{R''_{n_c}(\tau)}{\eta B_{IF}} = \frac{R''_{n_s}(\tau)}{\eta B_{IF}} \tag{C-30}$$

since, from Equation (C-5), it is clear that the quadrature components $n_c(t)$ and $n_s(t)$ have the same autocorrelation function $R_{n_{sc}}(\tau)$. In Section C.5, the appendix, it is shown that

$$\gamma''(0) = -\left(\pi^2 B_{IF}^2 / 3 \right) \tag{C-31}$$

Substituting Equation (C-31) into Equations (C-28) and (C-29),

$$N \approx (\sqrt{2\pi}/3)\,\pi^2 B_{IF}^2 B_m e^{-\rho} \left[\frac{\rho\pi^2 B_{IF}^2}{6} \right]^{-1/2} \left[1 + 12\rho(\Delta f/B_{IF})^2 \right]^{-1/2} \left[1 + 12\rho(\Delta f/B_{IF})^2 D \right] \tag{C-32}$$

$$D \approx \ln 4 \left[1 + 12\rho(\Delta f/B_{IF})^2 \right] \tag{C-33}$$

It is possible to further simplify Equation (C-32) by assuming $12\rho(\Delta f/B_{IF})^2 >> 1$; in the case of wideband FM, $B_{IF} \approx 2\Delta f$, and the assumption becomes $\rho >> 1/3$; for narrowband FM, $B_{IF} \approx 2f_m$ and the assumption becomes $\rho\beta >> 1/3$; then

$$N_s \approx 2\sqrt{\pi}\ \Delta\omega B_m e^{-\rho} D, \quad 12\rho \left(\frac{\Delta f}{B_{IF}}\right)^2 >> 1 \tag{C-34}$$

where $\Delta\omega$ is the peak radian frequency deviation and D is given by Equation (C-33).

It was shown before that the total output-noise power is the sum of the Gaussian smooth noise N_G and the spike noise N_S, as given by Equation (C-18). Moreover, it is well known that N_G is given by (Ref. C-7)

$$N_G = 4\pi^2 B_M^2/3\kappa\rho \tag{C-35}$$

Therefore, for the case of sinusoidal modulation, the approximate SNR obtained by the output autocorrelation function method is determined by using Equations (C-16), (C-18), (C-32), (C-33), and (C-35):

$$\frac{S_0}{N_0} \approx \frac{3}{2}\kappa\delta^2\rho\left(1 - e^{-\rho}\right)^2 \Bigg/ \Bigg\{1 + (\sqrt{2\pi}/4)B_{IF}^2\,\kappa\rho e^{-\rho}$$

$$\cdot \left[\frac{\rho\pi^2 B_{IF}^2}{6}\right]^{-1/2} \left[1 + 12\rho(\Delta f/B_{IF})^2\right]^{-1/2}$$

$$\cdot \left[1 + 12\rho(\Delta f/B_{IF})^2 D\right]\Bigg\} \tag{C-36}$$

where D is given by Equation (C-33). If the assumption $12\rho(\Delta f/B_{IF})^2 >> 1$ holds, then N_S is computed by Equation (C-34), instead of Equation (C-32):

$$\frac{S_0}{N_0} \approx \frac{(3/2)\kappa\delta^2\rho(1 - e^{-\rho})^2}{1 + (3/\sqrt{\pi})\delta\kappa\rho e^{-\rho} D}, \quad 12\rho\left(\frac{\Delta f}{B_{IF}}\right)^2 >> 1 \tag{C-37}$$

where, again, D is given by Equation (C-33). It can be seen that for large values of ρ, Equations (C-36) and (C-37) are reduced to Equation (C-16).

Under the same assumptions made earlier for the power spectra and autocorrelation function of the output spike noise components and for Gaussian process modulation, using the same procedures as in Equations (C-28) through (C-33), the spike noise is determined by (Ref. C-4)

$$N_S \approx (\sqrt{2\pi}/3)\,\pi^2 B_{IF}^2 B_m e^{-\rho}\left[\frac{\rho\pi^2 B_{IF}^2}{6}\right]^{-1/2}$$

$$\cdot\left[1 + 24\rho(\Delta f_{rms}/B_{IF})^2\right]^{-1/2}\left[1 + 24\rho(\Delta f_{rms}/B_{IF})^2 D\right] \tag{C-38}$$

where Δf_{rms} is given by Equation (C-12), the power in the baseband signal S_0 is assumed to be $(\Delta\omega_{rms})^2$ in the above representation of Equation (C-38), and

$$D \approx \ln 4\left[1 + 24\rho(\Delta f_{rms}/B_{IF})^2\right] \tag{C-39}$$

It can be seen that Equation (C-38) is very similar to Equation (C-32) in form.

Furthermore, similarly, it is possible to further simplify Equation (C-39) by assuming $24\rho(\Delta f_{rms}/B_{IF})^2 >> 1$; in the case of wideband FM, $B_{IF} \approx 2\Delta f_{rms}$ and the assumption becomes $\rho >> 1/6$; for narrowband FM, $B_{IF} \approx 2f_m$ and the assumption becomes $\rho\beta_{rms} >> 1/6$; then

$$N_S \approx 2\sqrt{2\pi}\,\Delta\omega_{rms} B_m e^{-\rho} D, \quad 24\rho\left(\frac{\Delta f_{rms}}{B_{IF}}\right)^2 >> 1 \tag{C-40}$$

where $\Delta\omega_{rms}$ is the rms radian frequency deviation and D is given by Equation (C-39). It should be noted that the above expressions $B_{IF} \approx 2\Delta f_{rms}$ and $B_{IF} \approx 2f_m$ are very rough approximations for the case of Gaussian modulation and a better general approximation is given by

$$B_{IF} \approx 2.5(3.5\ \Delta f_{rms} + f_m) \tag{C-41}$$

Again, for the Gaussian process type of modulation, the approximate SNR obtained by the output autocorrelation function method is obtained by using Equations (C-17), (C-18), (C-35), (C-38), and (C-39); this ratio is

$$\frac{S_0}{N_0} \approx 3\kappa\delta_{rms}^2\rho(1-e^{-\rho})^2 \Bigg/ \Bigg\{1 + (\sqrt{2\pi}/4)B_{IF}^2\kappa\rho e^{-\rho}\left[\frac{\rho\pi^2 B_{IF}^2}{6}\right]^{-1/2}\left[1 + 24\rho(\Delta f_{rms}/B_{IF})^2\right]^{-1/2}$$

$$\cdot\left[1 + 24\rho(\Delta f_{rms}/B_{IF})^2 D\right]\Bigg\} \tag{C-42}$$

where D is given by Equation (C-39). If the assumption $24\rho(\Delta f_{rms}/B_{IF})^2 >> 1$ holds, then N_s is computed by Equation (C-40) instead of Equation (C-38), which gives

$$\frac{S_0}{N_0} \approx \frac{3\kappa\delta_{rms}^2\rho(1-e^{-\rho})^2}{1 + (3\sqrt{2/\pi})\delta_{rms}\kappa\rho e^{-\rho}D}, \quad 24\rho\left(\frac{\Delta f_{rms}}{B_{IF}}\right)^2 >> 1 \tag{C-43}$$

where, again, D is given by (C-39). It is seen that for large values of ρ, above threshold, Equations (C-42) and (C-43) are reduced to Equation (C-17).

Using the same output autocorrelation function method, a "simple" formula for the demodulator output SNR has been derived (Ref. C-5), by the authors of Refs. C-3 and C-4. After some change of notations and adding the signal-suppression factor, $(1-e^{-\rho})^2$, the "simple" formula for the case of sinusoidal type of modulation is (Ref. C-5)

$$\frac{S_0}{N_0} \approx \frac{(3/2)\kappa\delta^2\rho(1-e^{-\rho})^2}{1 + \sqrt{3/\pi}\,\kappa^2\sqrt{\rho}\,e^{-\rho}\left[1 + 12\rho(\Delta f/B_{IF})^2\right]} \tag{C-44}$$

where some similarities between the denominators of Equations (C-44) and (C-36) can be observed. For the Gaussian-process type of modulation, the "simple" SNR formula is (Ref. C-5)

$$\frac{S_0}{N_0} \approx \frac{3\kappa\delta_{rms}^2 \rho(1-e^{-\rho})^2}{1 + \sqrt{3/\pi}\,\kappa^2\sqrt{\rho}\,e^{-\rho}\left[1 + 24\rho(\Delta f_{rms}/B_{IF})^2\right]} \tag{C-45}$$

where, again, Equation (C-45) should be compared to Equation (C-42).

C.3.4 "Empirical Formulation" Model

Davis (Ref. C-6) has shown that the results based on the Rice's "clicks" model are in error in the FM subthreshold region, principally because the clicks are no longer independent of one another as was assumed by Rice. An empirical formula for the spike noise has been formulated by Davis (Ref. C-6), at Bell Telephone Laboratories, which yields the following expression for the demodulator output SNR (Ref. C-11)

$$\frac{S_0}{N_0} = \frac{S(1 - e^{-\rho})^2}{(a/\rho)(1 - e^{-\rho})^2 + \left[8\pi B_{IF} B_m e^{-\rho} \Big/ \sqrt{2(\rho + 2.35)}\right]} \tag{C-46}$$

where

$$a \triangleq \frac{(2\pi)^2}{B_{IF}} \int_0^{B_m} f^2 e^{-\pi f^2/B_{IF}^2}\, df$$

$$= \frac{4\pi^2 B_m^2}{3\kappa}\left\{1 - \frac{6\pi}{10\kappa^2} + \frac{12\pi^2}{56\kappa^4} + \ldots\right\} \tag{C-47}$$

and S is the modulation signal power, which, from Equation (C-2), is given by

$$S = (\Delta\omega)^2 \overline{m^2(t)} \tag{C-48}$$

where, again, for sinusoidal modulation,

$$S = (\Delta\omega)^2/2 \tag{C-49}$$

and for Gaussian process modulation,

$$S = (\Delta\omega_{rms})^2 \qquad \text{(C-50)}$$

It can be seen that if the numerator and the denominator of Equation (C-46) are divided by $(4\pi^2 B_m^2/3\kappa\rho)$, which is the first term in the expansion form of Equation (C-47) over ρ, then for large values of ρ, Equation (C-46) will be reduced to Equation (C-16) or Equation (C-17) depending on the modulation type.

C.4 EFFECTS OF RAYLEIGH FADING ON OUTPUT SNR

It is well known that the rapid Rayleigh fading alters the demodulator output SNR performance markedly, washing out the sharp threshold and capture properties of FM. Also, rapid phase changes produce a random FM component in the receiver output that imposes an upper limit on obtainable output SNR.

To determine the average output signal and noise in the presence of Rayleigh fading only (no direct line-of-sight), a good quasistatic approximation (Ref. C-11), which expresses the output signal and noise as functions of CNR, ρ, and then averages over the statistics of ρ, has been provided. Using this model, the average signal power at the receiver output is (Ref. C-11)

$$\overline{S} = \rho_0^2 S/(\rho_0 + 1)^2 \qquad \text{(C-51)}$$

where ρ_0 is the average CNR at the demodulator input and S is the modulation signal power given by Equation (C-48), (C-49), or (C-50) depending on the modulation type. The average noise power at the receiver output is

$$\overline{N} = S\left[\frac{1}{(2\rho_0 + 1)} - \frac{1}{(\rho_0 + 1)^2}\right] + \frac{a}{\rho_0} \ln \frac{(1 + \rho_0)^2}{1 + 2\rho_0}$$

$$+ 8B_{IF}B_m \left[\frac{\pi}{2\rho_0(\rho_0+1)}\right]^{1/2} \exp\left[2.35(\rho_0+1)/\rho_0\right] \operatorname{erfc}\left\{\left[2.35(\rho_0+1)/\rho_0\right]^{1/2}\right\} \qquad \text{(C-52)}$$

where a is defined in Equation (C-47). The first term in Equation (C-52) is due to signal suppression noise generated by receiver loss of capture on the carrier, which is caused by the rapid random suppressions of the carrier at the demodulator input. The second term in Equation (C-52) is due to "above-threshold" noise, smooth noise N_G plus some correction factors, after it is averaged over the statistics of ρ; the last term is due to "threshold-and-below" noise, spike noise N_S, which is obtained by the same empirical formula used in obtaining Equation (C-46) and averaged over the statistics of ρ.

In addition to the above noise components, there is random FM noise in the baseband output caused by interference between waves of different Doppler frequency arriving at a mobile from various directions. The demodulator output random FM noise, when assuming uniform arrival angles, is given by (Ref. C-11)

$$N_{RFM} = 2\pi^2 f_d^2 \ln (10) \qquad \text{(C-53)}$$

where f_d is the maximum Doppler shift computed from

$$f_d = \frac{\nu}{\lambda} \qquad \text{(C-54)}$$

with ν being the mobile speed in m/s and λ is the wavelength of the transmitted carrier frequency in m.

It has been shown (Ref. C-11) that as the signal fades below FM threshold, a click may occur due to noise, and, at the same time, the random FM noise of the signal peaks to a value comparable to that of the click. The FM receiver output is a nonlinear function of the noise click and the signal random FM peak, so that the total output noise cannot be accurately approximated by addition of threshold noise, $\overline{N}$, and random FM noise, N_{RFM}, as separate contributions. Therefore, in general, the demodulator output average SNR, $\overline{S}/\overline{N}$, is determined from Equations (C-51) and (C-52). However, the random FM noise component imposes an upper limit on obtainable output SNR which is given by

$$(SNR)_{UL} = \frac{S}{N_{RFM}} = \frac{S}{2\pi^2 f_d^2 \ln (10)} \qquad \text{(C-55)}$$

where, again, S is determined by Equation (C-48), (C-49), or (C-50), depending on the modulation type.

C.5 DETERMINATION OF THE $\gamma''(0)$

The function $\gamma(\tau)$ was earlier defined as the normalized autocorrelation function of the quadrature components, $R_{n_{sc}}(\tau)$, which can be expressed as

$$\gamma(\tau) = \frac{R_{n_{sc}}(\tau)}{\eta B_{IF}} \tag{C-56}$$

Furthermore, the quadrature components are ideal low-pass processes with power spectral densities, as given by Equation (C-5), which is

$$S_{n_{sc}}(f) \triangleq S_{n_c}(f) = S_{n_s}(f) = \begin{cases} \eta, & |f| \leq \frac{B_{IF}}{2} \\ 0, & |f| \geq \frac{B_{IF}}{2} \end{cases} \tag{C-57}$$

and the autocorrelation of these processes are given by (Ref. C-12)

$$R_{n_{sc}}(\tau) \triangleq R_{n_c}(\tau) = R_{n_s}(\tau) = \eta \frac{\sin(\pi B_{IF}\tau)}{\pi\tau} \tag{C-58}$$

To find $R''_{n_{sc}}(0)$, we can use the fact (Ref. C-12, Table 10-1) that

$$-R''_{n_{sc}}(\tau) = \mathcal{F}^{-1}\left\{\omega^2 S_{n_{sc}}(\omega)\right\} \tag{C-59}$$

where $\mathcal{F}^{-1}$ denotes inverse Fourier transform and, therefore,

$$-R''_{n_{sc}}(0) = \frac{1}{2\pi}\int_{-\pi B_{IF}}^{\pi B_{IF}} \omega^2 S_{n_{sc}}(\omega)\, d\omega = \frac{\eta\pi^2 B_{IF}^3}{3} \tag{C-60}$$

Hence

$$\gamma''(0) = R''_{n_{sc}}(0)/\eta B_{IF} = -\frac{\pi^2 B_{IF}^2}{3} \qquad \text{(C-61)}$$

REFERENCES

C-1. Rice, S. O., "Noise in FM Receivers," in Proceedings, Symposium of Time Series Analysis, M. Rosenblatt (ed.), Wiley, New York, 1963, Chapter 25.

C-2. Kibe, S. V., "Zero-Crossing Analysis of FM Threshold," IEEE Trans. Commun., Vol. COM-30, No. 5, pp. 1249-1254, May 1982.

C-3. Shimbo, O., "Threshold Noise Analysis of FM Signals for a General Baseband Signal Modulation and Its Application to the Case of Sinusoidal Modulation," IEEE Trans. Inform. Theory, Vol. IT-16, No. 6, pp. 778-781, Nov. 1970.

C-4. Shimbo, O., "Threshold Characteristic of FM Signals Demodulated by an FM Discriminator," IEEE Trans. Inform. Theory, Vol. IT-15, No. 5, pp. 540-549, Sept. 1969.

C-5. Shimbo, O., "A Simple Formula for the Threshold Characteristics of FM Signals," Proc. IEEE, Vol. 56, pp. 1241-1242, July 1968.

C-6. Davis, B. R., "FM Noise with Fading Channels and Diversity," IEEE Trans. Commun. Technol., Vol. COM-19, No. 6, pp. 1189-1199, Dec. 1971.

C-7. Taub, H., and Schilling, D. L., Principles of Communication Systems, New York: McGraw-Hill, 1971, Chapter 10.

C-8. Yavuz, D., and Hess, D. T., "False Clicks in FM Detection," IEEE Trans. Commun. Technol., Vol. COM-18, No. 6, pp. 751-756, Dec. 1970.

C-9. Yavuz, D., "FM Click Shapes," IEEE Trans. Commun. Technol., Vol. COM-19, No. 6, pp. 1271-1273, Dec. 1971.

C-10. Selby, S. M., Standard Mathematical Tables, 9th ed., pp. 525-526. CRC Publishers, New York, New York, 1971.

C-11. Jakes, W. C., Microwave Mobile Communications, New York: Wiley-Interscience, 1974, Chapter 4.

C-12. Papoulis, A., Probability, Random Variables and Stochastic Processs, New York: McGraw-Hill, 1965, Chapter 10.

APPENDIX D

MEASUREMENT TECHNIQUES FOR QUANTITATIVE PERFORMANCE EVALUATION

In the previous appendices, various theoretical models for determination of the FM receiver output SNR in the presence of narrowband Gaussian noise and rapid Rayleigh fading (i.e., no direct line-of-sight signal) were examined.

Using this channel simulator, a large number of experiments have been carried out, including the FM receiver output SNR as a function of input CNR measurements under various conditions of narrowband Gaussian noise and rapid Rayleigh fading, with or without the satellite direct line-of-sight (LOS) signal.

The technique used in the receiver output Signal-to-Channel Impairment ratio, S/CI, measurements is shown in Figure D-1. The impairment could be any of the type mentioned before (e.g., background channel noise or cochannel/adjacent channel interference) or any other type envisioned for testing purposes (e.g., man-made environmental noise). The reference receiver and the test receiver shown in the figure are exactly identical, and are matched in terms of their group delay and characteristics of the components.

In summary, the S/CI measurements are conducted according to the following procedure:

(1) With the channel noise removed, the amplitude control is adjusted till the rms voltmeter reads a minimum value at the output of the differential amplifier. Then the rms voltage of the baseband signal, in the absence of channel impairment, is read. This reading actually gives the rms voltage for a composite signal that is the sum of the baseband signal, the distortions due to demodulation, and the reference receiver circuit noise.

(2) With both the baseband modulation and the channel impairment removed, and only the carrier present, the value of circuit noise at the output of each receiver is measured.

(3) With both the baseband modulation and the channel impairment present, the rms voltages of the baseband signal and the baseband impairment are measured. Then the rms voltage readings in steps (1) and (2) are used to obtain the true S/CI, by taking the effects of the circuit noises and signal suppression due to the addition of the channel impairment into account.

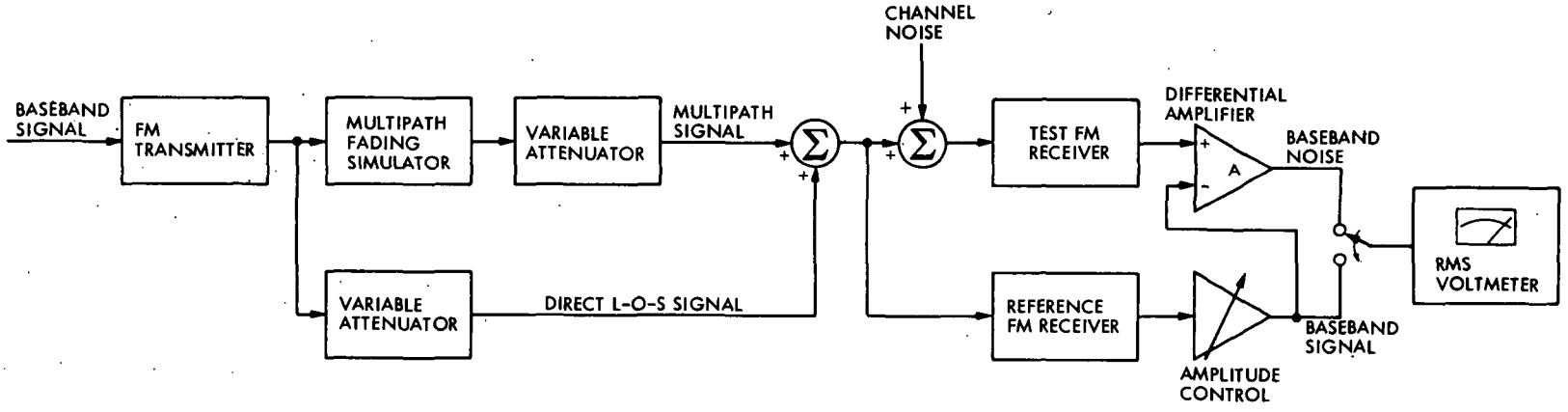

Figure D-1. The Experimental Setup for S/CI Measurements

D.1 FM RECEIVER MEASUREMENTS - SINUSOIDAL MODULATION

The general output from the FM receiver is x(t), which is comprised of the components:

$$x(t) = s(t) + s_H(t) + n(t) + n_{sxn}(t) + n_c(t) \qquad \text{(D-1)}$$

where,

s(t) is the desired signal,

$s_H(t)$ is the harmonics or distortion products of the desired signal,

n(t) is the noise (i.e., in general, noise is assumed to be any kind of impairment) of interest (theoretical noise),

$n_{sxn}(t)$ is a noise term arising from nonlinear interaction of signal and noise in the detection circuits,

$n_c(t)$ is circuit and instrumentation floor noise (it is nonzero when the receiver input is zero).

The signal-to-noise (SNR) ratio to be determined is

$$SNR = \frac{\langle s^2(t) \rangle}{\langle n^2(t) \rangle} \qquad \text{(D-2)}$$

where the desired signal power is divided by the theoretical noise power. Thus, the other components must be eliminated by measurement.

Noise component $n_c(t)$ is simply obtained by making an rms measurement of the receiver output when the input signal plus noise are zero (i.e., with the input terminated with its characteristic impedance and by making sure that the limiter is not oscillating).

A sinusoidal test signal is to be used. Thus the receiver signal output is given by

$$s(t) + s_H(t) = A_1 \cos(\omega_s t) + \sum_{n=2}^{\infty} A_n \cos[n\omega_s t + \phi_n] \qquad \text{(D-3)}$$

The amplitude coefficients, A_n, are a function of the receiver input SNR, ρ, where:

$$\rho = \frac{\text{carrier power at IF output}}{\text{noise power at IF output}} \tag{D-4}$$

and have the property

$$A_n\ (\rho < \infty) < A_n(\infty) \tag{D-5}$$

which arises from signal suppression by the noise in the limiter circuits.

Furthermore, $A_1(\rho)$ and $\sum_{n=2}^{\infty} A_n^2(\rho)$ must be determined by measurement. Consider the configuration of Figure D-2. Setting $\rho = \infty$, the phase is adjusted to maximize the dc voltmeter reading; then the amplitude is adjusted until the dc voltmeter reads zero. At this point, the desired signal component has been removed from the differential amplifier (with unit gain, G = 1) output, leaving only $S_H(t)$. Thus, the rms voltmeter readings give the following:

$$R_1(\infty) = \sqrt{\frac{1}{2}\sum_{n=2}^{\infty} A_n^2\ (\infty) + \left\langle n_c^2(t) \right\rangle} \tag{D-6}$$

$$R_2(\infty) = A_1(\infty)/\sqrt{2} \tag{D-7}$$

Now, since $\left\langle n_c^2(t) \right\rangle$ was previously measured as an rms reading (call it R_{n_c}), then:

$$\frac{1}{2}\sum_{n=2}^{\infty} A_n^2(\infty) = R_1^2(\infty) - R_{n_c}^2 \tag{D-8}$$

The input SNR is next set to the desired value of ρ. The dc voltmeter will show a nonzero reading because the desired signal component from the receiver has been suppressed relative to the reference signal applied to the differential amplifier. Adjustment of the reference amplitude is made to bring the dc voltmeter reading to zero. (Note: the phase adjustment

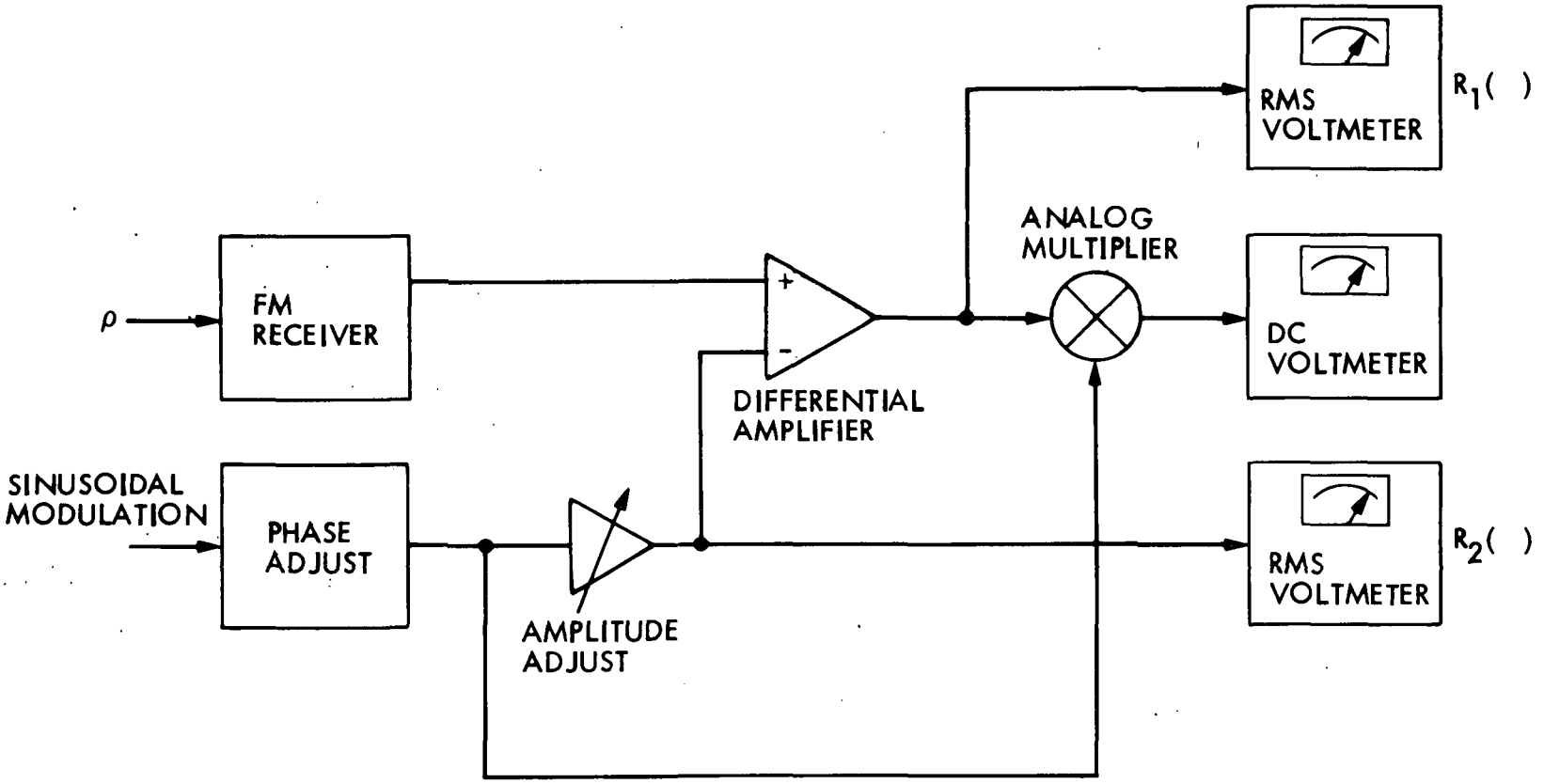

Figure D-2. The Experimental Setup for Sinusoidal Modulation Measurements

should be checked to ensure that the nonzero dc voltmeter reading is maximized.) The two rms readings are now given by

$$R_1(\rho) = \sqrt{\frac{1}{2}\sum_{n=2}^{\infty} A_n^2(\rho) + \left\langle n_c^2(t)\right\rangle + \left\langle n^2(t)\right\rangle + \left\langle n_{sxn}^2(t)\right\rangle} \qquad \text{(D-9)}$$

$$R_2(\rho) = A_1(\rho)/\sqrt{2} \qquad \text{(D-10)}$$

The signal voltage suppression factor is defined as

$$\alpha = \frac{A_1(\rho)}{A_1(\infty)} = \frac{R_2(\rho)}{R_2(\infty)} \qquad \text{(D-11)}$$

Assuming that the signal harmonics are also suppressed by α, we may then calculate the noise power components as:

$$\left\langle n^2(t)\right\rangle + \left\langle n_{sxn}^2(t)\right\rangle = R_1^2(\rho) - \frac{R_2^2(\rho)}{R_2^2(\infty)}\left[R_1^2(\infty) - R_{n_c}^2\right] - R_{n_c}^2 \qquad \text{(D-12)}$$

Although $\langle n^2(t)\rangle$ is sought, it is virtually impossible to determine $\langle n_{sxn}^2(t)\rangle$. However, $\langle n_{sxn}^2(t)\rangle$ will be quite small compared to $\langle n^2(t)\rangle$ for a good receiver. At most, its presence will result in a slightly lower measured SNR than that predicted by theory.

Finally, then, the measured SNR is given by:

$$\text{SNR (dB)} = 10\log_{10}\left\{\frac{R_2^2(\rho)}{R_1^2(\rho) - \frac{R_2^2(\rho)}{R_2^2(\infty)}\left[R_1^2(\infty) - R_{n_c}^2\right] - R_{n_c}^2}\right\} \qquad \text{(D-13)}$$

D.2 THEORETICAL CONSIDERATIONS - SINUSOIDAL MODULATION

The general output from the FM receiver when both signal and noise are present is

$$x(t) = s(t) + s_H(t) + n(t) + n_{sxn}(t) + n_c(t) \tag{D-14}$$

where

$$s(t) = A_1 \cos(\omega_s t + \phi_1) \tag{D-15}$$

$$s_H(t) = \sum_{n=2}^{\infty} A_n \cos[n\omega_s t + \phi_n] \tag{D-16}$$

When the noise is turned off (i.e., no impairment) the output of the differential amplifier y(t) is

$$y(t) = G[s(t) + s_H(t) + n_c(t) - R(t)] \tag{D-17}$$

where G is the gain of the differential amplifier and R(t) is the reference signal given by

$$R(t) = A' \cos(\omega_s t + \phi') \tag{D-18}$$

and, hence

$$y(t) = G[A_1 \cos(\omega_s t + \phi_1) + \sum_{n=2}^{\infty} A_n(\infty) \cos(n\omega_s t + \phi_n) + n_c(t) - A' \cos(\omega_s t + \phi')] \tag{D-19}$$

With no channel impairment, the output of the analog multiplier z(t) is

$$z(t) = y(t) \cdot A'' \cos(\omega_s t + \phi')$$

$$= G\left[A_1 \cos(\omega_s t + \phi_1) + \sum_{n=2}^{\infty} A_n(\infty)\cos(n\omega_s t + \phi_n) + n_c(t) - A' \cos(\omega_s t + \phi')\right] A'' \cos(\omega_s t + \phi')$$

$$= G\left[A_1 A'' \cos(\omega_s t + \phi_1)\cos(\omega_s t + \phi') + n_c(t)A'' \cos(\omega_s t + \phi') + \sum_{n=2}^{\infty} A_n(\infty)\, A'' \cos(n\omega_s t + \phi_n)\cos(\omega_s t + \phi') - A'A'' \cos^2(\omega_s t + \phi')\right] \quad \text{(D-20)}$$

By adjusting the phase ϕ', we set $\phi' = \phi_1$. Then

$$z(t) = G\left\{(A_1 A'' - A'A'')\left[\frac{1 + \cos(2\omega_s t + 2\phi_1)}{2}\right] + n_c(t)\, A'' \cos(\omega_s t + \phi_1) + \sum_{n=2}^{\infty} A_n(\infty)\, A'' \cos(n\omega_S t + \phi_n)\cos(\omega_s t + \phi_1)\right\} \quad \text{(D-21)}$$

The dc Component of z(t) would become

$$z_{dc}(t) = (G/2)\ (A_1 A'' - A' A'') \tag{D-22}$$

By adjusting the amplitude A' we can set the dc component equal to zero (dc meter reading is zero now) only if $\frac{G}{2}\ (A_1 A'' - A' A'') = 0$. Hence,

$$A_1 = A' \tag{D-23}$$

Now, the output of the differential amplifier will become

$$y(t) = G\left[\sum_{n=2}^{\infty} A_n(\infty) \cos\ (n\omega_s t + \phi_n) + n_c(t)\right] \tag{D-24}$$

Hence, if we read the rms value of y(t)

$$R_1(\infty) = \sqrt{G\left(\frac{1}{2}\sum_{n=2}^{\infty} A_n^2\ (\infty) + \langle n_c^2\ (t)\rangle\right)} \tag{D-25}$$

Now, if we take the modulation off with the input and its characteristic impedance terminated, then take a rms reading of y(t), we get (the gain of differential amplifier G should not be changed)

$$R_{nc} = \sqrt{G\langle n_c^2(t)\rangle} \tag{D-26}$$

Hence, we find the power in harmonics of the desired signal

$$R_1^2(\infty) - R_{nc}^2 = \frac{G}{2}\ \sum_{n=2}^{\infty} A_n^2(\infty) = G\langle s_H^2(t)\rangle_{\infty} \tag{D-27}$$

With the channel noise added, the input SNR is next set to the desired value of ρ. Then, the output of the differential amplifier $y(t)$ is

$$y(t) = G\,[s(t) + s_H(t) + n(t) + n_{sxn}(t) + n_c(t) - R(t)]$$

$$= G[A_1 \cos(\omega_s t + \phi_1) + S_H(t) + n(t) + n_{sxn}(t) + n_c(t)$$

$$- A' \cos(\omega_s t + \phi')]$$

$$z(t) = y(t) \cdot A'' \cos(\omega_s t + \phi')$$

$$= G[A_1 \cos(\omega_s t + \phi_1) + S_H(t) + n(t) + n_{sxn}(t) + n_c(t)$$

$$- A' \cos(\omega_s t + \phi')]\, A'' \cos(\omega_s t + \phi')$$

$$= G[A_1 A'' \cos(\omega_s t + \phi_1) \cos(\omega_s t + \phi') + s_H(t)\, A'' \cos(\omega_s t + \phi')$$

$$+ n(t)\, A'' \cos(\omega_s t + \phi') + n_{sxn}\, A'' \cos(\omega_s t + \phi')$$

$$+ n_c(t)\, A'' \cos(\omega_s t + \phi') - A'A'' \cos^2(\omega_s t + \phi')] \qquad \text{(D-28)}$$

We set $\phi' = \phi_1$; then

$$z(t) = G \left\{ (A_1 A'' - A'A'') \frac{1 + \cos(2\omega_s t + 2\phi_1)}{2} \right.$$

$$+ s_H(t) A'' \cos(\omega_s t + \phi_1) + n(t) A'' \cos(\omega_s t + \phi_1)$$

$$\left. + n_{sxn} A'' \cos(\omega_s t + \phi_1) + n_c(t) A'' \cos(\omega_s t + \phi_1) \right\} \qquad \text{(D-29)}$$

Again the dc component of z(t) is equal to zero only if

$$A_1 = A'$$

Now, the output of the differential amplifier will become

$$y(t) = G[s_H(t) + n(t) + n_{sxn}(t) + n_c(t)] \qquad \text{(D-30)}$$

We have already measured $G\langle s_H^2(t)\rangle_\infty$ when there was no channel impairment; when there is channel impairment, we can assume that the signal and the signal harmonics are suppressed by

$$\alpha = \frac{A_1(\rho)}{A_1(\infty)} = \frac{R_2(\rho)}{R_2(\infty)} \qquad \text{(D-31)}$$

So,

$$G\langle s_H^2(t)\rangle_\rho = \frac{R_2^2(\rho)}{R_2^2(\infty)}\left[R_1^2(\infty) - R_{nc}^2\right] \qquad \text{(D-32)}$$

Now, the rms reading of y(t) gives

$$R_1(\rho) = \sqrt{G\left[\langle s_H^2(t)\rangle_\rho + \langle n_c^2(t)\rangle + \langle n^2(t)\rangle + \langle n_{sxn}^2(t)\rangle\right.} \qquad \text{(D-33)}$$

and

$$R_2(\rho) = \frac{A_1(\rho)}{\sqrt{2}} \qquad \text{(D-34)}$$

Hence,

$$G\left[\langle n^2(t)\rangle + \langle n^2_{sxn}(t)\rangle\right] = R_1^2(\rho) - \frac{R_2^2(\rho)}{R_2^2(\infty)}\left[R_1^2(\infty) - R_{nc}^2\right] - R_{nc}^2 \qquad \text{(D-35)}$$

Finally, we obtain Equation (D-13) as

$$SNR(dB) = 10\ \log_{10}\left\{\frac{GR_2^2(\rho)}{R_1^2(\rho) - \frac{R_2^2(\rho)}{R_2^2(\infty)}\left[R_1(\infty) - R_{nc}^2\right] - R_{nc}^2}\right\} \qquad \text{(D-36)}$$

D.3 FM RECEIVER MEASUREMENTS - RANDOM SIGNAL MODULATION

Section D.1 provides an outline of a technique for accurate measurement of receiver output SNR when the modulation is a single sinusoid. An extension of the technique will now be presented for the measurement of SNR or S/I when the modulation is a random (noise) function.

The general output from the FM receiver given by Equation (D-1) is still valid for random modulations. Two cases are now of interest:

1 - The SNR case with

$$x(t) = s(t) + s_D(t) + n(t) + n_{sxn}(t) + n_c(t) \qquad \text{(D-37)}$$

where the components are defined in Section D.1 (the symbol s_D for distortion now replaces s_H for harmonics); and

2 - The S/I case with

$$x(t) = s(t) + s_D(t) + s_i(t) + n_c(t) \qquad \text{(D-38)}$$

where $s_i(t)$ includes all baseband interference components at the receiver output. SNR is defined as

$$SNR = \frac{\langle s^2(t) \rangle}{\langle n^2(t) \rangle} \qquad \text{(D-39)}$$

and S/I is defined as

$$S/I = \frac{\langle s^2(t) \rangle}{\langle s_i^2(t) \rangle} \qquad \text{(D-40)}$$

Since a random modulation is to be used, it should have the following properties and restrictions. First, s(t) should have a baseband bandwidth sufficiently within the baseband bandwidth of the FM receiver. For example, if the receiver baseband bandwidth is reasonably flat between, say, 400 Hz and 2.5 kHz, then the noise into the frequency modulator should be prefiltered to between 600 Hz and 2 kHz to insure that the receiver passband

has minimal effect on the noise signal. (Note: $s_i(t)$ will be an independent noise modulation which should also be prefiltered, in an identical fashion.)

Second, since the FM receiver output SNR is proportional to the square of the FM transmitter frequency deviation times the noise variance, the rms deviation of the FM transmitter should be accurately established. An HP 8901A modulation analyzer may be used to perform this measurement. Alternatively, the modulation sensitivity of the transmitter will have to be carefully measured and the rms level of the modulating voltage obtained with an rms meter. The rms deviation should not exceed the maximum given by the following equation (see Equation (B-45)):

$$\sigma \leq \frac{0.4B - f_m}{3.5} \tag{D-41}$$

where B is the IF -3 dB bandwidth, and f_m is the highest effective frequency of the noise modulation. (As an exmaple, if B = 30 kHz and f_m = 3 kHz, then $\sigma \leq$ 2.57 kHz.)

Figure D-3 shows the test configuration, which is very similar to that used for sinusoidal modulation SNR testing. The principal difference is that the reference signal phase-shifter is now replaced by a second FM receiver. This reference FM receiver is to be made as nearly identical to the test FM receiver as possible. The reference receiver output may be expressed as

$$x_r(t) = s_r(t) + s_{Dr}(t) + n_{cr}(t) \tag{D-42}$$

By matching the two receivers,

$$s_r(t) = s(t) \tag{D-43}$$

and

$$s_{Dr}(t) = s_D(t) \tag{D-44}$$

The floor noise from the reference receiver, $n_{cr}(t)$, should generally be uncorrelated with that from the test receiver.

The two receivers are matched in terms of (1) input group delay, (2) discriminator characteristic, and (3) output LPF. Input group delay from the FM transmitter to each receiver should be the same. This is accomplished by making the RF path length to each receiver the same. It may be checked by applying a sinusoidal test modulation and looking for any

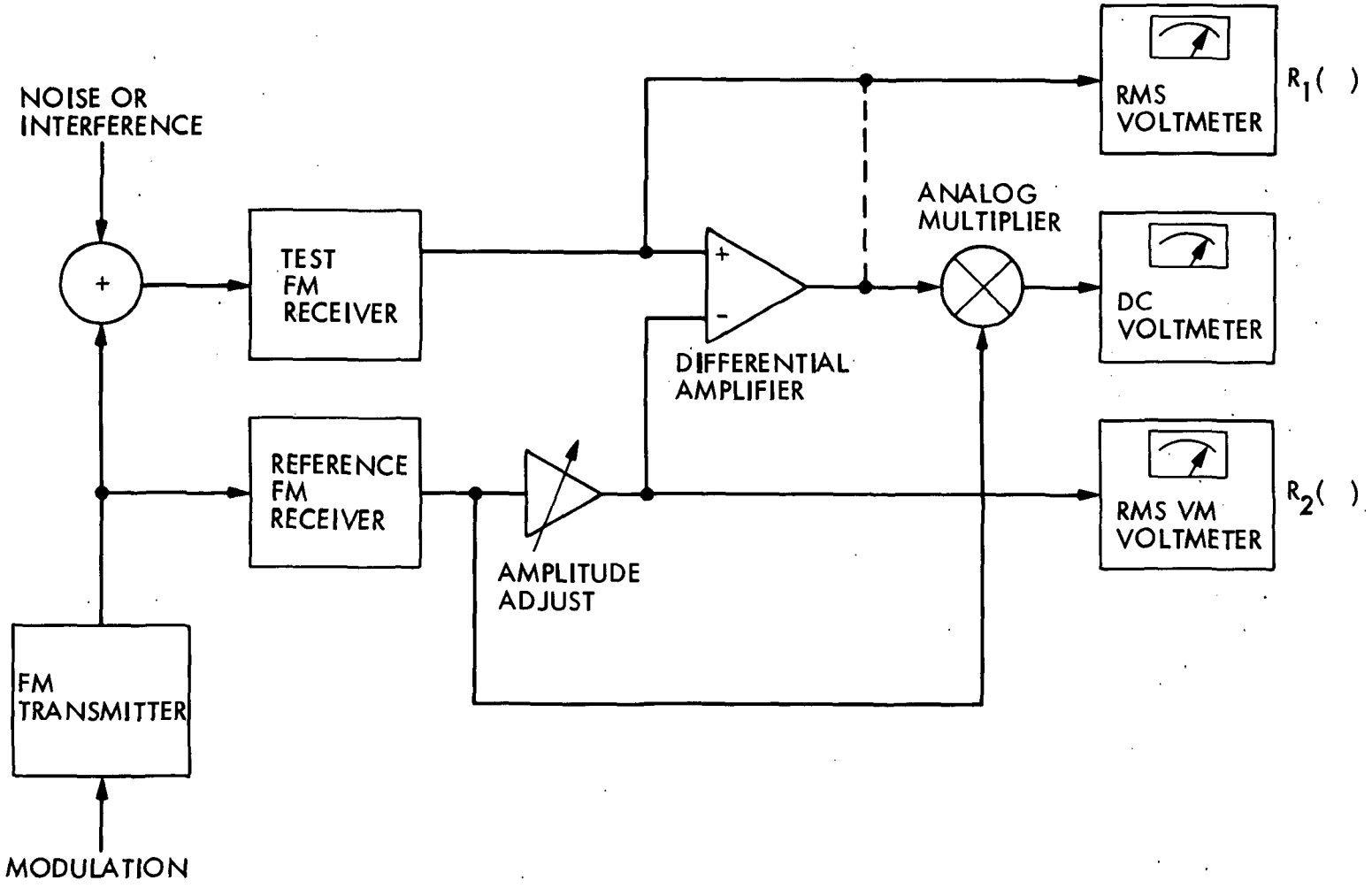

Figure D-3. The Experimental Setup for Random Function Modulation Measurements

demodulated signal phase delay between the two discriminator outputs. This is done after the reference discriminator characteristic is made as nearly identical to the test discriminator characteristic as possible. Once all of the individual elements are matched as closely as possible, a dynamic test is conducted. This is best accomplished by applying a swept frequency (between 300 Hz to 3 kHz) to the FM transmitter. By observing the differential amplifier output on a scope, and adjusting the reference amplitude for the largest cancellation possible, the residual waveform seen on the scope will represent the mismatch between the two receiving system characteristics. To minimize the residual, the input group delay, discriminator tuning, and LPF components of the reference receiver may all be trimmed. It is also important that the dc output from the analog multiplier be zero. In fact, adjusting for this latter condition should be at the expense of waveform minimization at the differential amplifier output.

The test measurements should be conducted according to the following procedure (both rms voltmeters connected to receiver outputs)

(1) Apply the noise modulation to the FM transmitter and set the desired rms deviation. (This should be monitored throughout the tests by checking the rms voltage of the noise signal to assure that it remains constant.)

(2) Adjust the reference amplitude until the dc voltmeter (or oscilloscope) indicates zero volts.

(3) Record the two rms voltmeter readings, $R_1'(\infty)$ and $R_2(\infty)$. The values are comprised of the components:

$$R_1'(\infty) = \sqrt{\langle s^2(t)\rangle + \langle s_D^2(t)\rangle + \langle n_c^2(t)\rangle} \qquad \text{(D-45)}$$

$$R_2(\infty) = \sqrt{\langle s_r^2(t)\rangle + \langle s_{Dr}^2(t)\rangle + \langle n_{cr}^2(t)\rangle} \qquad \text{(D-46)}$$

Since by virtue of receiver matching $s(t) \cong s_r(t)$ and $s_D(t) \approx s_{Dr}(t)$, any difference in the $R_1(\infty)$ and $R_2(\infty)$ readings should be due to the individual circuit noise components.

(4) Remove the modulation from the FM transmitter, and measure the circuit noise from each receiver. These measurements will be given the respective symbols R_{n_c} and $R_{n_{cr}}$. If in Step (3) $R_1'(\infty)$ and $R_2(\infty)$ did not exactly agree, and R_{n_c} is not identical to $R_{n_{cr}}$, then compute $R_1'^2(\infty) - R_{n_c}^2$ and $R_2^2(\infty) - R_{n_{cr}}^2$. These latter two values should be nearly equal. Any slight difference may be attributed to the mismatch between the two receiving subsystems.

(5) Connect the test receiver rms voltmeter to the differential amplifier output, and reapply the noise modulation to the FM transmitter. The dc voltmeter (or oscilloscope) should still read zero. Record the test rms voltmeter reading, $R_1(\infty)$. This should be comprised of three components;

$$R_1(\infty) = \sqrt{\langle s_0^2(t)\rangle + \langle n_c^2(t)\rangle + \langle n_{cr}^2(t)\rangle} \qquad \text{(D-47)}$$

where $s_0(t)$ is the residual signal component due to receiver mismatch. As a result, we should obtain $R_1(\infty) > R_1'(\infty)$.

(6) Add the noise or interference at the desired level ρ. Adjust the reference amplitude until the dc voltmeter or oscilloscope reads zero, and record $R_1(\rho)$ (where the rms voltmeter is still connected to the differential amplifier output) and $R_2(\rho)$.

This completes the measurement procedure. Calculation of the SNR or S/I follows. The no impairment and interference signal level is given by

$$s(\infty) = \sqrt{R_2^2(\infty) - R_{n_{cr}}^2} = \sqrt{\langle s_r^2(t)\rangle + \langle s_{DR}^2(t)\rangle} \tilde{=} \sqrt{\langle s^2(t)\rangle + \langle s_D^2(t)\rangle} \qquad \text{(D-48)}$$

Note that unlike the situation for sinusoidal modulation where it was possible to eliminate the signal harmonic components, the distortion component for random modulation cannot be easily eliminated. Thus, it will have to be included as part of the output signal.

When noise/interference is present, the output signal level is

$$s(\rho) = \sqrt{R_2^2(\rho) - R_{n_{cr}}^2} \qquad \text{(D-49)}$$

Signal suppression by the noise/interference is given by

$$\alpha = \frac{s(\rho)}{s(\infty)} = \sqrt{\frac{R_2^2(\rho) - R_{n_{cr}}^2}{R_2^2(\infty) - R_{n_{cr}}^2}} \qquad \text{(D-50)}$$

If it is assumed that the residual signal $s_o(t)$ is also suppressed by α, then the noise or interference output level is given by

$$n(\rho) \text{ or } I(\rho) = \sqrt{R_1^2(\rho) - \alpha^2\left[R_1^2(\infty) - R_{n_c}^2 - R_{n_{cr}}^2\right] - R_{n_c}^2 - R_{n_{cr}}^2} \qquad \text{(D-51)}$$

The SNR or S/I is then given in dB by

$$\text{SNR or S/I} = 10 \log_{10}\left\{s^2(\rho)/n^2(\rho)\right\}$$

$$= 10 \log_{10}\left\{\frac{R_2^2(\rho) - R_{n_{cr}}^2}{R_1^2(\rho) - \left[\frac{R_2^2(\rho) - R_{n_{cr}}^2}{R_2^2(\infty) - R_{n_{cr}}^2}\right]\left(R_1^2(\infty) - R_{n_c}^2 - R_{n_{cr}}^2\right) - R_{n_c}^2 - R_{n_{cr}}}\right\} \qquad \text{(D-52)}$$

Due to the distortion component having to be included in the signal output, the measured SNR may be slightly higher than theoretical predictions for large ρ.

D.4 ALTERNATE MEASUREMENT METHOD USING THE HP 3582A SPECTRUM ANALYZER

This approach is not recommended because of the need for time-consuming spectrum plotting and plot area measurement for each value of ρ. The approach procedure is being given here for information purposes.

Figure D-4 shows the manner by which the FM system must be viewed. The desired signal s(t) may be a filtered version of the modulation m(t), while all noise, interference, distortion, etc., must be lumped into a single term, $\nu(t)$, which will now be comprised of

$$\nu(t) = n(t) + s_D(t) + n_{sxn}(t) + n_c(t) \qquad \text{(D-53)}$$

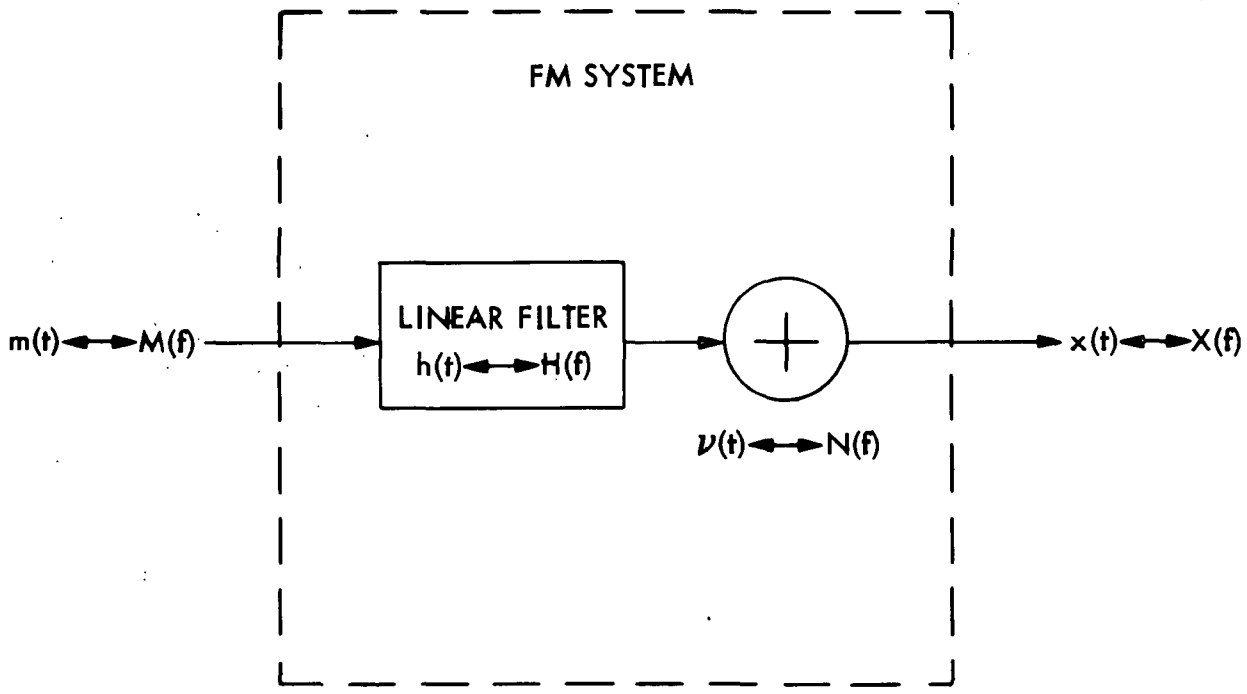

Figure D-4. Spectrum Analyzer Measurement Model for Random Function Modulation

The SNR (or S/I) that is ultimately measured using the spectrum analyzer approach is

$$SNR = \frac{\langle m^2(t)\rangle}{\langle v^2(t)\rangle}$$

$$= \frac{\langle m^2(t)\rangle}{\langle n^2(t)\rangle + \langle s_D^2(t)\rangle + \langle n_{sxn}^2(t)\rangle + \langle n_c^2(t)\rangle} \qquad \text{(D-54)}$$

which should be noted as different from the previously discussed approach in Section D.2, which gives

$$SNR \tilde{=} \frac{\langle s^2(t)\rangle + \langle s_D^2(t)\rangle}{\langle n^2(t)\rangle + \langle n_{sxn}^2(t)\rangle} \qquad \text{(D-55)}$$

However, if m(t) is sufficiently narrowband (set by prefiltering) so that $s(t) \approx m(t)$, i.e., the effects of the filter can be ignored, then the spectrum analyzer measured SNR becomes

$$SNR \tilde{=} \frac{\langle s^2(t)\rangle}{\langle n^2(t)\rangle + \langle s_D^2(t)\rangle + \langle n_{sxn}^2(t)\rangle + \langle n_c^2(t)\rangle} \qquad \text{(D-56)}$$

Note that as $\rho \to \infty$, this SNR will be bounded by

$$SNR(\rho \to \infty) = \frac{\langle s^2(t)\rangle}{\langle s_D^2(t)\rangle + \langle n_c^2(t)\rangle} \qquad \text{(D-57)}$$

While the SNR of the preferred approach tends toward ∞ as $\rho \to \infty$.

The HP 3582A spectrum analyzer computes a "coherence function" given by

$$\gamma^2(f) = \frac{\left|G_{XM}(f)\right|^2}{G_{MM}(f)\, G_{XX}(f)} \tag{D-58}$$

where

$$G_{MM}(f) = \overline{M(f)\, M^*(f)}$$

$$G_{XX}(f) = \overline{X(f)\, X^*(f)}$$

$$G_{XM}(f) = \overline{X(f)\, M^*(f)}$$

the overbar denoting average of many successively determined Fourier transforms. Under the previous assumptions, $\gamma^2(f)$ can be shown to be

$$\gamma^2(f) = \frac{G_{MM}(f)}{G_{MM}(f) + G_{NN}(f)} \tag{D-59}$$

Thus with $\gamma^2(f)$ and $G_{MM}(f)$, which are both produced by the spectrum analyzer, it is possible to calculate $G_{NN}(f)$ given by

$$G_{NN}(f) = \frac{1 - \gamma^2(f)}{\gamma^2(f)}\, G_{MM}(f) \tag{D-60}$$

The two power density spectra are frequency limited to the range 0 Hz to W Hz. Therefore, the SNR is calculated as

$$SNR = \frac{\int_0^W G_{MM}(f)\, df}{\int_0^W G_{NN}(f)\, df} \tag{D-61}$$

Note that this will be a time-consuming procedure as the spectrum analyzer will produce the plots $G_{MM}(f)$ and $\gamma^2(f)$ (these must be linear plots), and the plot $G_{NN}(f)$ must be made by hand, following which a planimeter can be used to obtain the areas. This procedure must be repeated for each value of ρ.

It is finally noted that the resolution accuracy of the spectrum analyzer method, comparable to that of the preferred approach, will require an average of 128 spectra.

APPENDIX E

COMPANDING FOR THE LMSS VOICE LINKS

E.1 INTRODUCTION AND BASIC REQUIREMENTS

Speech is a very complex process and rather difficult to characterize from a communication transmission system perspective. In fact, for the communication system design engineer, performance optimization of a voice radio link represents a compromise among several conflicting requirements.

The speech voltage waveform at the output of a microphone is very dynamic. Spoken words and phrases may be viewed as short bursts, called syllables, between which the microphone output is essentially zero. Figure E-1 is such a characterization. For the immediate discussion, each syllable may be represented in terms of its envelope, which may be thought of as a slowly varying function which undulates in accord with the peaks and valleys of the waveform as pictured in Figure E-1.

Syllables generally fall into two classes, voiced and unvoiced. Voiced syllables are those associated with vocal-cord vibration. The vowel letters are an example of voice sounds. Unvoiced syllables or sounds are formed by forcing air through a constricted area of the vocal tract (especially in the mouth and lips) to produce air turbulence. Thus, the unvoiced sounds tend to be "noise like" as compared with the voiced sound's periodic vibrations. Voiced syllables typically have a higher energy content than unvoiced syllables. Another way of stating this is that the waveform envelope for voiced segments is considerably larger than that for unvoiced segments. Thus, in Figure E-1, syllable No. 2 could be thought of as voiced while syllable No. 3 is unvoiced.

A peculiarity of speech is that the unvoiced sounds are more critical to intelligibility than are the voiced (especially vowel) sounds, yet they are the weaker. This, therefore, is one problem the communication system designer faces when the received signal-to-noise ratio (SNR) on a per-syllable basis is a direct function of the speaker's talking intensity. An analog FM link suffers from this fact, as the received-per-syllable SNR is directly proportional to the square of the transmitter's frequency deviation which, in turn, depends upon the voice voltage produced by the microphone. Weak syllables inherently have a lower SNR than do the stronger syllables, so that the resultant noise masking lowers intelligibility. Stated another way, the important unvoiced syllables don't have enough SNR, while the lesser important voiced syllables (in terms of intelligibility) often have an excessive SNR. For a given speaker, the dynamic range between the weakest to strongest syllables is about 20 dB.

If a communication link were to be used by only one select speaker, the link parameters could be adjusted so that the received SNR or intelligibility would meet some stated criterion. However, let a second speaker use the link without any readjustment of parameters, and the performance criterion may not be met. If the second speaker is a

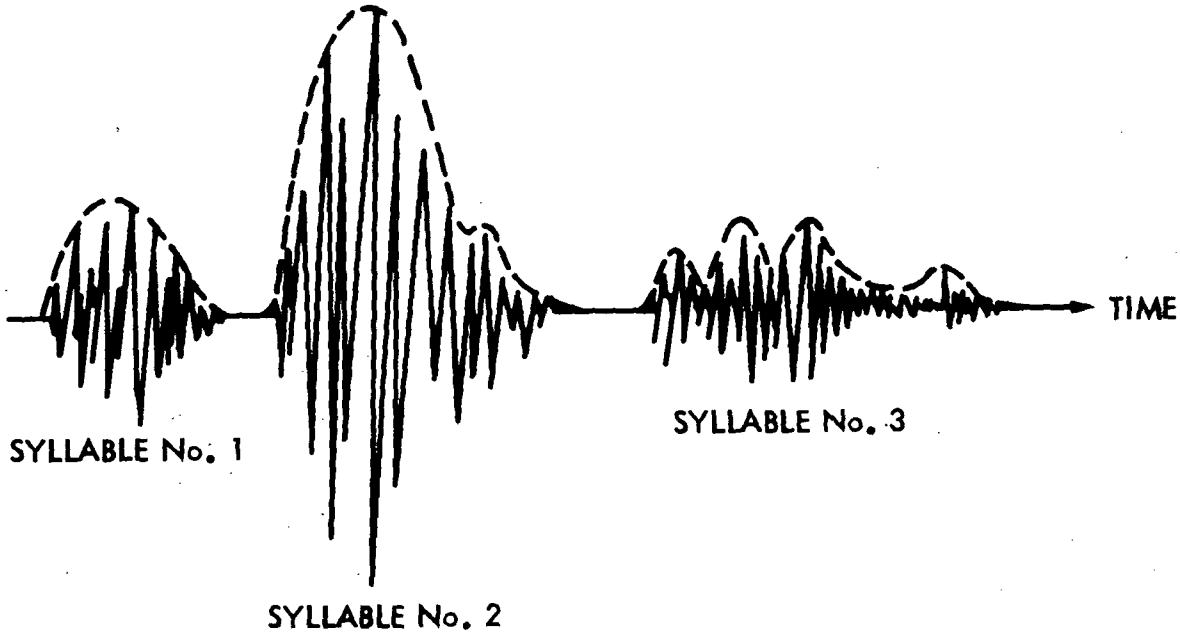

Figure E-1. Speech Waveform With Exact Envelope Representation

comparatively loud talker, the link overperforms (as long as a linearity is maintained), while if he/she is a comparatively soft talker, desired performance becomes degraded. Clearly, although the former case may be tolerated, the latter is unacceptable. One fix, then, is to design the link to meet the performance criterion with a soft spoken talker and accept the excesses for all other speakers. Again, from a communication designer's perspective, such an approach becomes wasteful. Over the total population of speakers, the dynamic range between the softest to the loudest is some 26 dB. Add to this the individual speaking dynamic range of 20 dB, and the engineer must provide for an overall dynamic range in excess of 46 dB. This is unreasonable from a number of measures: high transmitter power, large channel bandwidth, extreme linearity, and subjective listening variants. The means for alleviating these problems is known as companding, the essentials of which are now explored.

E.2 COMPANDOR TYPES AND OPERATION

A compressor is defined as a device that operates on the voice waveform to attenuate strong syllables and amplify weak syllables with respect to some chosen reference level. An expander functions in just the reverse manner. The two units in tandem (the compressor before the transmitter and the expander after the receiver) form the pair known as the compandor. Ideally, the compandor is voice-signal transparent.

There are a number of basic companding algorithms that may be classed either as instantaneous or syllabic. The latter is the type most applicable to voice links. A syllabic compressor will attenuate strong syllables and amplify weak syllables in a manner proportional to the syllable's energy or envelope.

Figure E-2 shows the functional form of the syllabic compressor and expander. The voice signal, $v_i(t)$ is input to a delay line and a syllabic estimator. The syllabic estimator measures in some fashion the intensity of each syllable and outputs a waveform, $e_s(t)$, that is slowly varying in accord with the overall syllable dynamics. Delay of the voice waveform is equal to that introduced by the syllabic estimator. The output of the compressor then becomes the delayed voice signal divided by the syllabic estimator's signal.

Expansion is accomplished in a nearly identical manner as shown. Again, a syllabic estimator produces an identical waveform, $e_s(t)$, to that of the compressor. Note, however, that this must be accomplished on the compressed waveform, $v_o(t)$; thus there is an intrinsic difference between the expander and compressor estimators. Expansion is affected by multiplying $v_o(t)$ by $e_s(t)$ to obtain $v_i(t)$.

Functionally, the compressor and expander operations are easily understood. Mechanistically, difficulties arise. Audiofrequency delays of tens of milliseconds are not easy to implement, and dividers and multipliers are complex and costly (although recent advances in LSI circuits have decreased this aspect). An estimator of any sophistication can also be complex and costly, and it must be remembered that the compressor and expander

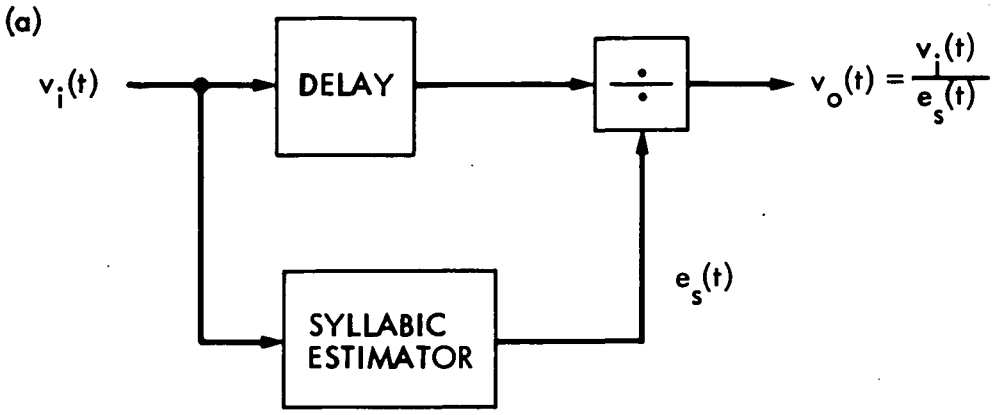

Figure E-2a. Functional Block Diagram of a Syllabic Compandor: Compressor

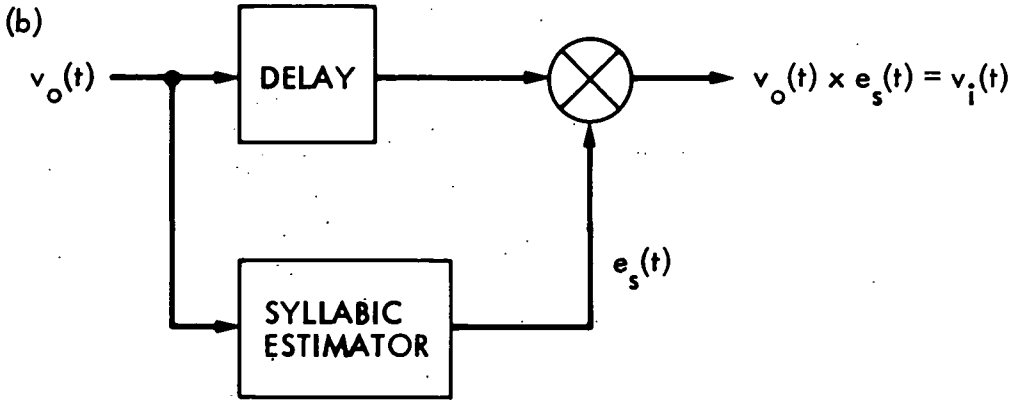

Figure E-2b. Functional Block Diagram of a Syllabic Compandor: Expander

syllabic estimators are different. Another problem with the expander's estimator is that when the degree of compression is large (which means that the compressor output's variation from syllable to syllable is small), and a significant amount of noise has been added to $v_o(t)$, the estimator may fail to produce a credible $e_s(t)$ and proper expansion will be compromised. A method for circumventing this problem, called linking, is to transmit the compressor's $e_s(t)$ along with the compressed signal $v_o(t)$. (More will be said about linking later). All in all, then, it is not surprising that most compandors found in commercial use only approximate the functional configuration of Figure E-2.

Compandors have been extensively used for wireline telephone service for over 30 years. It is only recently that they have been applied to mobile radio. They are also used on certain HF overseas links. The common commercial compressor has a 2:1 logarithmic input/output characteristic, that is, the output of the compressor changes 1 dB for every 2 dB of input signal change. Actually, it is an approximation to the signal's envelope that varies in this manner. Thus, at least ideally, if the input waveform has an rms value of σ_{v_i}, the output waveform has an rms value of σ_{v_o}, and the two values are related by the relationship:

$$\sigma_{v_o} = \sqrt{\sigma_{v_i}} \qquad \text{(E-1)}$$

Stated in other terms, the output signal's power is one-half that of the input signal. The waveform of Figure E-1 might appear as shown in Figure E-3 following 2:1 compression.

Figure E-4 shows the functional block diagram of a 2:1 compandor. The input signal is passed through a voltage-controlled amplifier (VCA) where the output, representing the compressed signal, is rectified (usually by a linear half-wave circuit), and then lowpass filtered (LPF) to form the control input to the VCA. This is simply a feedback regulator. The expander works in essentially the same fashion except that it is a feedforward regulator. Note that no delays are introduced into the signal path. On the other hand, the LPF does provide some delay in the feedback (or feedforward) path. Typically, the attack and recovery times of the units are 3 ms and 14 ms respectively, which are obtained by the use of a 20-ms time-constant R-C filter. What the rectifier and LPF jointly accomplish is an approximate measurement of the syllabic envelope as shown in Figure E-5, with the VCA gain being inversely proportional to the instantaneous approximate envelope value. Clearly, because of the simplistic mechanization of the 2:1 compandor, and especially a lack of delay compensation in the signal path, the compandor's output is not exactly equal to its input. Nevertheless, for very high SNR applications, and because the ear is reasonably insensitive to the companding error for narrowband voice signals, the overall performance is quite satisfactory.

Higher compression ratios have been investigated and implemented. In particular, a 4:1 logarithmic input/output characteristic has received considerable attention. Usually, such has been realized by cascading two 2:1 compressors at the transmitter and two 1:2 expanders at the receiver. This approach has not yielded wholly acceptable results, principally because of the

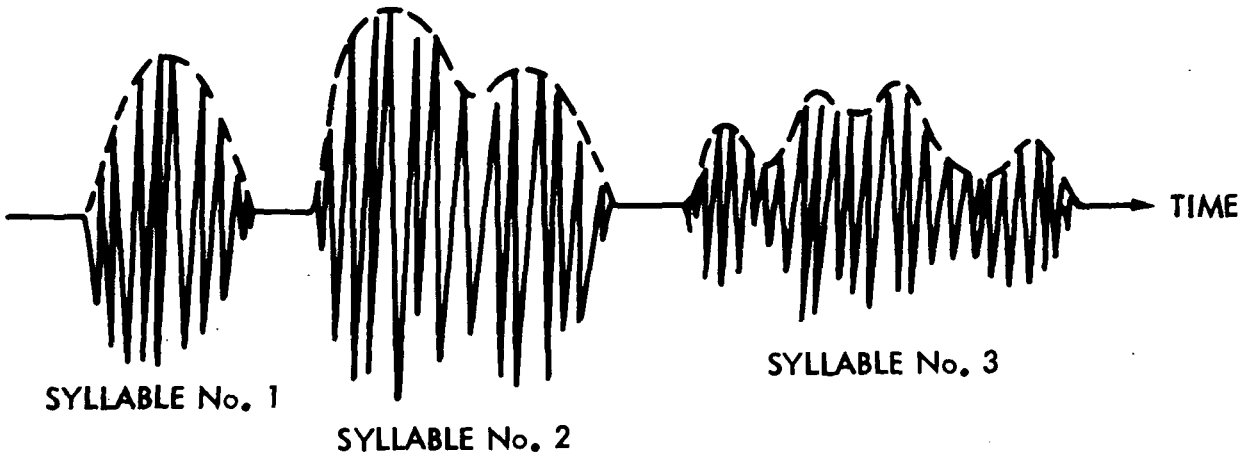

Figure E-3. Speech Waveform After 2:1 Compression

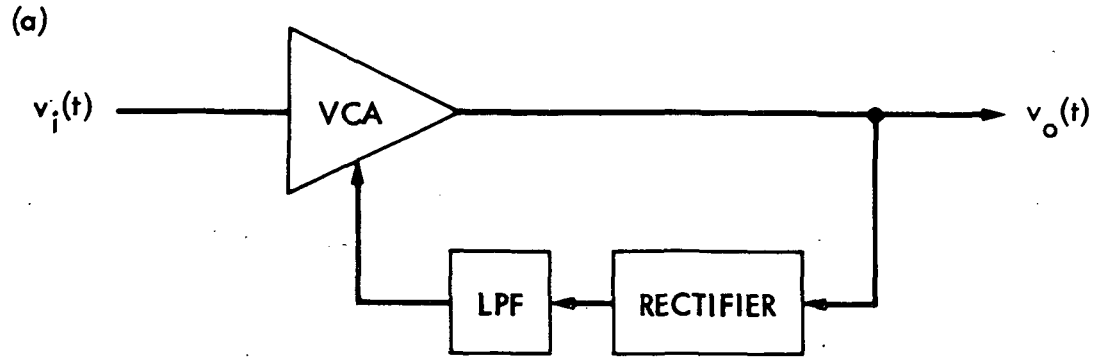

Figure E-4a. Functional Block Diagram of a 2:1 Compandor: 2:1 Compressor

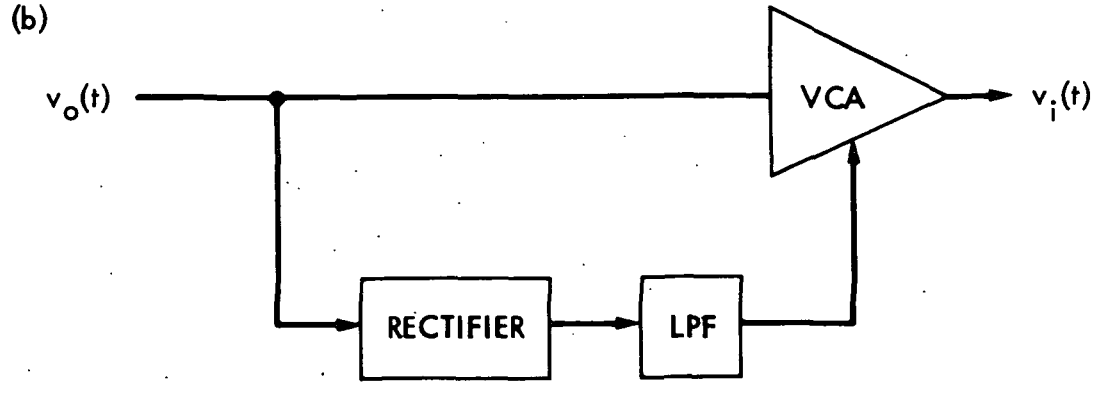

Figure E-4b. Functional Block Diagram of a 2:1 Compandor: 1:2 Expander

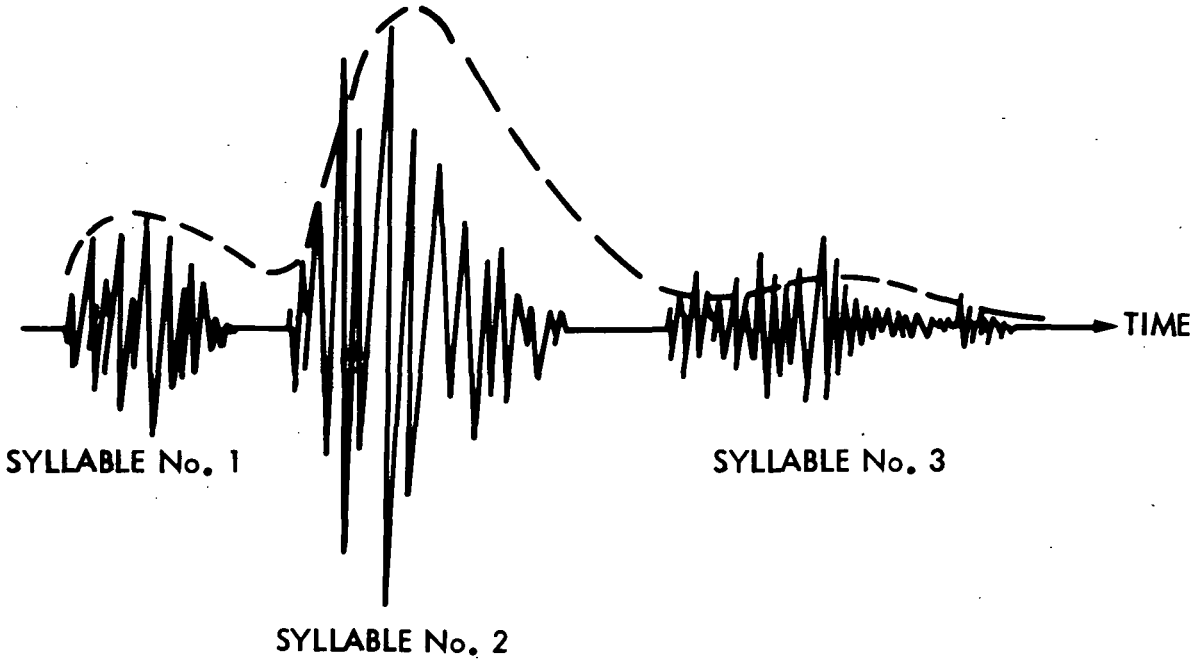

Figure E-5. Speech Waveform With Approximate Envelope Representation

lack of signal delay compensation, proliferation of the unequal input/output effect, and a lessened tolerance to additive noise by the expansion operation.

One problem concerning the use of companding for radio links is that under the conditions of fading, the expander actually exaggerates the effects of fading, making reception appear worse to the listener than it actually is. It might seem natural to ask: What happens if only compression is employed without the corresponding use of the expander at the receiver? Surprisingly, for high SNR situations, the intelligibility of the compressed voice signal is virtually the same as that for the uncompressed version. There is, however, some perceived unnaturalness, as the compressed syllables sound somewhat "plosive" and the speech dynamics are lacking. It is quality that primarily suffers.

A very impelling reason for not dispensing with the expander is that it provides an effective subjective improvement of SNR. If the noise level out of the receiver is not a function of the voice signal itself, then, between syllables and during speech pauses, the expander sees only the weak noise voltage at its input and acts to significantly attenuate the noise. Thus, a marked quieting takes place, which, to the listener, has the appearance of increasing the overall speech pattern SNR by some 6 to 10 dB. (Remember, with a voice signal present, the background noise is reasonably masked by the voice).

Given the fact, then, that expansion is a desirable attribute, a means for realizing its effectiveness for fading or other imparing conditions is required. The solution is to transmit the compressor's VCA control signal along with the compressed voice, and at the receiver recover the control signal for use by the expansion operation. This eliminates the need for the expander to derive its control waveform from the compressed voice signal. As previously mentioned, the method is called linking. Control signal transmission is effected by modulating the control signal onto a subcarrier or pilot tone placed above the voice audio frequency band. At the receiver, simple filtering permits separation of the voice and modulated subcarrier. For continuous (analog) control waveforms, modulation may be AM or FM. A commercial system which employs this approach is known as "Lincompex." Sometimes the control waveform is quantized (typically to 8 levels), and the information is transmitted using FSK modulation of the subcarrier. The commercial system is called "Syncompex." Clearly, the received control signal must have sufficient SNR (in the presence of fading) to foster acceptable expansion, and therefore must be apportioned the necessary power at the transmitter. Typically, it may be expected that a linked system would require less than a 25 percent transmitter power increase over a nonlinked system.

E.3 *ENVELOPE NORMALIZATION*

The ultimate compressor is one that takes the dynamic voice waveform and transforms it into a signal that has no envelope variations, i.e., a constant envelope signal. A means of accomplishing this result is to divide the voice signal by its own true envelope. Figure E-6 shows what results when the voice waveform of Figure E-1 is envelope normalized. If v(t) is the voice, the envelope of v(t) is mathematically given by

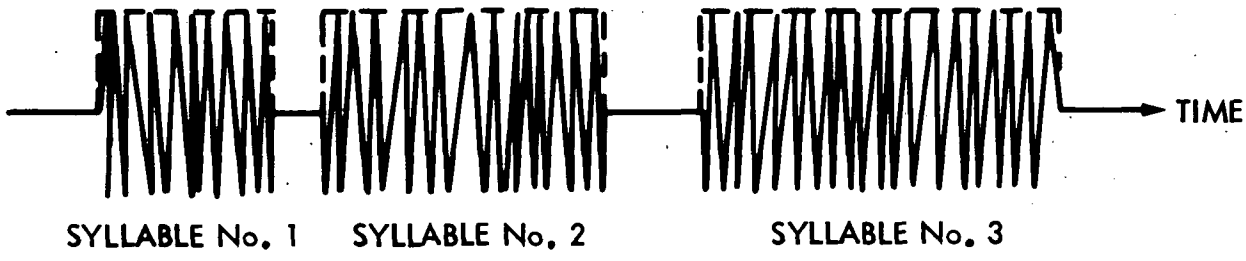

Figure E-6. Speech Waveform After Envelope Normalization

$$\text{evn}\{v(t)\} = \sqrt{v^2(t) + \hat{v}^2(t)} \qquad \text{(E-2)}$$

where $\hat{v}(t)$ is known as the Hilbert transform of $v(t)$. Electrically, $\hat{v}(t)$ may be obtained by passing $v(t)$ through a network that phase shifts each of $v(t)$'s frequency components by exactly 90 deg while at the same time renders the component amplitudes unchanged (i.e., amplitude all pass). The compressor out is given by:

$$v_o(t) = \frac{v(t)}{\text{env}\{v(t)\}} \qquad \text{(E-3)}$$

with the property that env $\{v_o(t)\}$ = unity (or some selected constant). It is interesting to note that the instantaneous amplitude distribution of $v_o(t)$ is identical to that of a sine wave. In fact, an alternate representation is:

$$v_o(t) = \cos[\theta(t)] \qquad \text{(E-4)}$$

with

$$\theta(t) = \tan^{-1}\left\{\frac{\hat{v}(t)}{v(t)}\right\} \qquad \text{(E-5)}$$

Envelope normalization is not widely known by the forms just presented. Yet, the essence of envelope normalization has found extensive use in single sideband communications, especially by radio amateurs. The common designation for the process is "RF clipping" and has been described in many references. Implementations based on the use of RF amplitude limiting circuits in conjunction with SSB signals are reasonably cumbersome. For SSB applications, use has been made of the technique without corresponding expansion at the receiving end, with the resultant limitations already discussed.

It should be clear that envelope normalization companding definitely requires the use of linking (even for a perfect noise-free communication channel) as the constant envelope nature of the compressed signal precludes derivation of an expander control signal at the receiver. (There is the possibility that a pseudoenvelope waveform might be synthesized using frequency analysis and voiced/unvoiced syllable detection. This, however, has not been experimentally verified). The means for accomplishing linking will likely be similar to that used for Lincompex or Syncompex. Figure E-7 is a functional block diagram for an envelope normalizing compandor. The input voice signal is summed with a bias (most likely a tone below or above the audio band) before being processed. Biasing is needed to

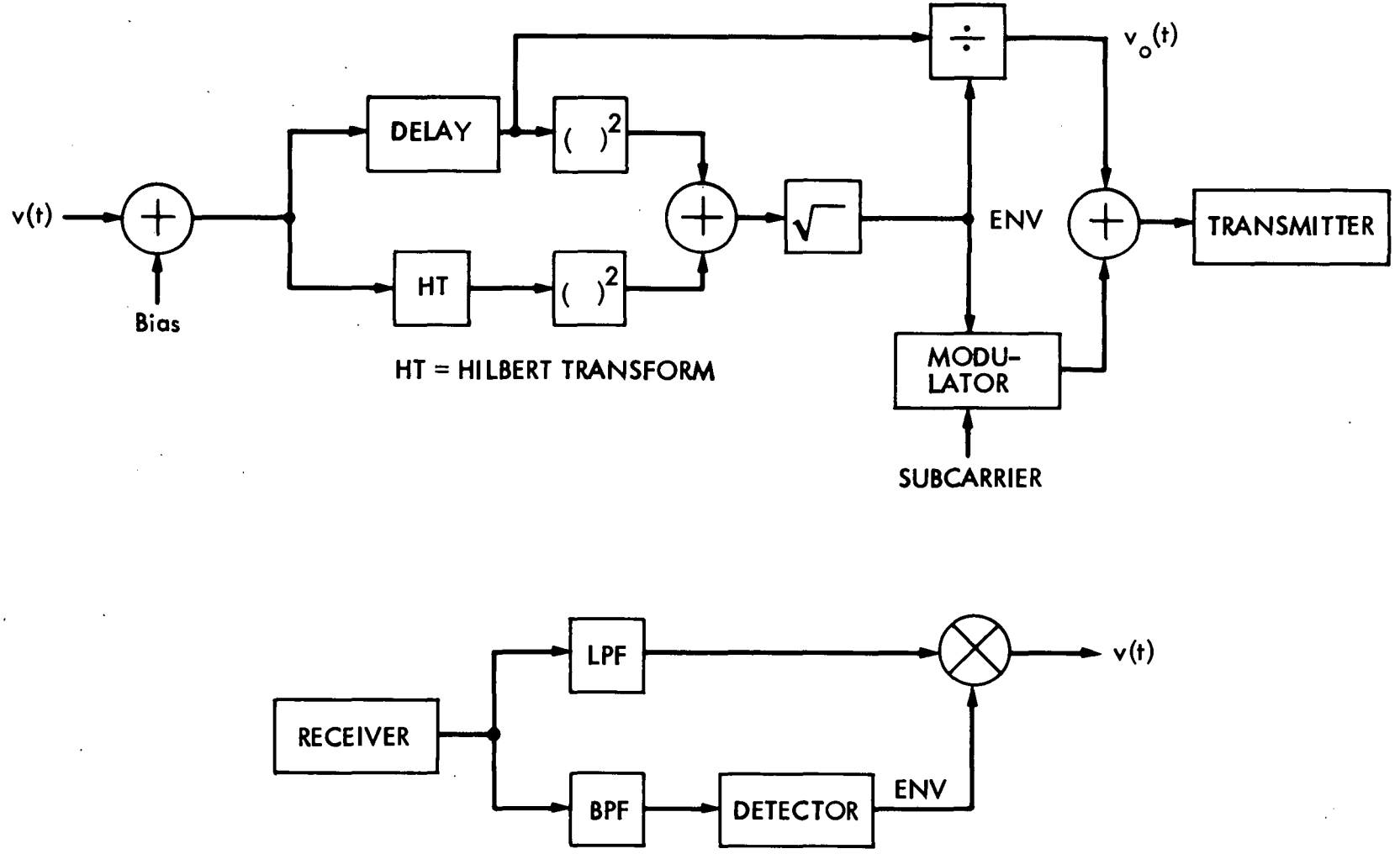

Figure E-7. Functional Envelope Normalization Compandor

prevent the divisor of the normalizing operation from becoming zero between syllables and during pauses. It also prevents circuit noise from being greatly amplified for the same conditions. The envelope (env) generating functions implement the previously defined mathematical form (Equation (E-2)).Division of the delayed voice waveform by the envelope produces the envelope normalized signal, $v_o(t)$. The envelope waveform is also modulated onto a subcarrier. the modulated subcarrier and $v_o(t)$ are then summed (with appropriate weightings) and passed to the transmitter. At the output of the receiver, these same components are extracted respectively by bandpass and low-pass filters. A detector recovers the envelope waveform, which is then used to perform the expansion of the envelope normalized voice.

There are a number of approaches - analog, digital, and hybrid - that can be used to realize Figure E-7. Nearly all of the identified functions are already available in LSI form. Some aspects are amenable to the use of charge-coupled devices. An implementation study, including the best means of handling the bias and subcarrier modulation, should be performed to attain a practical design.

E.4 COMPANDOR PERFORMANCE FOR THE LMSS

As discussed under Section E.1, the communication link must be designed to meet some minimum requirement for the soft-spoken talker. Experience has shown that if the soft talker's weak-syllable SNR is 12 dB, then an overall 90 percent intelligibility is obtained for such a speaker, and the subjective listening quality is judged to be "fair." The presence of background noise is very noticeable. Such performance is some 8 to 10 dB below minimum wireline telephone quality.

For a weak-syllable SNR of 12 dB, the corresponding rms voice SNR is 22 dB for uncompressed voice. As compression is employed, and the weak-syllable SNR is held to 12 dB, the rms SNR decreases. This produces undesirable effects as intelligibility and quality suffer. Thus, it is the soft talker's rms SNR that should be held constant as compression is applied, the net effect being to raise the weak-syllable SNR. Application of this criterion to the various compression ratios discussed under Section E.3 yields the performances tabulated in Table E-1. Note the wide variation in performance between speakers for the no-compression case. At the other extreme, envelope normalization provides a constant SNR for all syllables of all speakers. The subjective SNR improvement factor associated with expansion (as discussed under Section E.2) has not been included in the compression case SNR values of Table E-1 because of its incorporeal or perceived nature. (There is, in fact, no measurable syllable SNR change due to expansion).

The FM link must be designed to accommodate the peak values of a loud speaker's strong syllables. A peak allowance factor of 4.5 dB is appropriate for the no compression, the 2:1, and the 4:1 compression cases. For envelope normalization, the peak factor is 3 dB. FM deviation is calculated to obtain peak SNR values based upon a 10-dB IF SNR into the FM detector (discriminator). Using Carson's rule, together with a maximum voice frequency of 3 kHz, the required IF bandwidths are obtained. The results are found in Table E-2.

Table E-1. Voice SNRs as a Function of Voice Compression Ratio

Parameter	No Compression	2:1 Compression	4:1 Compression	Envelope Normalization
Loud Speaker				
Strong-Syllable SNR, dB	58	39	31	22
Rms SNR, dB	48	34	28	22
Weak-Syllable SNR, dB	38	29	25	22
Average Speaker				
Strong-Syllable SNR, dB	45	33	28	22
Rms SNR, dB	35	28	25	22
Weak-Syllable SNR, dB	25	23	22	22
Soft Speaker				
Strong-Syllable SNR, dB	32	27	25	22
Rms SNR, dB	22	22	22	22
Weak-Syllable SNR, dB	12	17	19	22

Table E-2. FM Parameters as a Function of Compression Type

Compression	Peak Deviation, kHz	IF Bandwidth, kHz	Improvement Relative to No Compression, dB
None	49.3	104.6	-
2:1	10.8	27.6	5.8
4:1	5.5	17.0	7.9
Envelope normalization	2.1	10.2	10.1

The improvement relative to no compression is simply calculated as the ratio of the corresponding IF bandwidths. This factor is important because, for a constant IF SNR of 10 dB for all compression types, it may be viewed as direct savings in required link transmitter power. Relative to the use of 2:1 compression, 4:1 compression reduces the transmitter power needed by 2.1 dB, and envelope normalization decreases the transmitter power requirement by 4.3 dB. Thus, the value of using the slightly more complex envelope normalization compression over 2:1 compression is clearly established. In reality, the improvement will not be quite 4.3 dB because of the need for linking, which requires some transmitter power. It is estimated that a linked envelope normalization system will save about 3.5 dB of transmitter power with respect to that needed for 2:1 compression.

E.5 CONCLUDING REMARKS

One strong motivation for using 2:1 voice compression is that fact that the Bell System has developed an experimental system using this compression ratio for its Advanced Mobile Phone Service (AMPS) Program. The AMPS mobile transceivers utilize FM and operate on the same 806- to 890-MHz band selected for the LMSS. Therefore, compatibility is a strong driver - a single mobile unit that will work with the AMPS local cellular stations and with the LMSS.

An AMPS transceiver requires modification for use with LMSS. It will not tune to the proposed LMSS RF channels. A lower receiver noise figure, and probable higher transmitter power, are also required. It does not seem, then, that the incorporation of two voice compression schemes, 2:1 compression and envelope normalization, into a single universal transceiver is unreasonable. A switch may simply select the proper method depending upon which service is to be employed.

This paper has developed a case for the use of voice envelope normalization with the LMSS. The prime reason is the considerable reduction of satellite transmitter power (3.5 dB over that needed for 2:1 voice compression) in a situation where prime power is severely limited. Some development engineering is required to implement a practical envelope normalization system. It is believed, however, that such costs will be significantly less than other possible system improvements that can claim the same improvement factor.

APPENDIX F

ANALYSIS OF COCHANNEL INTERFERENCE FOR FM SYSTEMS

F.1 INTRODUCTION

In this appendix we investigate the relationship between C/I at the input to an FM receiver and the power ratio of the desired baseband signal to the interfering baseband signal. We begin in Section F.2 with the case of a single interfering signal, and then in Section F.3 generalize to N > 1 interferers.

F.2 SINGLE-INTERFERER ANALYSIS

Let the desired signal be given by:

$$S(t) = \sqrt{2P}\cos\left[\omega_c t + \phi_s(t)\right] \tag{F-1}$$

Where the carrier power is P, and $\phi_s(t)$ is the modulation. For FM, the desired baseband signal is $\dot{\phi}_s(t)$, with the relationship:

$$\phi_s(t) = \int_{-\infty}^{t} \dot{\phi}_s(\lambda)d\lambda \tag{F-2}$$

The interfering signal is defined as:

$$S_i(t) = \sqrt{2P_i}\cos\left[\omega_c t + \phi_i(t)\right] \tag{F-3}$$

with carrier power P_i, and phase modulation $\phi_i(t) = \omega_D t + \phi_1(t)$. Here ω_D represents a small frequency difference between the desired and interfering signals, and $\phi_1(t)$ is a phase modulation arising from FM by the baseband signal $\dot{\phi}_1(t)$.

The two modulating terms, $\dot{\phi}_s(t)$ and $\dot{\phi}_1(t)$, are totally independent but have the same power spectrum $W_{\dot{\phi}}(f)$. Thus,

$$\overline{\dot{\phi}_s^2(t)} = \overline{\dot{\phi}_1^2(t)} = 2\int_0^\infty W_{\dot{\phi}_s}(f)\,df \triangleq \sigma_{\dot{\phi}_s}^2 \tag{F-4}$$

This relationship will be expanded upon and used later.

By definition,

$$C/I = P/P_i = u^{-2} \tag{F-5}$$

The coefficient u will arise in the subsequent analysis.

The input to the FM receiver is $S(t) + S_i(t)$, which can be written in the form:

$$S(t) + S_i(t) = \alpha(t) \cos [w_0 t + \psi(t)] \tag{F-6}$$

Since $\alpha(t) \geq 0$ for all t, the amplitude limiter that preceeds the FM demodulator removes $\alpha(t)$ from further consideration. The FM demodulator then functions to produce $\dot{\psi}(t)$, which is given in terms of the input signal parameters by:

$$\dot{\psi}(t) = \frac{d}{dt} \left\{ \tan^{-1} \left[\frac{\sin \phi_s(t) + u \sin \phi_i(t)}{\cos \phi_s(t) + u \cos \phi_i(t)} \right] \right\} \tag{F-6a}$$

$$= \frac{\dot{\phi}_s(t) + u^2 \dot{\phi}_i(t) + u [\dot{\phi}_s(t) + \dot{\phi}_i(t)] \cos [\phi_s(t) - \phi_i(t)]}{1 + u^2 + 2u \cos [\phi_s(t) - \phi_i(t)]} \tag{F-6b}$$

Equation (F-6b) may now be rewritten in the form:

$$\dot{\psi}(t) = a [\phi_s(t), \phi_i(t)] \dot{\phi}_s(t) + b [\phi_s(t), \phi_i(t)] \dot{\phi}_i(t) \tag{F-7}$$

with

$$a[\phi_s(t), \phi_i(t)] = \frac{1 + u \cos [\phi_s(t) - \phi_i(t)]}{1 + u^2 + 2u \cos [\phi_s(t) - \phi_i(t)]} \tag{F-8}$$

and

$$b[\phi_s(t), \phi_i(t)] = 1 - a[\phi_s(t), \phi_i(t)] \tag{F-9}$$

Now, since $\phi_s(t)$ and $\phi_i(t)$ are independent, we let $\omega_D = 0$, and

$$\phi \triangleq \phi_s + \phi_i \tag{F-10}$$

With variance σ_ϕ^2. (Note that we are also dropping the time-dependence designation since we will subsequently be dealing with statistical averages.) Thus, using Equations (F-9) and (F-10), Equations (F-7) and (F-8) are rewritten as:

$$\dot{\psi} = a(\phi)\,\dot{\phi}_s + [1 - a(\phi)\,]\,\dot{\phi}_i \tag{F-11}$$

$$a(\phi) = \frac{1 + u\cos(\phi)}{1 + u^2 + 2u\cos(\phi)} \tag{F-12}$$

Our task now is to calculate the fractional power of $\dot{\phi}_s$ contained in $\dot{\psi}$, and the amount of interference power. To facilitate evaluation, $\dot{\phi}_s$ and $\dot{\phi}_i$ are assumed to be Gaussian random processes. It is well known, then, that ϕ_s and ϕ_i are also Gaussian processes, with $\dot{\phi}_s$ and $\dot{\phi}_i$ being linearly independent, as are $\dot{\phi}_i$ and ϕ_i. Further,

$$\overline{\phi_s^2} = \overline{\phi_i^2} = 2\int_0^\infty f^{-2}\, W_{\dot{\phi}_s}(f)\, df \tag{F-13}$$

which, using Equation (F-4), may be written as:

$$\overline{\phi_s^2} = \overline{\phi_i^2} = \sigma_{\dot{\phi}_s}^2 \frac{\displaystyle\int_0^\infty f^{-2}\, W_{\dot{\phi}_s}(f)\, df}{\displaystyle\int_0^\infty W_{\dot{\phi}_s}(f)\, df} \tag{F-14}$$

The random process ϕ is also Gaussian with variance

$$\sigma_{\phi}^2 = 2\sigma_{\dot{\phi}_s}^2 \frac{\int_0^{\infty} f^{-2} W_{\dot{\phi}}(f)\, df}{\int_0^{\infty} W_{\dot{\phi}}(f)\, df} \qquad \text{(F-15)}$$

Before proceeding to the evaluation of the needed statistical averages, it is instructive to calculate a typical σ_{ϕ}^2. If Δf_p is the peak frequency deviation of the FM transmitter, and we assume a peak-to-rms deviation ratio of $\sqrt{10}$, then,

$$\sigma_{\dot{\phi}_s}^2 = \frac{(2\pi\Delta f_p)^2}{10} \qquad \text{(F-16)}$$

From Ref. C-11, we take $W_{\dot{\phi}}(f)$ to be proportional to:

$$W_{\dot{\phi}}(f) \propto f^6 \left[(f^2 + 70^2)(f^2 + 180^2)(f^2 + 400^2)(f^2 + 700^2)\right]^{-1} \qquad \text{(F-17)}$$

Where a 6-dB/octave preemphasis has been included. Evaluating the integrals of Equation (F-15) by use of a computer results in

$$\sigma_{\phi}^2 = 8.87 \times 10^{-6} (\Delta f_p)^2 \qquad \text{(F-18)}$$

Now, if we let Δf_p = 10 kHz (a typical LMSS value for 2:1 compressed speech), then $\sigma_{\phi}^2 = 887$ (rad^2). As we shall see, the fact that this is a very large value is significant to the results that follow.

Returning now to Equations (F-11) and (F-12), we first note that when u = 1 (i.e., C/I = 0 dB), $a(\phi) \equiv 1/2$ irrespective of the process ϕ. Thus:

$$\dot{\psi} = \frac{1}{2}\dot{\phi}_s + \frac{1}{2}\dot{\phi}_i \qquad \text{(F-19)}$$

from which we can easily see that the desired and interfering baseband signal powers are equal.

When $u < 1$, $a(\phi)$ may be expanded in an infinite series, viz,

$$a(\phi) = \sum_{n=o}^{\infty} (-u)^n \cos(n\phi) \tag{F-20}$$

Now, the fractional power of $\dot{\phi}_s$ contained in $\dot{\psi}$ depends upon the mean value of $a(\phi)$, denoted $\overline{a(\phi)}$, given by:

$$\overline{a(\phi)} = \sum_{n=0}^{\infty} -(u)^n \int_{-\infty}^{\infty} \cos(n\phi)\, p(\phi)\, d\phi \tag{F-21}$$

$$p(\phi) = (\sqrt{2\pi}\sigma_{\phi}) \exp\left[-\phi^2/2\sigma_{\phi}^2\right] \tag{F-22}$$

Integral tables readily yield the result:

$$\overline{a(\phi)} = \sum_{n=o}^{\infty} (-u)^n \exp\left[-n^2 \sigma_{\phi}^2/2\right] \tag{F-23}$$

But, using the previously calculated value of $\sigma_{\phi}^2 = 887$, we see that the only term of significance is the first term ($n = 0$) of the series, so that

$$\overline{a(\phi)} = 1 \tag{F-24}$$

for all $u < 1$. Recalling that $\overline{a(\phi)} = 1/2$ when $\mu = 1$, we see that $\overline{a(\phi)}$ has a jump discontintuity as $u \to 1$. (This is an interesting paradox observed in other works dealing with cw interference in spread-spectrum systems.) Thus, when $u < 1$ we take the fractional power of $\dot{\phi}_s$ contained in $\dot{\psi}$ to be

$$\text{power}\,(\dot{\phi}_s) = \left[\overline{a(\phi)}\right]^2 \left[\dot{\phi}_s^2\right] = \sigma_{\dot{\phi}_s}^2 \tag{F-25}$$

To calculate the interference power, we begin by examining the mean square value of $\dot{\psi}$, which from Equation (F-11), is given by:

$$\overline{\dot{\psi}^2} = \left[1 - \overline{2a(\phi)} + \overline{2a^2(\phi)}\right] \sigma_{\dot{\phi}_s}^2 \qquad \text{(F-26)}$$

Using Equation (F-24), Equation (F-26) becomes:

$$\overline{\dot{\psi}^2} = \left[\overline{2a^2(\phi)} - 1\right] \sigma_{\dot{\phi}_s}^2 \qquad \text{F-27)}$$

We must therefore calculate the mean square value of $a(\phi)$, which is given by:

$$\overline{a^2(\phi)} = \sum_{n=o}^{\infty} \sum_{m=o}^{\infty} (-u)^{n+m} \quad \overline{\cos(n\phi)\cos(m\phi)} \qquad \text{(F-28)}$$

Taking the indicated average on the cosine terms yields:

$$\overline{a^2(\phi)} = \frac{1}{2} \sum_{n=o}^{\infty} \sum_{m=o}^{\infty} (-u)^{n+m} \left\{ \exp\left[-(n+m)\frac{\sigma_\phi^2}{2}\right] + \exp\left[-(n-m)\frac{\sigma_\phi^2}{2}\right] \right\} \qquad \text{(F-29)}$$

Again, using $\sigma_\phi^2 = 887$, the only terms of significance result when $n = m$, giving

$$\overline{a^2(\phi)} = 1 + \frac{1}{2} \sum_{n=1}^{\infty} u^{2n} \qquad \text{(F-30a)}$$

$$= \frac{1}{2}\left[\frac{2 - u^2}{1 - u^2}\right], \quad u < 1 \qquad \text{(F-30b)}$$

Now we find a very definite problem here, for as $u \to 1$, $\overline{a^2(\phi)} \to \infty$, and therefore $\overline{\dot{\psi}^2} \to \infty$. This difficulty is due to the fact that even though $\phi(t)$ is a band-limited random process, $\cos[n\phi(t)]$ has a spectrum that mathematically extends to infinite frequency. Thus, if we are going to obtain a useful

result, the process $\dot{\psi}(t)$ will have to be low-pass filtered. We therefore define a new process as

$$Z(t) = a[\phi(t)] * h(t) \tag{F-31}$$

where $h(t)$ is the impulse response of the LPF, and * denotes convolution. We now proceed to find $\overline{Z^2}$.
It has been established (Ref. F-1) that

$$\overline{Z^2} = \int_{-\infty}^{\infty} \rho_h(\tau) K_a(\tau)\, d\tau \tag{F-32a}$$

$$= 2\int_{o}^{\infty} \left|H(f)\right|^2 W_a(f)\, df \tag{F-32b}$$

where $\rho_h(\tau)$ is the autocorrelation function of the LPF, and $|H(f)|$ is the magnitude squared of the LPF transfer function, with

$$\left|H(f)\right|^2 = \mathscr{F}\left\{\rho_h(\tau)\right\} \tag{F-33}$$

and $K_a(\tau)$ is the covariance function of the process $a[\phi(\tau)]$, with

$$W_a(f) = \mathscr{F}\left\{K_a(\tau)\right\} \tag{F-34}$$

The operator $\mathscr{F}$ is the Fourier transform.

Formally, $K_a(\tau)$ is given by:

$$K_a(\tau) = \sum_{n=o}^{\infty} \sum_{m=o}^{\infty} (-u)^{n+m} \left\{ \frac{}{\cos\left[n\phi(\tau_1)\right] \cos\left[m\phi(\tau_2)\right]} \right\} \tag{F-35}$$

with $\tau = \left|\tau_2 - \tau_1\right|$. Evaluation of the expectation is somewhat involved, so the details will not be presented here. The result is:

$$K_a(\tau) = \sum_{n=o}^{\infty} \sum_{m=o}^{\infty} (-u)^{n+m} \exp\left[-(n^2 + m^2)\frac{\sigma_\phi^2}{2}\right] \cosh\left[nm\,\sigma_\phi^2\,\rho_\phi(\tau)\right] \tag{F-36}$$

where $\rho_\phi(\tau)$ is the normalized covariance of the process $\phi(\tau)$.

We now examine Equation (F-36) for large σ_ϕ^2, and again find that the only significant terms are when n = m, with the result:

$$K_a(\tau) = 1 + \frac{1}{2}\sum_{n=1}^{\infty} u^{2n} \exp\left[-n^2\sigma_\phi^2\left\{1 - \rho_\phi(\tau)\right\}\right] \tag{F-37}$$

Let us define $K_n(\tau)$ by

$$K_n(\tau) = \exp\left[-n^2\,\sigma_\phi^2\,\left\{1 - \rho_\phi(t)\right\}\right] \tag{F-38}$$

Then,

$$K_a(\tau) = 1 + \frac{1}{2}\sum_{n=1}^{\infty} u^{2n}\, K_n(\tau) \tag{F-39}$$

and from Equation (F-32a),

$$\overline{Z^2} = 1 + \frac{1}{2}\sum_{n=1}^{\infty} u^{2n} \int_{-\infty}^{\infty} \rho_h(\tau) K_n(\tau)\, d\tau \tag{F-40}$$

Before proceeding with the final evaluation, we take stock of what it is that we are attempting to accomplish. Returning to Equation (F-11), we now write:

$$\dot{\psi}_f = Z\dot{\phi}_s + [1 - Z]\,\dot{\phi}_i \tag{F-41}$$

where we have assumed that the LPF has no effect on the band-limited functions $\dot{\phi}_s$ and $\dot{\phi}_i$. Then,

$$\overline{\dot{\psi}_f^2} = \left[1 - 2\bar{Z} + 2\overline{Z^2}\right]\sigma_{\dot{\phi}_s}^2 \tag{F-42}$$

It is readily determined that $\overline{Z} = 1$, so Equation (F-42) becomes:

$$\overline{\dot{\psi}_f^2} = \left[2\overline{Z^2} - 1 \right] \sigma_{\dot{\phi}_s}^2 \tag{F-43}$$

Now, the power in the interference is given by

$$\text{power (i)} = \overline{\dot{\psi}_f^2} - \sigma_{\dot{\phi}_s}^2 = 2 \left[\overline{Z^2} - 1 \right] \sigma_{\dot{\phi}_s}^2 \tag{F-44}$$

and substituting Equation (F-40) we have

$$\text{power (i)} = \sigma_{\dot{\phi}_s}^2 \sum_{n=1}^{\infty} u^{2n} \int_{-\infty}^{\infty} \rho_h(\tau) K_n(\tau)\, d\tau \tag{F-45}$$

or, alternatively, using the form of Equation (F-32b),

$$\text{power (i)} = 2\sigma_{\dot{\phi}_s}^2 \sum_{n=1}^{\infty} u^{2n} \int_0^{\infty} \left| H(f) \right|^2 W_n(f)\, df \tag{F-46}$$

where:

$$W_n(f) = \mathcal{F} \{ k_n(\tau) \} \tag{F-47}$$

Finally, the desired power ratio is:

$$R = \frac{\text{power} \left(\dot{\phi}_s \right)}{\text{power (i)}} = \left[2 \sum_{n=1}^{\infty} u^{2n} \int_0^{\infty} \left| H(f) \right|^2 W_n(f)\, df \right]^{-1} \tag{F-48}$$

It remains now to evaluate the integral in Equation (F-48). Fortunately, because we are dealing with a large phase modulation index, the task is simple because the spectrum $W_n(f)$ is proportional to the first-order probability density of the equivalent FM process, which is Gaussian. Thus,

$$W_n(f) = \left(\sqrt{2\pi}\, n\sigma_\phi\right) \exp\left[-f^2/2n^2\sigma_\phi^2\right] \qquad \text{(F-49)}$$

Further, if we assume that the LPF has an ideal rectangular response, i.e.,

$$\left|H(f)\right|^2 = \begin{cases} 1 & 0 \leq f \leq f_m \\ 0 & f > f_m \end{cases} \qquad \text{(F-50)}$$

then we may evaluate the integral in Equation (F-48) to obtain with the use of Equations (F-15) and (F-16) the final result, viz,

$$R = \left[\sum_{n=1}^{\infty} (u)^{2n} \operatorname{erf}\left\{\sqrt{5} f_m / (2\sqrt{2\pi n}\Delta f_p)\right\}\right]^{-1} \qquad \text{(F-51)}$$

where

$$\operatorname{erf}(x) = \frac{2}{\sqrt{\pi}} \int_0^x \exp\left[-\lambda^2\right] d\lambda \qquad \text{(F-52)}$$

Since erf (x) is a monotonic function that goes to zero as $x \to 0$, we note in Equation (F-51) that for fixed f_m and u, the value of R becomes larger as the peak deviation, Δf_p, increases. As specific examples, R has been calculated for the values of f_m = 3 kHz, Δf_p = 10 kHz and 20 kHz, and various values of C/I = u^{-2}. The results are tabulated as Tables F-1 and F-2 (where R has been denoted by S/I).

As noted earlier, for C/I = 0 dB, we have S/I = 0 dB for all conditions. Note, however, at C/I = 1 dB, there is a very significant change in S/I. This phenomenon is often called the "capture effect". In the laboratory this may be dramatically demonstrated when the two carrier modulations are speech waveforms. At C/I = 0 dB the reproduced sound is garbled and unintelligible. Yet, when C/I = 1 dB, the stronger speech signal becomes clear and quite intelligible, although the background interferring speech signal is very annoying.

Note also from the tables that as C/I is further increased, the improvement in S/I is proportionally smaller, and that when C/I > 10 dB, the improvement in S/I is only 1 dB for each 1-dB increase in C/I (tit for tat). Additionally, the relative improvement in S/I for any fixed C/I is about 3 dB as Δf_p goes from 10 kHz to 20 kHz. Other calculations show another 3-dB

Table F-1. Values of C/I vs S/I for f_m = 3 kHz and Δf_p = 10 kHz

C/I = 0 dB	S/I = 0.00 dB
C/I = 1 dB	S/I = 8.71 dB
C/I = 2 dB	S/I = 10.72 dB
C/I = 3 dB	S/I = 12.28 dB
C/I = 4 dB	S/I = 13.65 dB
C/I = 5 dB	S/I = 14.90 dB
C/I = 6 dB	S/I = 16.09 dB
C/I = 7 dB	S/I = 17.23 dB
C/I = 8 dB	S/I = 18.33 dB
C/I = 9 dB	S/I = 19.42 dB
C/I = 10 dB	S/I = 20.48 dB
C/I = 11 dB	S/I = 21.53 dB
C/I = 12 dB	S/I = 22.56 dB
C/I = 13 dB	S/I = 23.59 dB
C/I = 14 dB	S/I = 24.62 dB
C/I = 15 dB	S/I = 25.63 dB
C/I = 16 dB	S/I = 26.65 dB
C/I = 17 dB	S/I = 27.66 dB
C/I = 18 dB	S/I = 28.67 dB
C/I = 19 dB	S/I = 29.68 dB
C/I = 20 dB	S/I = 30.68 dB
C/I = 21 dB	S/I = 31.69 dB
C/I = 22 dB	S/I = 32.69 dB
C/I = 23 dB	S/I = 33.69 dB
C/I = 24 dB	S/I = 34.70 dB
C/I = 25 dB	S/I = 35.70 dB
C/I = 26 dB	S/I = 36.70 dB
C/I = 27 dB	S/I = 37.70 dB
C/I = 28 dB	S/I = 38.70 dB
C/I = 29 dB	S/I = 39.70 dB
C/I = 30 dB	S/I = 40.70 dB

Table F=2. Values of C/I vs S/I for f_m = 3 kHz and Δfp = 20 kHz

C/I = 0 dB	S/I = 0.00 dB
C/I = 1 dB	S/I = 11.72 dB
C/I = 2 dB	S/I = 13.72 dB
C/I = 3 dB	S/I = 15.29 dB
C/I = 4 dB	S/I = 16.65 dB
C/I = 5 dB	S/I = 17.91 dB
C/I = 6 dB	S/I = 19.10 dB
C/I = 7 dB	S/I = 20.23 dB
C/I = 8 dB	S/I = 21.34 dB
C/I = 9 dB	S/I = 22.42 dB
C/I = 10 dB	S/I = 23.48 dB
C/I = 11 dB	S/I = 24.53 dB
C/I = 12 dB	S/I = 25.57 dB
C/I = 13 dB	S/I = 26.60 dB
C/I = 14 dB	S/I = 27.62 dB
C/I = 15 dB	S/I = 28.64 dB
C/I = 16 dB	S/I = 29.65 dB
C/I = 17 dB	S/I = 30.66 dB
C/I = 18 dB	S/I = 31.67 dB
C/I = 19 db	S/I = 32.68 dB
C/I = 20 dB	S/I = 33.69 dB
C/I = 21 dB	S/I = 34.69 dB
C/I = 22 dB	S/I = 35.69 dB
C/I = 23 dB	S/I = 36.70 dB
C/I = 24 dB	S/I = 37.70 dB
C/I = 25 dB	S/I = 38.70 dB
C/I = 26 dB	S/I = 39.70 dB
C/I = 27 dB	S/I = 40.70 dB
C/I = 28 dB	S/I = 41.71 dB
C/I = 29 dB	S/I = 42.71 dB
C/I = 30 dB	S/I = 43.71 dB

increase as Δf_p goes from 20 kHz to 40 kHz. We may therefore postulate a simple relationship between the variables involved, viz.,

$$S/I(dB) = C/I(dB) + 10.7 + 10 \log (\Delta f_p/10) \qquad \text{(F-53)}$$

for the conditions C/I > 10 dB, Δf_p > 10 kHz, and f_m = 3 kHz.

We now turn briefly to the case of sinusoidal modulations of the carrier. For this situation we let

$$\dot{\phi}_s(t) = 2\pi \Delta f_p \sin (\omega_1 t) \qquad \text{(F-54)}$$

and

$$\dot{\phi}_i(t) = 2\pi \Delta f_p \sin (\omega_2 t) \qquad \text{(F-55)}$$

Because of the nonlinear behavior of the demodulation process, the receiver output will now contain the desired frequency f_1, the interfering frequency f_2, and the intermodulation products of f_1 and f_2.

With periodic modulations, a convenient way to evaluate the desired result is to perform a Fourier analysis of Equation (F-6b) using a computer. Here we define R as

$$R = \frac{\text{power } (\dot{\phi}_s(t))}{\text{power } (\dot{\phi}_i(t))} \qquad \text{(F-56)}$$

where we ignore the in-band intermodulation components. The result for f_1 = 875 Hz, f_2 = 500 Hz and Δf_p = 10 kHz is tabulated in Table F-3. Also included are some measured values that show fairly good agreement with the calculations. Some difficulty was encountered in obtaining the experimental values as it was found that the measurements were very sensitive to the setting of the modulation index and the level of the voltage drive to the hardware receiver. A wave analyzer was used to obtain the receiver output power of $\dot{\phi}_s(t)$ and $\dot{\phi}_i(t)$.

By comparing the results of Table F-3 to Table F-1, it is noted that S/I based upon sinusoidal modulations is not a good measure of performance of S/I when the modulations are broadband and random. Thus, the utility of using sinusoidal modulations is only in verification of proper hardware receiver performance.

Table F-3. Values of C/I vs Calculated and Measured Values of S/I for f_1 = 875 Hz, f_2 = 500 Hz, and Δf_p = 10 kHz[a]

C/I	S/I (CALC)	S/I (MEAS)
0	.0	0.0
1	10.6	8.9
2	17.7	15.8
3	21.9	19.5
4	24.7	23.5
5	26.8	26.0
6	28.4	27.8
7	29.7	29.2
8	30.9	29.6
9	32.1	32.7
10	33.2	33.8
11	34.3	
12	35.4	
13	36.5	
14	37.6	
15	38.6	
16	39.6	
17	40.6	
18	41.6	
19	42.6	
20	43.6	

[a]All entries in dB.

F.3 MULTIPLE INTERFERER ANALYSIS

For the case of multiple equal-power interferers we take

$$S_i(t) = \sqrt{2P_i} \sum_{n=1}^{N} \cos\left[\omega_c t + \phi_n(t)\right] \tag{F-57}$$

where the $\phi_n(t)$ are independent phase-modulating signals. The same conditions that were earlier imposed on the single interferer $\phi_i(t)$, are now also applied to each $\phi_n(t)$.

Combining Equation (F-57) with Equation (F-1), the equivalent phase modulation seen by the ideal FM demodulator is now

$$\psi(t) = \tan^{-1}\left\{\frac{\sqrt{2P}\,\sin\left[\phi_s(t)\right] + \sqrt{2P_i}\sum_{n=1}^{N}\sin\left[\phi_n(t)\right]}{\sqrt{2P}\,\cos\left[\phi_s(t)\right] + \sqrt{2P_i}\sum_{n=1}^{N}\cos\left[\phi_n(t)\right]}\right\} \tag{F-58a}$$

$$= \tan^{-1}\left\{\frac{\sin\phi_s + u\sum_{n=1}^{N}\sin\phi_n}{\cos\phi_s + u\sum_{n=1}^{N}\cos\phi_n}\right\} \tag{F-58b}$$

where $u = \sqrt{P_i/P}$ as before. However, now

$$\frac{C}{I} = \frac{P}{NP_i} \tag{F-59}$$

so that,

$$\frac{C}{I} = \frac{1}{Nu^2} \tag{F-60}$$

or

$$u = \left(N\,\frac{C}{I}\right)^{-2} \tag{F-61}$$

Differentiating $\psi(t)$ with respect to t yields

$$\dot{\psi} = \frac{\dot{\phi}_s + u\sum_{n=1}^{N}(\dot{\phi}_s - \dot{\phi}_n)\cos(\phi_s - \phi_n) + u^2\sum_{n=1}^{N}\sum_{m=1}^{N}\dot{\phi}_n\cos(\phi_n - \phi_m)}{1 + 2u\sum_{n=1}^{N}\cos(\phi_s - \phi_n) + u^2\sum_{n=1}^{N}\sum_{n=1}^{N}\cos(\phi_n - \phi_m)} \qquad \text{(F-62)}$$

As was done previously for the single interferer, Equation (F-62) may be written as:

$$\dot{\psi} = a\left[\phi_s, \phi_n\right]\dot{\phi}_s + b\left[\phi_s, \phi_n\right]\sum_{n=1}^{N}\dot{\phi}_n \qquad \text{(F-63)}$$

where

$$a\left[\phi_s, \phi_n\right] = \frac{1 + u\sum_{n=1}^{N}\cos(\phi_s - \phi_n)}{1 + 2u\sum_{n=1}^{N}\cos(\phi_s - \phi_n) + u^2\sum_{n=1}^{N}\sum_{m=1}^{N}\cos(\phi_n - \phi_m)} \qquad \text{(F-64)}$$

and

$$b\left[\phi_s, \phi_n\right] = 1 - a\left[\phi_s, \phi_n\right] \qquad \text{(F-65)}$$

Equation (F-64) may be simplified somewhat by letting $\phi_n - \phi_m = (\phi_n - \phi_s) - (\phi_m + \phi_s)$ in the double summation and expanding cos $[(\phi_s - \phi_m) - (\phi_s - \phi_n)]$. The result is:

$$a\left[\phi_s, \phi_n\right] = \frac{1 + u\sum_{n=1}^{N}\cos(\phi_s - \phi_n)}{\left[1 + u\sum_{n=1}^{N}\cos(\phi_s - \phi_n)\right]^2 + \left[u\sum_{n=1}^{N}\sin(\phi_s - \phi_n)\right]^2} \qquad \text{(F-66)}$$

Now letting $\phi_s - \phi_n = \theta_n$, we have:

$$a\left[\theta_n\right] = \frac{1 + u\sum_{n=1}^{N}\cos\left(\theta_n\right)}{\left[1 + u\sum_{n=1}^{N}\cos\left(\theta_n\right)\right]^2 + \left[u\sum_{n=1}^{N}\sin\left(\theta_n\right)\right]^2} \qquad \text{(F-67)}$$

This, then, is the form of the coefficient for which the mean and covariance must be evaluated if we are to ultimately obtain the ratio of desired-to-interference power at the output of the FM demodulator. Note that when N = 1, Equation (F-67) reduces to Equation (F-12) for the case of a single interferer.

Unfortunately, Equation (F-67) does not lend itself to ready evaluation of the mean and covariance. Nor may we expand Equation (F-67) in a simple series as we did with Equation (F-12), i.e., Equation (F-20).

We may, however, make the following observations and approximations. Since, as was the case for a single interferer the variance, $\sigma_{\theta_n}^2$, of the Gaussian process θ_n is very large, it is reasonable to view this Gaussian process mod (2π) as a uniformly distributed process on $(-\pi, \pi)$. In turn, the variables

$$x \triangleq \sum_{n=1}^{N}\cos\theta_n \qquad \text{(F-68)}$$

and

$$y \triangleq \sum_{n=1}^{N}\sin\theta_n \qquad \text{(F-69)}$$

may be seen as orthogonal Gaussian random variables, having zero mean and variance $\sigma^2 = N/2$, provided N is sufficiently large. Thus,

$$a(x, y) = \frac{1 + ux}{[1 + ux]^2 + [uy]^2} \qquad \text{(F-70)}$$

The mean of Equation (F-70) may be evaluated, but the second moment and covariance still defy attempts to obtain closed-form solutions. (It appears impossible to carry out the integrations.)

To conclude this section, let us return to Equation (F-57) and rewrite $S_i(t)$ as

$$S_i(t) = \sqrt{2P_i} \sum_{n=1}^{N} \cos\left[\theta_n(t)\right] \cos(\omega_c t) - \sqrt{2P_i} \sum_{n=1}^{N} \sin\left[\theta_n(t)\right] \sin(\omega_c t) \tag{F-71}$$

Now, defining

$$\eta_c(t) = \sqrt{2P_i} \sum_{n=1}^{N} \cos\left[\theta_n(t)\right] \tag{F-72}$$

and

$$\eta_s(t) = \sqrt{2P_i} \sum_{n=1}^{N} \sin\left[\theta_n(t)\right] \tag{F-73}$$

Equation (F-71) becomes:

$$S_i(t) = \eta_i(t) \cos(\omega_c t) - \eta_s(t) \sin(\omega_c t) \tag{F-74}$$

Equation (F-74) is seen to be the usual representation of a bandpass random process. Again, with N sufficiently large, $\eta_i(t)$ and $\eta_s(t)$ may be considered as orthogonal Gaussian random variables having zero means and variance NP_i. This is the usual simplifying assumption made for a large number of cochannel interferers so that the ensemble may be regarded as another additive noise process.

F.4 LABORATORY SIMULATION OF COCHANNEL INTERFERENCE

As just outlined, cochannel interference might be simulated by additive Gaussian bandpass noise, although not necessarily spectrally flat over the input bandwidth to the FM demodulator. For the LMSS, however, the number of cochannels may not be sufficiently large to justify this approximation. (As an example, the base station-to-satellite link with a seven-frequency reuse pattern has only three cochannel interferers, while the satellite-to-mobile link has but six significant cochannel signals.)

One way to simulate a limited number of cochannel interference signals is to have N FM transmitters, each modulated by independent speech waveforms, and sum the transmitter outputs to obtain the composite interference. However, this may be an expensive and somewhat inflexible approach.

A second solution is to modulate a quadrature carrier set by $\eta_c(t)$ and $\eta_s(t)$ (as per Equation (F-74), or, alternatively, amplitude and phase modulate a single carrier in the form:

$$S_i(t) = A_I(t) \cos\left[\omega_c t + \psi_I(t)\right] \tag{F-75}$$

where

$$A_I(t) = \sqrt{\eta_c^2(t) + \eta_s^2(t)} \tag{F-76}$$

and

$$\psi_I(t) = \tan^{-1}\left[\frac{\eta_s(t)}{\eta_c(t)}\right] \tag{F-77}$$

It simply remains, then, to generate the signals $\eta_c(t)$ and $\eta_s(t)$, or $A_I(t)$ and $\psi_I(t)$.

Let $\upsilon_n(t)$ be one of the independent interferring speech signals. $\upsilon_n(t)$ is assumed to have been preprocessed in terms of filtering, preemphasis, and compression. The phase-modulation equivalent, $\theta_n(t)$ is then simply given by

$$\theta_n(t) = k_f \int \upsilon_n(t)\, dt \tag{F-78}$$

where k_f is the FM transmitter sensitivity, i.e., $k_f \left|\upsilon_n(t)\right|_{max} = \Delta f_p$, with Δf_p being the peak FM deviation.

Thus, $\theta_n(t)$ may be simply obtained by integrating and scaling $\upsilon_n(t)$. Integration can be suitably accomplished using an operational integrator or a 6-dB-per-octave preemphasis network. The remainder of the operations needed to form $\eta_c(t)$ and $\eta_s(t)$ (or alternatively $A_I(t)$ and $\psi_I(t)$) are most easily performed using a computer.

The process of simulating cochannel interference involves two steps: (a) generation of $\eta_c(t)$ and $\eta_s(t)$ (or $A_I(t)$ and $\psi_I(t)$) sample data tape in nonreal time, and (b) carrier modulation based on the samples read from the data tape in real time.

Realization of the data tape may be accomplished as follows. The general configuration is shown in Figure F-1. The first integrated speech signal, $Z_1(t)$ is sampled (at, say, 10 kHz) to produce the samples $Z_1(i)$. The computer then calculates $\eta_{c1}(i) = \cos\left[K_f Z_1(i)\right]$ and $\eta_{s1}(i) = \sin\left[K_f Z_1(i)\right]$, and writes each pair onto Tape No. 1. This operation continues until the desired number of samples have been obtained. The second speech signal

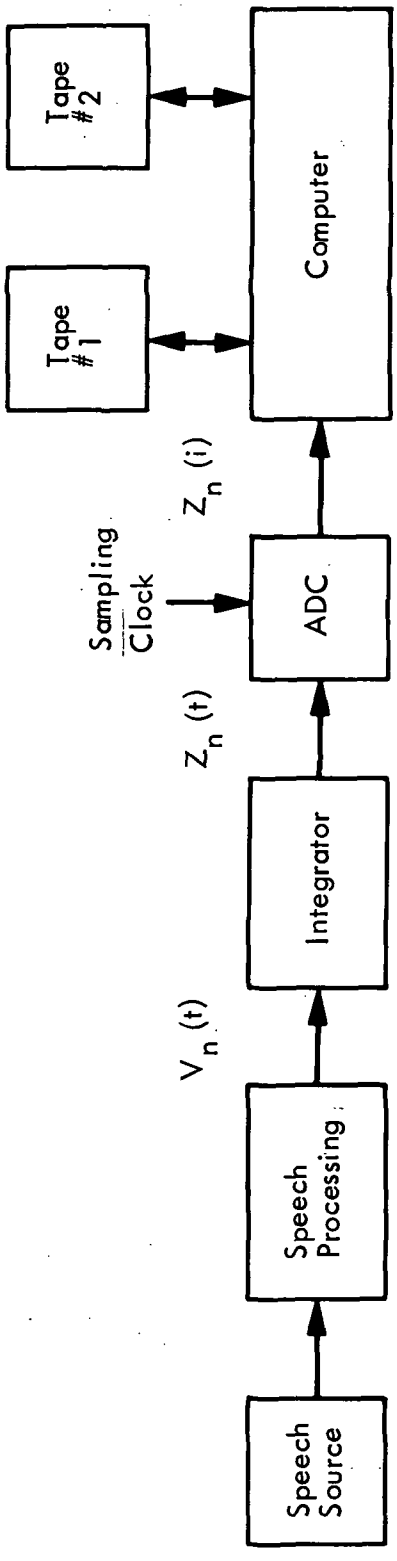

Figure F-1. Data Tape Generation Configuration

$Z_2(t)$ is next sampled to produce the samples $Z_2(i)$, with the computer calculating the terms $\eta_{c2}(i) = \cos [K_f Z_2(i)]$ and $\eta_{s2}(i) = \sin [K_f Z_2(i)]$. The sample pair $\eta_{c1}(i)$ and $\eta_{s1}(i)$ are read from Tape No. 1, the sums $\eta_c(i) = \eta_{c1}(i) + \eta_{c2}(i)$ and $\eta_s(i) = \eta_{s1}(i) + \eta_{s2}(i)$ formed, with the pair $\eta_c(i)$ and $\eta_s(i)$ then being written onto Tape No. 2. This operation continues until the necessary number of samples has been generated. Tape No. 2 now becomes the source tape for the next cycle which involves the speech samples $Z_3(i)$; the computed results are written onto Tape No. 1. The general operation continues until N speech signals have been processed, producing a final data tape containing the pairs

$$\eta_c(i) = \sum_{n=1}^{N} \cos \left[K_f Z_n(i)\right] \tag{F-79}$$

and

$$\eta_s(i) = \sum_{n=1}^{N} \sin \left[K_f Z_n(i)\right] \tag{F-80}$$

Finally, if they are to be used, the equations

$$A_I(i) = \sqrt{\eta_c^2(i) + \eta_s^2(i)} \tag{F-81}$$

and

$$\psi_I(i) = \tan^{-1} \left[\frac{\eta_s(i)}{\eta_c(i)}\right] \tag{F-82}$$

are calculated and written onto a tape. (Note that $\tan^{-1} [\ ]$ should be placed in the proper quadrant, i.e., the range is $-\pi, \pi$.)

For cochannel interference simulation, the appropriate sample pairs are output in real time (the output sampling clock is the same as the original speech-samples clock) through DACs and LPFs, as shown in Figure F-2. The two modulator options are shown in Figure F-3. In all cases, the amplitude modulators are linear modulators (not saturated mixers). The possible advantage of the option shown in Figure 3b is that the phase and amplitude modulators are already existing in the RF test console.

Note also that the $\sqrt{2P_i}$ scaling (see Equations (F-71), (F-72), and (F-73)) will be accomplished using the hardware C/I mixer.

REFERENCE

F-1. Middleton, D., An Introduction to Statistical Communication Theory. McGraw-Hill, New York, New York, 1960.

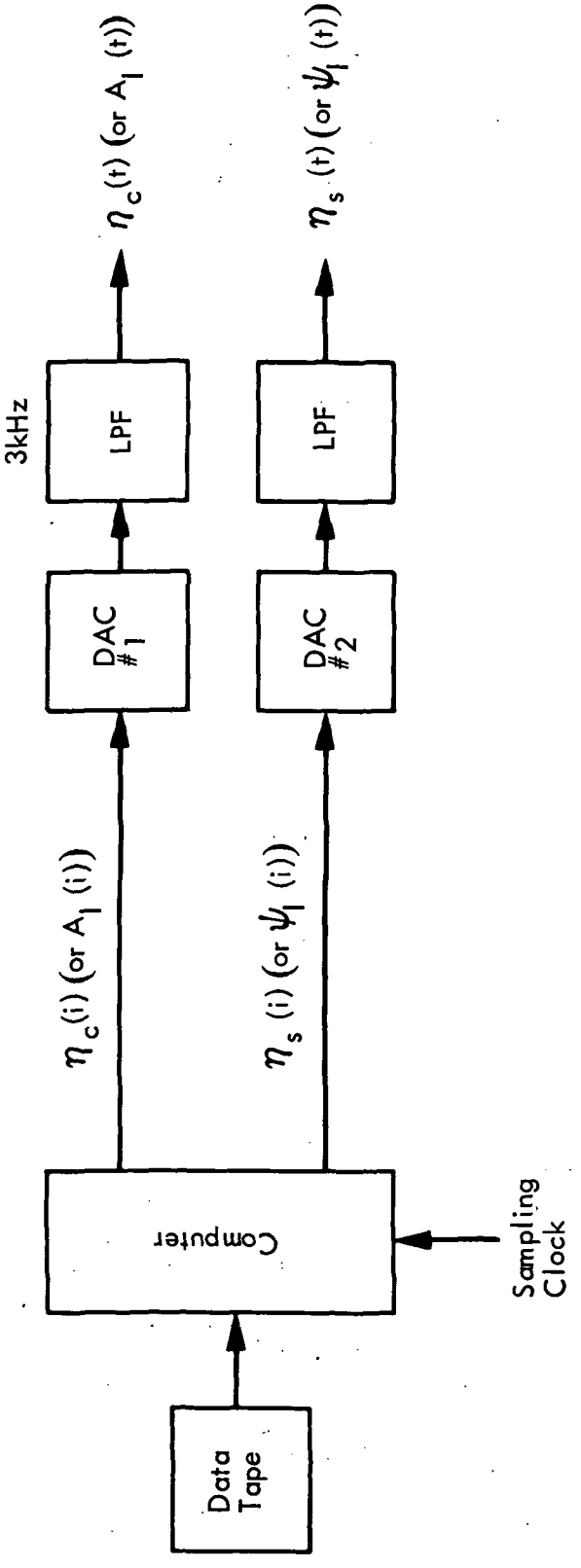

Figure F-2. Real-Time Sample Outputs

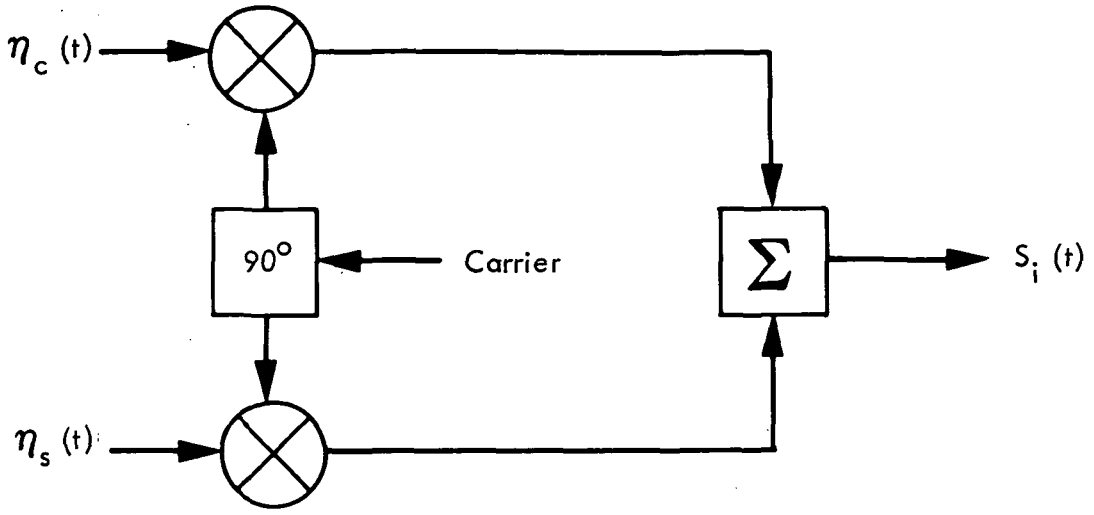

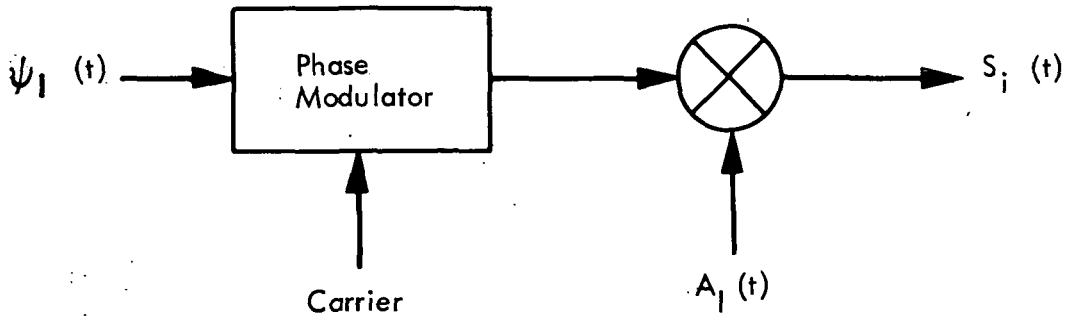

Figure F-3. Two Modulator Options

APPENDIX G

CIRCUIT DIAGRAMS AND FUNCTIONAL CHARACTERISTICS OF THE ELEMENTS IN THE SIGNAL-PATH SIMULATOR

In this appendix, detailed circuit diagrams (Figures G-1 through G-23) along with complete functional characteristics (Tables G-1 through G-15) are provided for each one of the functional elements in the signal-path simulator.

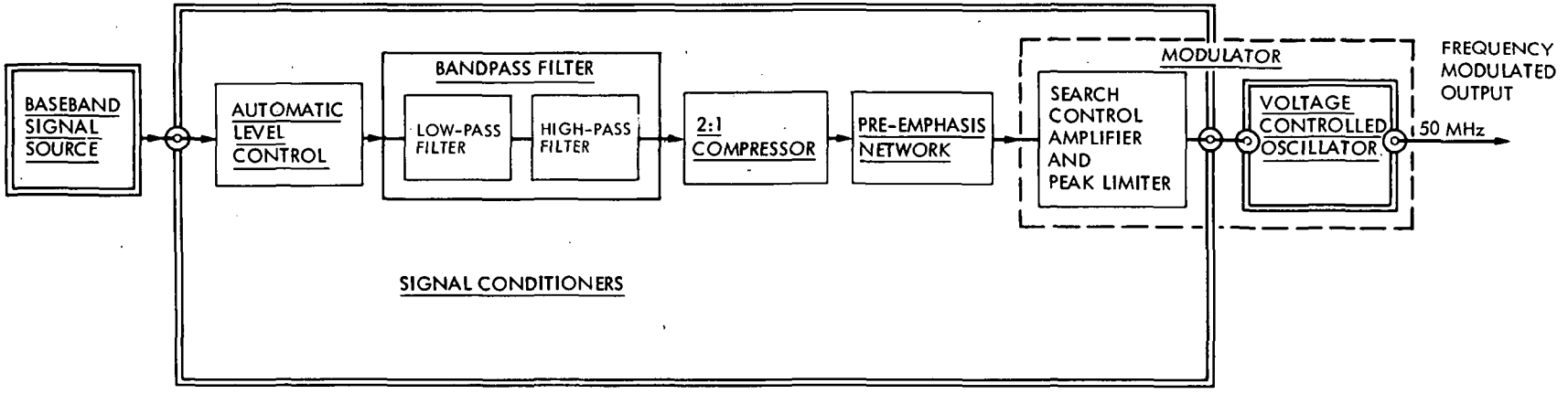

Figure G-1. FM Transmitter-Conditioner Block Diagram

Table G-1. Automatic Level Control Amplifier Functional Characteristics

Characteristic	Specified Performance
Input impedance	<2 kΩ
Input signal levels[a]	0.06 V_{rms} to 0.95 V_{rms}
Dynamic range (input rms variations)	30 dB
Nominal output signal level	0.13 V_{rms}
Max output current	±0.02 A
Frequency response	10 Hz to 20 kHz
Low-pass filter time constant	22 ms
Dc power required	+15 Vdc

[a]Voice-simulated signal

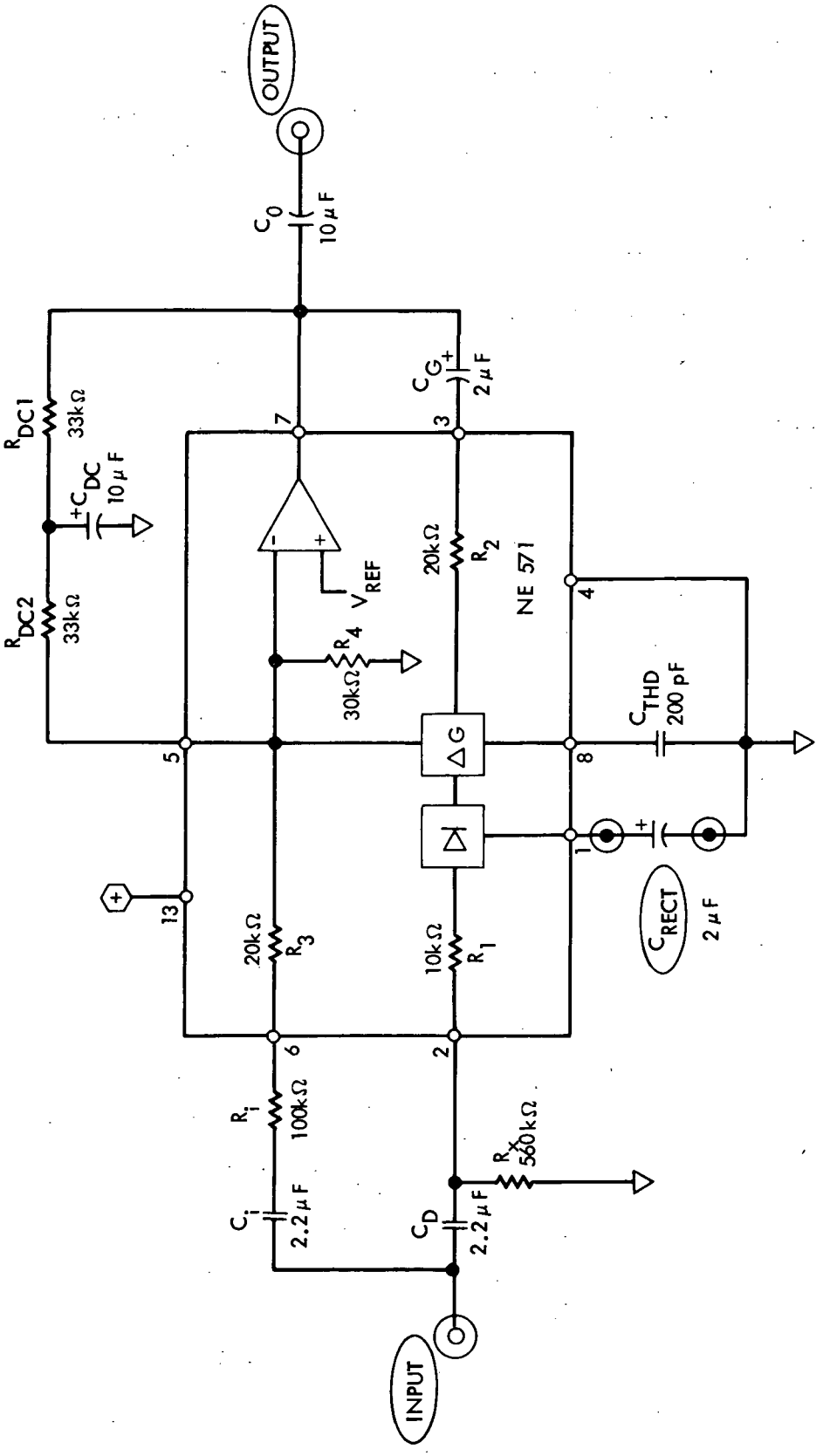

Figure G-2. Automatic Level Control Amplifier

Table G-2. Low-Pass Filter Functional Characteristics

Characteristic	Specified Performance
Filter type	5th-order Butterworth multiple feedback
Input impedance	2 kΩ
Max input signal level[a]	0.5 V_{rms}
Max output signal level	±10 V into 2 kΩ load
Max output current	±5 mA
Filter frequency response	dc - 3 kHz (±1%)
Amplifier frequency response	dc - 100 kHz
Cutoff frequency	3 kHz
Attenuation at cutoff	3 dB
Attenuation slope (roll-off rate)	30 dB/oct
Gain	1
Dc power required	±15 Vdc

[a]Voice-simulated signal

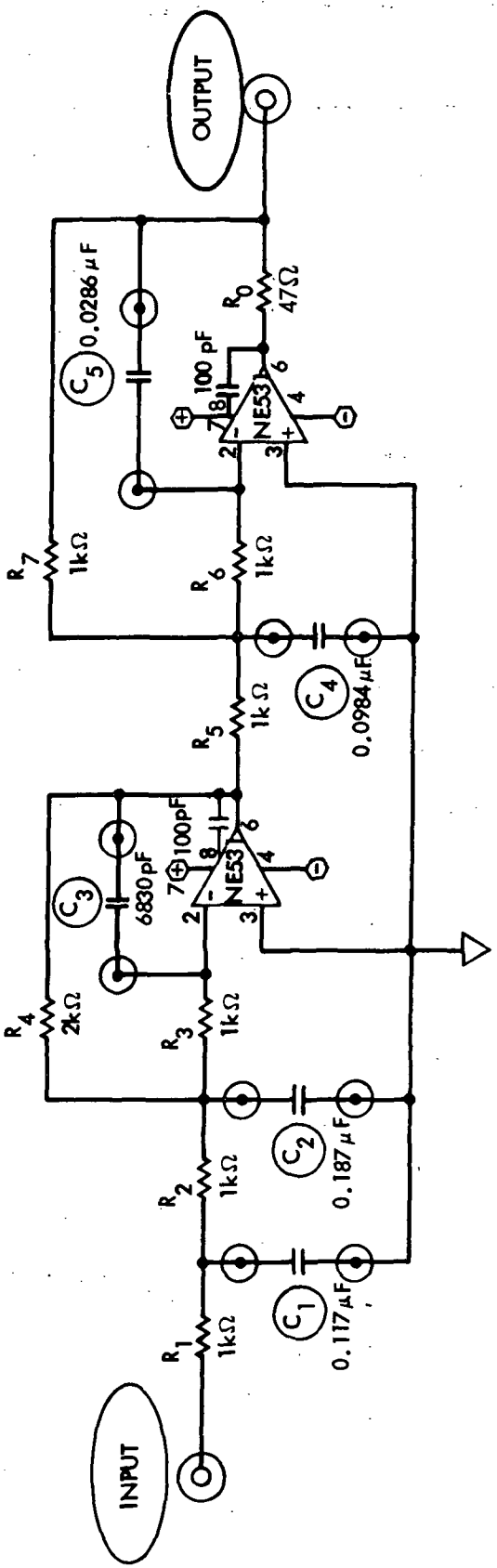

Figure G-3. Low-Pass Filter

Table G-3. High-Pass Filter Functional Characteristics

Characteristic	Specified Performance
Filter type	3rd-order Butterworth multiple feedback
Input impedance	1 kΩ
Max input signal level[a]	0.8 V_{rms}
Max output signal level	±10 V into 2 kΩ load
Max output current	±5 mA
Filter frequency response	300 Hz to 100 kHz (±1%)
Amplifier frequency response	dc - 100 kHz
Cutoff frequency	300 Hz
Attenuation at cutoff	3 dB
Attenuation slope (roll-off rate)	18 dB/oct
Gain	1
Dc power required	±15 Vdc

[a]Voice-simulated signal

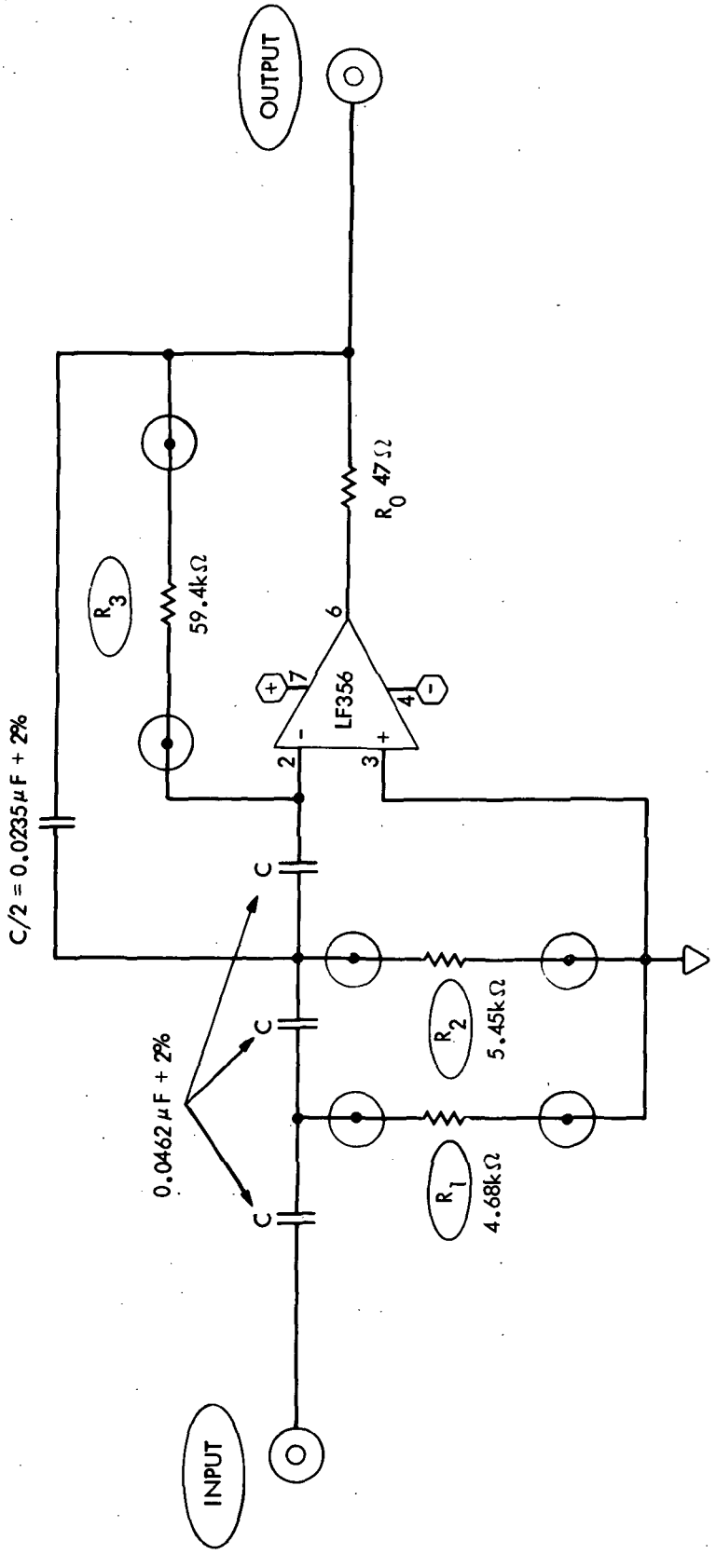

Figure G-4. High-Pass Filter

Table G-4. 2:1 Compandor Compressor Functional Characteristics

Characteristic	Specified Performance
Syllabic commanding law	2 to 1 (dB)
Input impedance	20 kΩ
Max input signal level[a]	0.055 V_{rms}
Max output signal level[a]	0.21 V_{rms}
Max output current	±20 mA
Frequency response	4 Hz - 50 kHz
Distortion	0.33% at 300 Hz to 0.1% at 1 kHz
Dynamic range (input rms variations)	70 dB
Low-pass filter (envelope) time constant	22 ms
Attack time	3 ms
Recovery time	13.5 ms
Dc power required	+15 Vdc

[a]Voice simulated signal

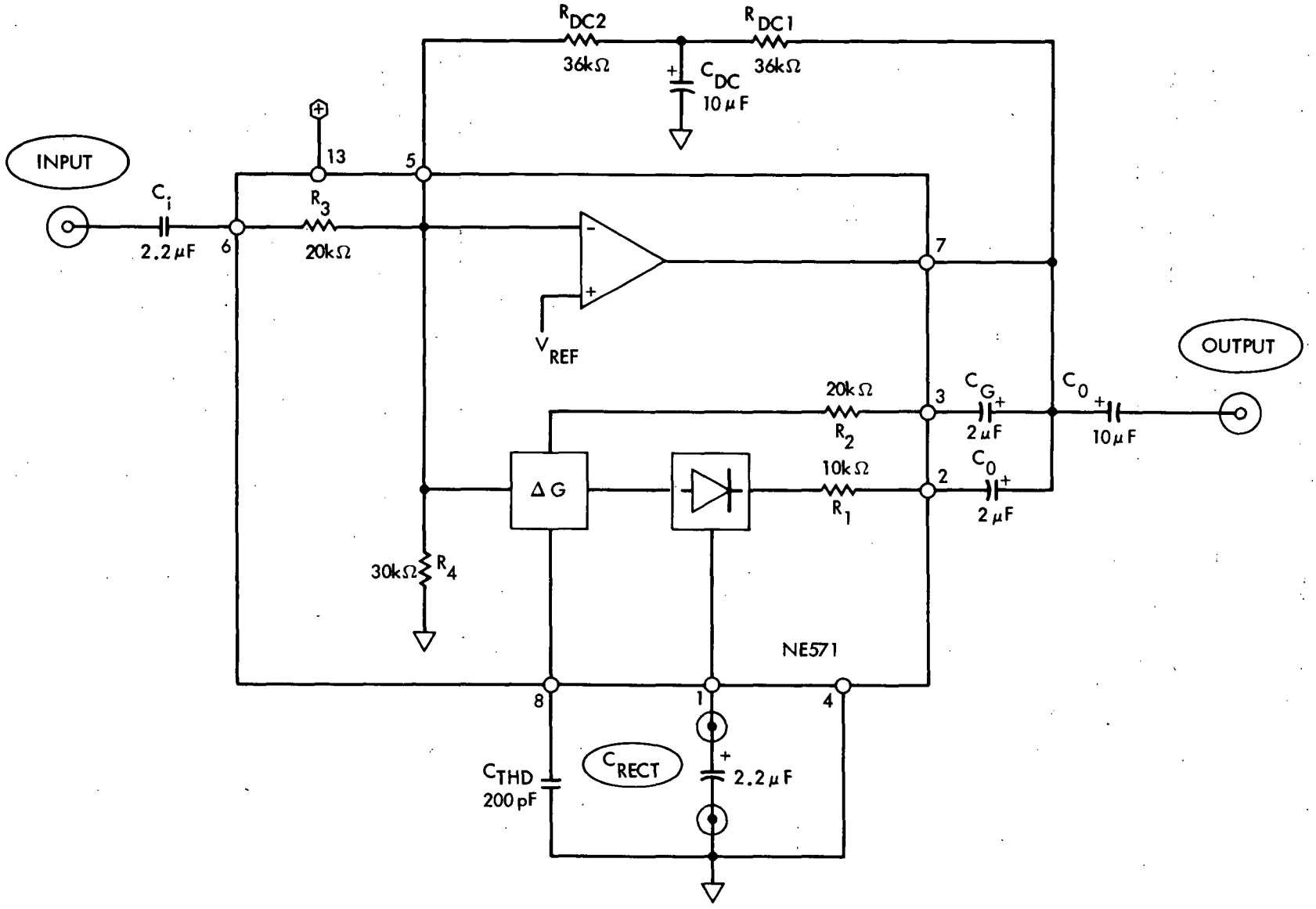

Figure G-5. 2:1 Compandor Compressor

Table G-5. Preemphasis Network Functional Characteristics

Characteristic	Specified Performance
Input impedance	10 kΩ
Accentuation (roll-up rate)	6 dB/oct
Applicable frequency range	300 Hz to 3 kHz
Max input signal level[a]	0.34 V_{rms}
Max output signal level[a]	0.85 V_{rms}
Max output current	±5 mA
Max output voltage	±10 V into 2 kΩ load
Time constant (R-C)	0.536 ms
Gain	21
Dc power required	±15 Vdc

[a]Voice simulated signal

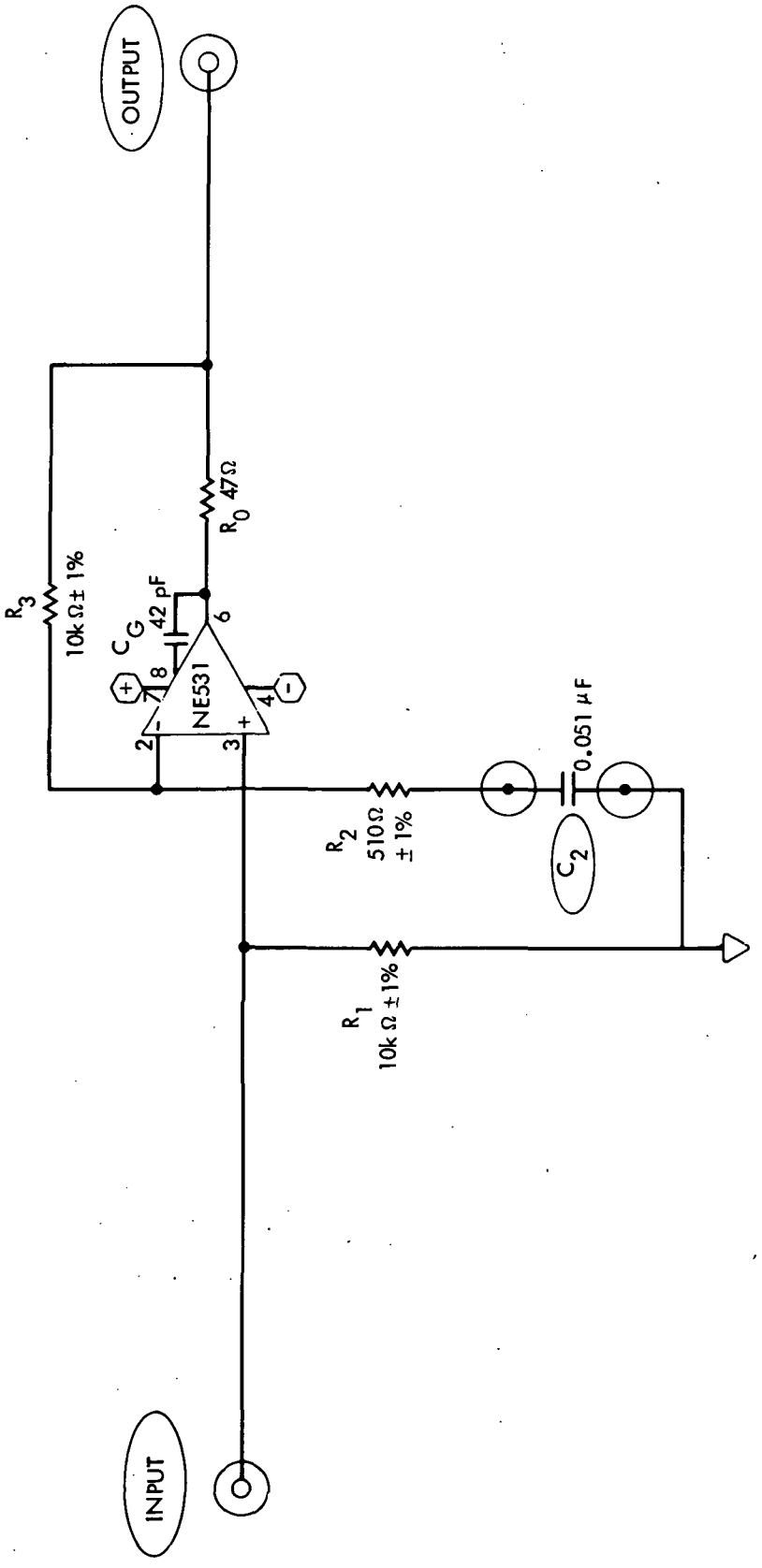

Figure G-6. Preemphasis Network

Table G-6. Peak Limiter and Search Control Amplifier Functional Characteristics

Characteristic	Specified Performance
Input impedance	>1.5 kΩ
Amplifier gain (variable)	0.33 to 2
Max input peak limiting (diode)	±1.2 V
Peak limiter range	Variable up to max (±1.2 V)
Max input signal level[a]	0.29 V_{rms}
Max output signal level[a]	0.55 V_{rms}
Max output current	±100 mA
Nominal dc offset	-6.05 V
Max output voltage swing from nominal dc offset	±5 V
Carrier frequency stability provided	±100 Hz
Frequency response	1 Hz to 500 kHz
Dc power required	±15 Vdc

[a]*Voice simulated signal*

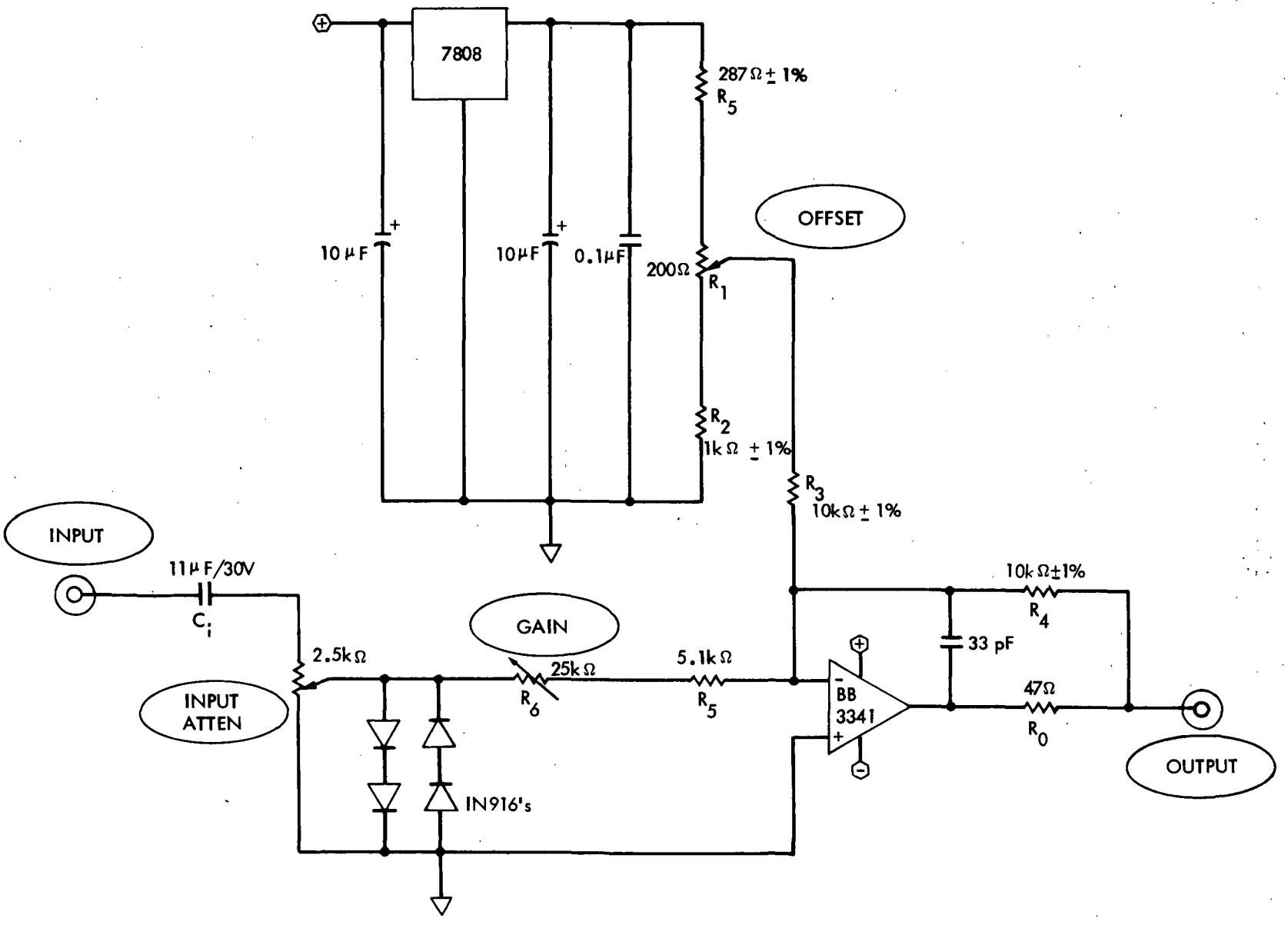

Figure G-7. Peak Limiter and Search Control Amplifier

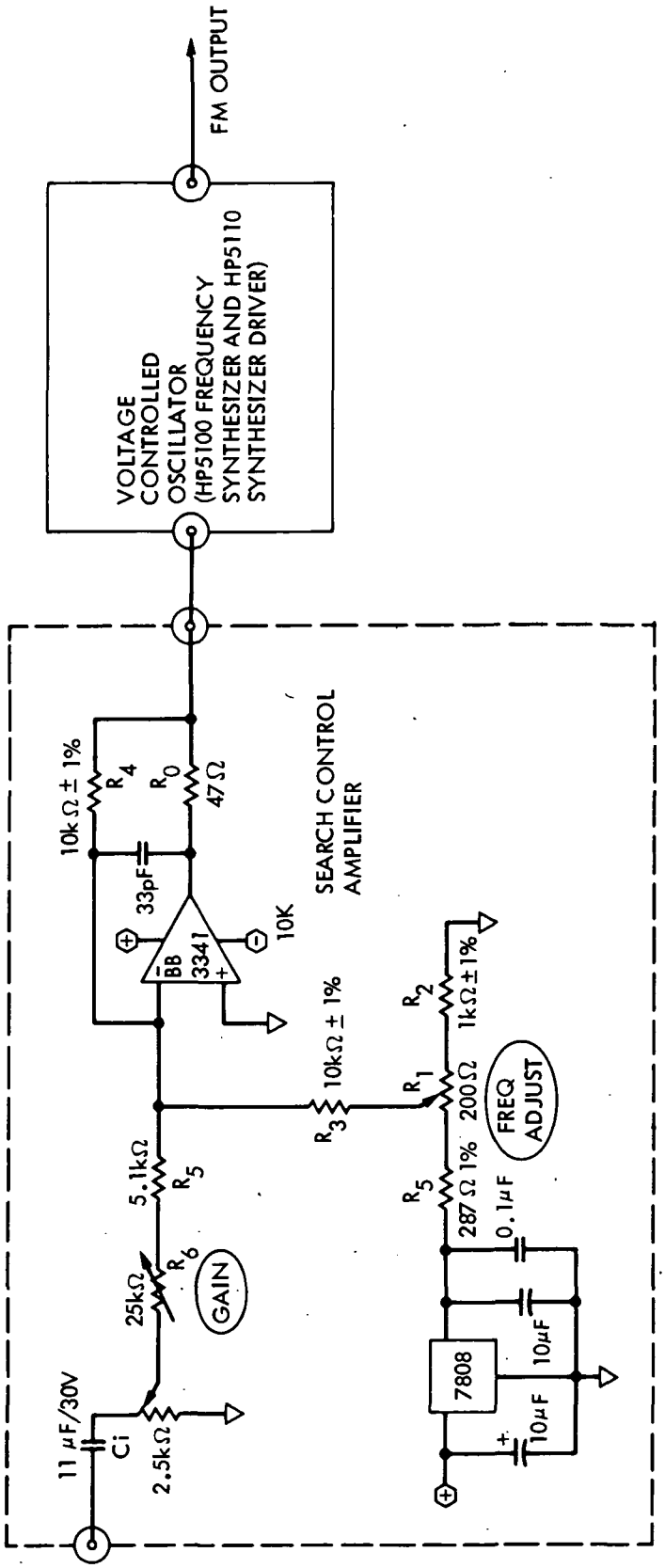

Figure G-8. Direct FM Modulator and Transmitter

Table G-7. Multipath Fading Simulator Functional Characteristics

Characteristic	Specified Performance
Input and output impedance	50 Ω
Max input RF signal level	7 dBm
Output RF signal level range	-12 dBm to 40 dBm
Input frequency	50 MHz
PN noise generators bit length	536870911
PN noise generator frequency response[a]	Dc - 200 kHz
PN noise generator clock frequency	Variable (max frequency ≙ 1 MHz)
I and Q channels phase difference	90 deg ±4 deg (at 50 MHz)
Peaking filter (shaping filter)[b]	Active twin-T band-pass filter
Low-pass filter (shaping filter)	Active 5th-order Butterworth
Shaping filter doppler frequency (Vehicle speed)	104 Hz (80 ± 0.2 mph) 72 Hz (55 ± 0.7 mph) 20 Hz (15 ± 0.2 mph)

[a]White noise up to about 1/5 of the clock frequency value.

[b]See Section 3.

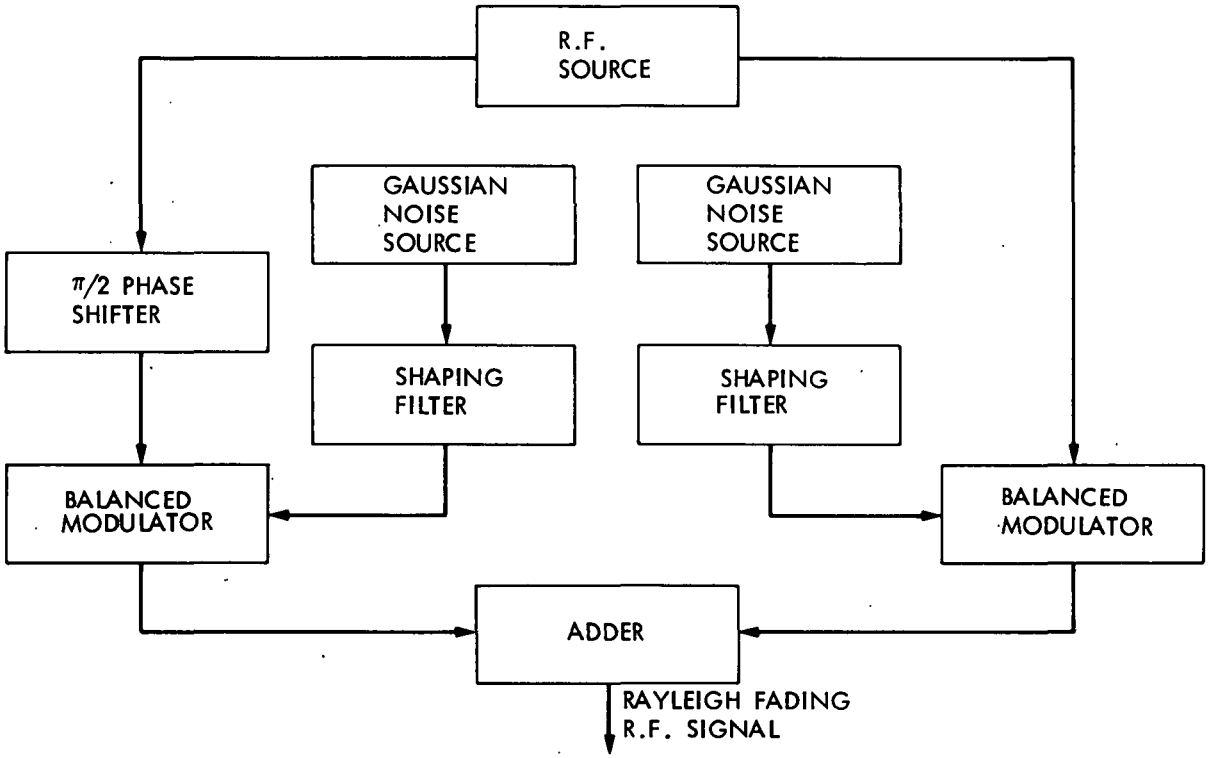

Figure G-9. Multipath Fading Simulator Block Diagram

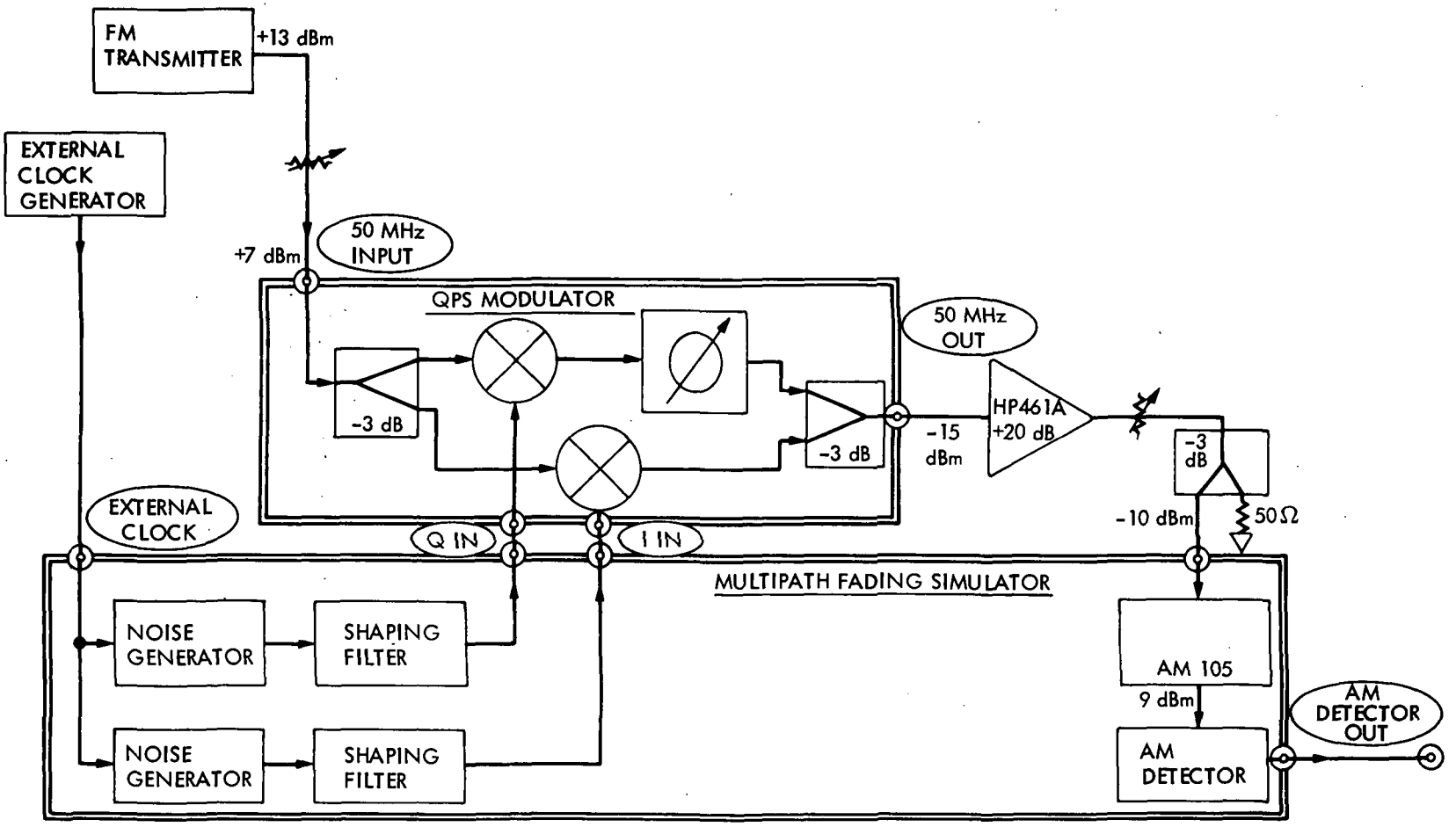

Figure G-10. Multipath Fading Simulator Detailed Block Diagram

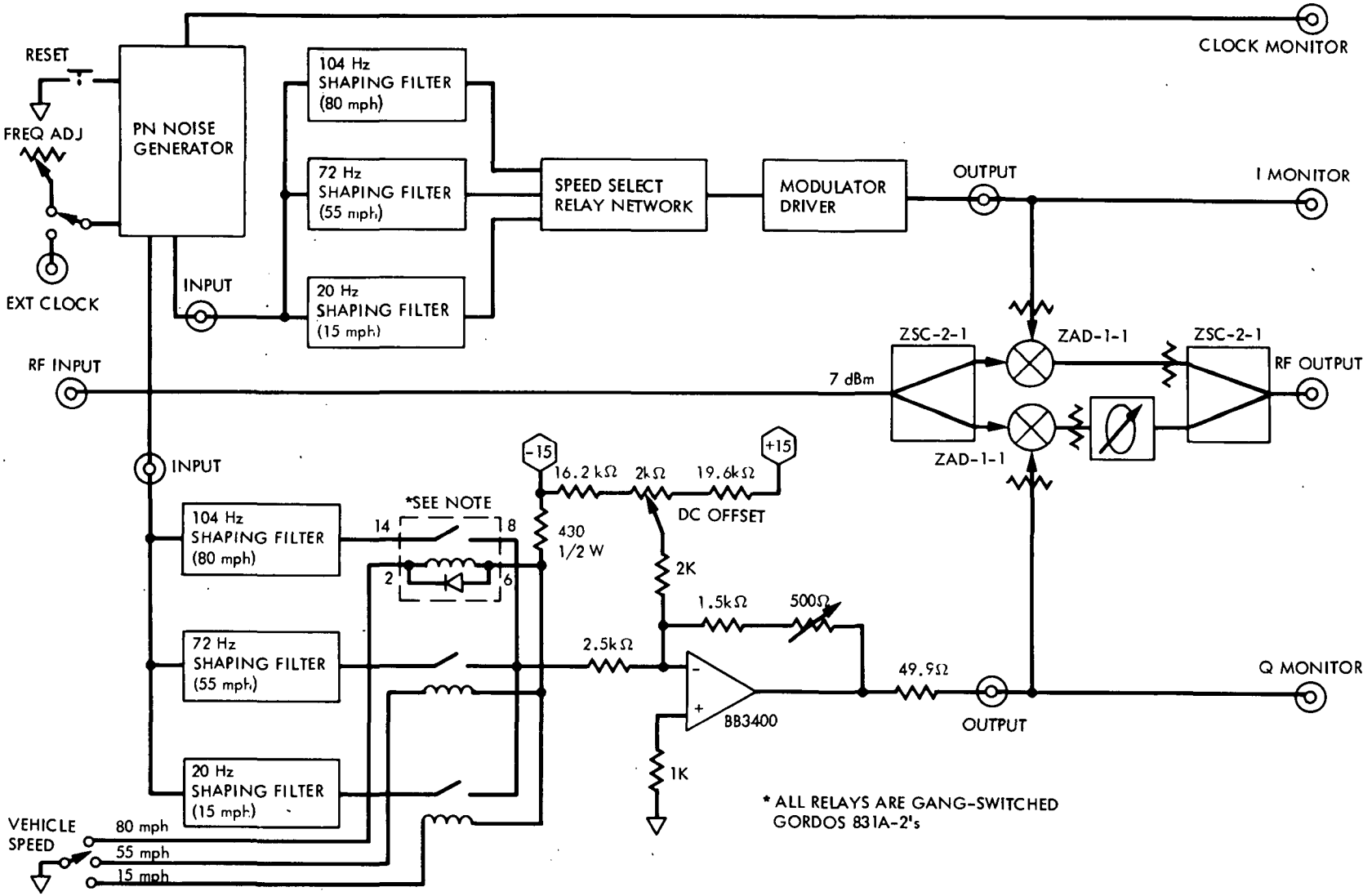

Figure G-11. Multipath Fading Simulator With RF Modulator And Modulator-Driver Detail

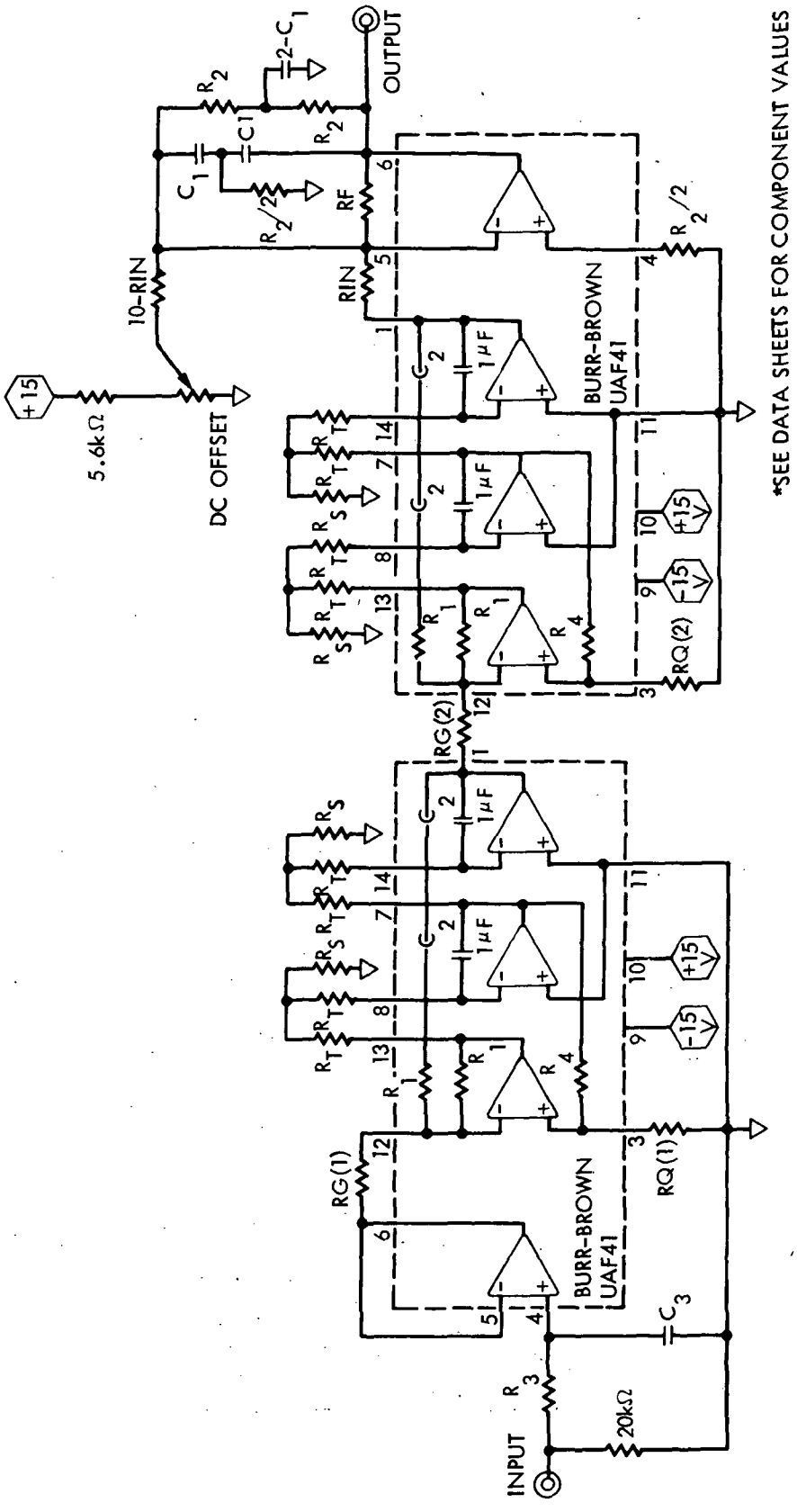

Figure G-12. Shaping Filter-Multipath Fading Simulator

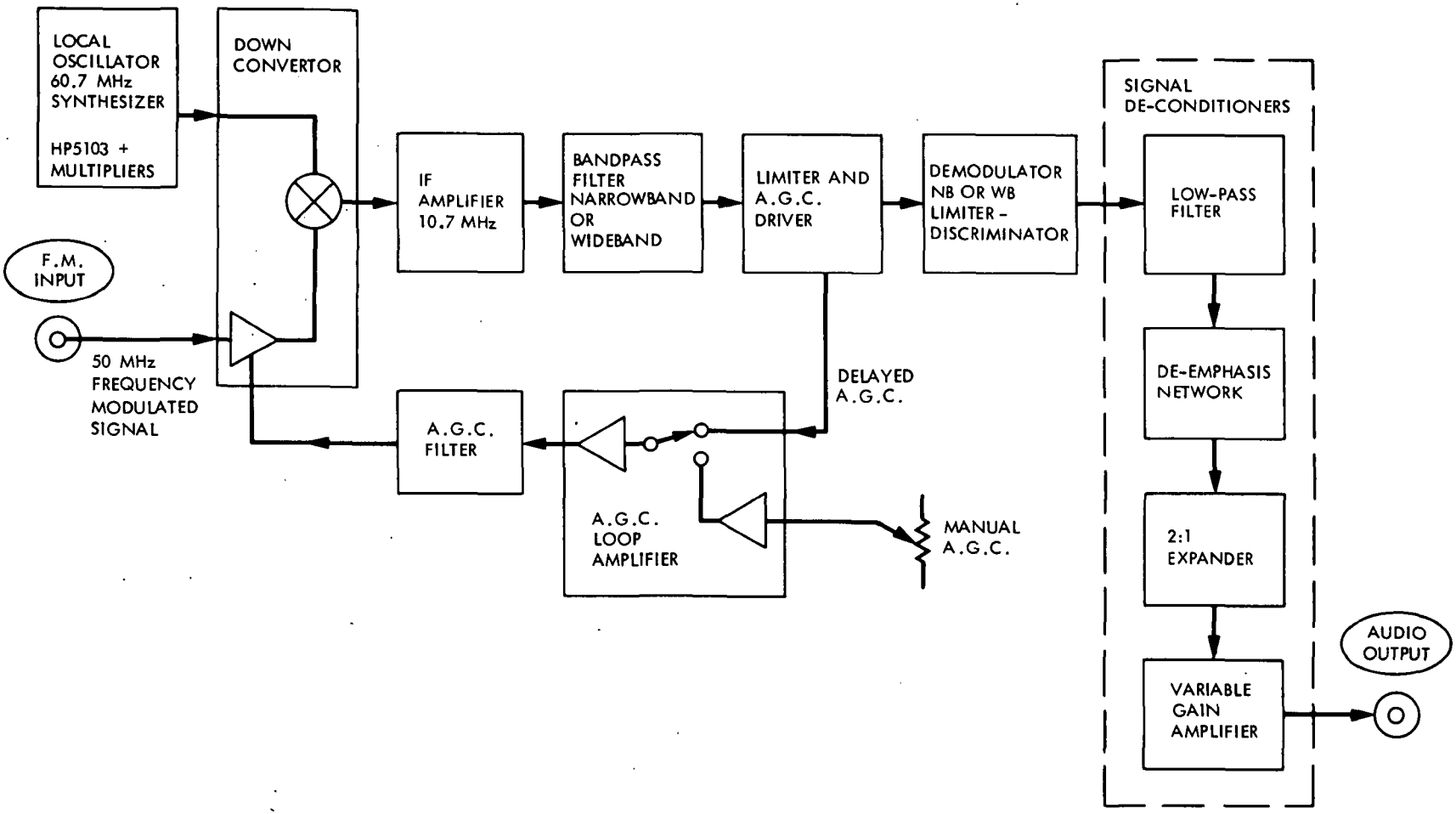

Figure G-13. Frequency Modulated Receiver Block Diagram

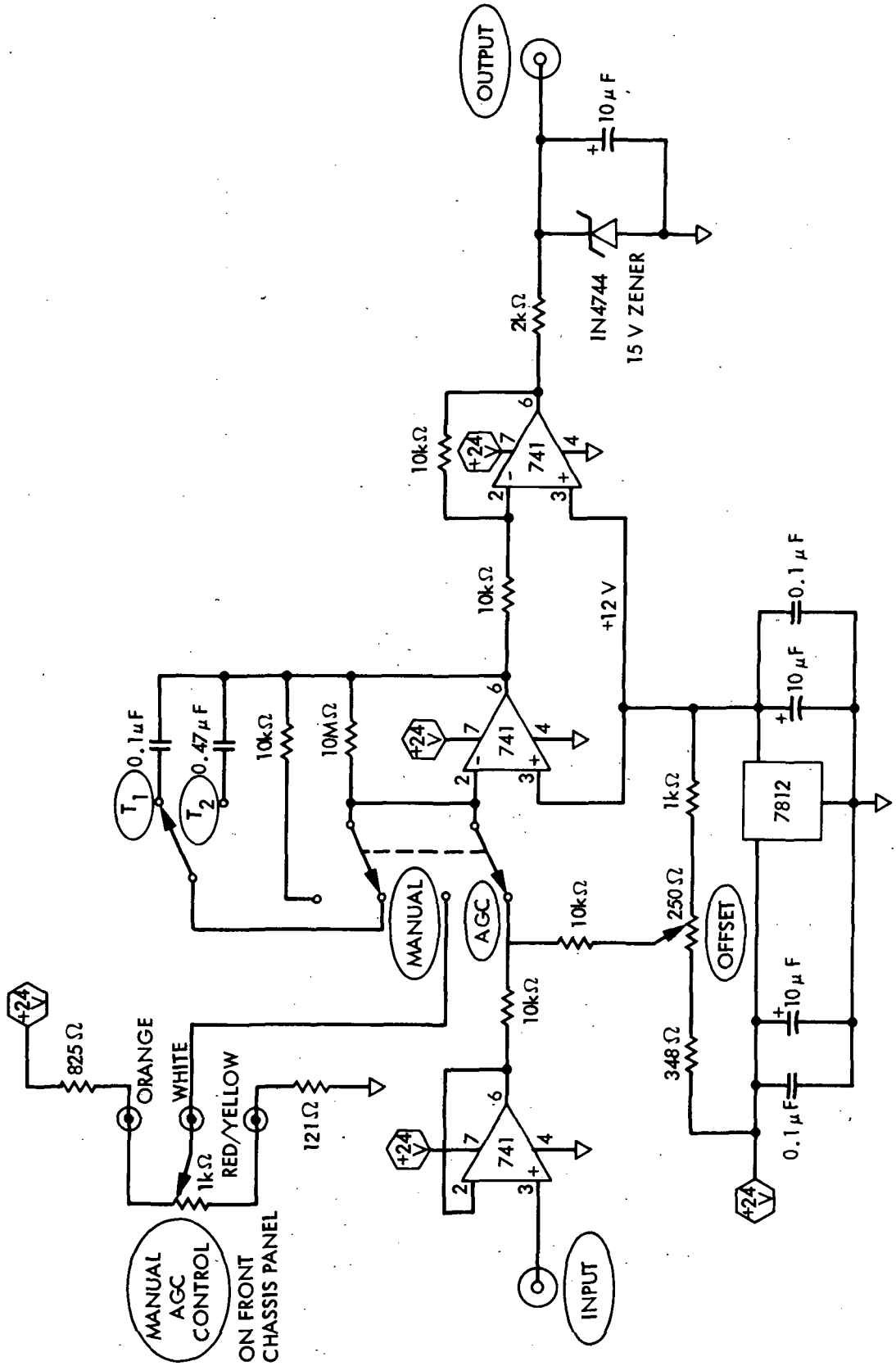

Figure G-14. AGC Loop Filter Amplifier

Table G-8. IF Down Converter Functional Characteristics

Characteristic	Specified Performance
Input impedance	50 Ω
Input frequency	50 MHz
Input RF signal-level range	-120 dBm to 60 dBm
Nominal input RF signal level	-80 dBm
Noise figure	$\leq$4 dB
IF frequency	10.7 MHz
3rd-order intermodulation product	$\leq$-60 dB
All other spurious signals	$\leq$80 dB
Reference LO frequency stability[a]	$\pm 2 \times 10^{-10}$ (for 1°C to 55°C)
Reference LO spurious signals	<70 dB
AGC dynamic range	40 dB
AGC resolution	±1 dB

[a]LO is a HP-5103A frequency synthesizer

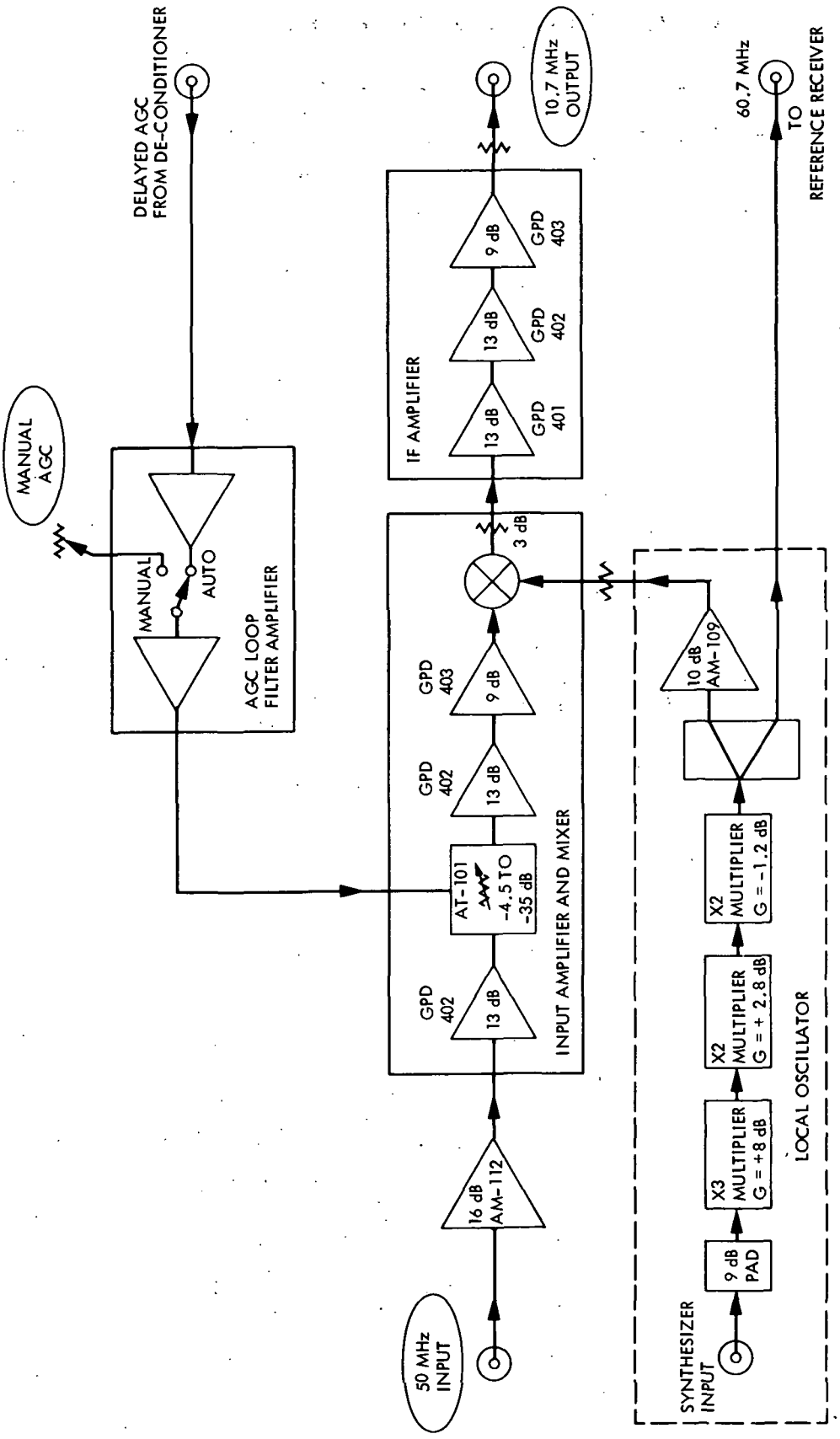

Figure G-15. IF Down Converter

Table G-9. IF Bandpass Filter (Narrowband) Functional Characteristics

Characteristic	Specified Performance
Filter type	Integrated crystal, 8 poles
Input and output impedance	50Ω
Max input IF signal level	10 dBm
Center frequency	10.7 MHz
3-dB bandwidth	27.7 kHz ±100 Hz
6-dB bandwidth	30 kHz ±100 Hz
60-dB bandwidth	60 kHz ±100 Hz
80-dB bandwidth	80 kHz ±100 Hz
Noise bandwidth (measured)	25.192 kHz
Ultimate attenuation	100 dB
Spurious responses	<-80 dB
Shape factor	2
Ripple	1.5 dB
Insertion loss	1.6 dB
Operating temperature	-30° to 80°C

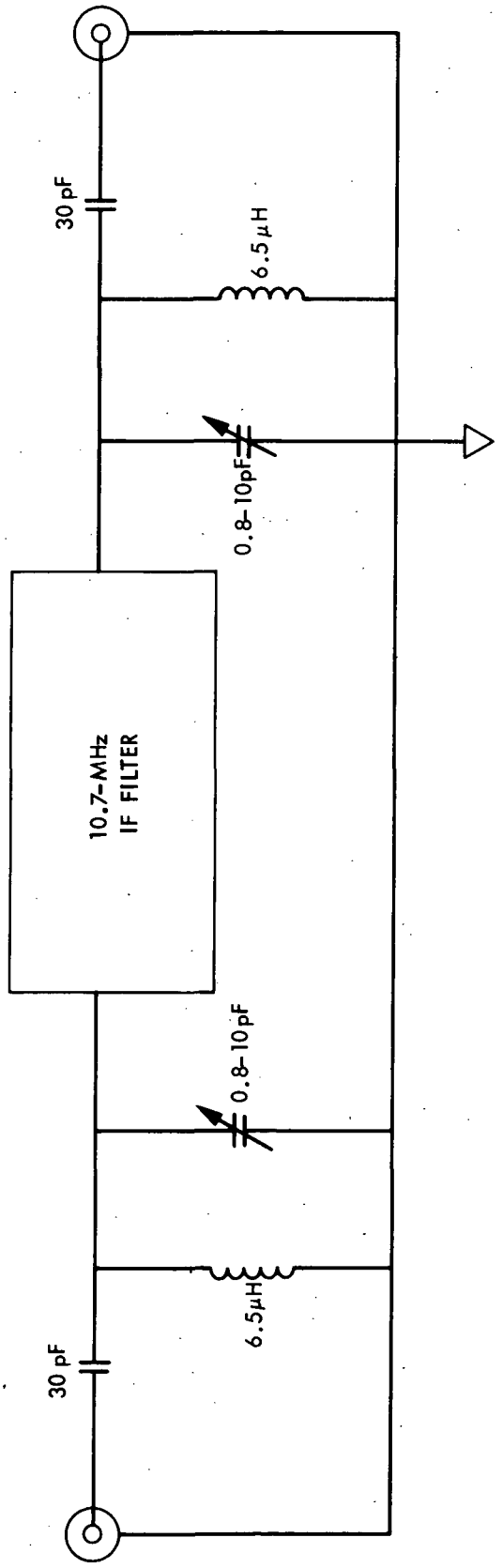

Figure G-16. IF Narrowband Bandpass Filter

Table G-10. IF Bandpass Filter (Wideband) Functional Characteristics

Characteristic	Specified Performance
Filter type	2 cascaded ceramic
Input and output impedance	50Ω
Max input IF signal level	10 dBm
Center frequency	10.7 MHz
3-dB bandwidth	216 ±1 kHz
6-dB bandwidth	270 ±1 kHz
40-dB bandwidth	570 ±1 kHz
Noise bandwidth (measured)	224.925 kHz
Ripple	<1 dB
Insertion loss	14 dB
Spurious responses	<-60 dB

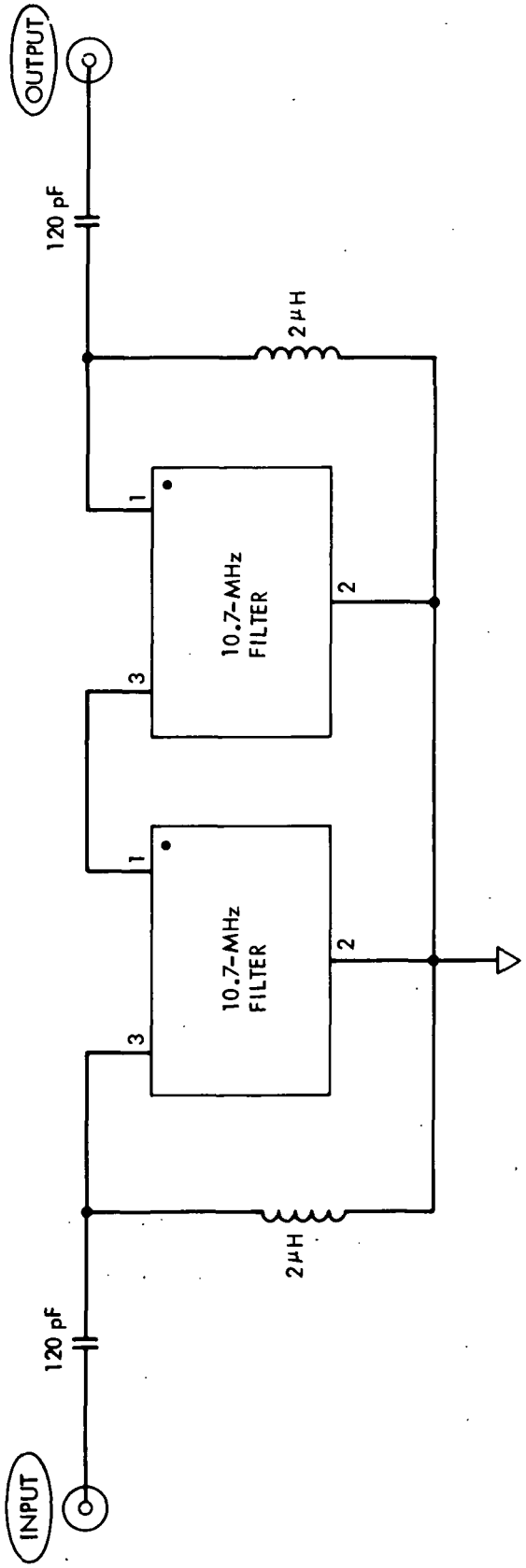

Figure G-17. IF Wideband Bandpass Filter

Table G-11. FM Limiter-Discriminator[a] (Narrowband) Functional Characteristics

Characteristic	Specified Performance
Discriminator type	Quadrature detector[b]
Input impedance	50 Ω
Max input IF signal level	0 dBm
Nominal audio output level	0.78 V_{rms}
Dynamic range	50 dB
Center frequency	10.7 MHz
Discriminator peak frequencies	10.7 MHz ±15 kHz
Discriminator linear frequency range	10.7 MHz ±12 kHz
Signal-to-noise ratio	50 dB
Total harmonic distortion:	
at 10.7 MHz ±2 kHz	0.6%
at 10.7 MHz ±5 kHz	1.2%
Operating temperature	-30° to 70°C
Dc power required	+15 Vdc

[a]Commercial IC (National Semiconductor Corporation, IC # LM 3089).

[b]Monolithic crystal filter (2-pole).

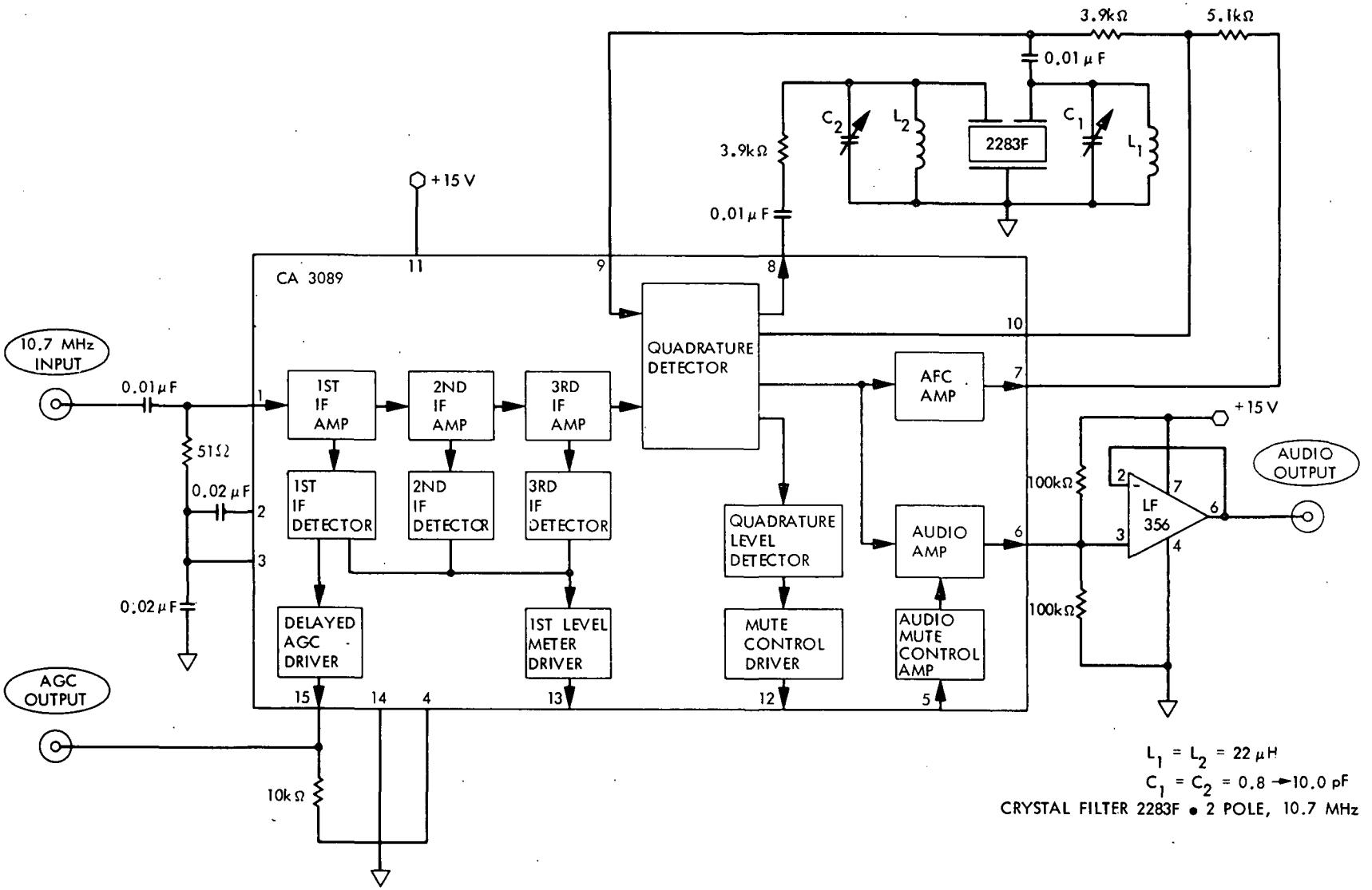

Figure G-18. FM Limiter-Discriminator (Narrowband)

Table G-12. FM Limiter-Discriminator (Wideband) Functional Characteristics

Characteristic	Specified Performance
Discriminator type	Single-tuned detector coil[a]
Input impedance	50 Ω
Max input IF signal level	0 dBm
Nominal audio output level	0.78 V_{rms}
Dynamic range	70 dB
Center frequency	10.7 MHz
Discriminator peak frequencies	10.7 MHz ±250 kHz
Discriminator linear frequency range	10.7 MHz ±120 kHz
Operating temperature	-30°C to 70°C
Dc power required	+15 Vdc

[a]Quadrature detector

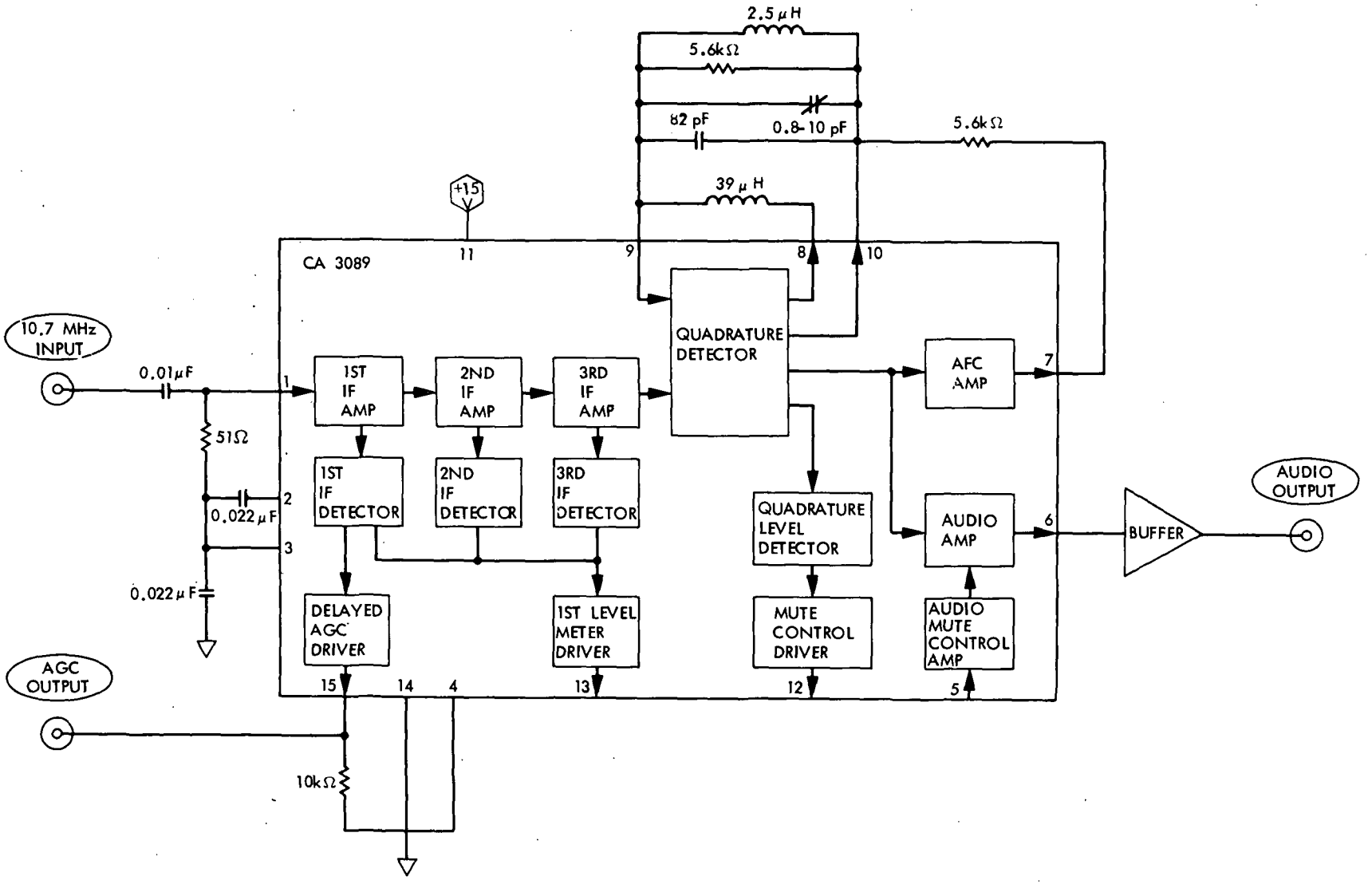

Figure G-19. FM Limiter-Discriminator (Wideband)

Table G-13. De-emphasis Network Functional Characteristics

Characteristic	Specified Performance
Input impedance	2 kΩ
Attenuation (roll-off rate)	6 dB/oct
Applicable frequency range	300 Hz to 3 kHz
Max input signal level[a]	2.1 V_{rms} (Gain = 1)
Max output signal level[a]	0.7 V_{rms} (Gain = 1)
Max output current	±5 mA
Max output voltage	±10 V into 2 kΩ load
Time constant (R-C)	0.53 ms
Gain	$\geq$1 (variable)
Dc power required	±15 Vdc

[a]Voice simulated signal

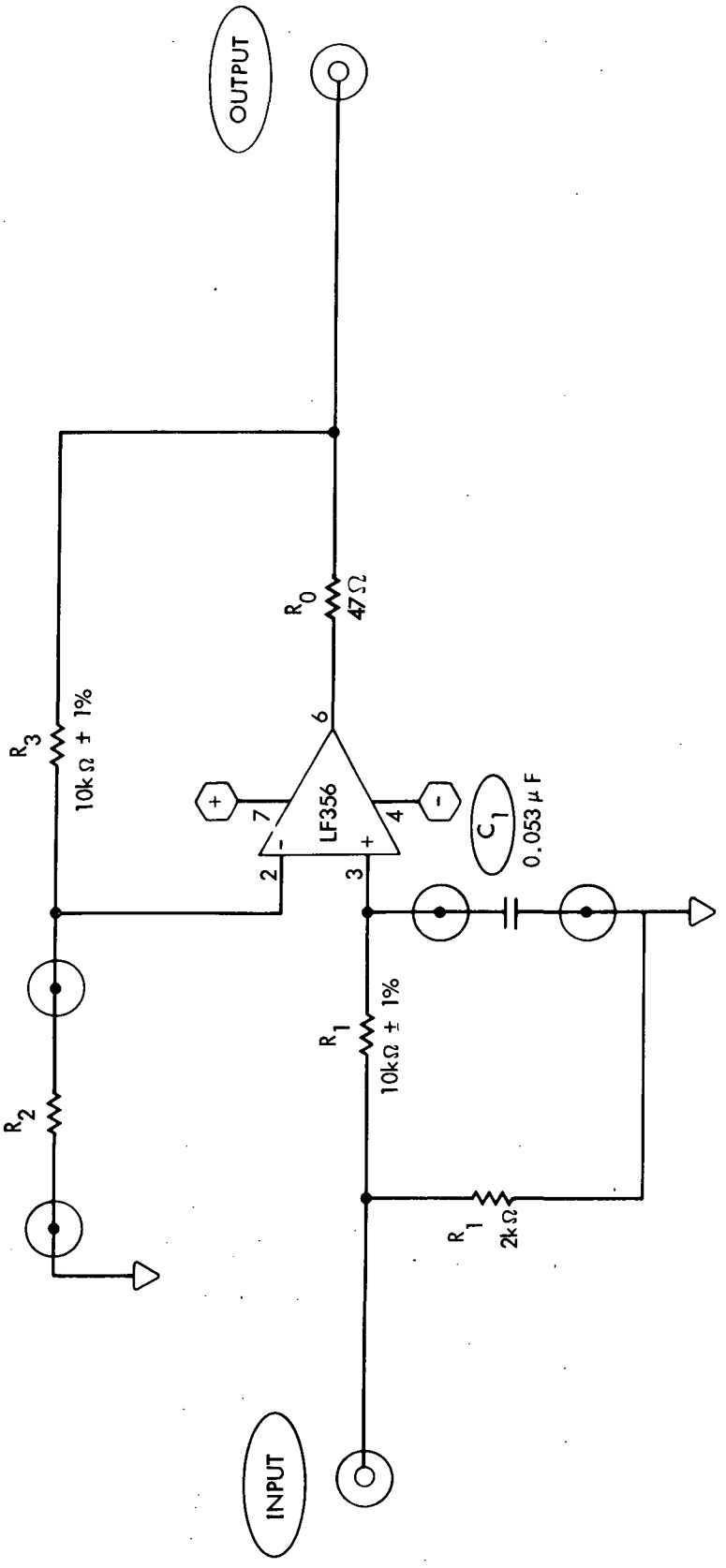

Figure G-20. De-Emphasis Network

Table G-14. 2:1 Compandor Expander Functional Characteristics

Characteristic	Specified Performance
Syllabic companding law	2 to 1 (dB)
Input impedance	>2 kΩ
Max input signal level[a]	0.2 V_{rms}
Max output signal level[a]	0.048 V_{rms}
Max output current	±20 mA
Frequency response	10 Hz to 40 kHz
Input tracking error	±0.1 dB
Dynamic range (input rms variations)	40 dB
Low-pass filter (envelope) time constant	22 ms
Dc power required	+15 Vdc

[a]Voice simulated signal

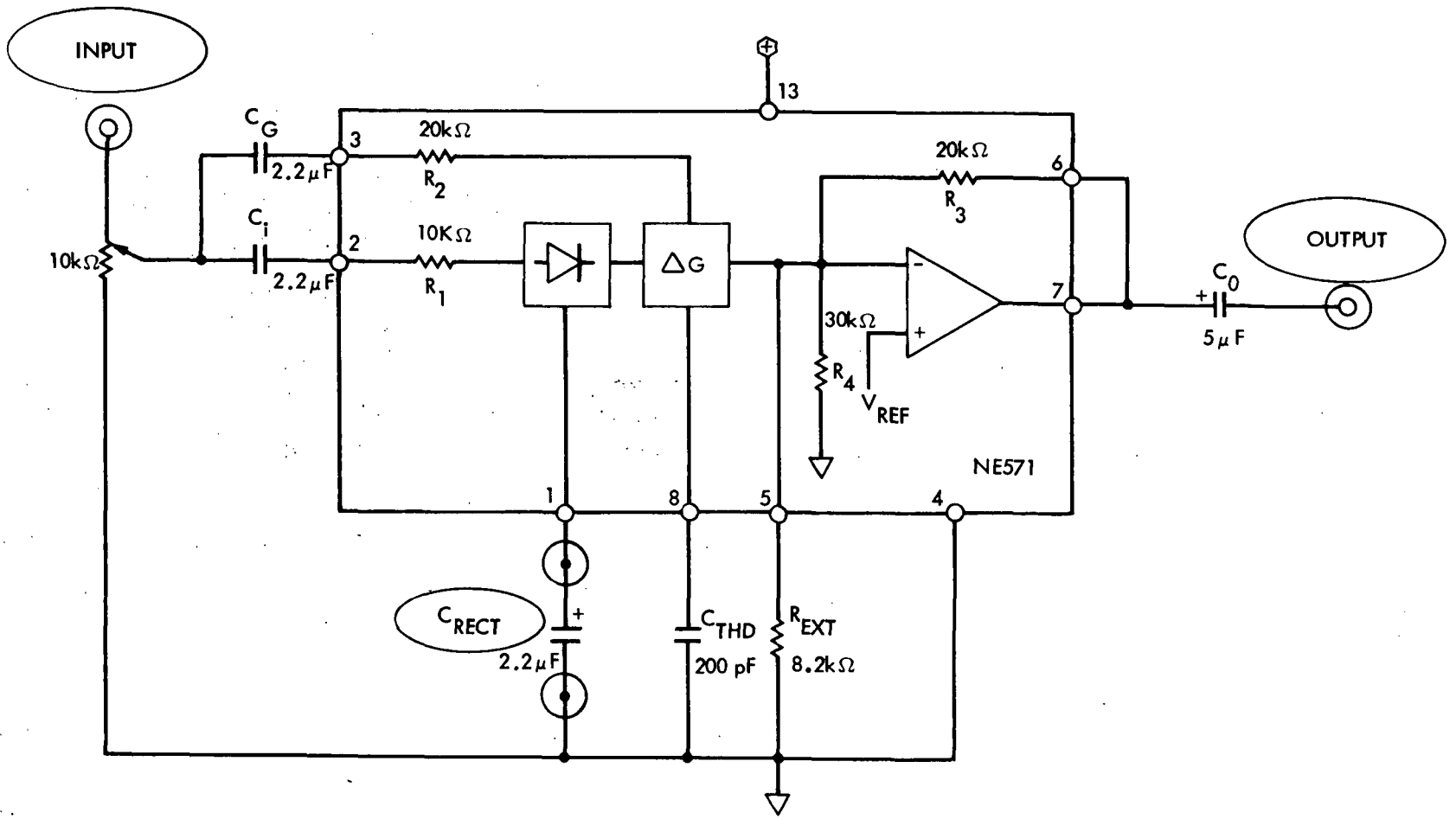

Figure G-21. 2:1 Compandor Expander

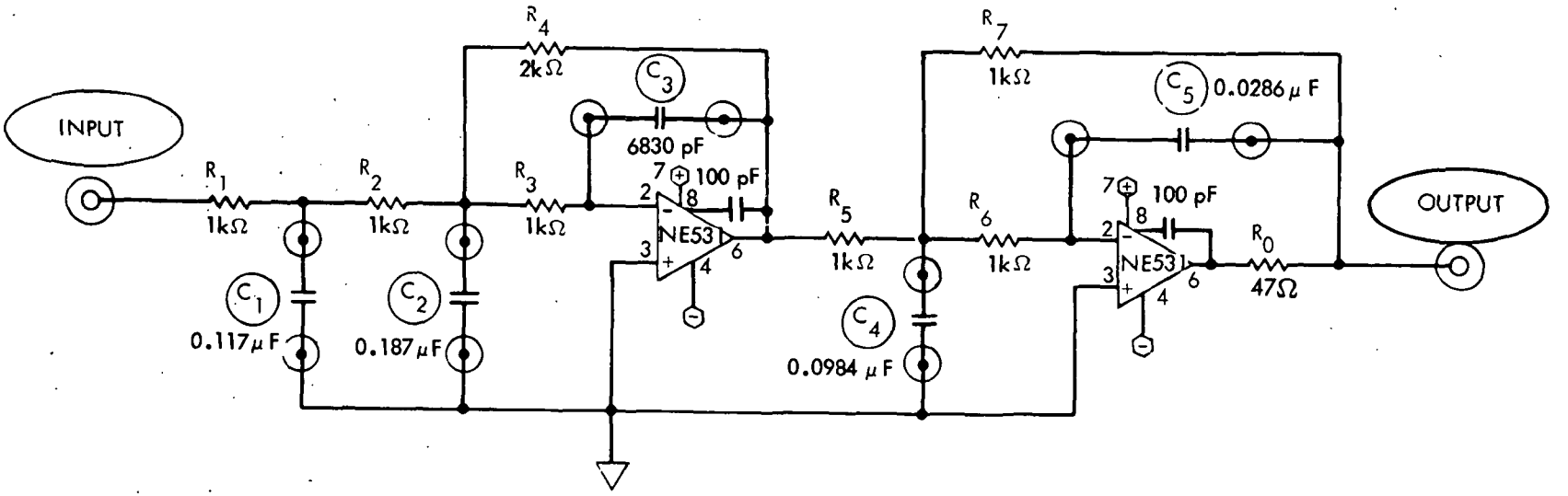

Figure G-22. Compandor-Expander Low-Pass Filter

Table G-15. Variable Gain Amplifier[a] Functional Characteristics

Characteristic	Specified Performance
Input impedance	620 Ω to 10.62 kΩ[b]
Output impedance	50 Ω
Max output current	±100 mA
Frequency response	20 Hz to 10 MHz
Operating temperature	-25°C to 80°C
Dc power required	±15 Vdc

[a]50 Ω Line driver (operational amplifier)

[b]Depends on the gain setting

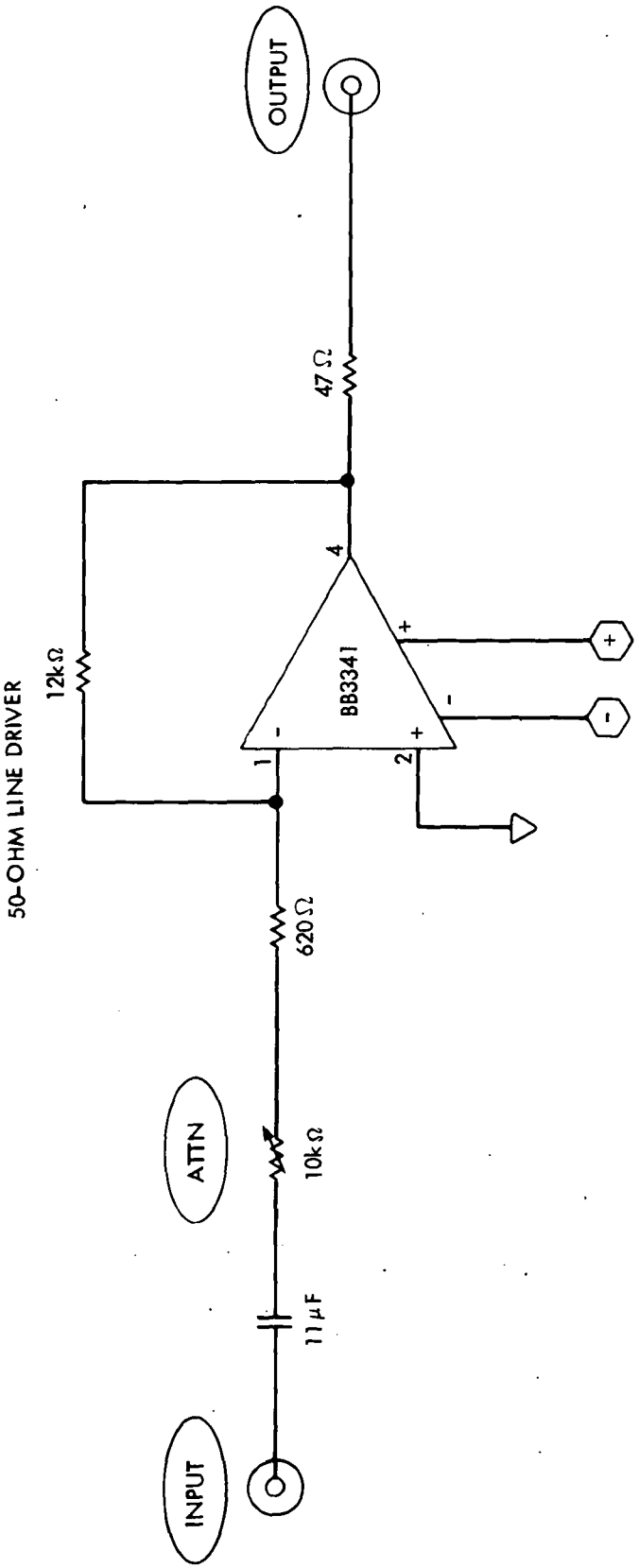

Figure G-23. Variable Gain Amplifier